NUREG-1313

Safety Evaluation Report

related to the Evaluation of Low-Enriched Uranium Silicide-Aluminum Dispersion Fuel for Use in Non-Power Reactors

U.S. Nuclear Regulatory Commission

Office of Nuclear Reactor Regulation

July 1988

NOTICE

Availability of Reference Materials Cited in NRC Publications

Most documents cited in NRC publications will be available from one of the following sources:

1. The NRC Public Document Room, 1717 H Street, N.W.
   Washington, DC 20555
2. The Superintendent of Documents, U.S. Government Printing Office, Post Office Box 37082, Washington, DC 20013-7082
3. The National Technical Information Service, Springfield, VA 22161

Although the listing that follows represents the majority of documents cited in NRC publications, it is not intended to be exhaustive.

Referenced documents available for inspection and copying for a fee from the NRC Public Document Room include NRC correspondence and internal NRC memoranda; NRC Office of Inspection and Enforcement bulletins, circulars, information notices, inspection and investigation notices; Licensee Event Reports; vendor reports and correspondence; Commission papers; and applicant and licensee documents and correspondence.

The following documents in the NUREG series are available for purchase from the GPO Sales Program: formal NRC staff and contractor reports, NRC-sponsored conference proceedings, and NRC booklets and brochures. Also available are Regulatory Guides, NRC regulations in the *Code of Federal Regulations,* and *Nuclear Regulatory Commission Issuances.*

Documents available from the National Technical Information Service include NUREG series reports and technical reports prepared by other federal agencies and reports prepared by the Atomic Energy Commission, forerunner agency to the Nuclear Regulatory Commission.

Documents available from public and special technical libraries include all open literature items, such as books, journal and periodical articles, and transactions. *Federal Register* notices, federal and state legislation, and congressional reports can usually be obtained from these libraries.

Documents such as theses, dissertations, foreign reports and translations, and non-NRC conference proceedings are available for purchase from the organization sponsoring the publication cited.

Single copies of NRC draft reports are available free, to the extent of supply, upon written request to the Division of Information Support Services, Distribution Section, U.S. Nuclear Regulatory Commission, Washington, DC 20555.

Copies of industry codes and standards used in a substantive manner in the NRC regulatory process are maintained at the NRC Library, 7920 Norfolk Avenue, Bethesda, Maryland, and are available there for reference use by the public. Codes and standards are usually copyrighted and may be purchased from the originating organization or, if they are American National Standards, from the American National Standards Institute, 1430 Broadway, New York, NY 10018.

NUREG-1313

Safety Evaluation Report

related to the Evaluation of Low-Enriched Uranium Silicide-Aluminum Dispersion Fuel for Use in Non-Power Reactors

U.S. Nuclear Regulatory Commission

Office of Nuclear Reactor Regulation

July 1988

ABSTRACT

Low-enriched uranium silicide-aluminum dispersion plate-type fuels have been extensively researched and developed under the international program, Reduced Enrichment in Research and Test Reactors. The international effort was led by Argonne National Laboratory (ANL) in the United States. This evaluation is based primarily on reports issued by ANL that discuss and summarize the developmental tests and experiments, including postirradiation examinations, of both miniature and full-sized plates of prototypical fuel compositions. This evaluation concludes that plate-type fuels suitable and acceptable for use in research and test reactors can be fabricated with U_3Si_2-Al dispersion compacts with uranium densities up to 4.8 g/cm^3.

CONTENTS

FIGURE

1 INTRODUCTION

In 1978, the United States took the lead in initiating a program, Reduced Enrichment in Research and Test Reactors (RERTR), to help provide the capability for research and test (nonpower) nuclear reactors to convert from the use of high-enriched uranium (HEU) to low-enriched uranium (LEU) fuels. Some of the world's operating nonpower reactors could have successfully made the conversion with fuel types that were technically feasible at that time. However, many of the higher powered and higher performance reactors were designed for and operating with HEU fuels in which the uranium concentration was already close to the practical maximum. Therefore, a fuels review and development program was initiated to provide the capability for more of these reactors to convert without serious detriment to their research projects. Under that program, established at the Argonne National Laboratory (ANL), a dispersion-type fuel containing uranium silicide in aluminum has been developed and tested. This fuel provides a total uranium concentration significantly higher than that previously available in the plate geometry. The fuel has the capability of maintaining a concentration of uranium-235 that is sufficient for operational use in nonpower reactors at a uranium-235 enrichment that is as low as 20 percent.

The developmental work on the U_3Si_2-Al dispersion fuel performed under the auspices of the worldwide RERTR programs has been presented, discussed, and summarized in two reports issued by ANL. These reports, which have been reviewed and evaluated by the Idaho National Engineering Laboratory (INEL), provide the principal bases for the U.S. Nuclear Regulatory Commission's (NRC's) acceptance of the use of this new fuel type in nonpower reactors that NRC licenses to operate. The two ANL reports are included as Appendices A and B in this evaluation report.

R. E. Carter, Project Manager, Office of Nuclear Reactor Regulation, NRC, initiated and coordinated the review and evaluation of the ANL reports. A. Adams, Jr., a project manager in the same office, continued and completed the task. R. R. Hobbins (INEL) conducted the principal technical review under contract to the NRC.

2 DISCUSSION

The ANL reports (Appendices A and B in this report) summarize the results obtained from preirradiation and postirradiation tests on miniature (mini) plates and full-sized fuel elements, with the irradiations performed at the Oak Ridge Research Reactor (ORR). Typical maximum power developed in a test fuel element was approximately 1 MW, leading to about 1.4 MW/m^2 heat flux and a maximum fuel-meat temperature of approximately 130°C. These parameters define the upper limits for the range of conditions actually tested and, therefore, define the upper limits for the range over which the conclusions of the reports apply. However, there appear to be no tested parameters of these fuels that are strongly correlated to power level or power density, so extrapolation

of the conclusions to higher ranges is not ruled out. In addition, the conclusions also apply to the entire range below these limits and, therefore, to all lower powered reactors with approximately the same number of fuel plates.

Tests were run on fuels consisting primarily of the U_3Si-Al and the U_3Si_2-Al matrices. The data show that many more tests and evaluations of U_3Si_2-Al were performed than of any other fuel type. Nevertheless, results and conclusions drawn indicate that the U_3Si-Al matrix is less suitable than U_3Si_2-Al for long-term and high burnup reliability because of gas bubble morphology and the exothermic U_3Si-Al reaction. The U_3Si-Al fuels are not yet sufficiently developed and understood to merit generic NRC acceptance for use in nonpower reactors. They might be acceptable for specific applications, especially where burnup will be low, and should then be evaluated on a case-by-case basis.

Most of the irradiations were performed in the ORR, where essentially a full-core irradiation program also was conducted. No results of the latter are discussed in the ANL reports. ANL will report on the full-core irradiation program and on any observations or results from the full-core test that conflict with or shed more light on the individual plate and fuel element tests discussed in Appendices A and B in this report. However, discussions with ANL staff indicate that no fuel failure or unpredicted behavior occurred during irradiation of the full core in the ORR, and preliminary results support the conclusions in Appendices A and B.

The results presented are confined to characteristics of the fuel itself and were not intended to constitute a full safety review of the use of the U_3Si_2-Al fuel system in operating reactors. The data are usable, however, not only to compare the U_3Si_2-Al fuel with the UAl_x-Al and U_3O_8-Al fuels in current use, but also to extend the evaluations to burnup regimes not recently or previously tested using UAl_x-Al and U_3O_8-Al fuels.

Many of the physical parameters of the LEU U_3Si_2-Al fuel system are similar to the corresponding ones of the HEU Materials Testing Reactor (MTR)-type fuels. However, the influence of exothermic U_3Si_2-Al interaction at high temperature, which is more energetic than the UAl_x interaction, requires analysis to show the potential consequences of the use of U_3Si_2-Al fuel in specific reactor applications. There appear to be no new operating or accident concerns introduced by the use of U_3Si_2-Al fuel; only the magnitudes of some reactor operational conditions may change.

It appears that even the existence of the exothermic reaction does not introduce a significant new parameter; however, both this and other operational and potential accident differences caused by conversion of a reactor from its current fuel (for example, HEU UAl_x-Al) to LEU U_3Si_2-Al must be considered in each case.

All three of the major fuel vendors, Babcock & Wilcox (B&W),* CERCA,** and NUKEM*** fabricated fuel used in the reported tests or examinations. There were

---

*Babcock & Wilcox Company, Lynchburg, Virginia, USA.
**Compagnie pour l'Etude et la Realisation de Combustibles Atomiques, Romans-sur-Isere, France.
***NUKEM GmbH, Hanau, Federal Republic of Germany.

some differences in the characteristics and the responses to irradiation of samples from the three fabricators, but the differences, which are discussed, are not significantly harmful. However, acceptance specifications should be developed and required for all three vendors to ensure that the fuel samples tested were representative of the fuel elements to be produced under future industrial production-type conditions. The full-core tests mentioned above also included products from all three vendors and may provide additional information about their relative performance. The information currently available supports acceptance of the U_3Si_2-Al fuel for use in NRC-licensed reactors. However, unqualified approval of the U_3Si_2-Al fuel is contingent on the following two conditions: (1) acceptance specifications and (2) evaluations of the results of the full-core tests in the ORR.

3 EVALUATION

In this section, a brief description of the uranium-silicide fuel system and an evaluation of the physical properties and irradiation performance of this system are given. This fuel system also is compared with the currently accepted uranium-aluminide fuel system.

3.1 Fuel System Description

The development of the uranium-silicide fuel system is similar to the earlier development of the uranium-aluminide fuel system, with the compound U_3Si_2 being substituted for UAl_x as the fuel dispersed in an aluminum matrix in the core or "meat" of a fuel plate clad in aluminum. The same basic procedure is used to fabricate either uranium-silicide fuel plates or uranium-aluminide fuel plates. The uranium-silicide fuel is produced by melting stoichiometric amounts of uranium and silicon, followed by comminution to produce a powder. The fuel powder is mixed with aluminum powder and formed under pressure into a powder metallurgical compact. The compact is placed in an aluminum picture frame and aluminum cover plates and hot and cold rolled to produce the fuel plate.

The use of a high volume percent (40 to 50 percent) of fuel in the fuel core, considerably in excess of the loadings of HEU dispersion fuels, dictates that special consideration be given to fabrication procedures and/or specifications in order to obtain cost-effective yields of acceptable plates. Problems associated with the fabrication of dispersion fuel plates that are made worse by the use of high volume percentage fuel are dogboning, minimum cladding thickness, and stray fuel particles. These problems were successfully overcome in the fabrication of miniplates and full-sized elements tested in the ORR and, therefore, constitute problems that can be solved by the use of appropriate fabrication procedures and specifications. Dogboning is the thickening of the fuel core at the ends of the plate and can lead to increased areal uranium density and concomitantly high surface heat fluxes during irradiation. Requirements for minimum cladding thickness and removal of stray fuel particles prevent the exposure of the fuel to the coolant.

Oxidation of fuel particles at the surface of the compact may occur if precautions are not taken to prevent air from freely entering the rolling billet during the initial heating. Such oxidation is undesirable because blistering during postirradiation annealing initiates at the sites of oxidized fuel.

In practice, it is impossible to produce a fuel powder with precisely the stoichiometric composition U_3Si_2. Instead, a fuel that is predominantly U_3Si_2 but that contains some USi, U(Si), and U_3Si results. As illustrated in the phase diagram in Figure 1, deviations from stoichiometry on the silicon-rich side produce some USi, while deviations on the uranium-rich side produce a solid solution of silicon in uranium [U(Si)], which undergoes a peritectoid reaction with U_3Si_2 to generate U_3Si.

As discussed more thoroughly in Section 3.3.1, the compound U_3Si is undesirable, but USi and U(Si) are benign. Therefore, it is preferable to use a fuel composition slightly on the silicon-rich side of U_3Si_2 and to avoid heat treating steps in the fabrication process that promote the peritectoid formation of U_3Si.

3.2 Materials Properties

In the following sections, the properties of U_3Si_2 dispersion fuel are compared with those of the UAl_x dispersion fuel currently in use in research reactors.

3.2.1 Fuel Core Porosity

Porosity remaining in the fuel core after fabrication is useful in accommodating the swelling of fuel particles caused by the generation of fission products within the fuel. Fuel core porosity increases with the volume fraction of fuel dispersed in the aluminum matrix because the aluminum cannot flow completely around all the fuel particles during the fabrication process. An empirical relationship between porosity and volume fraction of fuel in the core is given in Appendix A that is based on measurements in miniplates. However, as noted in Appendix A, porosities of fuel produced by different plate manufacturers vary. Porosity was found to vary from 4 to 10 percent among three manufacturers (B&W, CERCA, NUKEM) of full-sized elements irradiated in the ORR. The lowest porosity allows fuel plate swelling to be about 30 to 45 μm greater than that for the plate with the highest porosity, but this difference is small compared with normally allowed tolerances in cooling channel thickness [e.g., 2.64-mm minimum gap in the ORR (see Appendix B)]. Similar variations in porosity are found in the UAl_x fuels currently used in research reactors. Therefore, the normal variation in as-fabricated porosity among manufacturers should have no safety implications.

3.2.2 Heat Capacity

The heat capacity of the fuel core is the sum of the heat capacities of the fuel and the aluminum of the matrix, taking into account the fabrication porosity. The volumetric heat capacities of aluminum, U_3Si_2, and UAl_x are all very similar, so that the principal factor affecting the heat capacity at room temperature of a U_3Si_2 fuel core is the porosity. In Appendix A, the heat capacity at room temperature of a U_3Si_2 fuel core is given as decreasing from 2.44 to 2.13 $J/cm^3 \cdot K$ as the fuel volume fraction increases from 0 to 0.5. This decrease in heat capacity with increasing fuel fraction is a result of the increase in porosity that accompanies the increasing fuel content. Similar values and behavior with increasing fuel content are found for the heat capacity of UAl_x dispersion cores (Stahl, 1982).

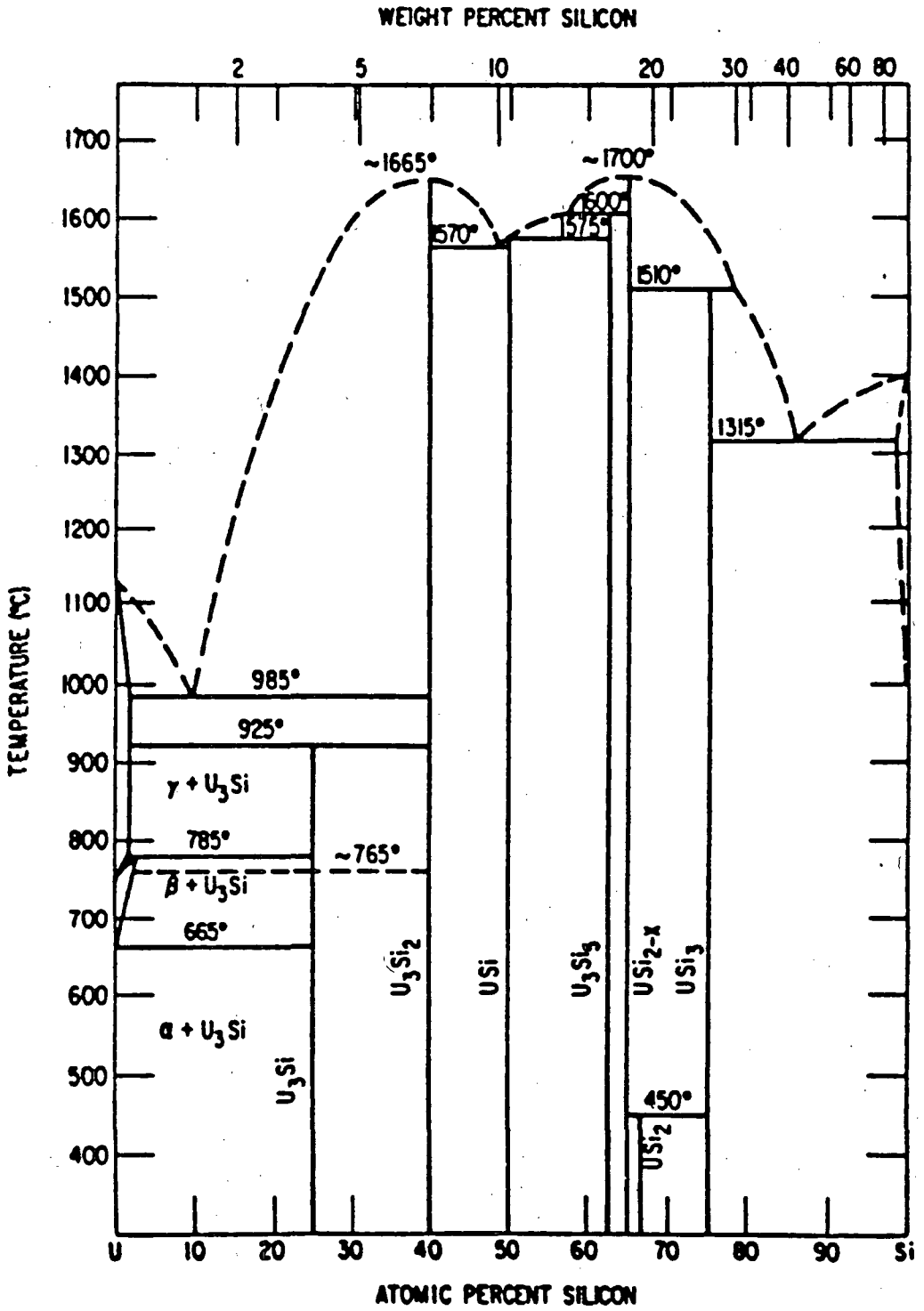

Figure 1 The uranium-silicide system
Source: Appendix A of this report.

3.2.3 Thermal Conductivity

As demonstrated in Appendix A, the thermal conductivity of U_3Si_2 dispersion fuel plates is a strong function of the fuel content of the core because the conductivity of U_3Si_2 is about 7 percent that of aluminum. For 45 volume percent fuel plus porosity, the thermal conductivity of a U_3Si_2 fuel plate is about 52 W/m·K at 333 K (Appendix A), similar to, but somewhat lower than, the value of about 60 W/m·K for a UAl_x fuel plate at 367 K (Nazare et al., 1975).

The temperature coefficient of thermal conductivity of U_3Si_2 reported in Appendix A is a small positive value that averages about 0.06 W/m·K^2 for eight samples. A temperature coefficient derived from conductivities reported by Stahl (1982) for U-Al alloy fuel (a dispersion of UAl_4 particles in an aluminum matrix without appreciable porosity) is a small negative value of about 0.03 W/m·K^2. These data suggest that the thermal conductivity of U_3Si_2 fuel plates is similar to that of UAl_x fuel plates. Also similar is the weak temperature dependence of the thermal conductivity in both fuel systems, although the data suggest a slightly increasing thermal conductivity for U_3Si_2 and a slightly decreasing thermal conductivity for UAl_x with increasing temperature. The positive temperature coefficient of thermal conductivity of U_3Si_2 fuel plates should contribute to fuel plate temperature stability under off-normal conditions and is, therefore, beneficial in regard to safety.

3.2.4 Compatibility of U_3Si_2 and Aluminum

A reaction between U_3Si_2 and aluminum occurs at elevated temperatures to produce $U(Al,Si)_3$ and approximately 350 J/g of U_3Si_2 that has reacted. The $U(Al,Si)_3$ has the UAl_3 crystal structure and some substitution of silicon in aluminum positions. The reaction is insignificant during normal irradiation at temperatures less than 570 K, but becomes rapid at temperatures of about 890 K, which is above the solidus point of the aluminum alloys used in the matrix of the fuel core and in the cladding. The reaction itself does not cause a loss of fuel element geometry because aluminum melting is necessary to cause the reaction to proceed at a significant rate. The heat of reaction approximates the heat of fusion of aluminum (397 J/g) and, therefore, results in essentially no net heat production or consumption for fuels containing about 45 volume percent U_3Si_2 in the fuel core because these fuel plates contain approximately equal weights of U_3Si_2 and aluminum. In the uranium-aluminide fuel system, an exothermic reaction occurs between the UAl_3 fuel and the aluminum matrix, but the heat generated is less than one-third that of the reaction of U_3Si_2 with aluminum for the same uranium content. The influence of this more energetic chemical reaction between fuel and matrix materials in the fuel core in the uranium-silicide system should be evaluated in safety analyses if postulated accidents lead to aluminum melting.

3.2.5 Corrosion Behavior

The corrosion resistance of U_3Si_2 was tested by immersing in boiling water a miniplate in which a hole had been drilled completely through the cladding and fuel core. No pickup of radioactivity in the water and no weight changes were measured after 168 hours. As concluded in Appendix A, the corrosion of U_3Si_2 dispersed in aluminum is negligibly small. A similar conclusion was made for the corrosion of UAl_x in hot water (Gibson, 1967).

3.3 Irradiation Behavior

Miniplates and full-sized fuel elements have been irradiated in the ORR and subjected to postirradiation examination. The irradiation included high flux positions in this 30-MW reactor resulting in heat generation rates up to 1.4 MW/m^2 and burnups of up to 98 percent of the uranium-235. Fuel loadings up to the practical limit for fabrication (about 50 volume percent) have been tested. No indications of fission product leakage, excessive fuel plate swelling, fuel plate warping, blistering, or other unusual conditions were observed. Three key aspects of irradiation behavior are discussed in the following sections: swelling, blister resistance, and fission product release.

3.3.1 Swelling

The fuel particles in the core swell as a function of burnup to accommodate fission products, both solid and gaseous, that occupy a greater volume than the fissioning uranium. The U_3Si_2, USi, and UAl_x fuel particles all exhibit linear swelling behavior with increasing burnup and are, therefore, predictably stable fuels, whereas U_3Si undergoes breakaway swelling and is unstable above about 4×10^{27} fissions/m^3 of fuel particle. The swelling rates per unit fission density for U_3Si_2 (Appendix A) and UAl_x (Beeston et al., 1980) are practically the same--6.2 percent and 6.0 percent per 1×10^{27} fissions/m^3 of fuel particle, respectively. The fuel core swelling of U_3Si_2 and UAl_x dispersion fuels can be reliably predicted for a given fission density from the above fuel particle swelling rates, the fuel volume fraction, and the as-fabricated porosity. The stable swelling behavior of U_3Si_2 is attributable to the formation of small gas bubbles (0.4 to 0.8 μm) within the fuel that remain small and independent of one another even at high burnup and the resulting high bubble density (Appendix A). On the other hand, it has been observed that bubble agglomeration is the cause of the unstable swelling in U_3Si fuel. Therefore, it is necessary to control the amount of U_3Si in U_3Si_2 fuel by suitable fabrication specifications and careful fabrication practices. Full-sized fuel elements produced by three different commercial fabricators were irradiated in the ORR, and acceptable swelling at very high burnups resulted (Appendix B). This experience suggests that adequate control of U_3Si content is a problem that can be managed relatively easily.

3.3.2 Blister Resistance

The resistance of a fuel plate to blistering (caused by gas bubble agglomeration) when it is heated to elevated temperatures has been used as a measure of fuel plate stability for many years in the development of dispersion fuels (Beeston, 1980). The blister threshold measured on U_3Si_2 fuel plates ranged from 788 to 848 K and does not appear to be affected significantly by either burnup or fuel volume loading (Stahl, 1982). This blister behavior is excellent and is similar to that in UAl_x fuels (Beeston, 1980).

3.3.3 Fission Product Release

As discussed in Appendix A, measurements of fission product release from fuels dispersed in an aluminum matrix generally have shown that the first release is

associated with the blister threshold. A major release coincides with the melting of the aluminum in the fuel plate. Another significant release point is the temperature at which the fuel reacts with the matrix. These results have been found with UAl_x, U_3O_8, and U_3Si fuels dispersed in an aluminum matrix.

Although measurements of fission product release have not been made on U_3Si_2 fuel, it is reasonable to expect that initial releases of fission products will occur at the blister threshold of about 800 K followed by a much larger release at the solidus temperature of the cladding (about 855 K) where the fuel begins to react with aluminum. The fission product behavior expected from U_3Si_2 fuel should be comparable to that of the UAl_x fuel currently used in research reactors.

3.4 Summary

The development and testing of LEU U_3Si_2 fuel are similar to the earlier development and testing of the HEU UAl_x fuel currently used in many research reactors.

Extensive experience with fabrication and irradiation performance has been gained with miniplates and full-sized fuel elements. The testing program has demonstrated excellent fuel performance comparable to that of the HEU UAl_x fuel.

The physical and chemical properties of the U_3Si_2 fuel system are well known and provide a basis for understanding the performance characteristics of the fuel. The influence of the exothermal reaction of U_3Si_2 with molten aluminum must be addressed in safety analyses in which fuel plate temperatures in excess of the solidus point of the aluminum alloys used are calculated to be possible. The use of LEU U_3Si_2 fuel in nonpower reactors is considered to provide a level of safety comparable to that associated with the use of HEU UAl_x fuel.

4 CONCLUSIONS

The tests and examinations summarized in Appendices A and B, including the extensive references to U_3Si_2-Al MTR (plate)-type fuel, provide the necessary bases for the staff's evaluations. On the basis of the currently available information, the staff concludes that the described fuel* is acceptable for use in licensed nonpower reactors provided individual safety analyses do not introduce new safety considerations. The staff will review the report on the full-core irradiation program once it is submitted, and if necessary, a supplement to the report will be issued if new safety considerations come to light. This conclusion also is contingent on the use of a uniform set of acceptance specifications consistent with those used for the fabrication of the test specimens.

5 REFERENCES

Beeston, J. M., R. R. Hobbins, G. W. Gibson, and W. C. Francis, "Development and Irradiation Performance of Uranium Aluminide Fuels in Test Reactors," Nuclear Technology, Vol. 49, pp. 136-149, June 1980.

*The U_3Si_2 dispersion in aluminum, with uranium densities up to 4.8 g/cm^3 in the fuel meat.

Gibson, G. W., The Development of Powdered Uranium-Aluminide Compounds for Use as Nuclear Reactor Fuels, IN-1133, Idaho Nuclear Corporation, Idaho Falls, Idaho, December 1967.

Nazare, S., G. Ondracek, and F. Thummler, "Investigations on UAl_x-Al Dispersion Fuels for High-Flux Reactors," Journal of Nuclear Materials, Vol. 56, pp. 251-259, 1975.

Stahl, D., Fuels for Research and Test Reactors, Status Review, ANL-85-5, Argonne National Laboratory, Argonne, Illinois, December 1982.

APPENDIX A

THE USE OF U_3SI_2 DISPERSED IN ALUMINUM IN PLATE-TYPE FUEL ELEMENTS FOR RESEARCH AND TEST REACTORS ANL/RERTR/TM-11

Distribution Category:
Nuclear Converter Reactor Fuel Cycle
Technology: Base Technology (UC-83)

ANL/RERTR/TM-11

ARGONNE NATIONAL LABORATORY
9700 South Cass Avenue
Argonne, Illinois 60439

THE USE OF U_3Si_2 DISPERSED IN ALUMINUM IN PLATE-TYPE FUEL ELEMENTS FOR RESEARCH AND TEST REACTORS

by

J. L. Snelgrove, R. F. Domagala, G. L. Hofman, and T. C. Wiencek

Argonne National Laboratory

and

G. L. Copeland, R. W. Hobbs, and R. L. Senn

Oak Ridge National Laboratory

October 1987

The Use of U_3Si_2 Dispersed in Aluminum in Plate-Type Fuel Elements for Research and Test Reactors

J. L. Snelgrove, R. F. Domagala, G. L. Hofman, and T. C. Wiencek

Argonne National Laboratory
Argonne, Illinois 60439

and

G. L. Copeland, R. W. Hobbs, and R. L. Senn

Oak Ridge National Laboratory
Oak Ridge, Tennessee 37831

ABSTRACT

A high-density fuel based on U_3Si_2 dispersed in aluminum has been developed and tested for use in converting plate-type research and test reactors from the use of highly enriched uranium to the use of low-enriched uranium. The results of preirradiation testing and the irradiation and postirradiation examination of miniature fuel plates and full-sized fuel elements are summarized.

The swelling of the U_3Si_2 fuel particles is a linear function of the fission density in the particle to well beyond the fission density achievable in low-enriched fuels. The U_3Si_2 particle swelling rate is approximately the same as that of the commonly used UAl_x fuel particle. The presence of minor amounts of U_3Si or uranium solid solution in the fuel result in greater, but still acceptable, fuel swelling. Blister threshold temperatures are at least as high as those of currently used fuels. An exothermic reaction occurs near the aluminum melting temperature, but the measured energy releases were low enough not to substantially worsen the consequences of an accident.

It is concluded that U_3Si_2-aluminum dispersion fuel with uranium densities up to at least 4.8 Mg/m^3 is a suitable LEU fuel for typical plate-type research and test reactors.

Table of Contents

Table of Contents (Cont.)

List of Tables

List of Figures

The Use of U_3Si_2 Dispersed in Aluminum in Plate-Type Fuel Elements for Research and Test Reactors

1. INTRODUCTION

The U.S. Reduced Enrichment Research and Test Reactor (RERTR) Program was established by the U.S. Department of Energy in 1978 to provide the technical means to convert research and test reactors from the use of highly enriched uranium (HEU) fuel to the use of low-enriched uranium (LEU) fuel. In order to maintain the required excess reactivity of the reactor core, the amount of ^{235}U must be increased by 10 to 15% to overcome the additional neutron absorption of the greatly increased ^{238}U content in LEU fuel and the effects of a harder neutron spectrum. This additional ^{235}U and ^{238}U can be accommodated by increasing the uranium density of the fuel and/or by redesigning the fuel element to increase the volume fraction of fuel in the reactor core. The RERTR Program has vigorously pursued both paths with major efforts in fuel development and demonstration and in reactor analysis and design.[1]

Research and test reactor fuel elements consist of assemblies of fuel-containing plates or rods. The RERTR Program has concentrated its efforts on plate-type fuels since plate-type research and test reactors consume much more HEU than do rod-type reactors. High-density LEU rod-type fuels have been developed by GA Technologies for TRIGA reactors[2] and by Atomic Energy of Canada, Ltd.[3] Rod-type fuels will not be discussed further in this report.

The fuel plates used in the fuel elements for most research and test reactors consist of a fuel core, or "meat," in an aluminum alloy cladding. Originally, cast and wrought alloys of uranium and aluminum, consisting of UAl_3 and UAl_4 precipitates in an aluminum matrix, were used for the fuel meat. Fabrication of alloy cores with uranium densities above ~1.1 Mg U/m^3 is difficult, however, and powder metallurgical cores, with UAl_x (a combination of UAl_2, UAl_3, UAl_4, and Al phases) or U_3O_8 dispersed in aluminum, are now used in most cases. In 1978 the densest UAl_x fuel in use contained ~1.7 Mg U/m^3 in the fuel meat (~37 vol% UAl_x), and the densest U_3O_8 fuel in use contained ~1.3 Mg U/m^3 in the fuel meat (~18 vol% U_3O_8). The RERTR Program has developed and tested UAl_x and U_3O_8 dispersion fuels for LEU applications up to their practical fabrication limits--2.4 and 3.2 Mg U/m^3, respectively.

In order to minimize the need to redesign fuel elements to increase the fuel volume fraction and to make significant enrichment reductions in high-performance reactors even feasible, higher densities yet were needed. One approach, followed by the French Commissariat à l'Energie Atomique (CEA), utilized small wafers of sintered UO_2 contained in compartments of a fuel

plate produced by diffusion bonding Zircaloy frames, spacer wires, and cladding plates.[4] The 7%-enriched "caramel" fuel has performed well in OSIRIS;[5] however, fabricators of conventional plate-type fuels would have to implement a completely new fabrication process to produce caramel fuel.

The RERTR Program chose to pursue the use of high-density uranium-silicon alloys in place of UAl_x and U_3O_8 in conventional aluminum-matrix dispersion fuel in order to take advantage of the large commercial base of equipment for and experience in fabrication of such fuels. One uranium silicide compound, U_3Si_2, has been found to perform extremely well under irradiation and can provide a uranium density of at least 4.8 Mg/m^3.

The development and testing of uranium silicide fuels has been an international effort, involving other national reduced enrichment programs, several commercial fuel fabricators, and several test reactor operators. In particular, the testing of full-sized fuel elements has been performed cooperatively, with the U.S. Government providing the enriched uranium, the fuel fabricators providing the fabrication, and the U.S. Government or other governments providing the irradiations and postirradiation examinations.

Numerous results of the development and testing of uranium silicide-aluminum dispersion fuels have been published previously. The results for U_3Si_2 dispersions are summarized in this report to facilitate the preparation and review of requests to use this fuel in research and test reactors.

2. PROPERTIES OF U_3Si_2 AND OTHER URANIUM SILICIDES

2.1 Uranium Silicide Phases

As is the case for uranium aluminide, uranium silicide normally consists of a mixture of intermetallic compounds, or phases. The quantity of each phase present depends upon the composition and homogeneity of the alloy and on its heat treatment. Since, as will be discussed later, the different uranium silicide phases behave differently under irradiation, knowledge of the phases to be expected in the fuel is necessary to correctly interpret the test results and to prepare specifications. A brief discussion of this topic follows; more detail can be found in Ref. 6.

The U-Si phase diagram is shown in Fig. 1. In the region of the phase diagram between 7.3 and 10.6 wt% Si, the two phases U_3Si_2 and USi exist, at equilibrium, in the proportions shown in Fig. 2. These two phases form directly upon cooling from the liquid state. The situation is more complicated for Si contents of less than 7.3 wt% because U_3Si is formed by a peritectoid (solid state) reaction. The as-cast alloy consists of primary U_3Si_2 with a

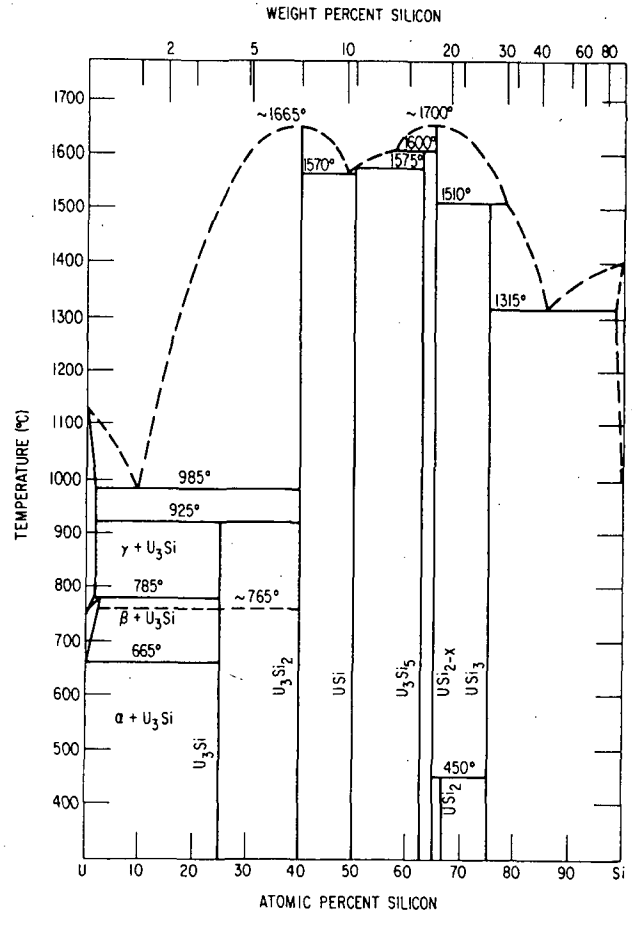

Fig. 1. The U-Si System.

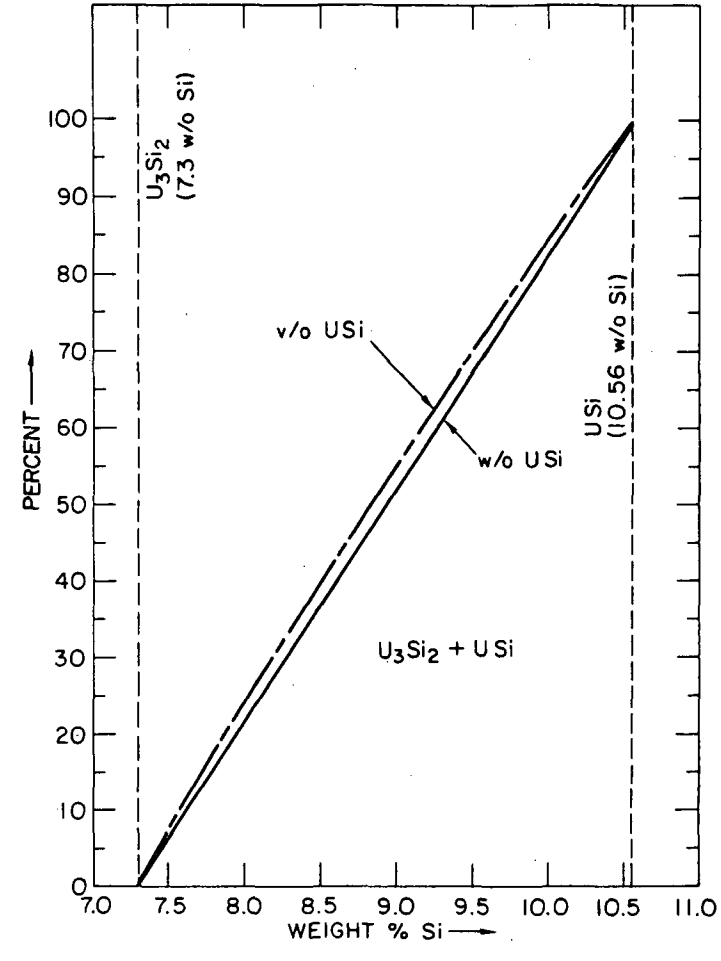

Fig. 2. Weight % (w/o) and Volume % (v/o) of USi vs. Weight % Si for Alloys at Equilibrium.

eutectic matrix of uranium solid solution (U_{ss}) and U_3Si_2. The proportions of U_3Si_2 and U_{ss} are shown in Fig. 3. Following prolonged heat treatment below the 925°C peritectoid temperature, U_{ss} reacts with U_3Si_2 to form U_3Si. Heat treatment of arc-cast ingots for 72 h at 800°C has been found to be sufficient to carry the reaction to completion. At equilibrium in the heat-treated alloy, the proportions of U_3Si and U_3Si_2 for Si contents between 3.9 and 7.3 wt% are shown in Fig. 4. Below 3.9 wt% Si the heat-treated alloy contains both U_3Si and U_{ss}.*

In practice it is essentially impossible to produce a perfectly homogeneous alloy at the exact stoichiometric composition of U_3Si_2 or to obtain equilibrium conditions. Therefore, the alloy can always be expected to contain two or more phases.† If the average composition is close to 7.3 wt%, local inhomogeneities may result in some regions of the as-cast alloy containing U_3Si_2 and USi and other regions containing U_3Si_2 and U_{ss}. If the alloy is then heat treated, the U_{ss} will be converted to U_3Si.

The practice at ANL has been to produce alloys slightly to the Si-rich side of U_3Si_2, typically 7.5 wt% Si, in order to minimize the possibility of the alloy containing measurable quantities of either U_{ss} or U_3Si. The U_3Si_2 irradiation tests discussed in this report have been obtained for fuels with Si contents ranging from ~7.2 to ~7.7 wt%. Some of the fuel was heat treated and some was used in the as-cast condition. The maximum amounts of secondary phases estimated to be present were 2 to 3 vol% of U_{ss}, 10 vol% of U_3Si, or 15 vol% of USi.

In this report and in other literature discussing uranium silicide-aluminum dispersion fuels, the convention is to use the name of the dominant phase for those alloys with average composition near that of the dominant phase. It must be remembered, however, that other minor phases will also be present and may contribute to the macroscopic behavior of the fuel.

2.2 Selected Physical and Mechanical Properties

Both U_3Si_2 and USi are brittle while U_3Si is tough and relatively soft. The measured hardness of U_3Si_2 was 742 DPH, compared to 265 DPH for U_3Si.[7]

---

*At its experimentally determined composition, 3.9 wt% Si, U_3Si actually contains 1.03 atoms of Si for every three atoms of U.

†The presence of impurities, which are not being considered here, complicates the situation further, since they may lead to the existence of still other phases.

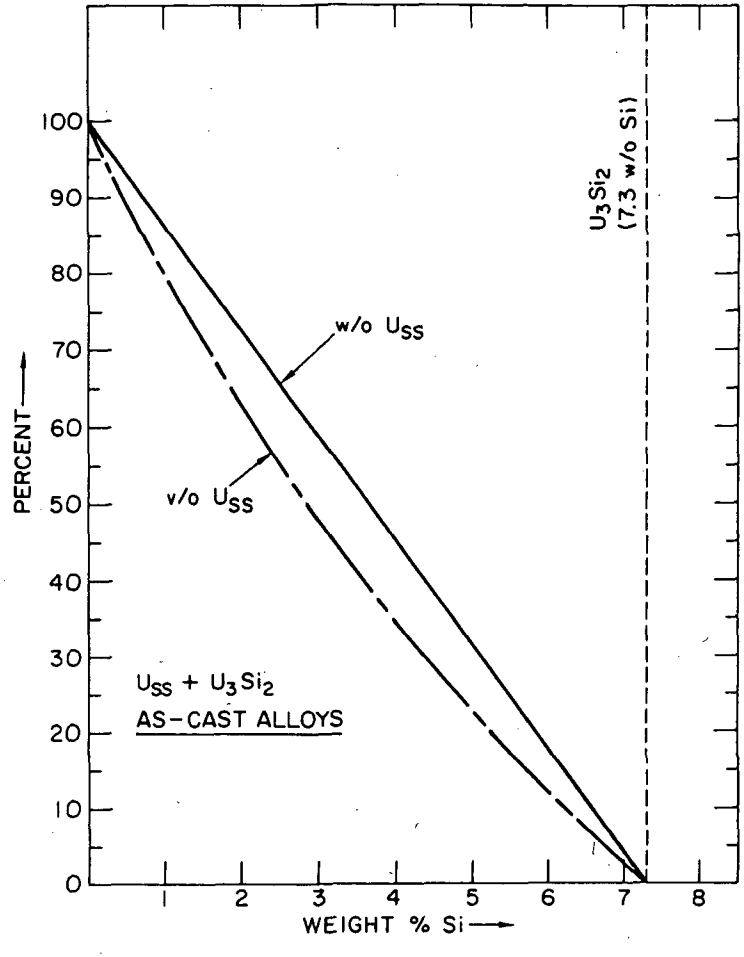

Fig. 3. Weight % (w/o) and Volume % (v/o) of Uranium Solid Solution (U_{SS}) vs. Weight % Si for As-Cast Alloys.

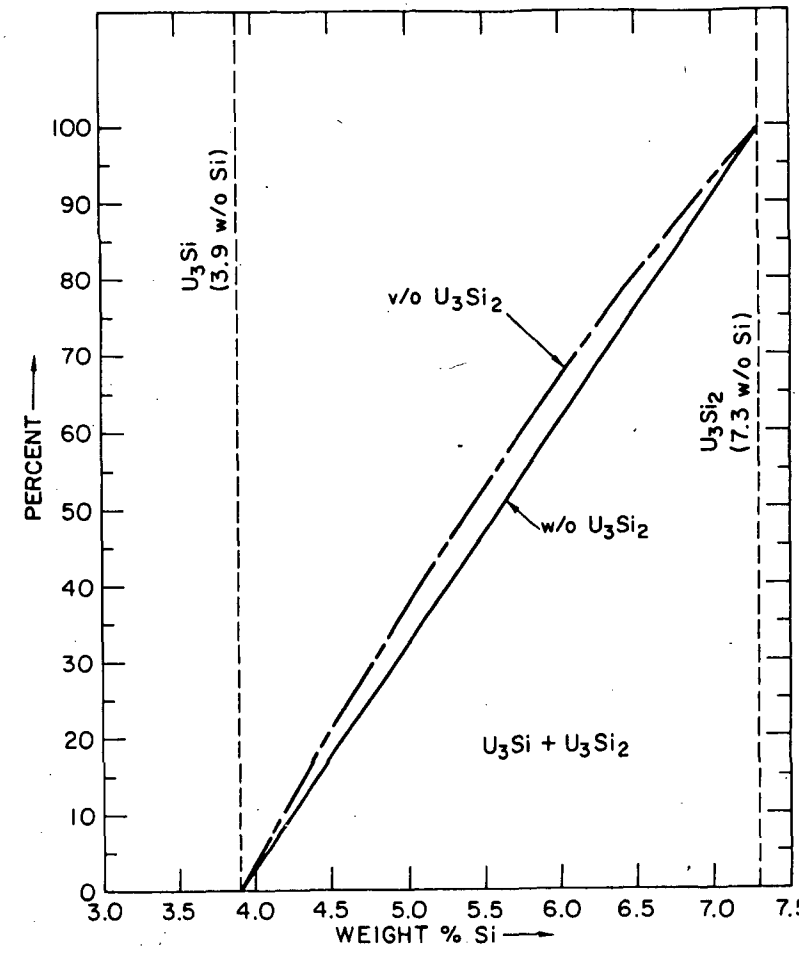

Fig. 4. Weight % (w/o) and Volume % (v/o) of U_3Si_2 vs. Weight % Si for Alloys at Equilibrium and Temperature <925°C.

The average thermal expansion coefficients of U_3Si_2 and U_3Si over the range 20 to 600°C are 15.2×10^{-6} and 15.8×10^{-6} per °C, respectively.[8]

A least squares quadratic fit of measured density vs. Si content for a series of depleted U-Si alloys with composition ranging from 4.0 to 7.5 wt% Si[7] and for USi[9] yields 12.2 and 15.4 Mg/m^3 for the densities of stoichiometric U_3Si_2 and U_3Si, respectively. For the fit the density of (depleted) USi was taken to be 10.86 Mg/m^3.[9] These densities are reduced by a negligible 0.2% for 20%-enriched uranium and by 1.1% for 93%-enriched uranium.

Both U_3Si_2 and U_3Si have a thermal conductivity of ~15 W/m•K.[8] Plots of specific heat data for stoichiometric U_3Si and for a U-Si alloy at 6.1 wt% Si are found in Ref. 10. From these data the specific heats of U_3Si_2 and U_3Si as a function of temperature (T, °C) have been derived:

$$C_p(U_3Si_2) = 199 + 0.104T \quad J/kg•K \tag{1}$$

$$C_p(U_3Si) = 171 + 0.019T \quad J/kg•K. \tag{2}$$

3. FUEL PLATE FABRICATION

3.1 Procedures

The procedures which have been used in fabricating U_3Si_2 fuel plates for irradiation tests are very similar to those already in use for UAl_x fuel. The procedures used at ANL to fabricate miniature fuel plates (miniplates) for irradiation testing are discussed in Ref. 11. Each of the commercial fabricators participating with the RERTR Program in the development and testing of U_3Si_2 fuel was encouraged to use its standard fabrication techniques and materials as much as was possible. A very brief general discussion of fabrication techniques follows.*

3.1.1 Fuel Powder

The uranium silicide alloys used in all of the irradiation tests were produced by melting uranium metal and elemental silicon in proper proportions in an arc furnace. The ingots were flipped and remelted from three to six times to produce a homogeneous material. Induction melting can also be used.

As discussed in Section 2.1, heat treatment (72 h at 800°C) is necessary only in those cases in which U_3Si is to be one of the end phases. In the

*A full set of procedures followed at ANL to produce miniplates is available on request from the authors.

early development work at ANL and, consequently, for the first U_3Si_2 ORR test elements produced by NUKEM* and CERCA,† the U_3Si_2 ingots were heat treated. The primary concern was that there be no U_{ss} present in the fuel plates. In later work, it was decided that heat treatment of U_3Si_2 ingots served no practical purpose, and, since it would add cost to commercial fabrication, the heat treatment step was eliminated. Hence, the fuel for all but the first four miniplates fabricated at ANL and for the ORR test elements produced by B&W** was not heat treated.

Both U_3Si_2 and USi are brittle and easily reduced to powder. In fact, the biggest concern is not to reduce the particle size too much. For the small volumes of powder needed at ANL, the U_3Si_2 was comminuted by hand using a steel mortar and pestle. Jaw crushers and/or hammer mills or ball mills were used by the commercial fabricators. Particle sizes ranged from <40 or <44 μm (fines), depending on whether metric or U.S. standard sieves were used, to 150 μm. The amount of fines in the irradiation test specimens ranged from 15 to 40 wt%. It should be noted that because of the brittle nature of U_3Si_2 and because of the high volume loading of fuel in high-density fuels, many of the larger fuel particles are broken during rolling, effectively increasing the number of fines. Uranium silicide is pyrophoric, and care must be taken when working with the powder in air. All fabricators conducted comminution in a glovebox with a neutral (N_2 or Ar) atmosphere. Average compositions and impurities of U_3Si_2 powders used to fabricate miniature plates and full-sized plates for irradiation testing are listed in Table I.

3.1.2 Fuel Plates

Fabrication of fuel plates followed the same procedures which had been established for UAl_x and U_3O_8 dispersion fuels. Fuel powder and aluminum powder were mixed in the desired proportions and formed under pressure into a powder-metallurgical compact. The compact was placed in the cavity of a "picture" frame, and cover plates to form the top and bottom cladding were welded in place to form a rolling billet. The billets were first hot rolled and then cold rolled to produce a plate of proper thickness. After hot rolling, a one-hour anneal at approximately the rolling temperature was conducted to test for the generation of blisters, indicating faulty bonding

*NUKEM GmbH, Hanau, Fed. Rep. of Germany.

†Compagnie pour l'Etude et la Réalisation de Combustibles Atomiques, Romans-sur-Isere, France.

**Babcock and Wilcox Company, Lynchburg, Virginia, U.S.A.

Table I. Reported Average U_3Si_2 Powder Compositions and Impurities

		Fabricator		
Major Constituent, wt%	ANL	B&W	CERCA	NUKEM
U	92.3	91.8 (91.2-92.3)	92.1	---
Si	7.5	7.4 (7.2- 7.7)	---	7.3
Impurity, ppm				
Al	26	4	---	400
B	---	5	<10	0.9
C	270	607	337	400
Cd	---	<0.5	<10	<5
Co	---	---	---	<5
Cu	---	7	---	96
Fe	96	6	---	550
H	6	---	13	---
Li	---	---	<5	<5
N	90	---	1672	---
Ni	---	5	---	---
O	429	806	1290	---
Zn	---	<2	---	<10

between cover and frame or between cover and fuel meat. Following shearing or machining to final size, the homogeneity of the uranium in the fuel meat was checked, either by real-time x-ray attenuation scanning or by densitometry of an x-radiograph. Full-sized plates for fuel elements were also inspected ultrasonically for areas of nonbond.

3.2 Special Considerations for High-Density U_3Si_2 Dispersion Fuel

Most of the fuel plates fabricated for irradiation testing contained between 40 and 50 vol% of fuel in the fuel meat, considerably in excess of the loadings of HEU dispersion fuels. Accordingly, special consideration must be given to certain fabrication procedures and/or specifications in order to achieve cost-effective yields of acceptable plates. The most important of these are briefly discussed below.

3.2.1 Dogbone

As the volume of fuel in the core increases, the core gets stronger. When the core is stronger than the frame and covers, the rolling process leaves the ends of the core thicker than the middle. A longitudinal cross section of the long, narrow fuel core with thickened ends resembles a bone, hence the name. A dogbone has two undesirable consequences: reduced cladding thickness and increased areal uranium density (the amount of uranium beneath a unit area of plate surface). The latter may result in excessively high surface heat fluxes during irradiation and be cause for rejection of the plate.

Two methods have been employed to reduce or eliminate "dogboning." If allowed by the specifications, a stronger aluminum alloy can be used for the frame and, possibly, the covers to more nearly match the strength of the fuel core. Of course, it is the strength at the rolling temperature (425 to 500°C) which is important. If the strength of the fuel core still exceeds the strength of available aluminum alloys, the ends of the compact can be tapered to compensate for the thickening at the ends of the rolled fuel core. Both methods have been successfully employed in producing high-density U_3Si_2 fuel plates for irradiation testing.

3.2.2 Minimum Cladding Thickness

As the volume loading of fuel particles increases so does the probability that fuel particles will come in contact with one another during rolling and that some will be projected into the cladding. Since the particle distribution in a dispersion fuel core is random, one cannot predict the location and depth of the penetrating particles.

Requirements for minimum cladding thickness in most specifications for HEU fuel plates date from the time of alloy cores. Once a proper set of rolling parameters had been determined for a fuel plate with an alloy core, the process was very repeatable. Core and cladding thickness could be reliably determined by examining a few metallographic sections of a few fuel plates. Unless a sophisticated and expensive device which can nondestructively measure the cladding thickness over single fuel particles is available, it is impossible to determine the actual minimum cladding thickness of a dispersion fuel plate. A statistical basis can be established for estimating minimum cladding thickness from the distribution of measured minima observed in metallographic sections of typical fuel plates.[12] Such a basis can be used to set acceptance criteria for the number of particles observed to penetrate to within a given distance of the cladding surface. One must always accept, however, the possibility that the cladding over some particles may be thinner than the stated minimum.

If a dogbone exists, there is a high probability that the point of minimum cladding exists in the dogbone region. Therefore, reducing the dogbone should increase the minimum cladding thickness. A reduction in the maximum allowed fuel particle size should decrease the penetration distance into the cladding, thereby increasing the minimum cladding thickness.

The minimum allowable cladding thickness for miniplates irradiated in the ORR was 0.20 mm. The minimum cladding thickness for full-sized fuel plates for use in test fuel elements was specified to be 0.25 mm; however, in some instances fuel plates were accepted from a batch exhibiting slightly smaller minima. No detrimental effects attributable to thin cladding were observed during testing.

3.2.3 Stray Fuel Particles

Another consequence of increased fuel loading is an increased number of fuel particles at the surface of the compact. Some of these exposed particles can be dislodged during assembly of the rolling billet or during rolling and deposited between the frame and covers--regions of the fuel plate which are supposed to be fuel free. The occurrence of stray fuel particles can be detected by examination of properly exposed x-radiographs, where the stray particles are seen as "white spots." Stray fuel particles are sources of both heat and fission products during irradiation. Unless the concentration of fuel particles is large, however, heat generation is small and of no practical consequence. Hence, the main concern is that the fuel particles not be in locations where they might become exposed to the coolant.

The occurrence of stray fuel particles can be minimized by use of adequate compacting pressure to lock most surface particles into the compact and by careful assembly of the rolling billet. NUKEM reports that the problem of stray particles can be completely eliminated by coating the compact with a thin layer of aluminum.[13,14]

Many full-sized fuel plates which should have been rejected according to the specifications were accepted on a case-by-case basis for the irradiation test elements. In some cases stray particles very near the edges or ends of a fuel plate were removed by filing.

3.2.4 Surface Oxidation of Compact

At temperatures above 177°C U_3Si_2 reacts readily with oxygen.[15-17] Since hot rolling temperatures range between 425 and 500°C, substantial oxidation of fuel particles at the surface of the compact may occur if adequate precautions are not taken to prevent air from freely entering the rolling billet during the initial heating. Recent evidence from postirradiation examinations indicates that blistering during a postirradiation anneal initiates at the sites of oxidized fuel.

4. PROPERTIES OF UNIRRADIATED U_3Si_2 DISPERSION FUEL

4.1 Fuel Meat Porosity

Porosity remaining after fabrication of dispersion fuel meat provides space to accommodate the initial swelling of the fuel particles under irradiation. The amount of as-fabricated porosity increases significantly as the volume loading of fuel increases because it becomes more difficult for the matrix aluminum to flow completely around all fuel particles, especially those in contact with one another.[18] Data obtained at ANL from measurements on U_3Si_2 miniplates are plotted in Fig. 5. These data are fit well by the cubic function

$$V_P = 0.072V_F - 0.275V_F^2 + 1.32V_F^3, \qquad (3)$$

where V_P and V_F are volume fractions of porosity and fuel in the meat, respectively.

Other parameters also have an important effect on the amount of as-fabricated porosity, although individual contributions have not been isolated. For example, consider the nominally identical U_3Si_2 elements fabricated by B&W, CERCA, and NUKEM for irradiation testing in the ORR. The porosity content of the fuel cores produced by a given fabricator remained virtually

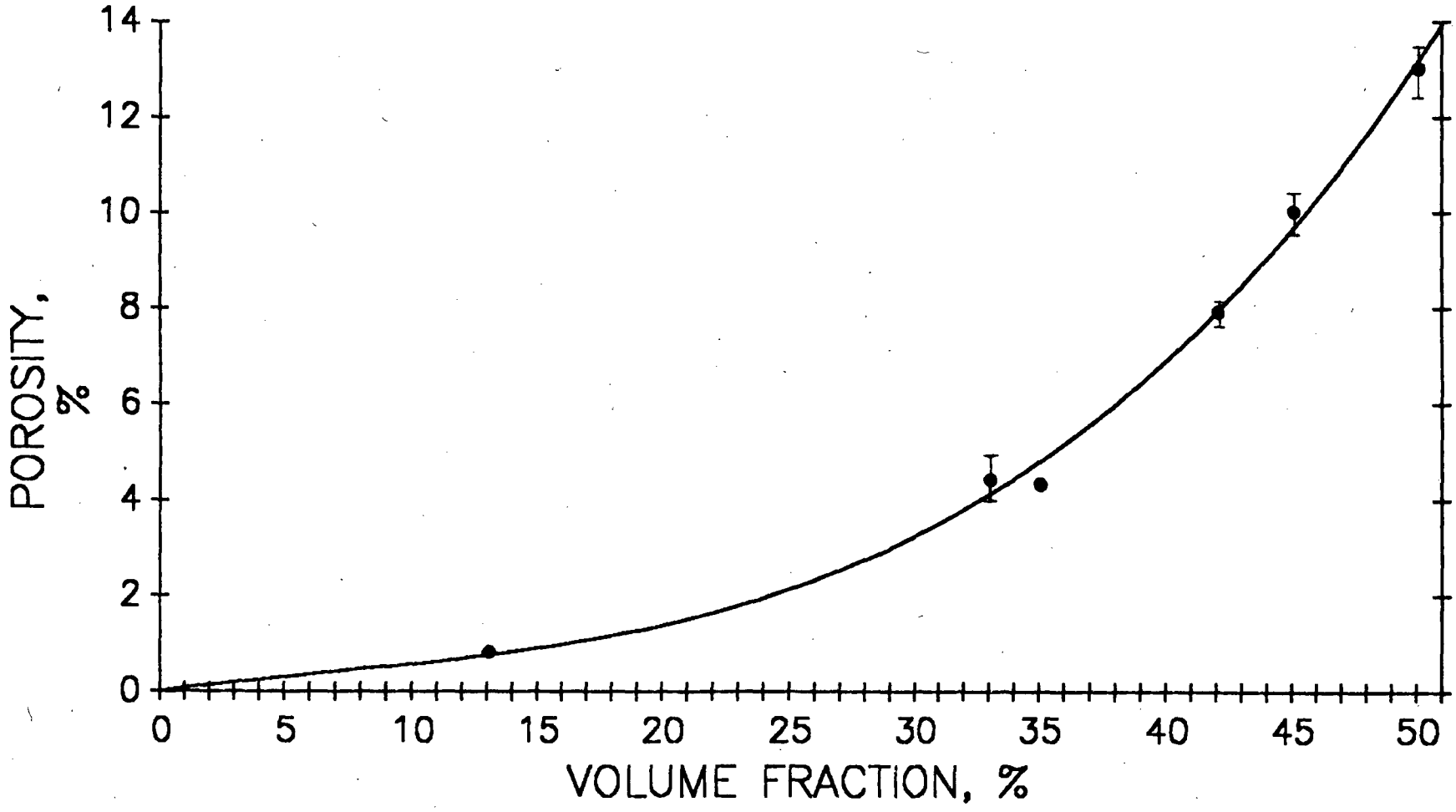

Fig. 5. Percent Porosity as a Function of the Volume Percent Fuel.

constant, but there was a variation from fabricator to fabricator: 4 vol% for CERCA, 7 to 8 vol% for NUKEM, and 9 to 10 vol% for B&W. Differences in material or fabrication parameters which might have contributed to the different amounts of porosity include: (1) strength of the aluminum alloy used for frames and covers--the CERCA alloy was by far the strongest while the B&W alloy was the weakest; (2) the rolling temperature--425°C for CERCA and NUKEM and ~500°C for B&W; (3) the amount of fines in the U_3Si_2 powder--40 wt% for CERCA and 17-18 wt% for NUKEM and B&W; (4) the rolling schedule, especially the amount of cold reduction; and (5) the relationship between the size of the compact and the size of the cavity in the frame.

Differences in the as-fabricated porosity in fuel plates will manifest themselves as differences in swelling of the plates during irradiation. Since much less constraint to swelling is offered in the thickness direction than in the length and width directions of plates, effectively all of the swelling results in a thickness increase. Early in the irradiation the plates will actually become thinner as irradiation-enhanced sintering occurs. Net swelling begins when the fuel particles have swelled enough to fill the pores. Under the same irradiation conditions, a difference of 6 vol% in as-fabricated porosity translates to a difference of 6% of the meat thickness in the final thickness of the plate. This value, ~30 to 45 μm for typical fuel meat thicknesses, is much less than the tolerances normally allowed for cooling channel thickness. Therefore, it is not expected that the normal variation of as-fabricated porosity among fabricators will have any safety implications.

4.2 Heat Capacity

The heat capacity of the fuel meat is the sum of the heat capacities of the fuel and the aluminum of the matrix. The heat capacity of U_3Si_2 is given by Eq. (1) and the heat capacity of aluminum as a function of its temperature (T, °C) is given by[19]

$$C_p(Al) = 892 + 0.46T \quad J/kg \cdot K. \tag{4}$$

The volumetric heat capacity of the fuel meat with LEU is

$$C_p(U_3Si_2\text{-}Al) = 0.0122V_F C_p(U_3Si_2) + 0.0027(1 - V_F - V_P)C_p(Al) \ MJ/m^3 \cdot K. \tag{5}$$

Using the pore volume given by Eq. (3), it is seen that the heat capacity of the fuel meat at room temperature decreases from 2.44 to 2.13 $MJ/m^3 \cdot K$ as the fuel volume fraction increases from 0 to 0.5. The decrease is primarily a result of the increase in porosity as the fuel volume fraction increases, since the volumetric heat capacities of aluminum and U_3Si_2 are very similar.

4.3 Thermal Conductivity

Values of thermal conductivities of the fuel meat in unirradiated U_3Si_2 dispersion fuel plates, measured at 60°C, are listed in Table II and plotted in Fig. 6.[20] Most of the samples were cut from miniature fuel plates produced at ANL for use in out-of-pile studies. Two samples came from a full-sized plate from a lot of plates fabricated by CERCA for the ORR test elements. The porosities of these miniature plates follow the trend discussed in Section 4.1 but are somewhat larger, owing, presumably, to the different shape of the fuel zone than in the miniplates fabricated for irradiation testing (cylindrical rather than rectangular compacts were used).

It is seen that the thermal conductivity decreases rapidly as the volume fraction of fuel plus porosity increases (and the volume fraction of matrix aluminum decreases), owing to the ~14 times larger thermal conductivity of aluminum than U_3Si_2. For very low volume loadings of fuel, it would be expected that the thermal conductivity of the dispersion would be proportional to the amount of aluminum present, since the aluminum matrix should provide a continuous thermal path. Indeed, this is the case for sample CS148. At higher volume fractions of fuel plus void, however, the aluminum ceases to be the continuous phase, and the thermal conductivity decreases more rapidly than does the volume fraction of aluminum. At very high loadings the aluminum ceases to play a significant role, and the thermal conductivity approaches that of the fuel. It may even become lower than that of the fuel alone because of poor thermal contact between fuel particles. The microstructure of the meat, specifically the distribution of the voids, can significantly affect the thermal conductivity. It appears that thin planar regions in which voids are associated with fractured fuel particles are responsible for the large difference in thermal conductivity exhibited by the CERCA samples and sample CS143. The larger void content of the CS samples than measured in the miniplates fabricated for irradiation testing or in full-sized plates most likely indicates the presence of more of such planar void regions. Therefore, it is believed that the thermal conductivity curve in Fig. 6 represents essentially a lower limit for the thermal conductivities of full-sized fuel plates.

The data for U_3Si_2 dispersions are virtually indistinguishable from those obtained in the same series of measurements for U_3Si dispersions. They are also quite similar to data obtained in other measurements of thermal conductivities of UAl_x dispersions[21] and U_3O_8 dispersions.[22] The U_3O_8 data fall somewhat below the U_3Si_2 data, possibly because the friable nature of U_3O_8 leads to the formation of more planar void regions than are present in U_3Si_2 fuel.

Table II. Thermal Conductivities of U_3Si_2-Aluminum Dispersions

Sample Identification	Fraction of Fuel -325M Mesh, wt%	Fuel Volume[1] Fraction, %	Porosity,[2] vol%	Thermal Conductivity of Dispersion at 60°C, W/m•K	Temperature Coefficient, W/m•K[2]
CS148	15	13.7	1.9	181	0.148
CS106	15	32.3	6.0	78	0.029
CS140	0	39.4	9.2	40	0.014
CS141	15	37.0	9.3	48	5×10^{-4}
CS142	25	39.1	9.5	40	0.017
CERCA #1	41.5	46.4	4.0	59	0.161
CERCA #2	41.5	46.4	4.0	59	0.076
CS143	15	46.4	15.4	13.9	0.010

[1]Determined on the thermal conductivity specimens using a radiographic technique.
[2]Average value for the roll-bonded fuel plate.

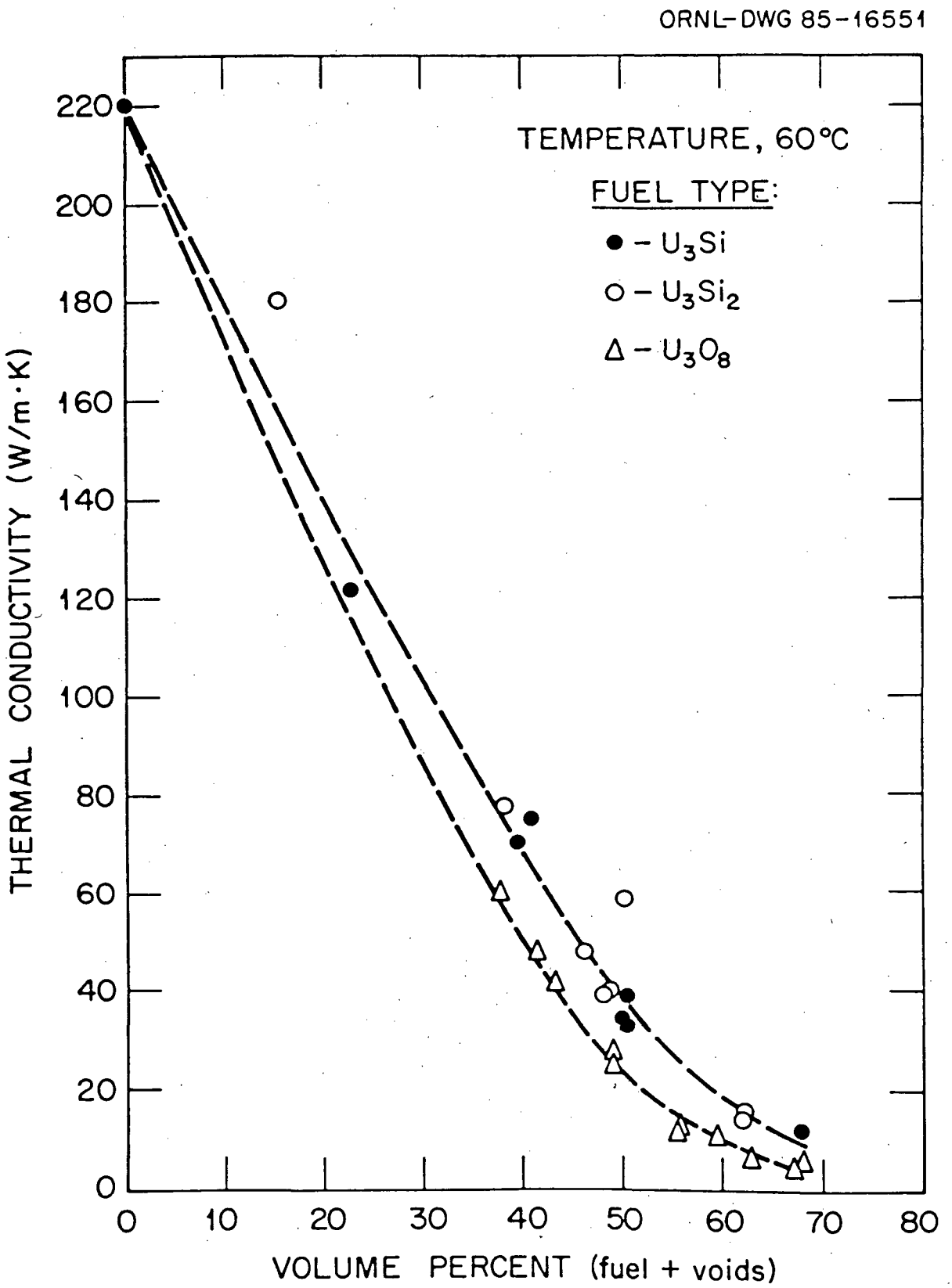

Fig. 6. Thermal Conductivities of Uranium Silicide- and U_3O_8-Aluminum Dispersion Fuels as a Function of Volume Fraction of Fuel Plus Voids (Porosity).

Even though this section properly deals with unirradiated fuel, some considerations will be set forth on how the thermal conductivity might change as the fuel is irradiated (no known data exist). Little change is expected either for very low or for very high fuel volume fractions. In the former case the thermal conductivity is essentially proportional to the amount of aluminum present in the matrix, which is effectively unchanged by the swelling fuel particles. In the latter case the thermal conductivity is much lower, approximately that of the fuel and would not be expected to change appreciably. For intermediate loadings, however, the thermal conductivity is quite sensitive to the amount of aluminum in the matrix and to the microstructure of the fuel meat. During the time that swelling fuel particles cause a reduction in the amount of as-fabricated porosity, the thermal conductivity might increase slightly, especially if planar void regions are eliminated. When the porosity has been eliminated, usually after medium burnup, irradiation-enhanced creep of the matrix aluminum toward the cladding is induced by pressure from swelling fuel particles, reducing the amount of aluminum in the matrix. This should result in a gradual decrease in thermal conductivity. As fission gas bubbles form in the fuel particles at high burnup, the conductivity might be even further reduced.

4.4 Compatibility of U_3Si_2 and Aluminum

Knowledge of the degree of compatibility of the fuel and cladding is important for any fuel system. Above about 600°C U_3Si_2 reacts rather rapidly with Al, as discussed in Section 4.5. At or below rolling temperatures (425 to 500°C), this reaction is very slow. No reaction zone surrounding the U_3Si_2 particles can be seen in optical micrographs of unirradiated fuel. Phase equilibria studies[9] indicate that the reaction product is $U(Al,Si)_3$, a phase based on UAl_3 wherein some of the Al atoms have been replaced by Si atoms in the crystal lattice.

Long-term thermal anneals of U_3Si_2 dispersions have been performed to study the compatibility of U_3Si_2 and Al.[15,16,23] In the work at ANL miniature fuel plates were fabricated by standard procedures using cylindrical compacts. Plates were annealed at 400 ± 5°C for incremental times up to 1981 hours. The plates were periodically withdrawn from the furnace, measured for volume increase, and returned to the furnace for additional annealing. The results for both 32- and 45-vol% fuel loadings are shown in Fig. 7. For comparison, data for U_3Si fuel are also shown.

The growth of uranium silicide dispersions during thermal anneals appears to be a two-step process:[23] First, the uranium silicide reacts with the aluminum of the matrix and cladding to form a less-dense product, $U(Al,Si)_3$. The early stages of swelling are due to this phenomenon. Then, as a result of

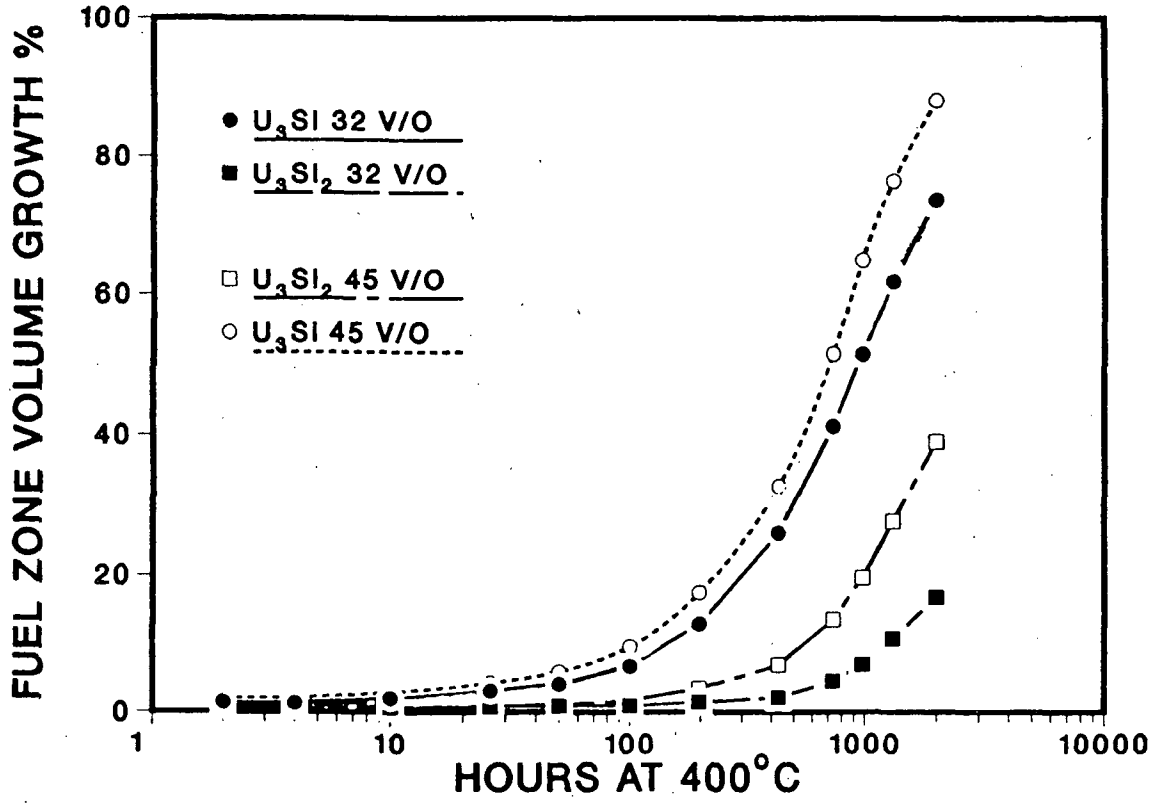

Fig. 7. Volume Percent Growth in the Fuel Zone for Uranium Silicide Fuels at 400°C.

the reaction, hydrogen, contained as an impurity in the reacting materials, is released as a gas into the pores of the meat. The strength of the fuel meat decreases as the reaction proceeds, and the pores become connected. When the internal pressure of the hydrogen exceeds the external pressure on the cladding, the cladding begins to creep and, finally, the plate "pillows".

The reaction noted above is diffusion controlled and, therefore, exponentially dependent on temperature. The rates of reaction at temperatures of 300°C or less have been demonstrated to be very low.[11] Since, as will be discussed later, there appears to be little reaction between U_3Si_2 and Al during irradiation, the mechanism of hydrogen release discussed here should not affect the swelling of U_3Si_2 dispersion fuel during irradiation at temperatures below 300°C. All evidence from irradiated plates supports this conclusion.

4.5 Exothermic Energy Releases

Early work on uranium silicide-aluminum dispersions suggested that a rapid exothermic reaction between uranium silicide and aluminum occurs at ~620°C.[24] Measurements, using differential thermal analysis (DTA) techniques, have been performed at ANL to determine the temperature regime and enthalpies of these reactions.[25] Results of similar measurements have also been reported by others.[17,26] Samples for the measurements were punched from miniature fuel plates fabricated using cylindrical compacts. Results of the DTA measurements are given in Table III, which includes values for U_3Si and U_3O_8[27] for comparison. Typical thermograms are shown in Fig. 8. The large negative ΔT is the aluminum melting endotherm. This endotherm occurs over an extended temperature range because the solidus point of the Al 6061 cladding is 582°C and the liquidus point is 652°C. The exothermic uranium silicide-aluminum reaction results in the reversal of the ΔT trace at ~640°C. Upon cooling and reheating, very little additional reaction was detected. The net effect for fuel loadings up to ~5 Mg U/m^3 was always an endotherm. For samples at 45 vol% U_3Si in the fuel zone (~6.6 Mg U/m^3), the net effect for the first heating was a very slight exotherm. No event (either exothermic or endothermic) was detected between temperatures of 660 and 1300°C.

Complete reaction of all fuel with aluminum should result in the release of the same amount of energy per unit mass of fuel for each sample tested. Insensitivity of the DTA technique to slow energy releases may be responsible for the different values determined for the different fuel loadings. The data indicated that sufficient aluminum was available in the matrix to complete the reaction in the lower-loaded U_3Si_2 samples but not in the higher-loaded U_3Si_2 samples or in the U_3Si samples. Since the reaction is diffusion controlled and since the cladding aluminum had to move larger distances to participate in

Table III. Energy Released from the Exothermic Reaction of Uranium Silicide or U_3O_8 with Aluminum in Fuel Plates

Fuel Type	Volume Loading, vol%	Reaction Energy, kJ/kg	Onset Temperature, °C
U_3Si_2	32	349 ± 44	590
U_3Si_2	45	304 ± 18	590
U_3Si	32	486 ± 54	580
U_3Si	45	379 ± 13	590
U_3O_8	44[a]	243 ± 126	890
U_3O_8	44[a]	71 ± 18	900

[a]Different cladding-to-meat-thickness ratios. Data from Ref. 27.

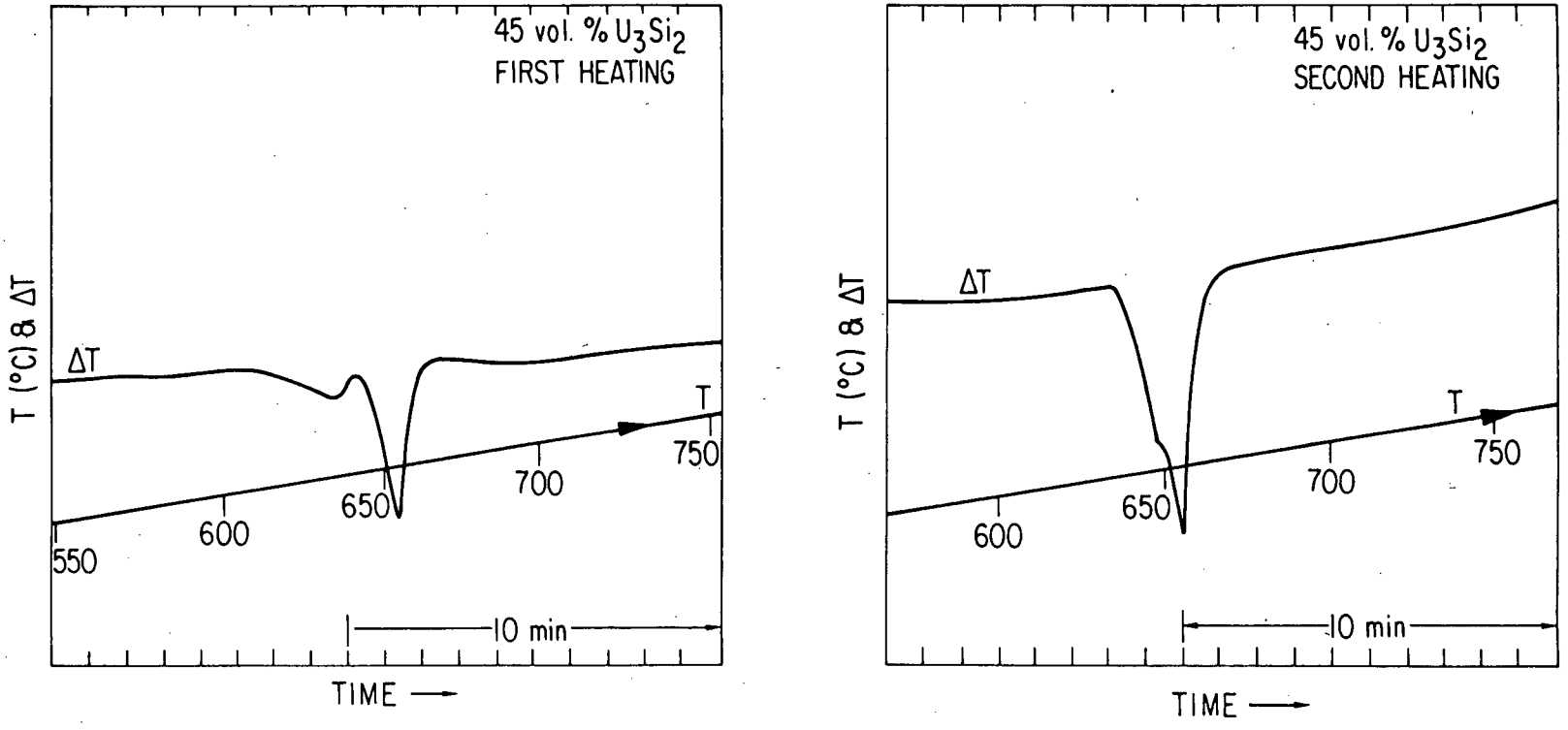

Fig. 8. Thermograms Obtained During Differential Thermal Analysis of U_3Si_2-Al Fuel Samples.

the reaction, it is possible that part of the reaction occurred too slowly to be detected by the DTA technique. If such were the case, the true reaction energy would have to be determined by extrapolation of the measured data to low volume loadings of fuel. For the U_3Si_2 fuel the extrapolated value should not be very much larger than the value for the 32-vol% case since sufficient aluminum was available in the matrix to complete the reaction.

As evident in Fig. 8, the reaction in dispersion fuel meat occurs over a period of minutes. A similar exothermic reaction in U_3O_8 dispersion fuel plates has been referred as a "thermite" reaction because of large reported energy releases.[28] More recent work[27] has shown that that reaction occurs much more slowly in fuel plates, consistent with the results for uranium silicide dispersion fuel plates. The relative slowness of the exothermic reaction means that the amount of energy supplied by the reaction will be small compared to the energy supplied by the heat source responsible for raising the temperature of the fuel plate to the reaction onset temperature. For example, an LEU fuel element containing 240 g of ^{235}U will contain ~1.3 kg of U_3Si_2, and ~450 kJ would be released by the reaction of all of the fuel in the element. That same element in a typical 2-MW reactor would produce between 50 and 100 kW, taking only 4.5 to 9 s to produce 450 kJ. After shutdown, decay heat would typically be of the order of 1% of the operating power, requiring 450 to 900 s to produce 450 kJ. Therefore, whether the initiating event were to be a flow blockage at full power or a loss of coolant, it is seen that over the course of the event and its aftermath, the contribution of the exothermic reaction is relatively small. It should also be noted that significant energy release from the exothermic reaction occurs only at temperatures above the solidus temperatures of commonly used cladding alloys; therefore, the exothermic reaction itself will not cause loss of cladding integrity.

4.6 Corrosion Behavior

A test of the corrosion resistance of U_3Si_2 dispersion fuel has been performed[11] by drilling a 3.25-mm (0.128-in.)-diam hole completely through the cladding and fuel meat of a miniplate and boiling the plate in distilled water for 168 h. The plate was withdrawn periodically during the test for weighing and examination. No radioactivity was detected in the water, nor was loose radioactivity present on the plate after the test. The plate darkened during the test, but no other changes were noted. It is concluded that the solubility in water at temperatures up to 100°C of U_3Si_2 dispersed in aluminum is negligibly small.

It should be noted that the cladding alloys used in all of the fuel tests and anticipated to be used in production fuel elements are the same alloys

which have been used in research and test reactors for many years. The corrosion behavior of these alloys is well established.

5. IRRADIATION BEHAVIOR OF U_3Si_2 DISPERSION FUEL

5.1 Irradiation Testing

The irradiation testing of fuels being developed by the RERTR Program has followed a two-stage process. First, miniplates were irradiated to determine the basic irradiation behavior of the candidate fuel. Following the miniplate irradiations, full-sized elements of a successful candidate fuel were irradiated to confirm the expected behavior of the fuel when fabricated and irradiated under typical conditions. In many instances fabrication of the elements began before complete results were available from the miniplates, in order to compress the development and testing schedule. Therefore, the test element specifications did not always reflect all that was ultimately to be learned from the miniplates. As will be seen, the resulting variety of as-fabricated properties greatly increased the value of the tests.

5.1.1 Test Samples

5.1.1.1 Miniplates

The miniature fuel plates for irradiation testing were 114 mm long by 50 mm wide and either 1.27 mm or 1.52 mm thick. The fuel meat could be up to 109 mm long by 46 mm wide. The thickness of the fuel meat was a parameter in some of the tests; its maximum was limited by the 0.20-mm minimum cladding requirement. The fuel meat and plate thicknesses were typical of those anticipated to be used in reactor conversions. The width and length of the miniplates were chosen to be sufficient to provide protypical conditions with regard to constraint of the fuel meat by the cladding and frame, i.e., the fuel meat length and width were very much greater than its thickness. The miniplate specifications[29] required that the cladding of the finished miniplate be in the O-temper condition to assure uniformity of cladding constraint conditions among miniplates produced by different fabricators. As testing progressed, it was decided that cladding temper did not play a major factor in miniplate performance, and this requirement was abondoned in order to more nearly simulate the conditions of commercially produced full-sized plates.

Miniplate irradiation testing, conducted in the Oak Ridge Research Reactor (ORR), proceeded in two phases: the screening of primary candidate fuels followed by more extensive tests of those performing acceptably. In the first series of irradiations, conducted between July 1980 and June 1983, four

U_3Si_2 and 18 U_3Si miniplates were irradiated. The second series of irradiations, conducted between March 1984 and January 1987, included ten USi, 35 U_3Si_2, and 34 U_3Si miniplates. Some plates contained fuel produced with 40%-enriched and with 93%-enriched uranium in order to establish failure thresholds and with depleted uranium in order to determine the effects of fast neutrons, as opposed to fission fragments, on the fuel. Postirradiation examinations of a number of miniplates have been completed, and the results will be discussed in Section 5.2.

5.1.1.2 Full-Sized Elements

Six full-sized U_3Si_2 fuel elements irradiated in the ORR[30] and one irradiated in the SILOE reactor at the Centre d'Etudes Nucléaires de Grenoble (CEN-G) in France in cooperation with the French CEA[31] have provided irradiation performance data under typical reactor conditions. Prior to testing a full element, CEN-G irradiated four full-sized plates, in lieu of miniplates, in SILOE. They have also irradiated four full-sized plates and a full-sized element containing U_3Si fuel.* Many more U_3Si_2 elements have been irradiated as part of a whole-core demonstration in the ORR (see Section 5.3). The ORR elements were fabricated by B&W, CERCA, and NUKEM, and the SILOE elements and plates were fabricated by CERCA. Each fabricator used its normal materials and fabrication practices, with minor modifications necessitated by the new fuel type.

The fuel elements for the ORR and SILOE were essentially identical geometrically to their standard HEU elements. The SILOE elements were assembled in such a manner that two plates were removable for interim thickness measurements. Specifications for the elements followed very closely their HEU counterparts. The nominal uranium loading in the fuel meat of the ORR elements was 4.75 Mg/m^3; the as-fabricated loadings ranged between 4.6 and 5.2 Mg/m^3. The SILOE element contained 5.2 Mg U/m^3. The ORR elements contained 19 curved plates, and the SILOE element contained 23 flat plates.

---

*Tests of U_3Si_2 elements are underway in the R2 reactor at Studsvik, Sweden, and U_3Si_2 elements are currently being fabricated for tests in the High Flux Reactor at Petten, The Netherlands. These irradiations will provide data on fuel elements containing plates with 0.76-mm-thick fuel meat and, consequently, with much higher total ^{235}U contents. These tests are not considered necessary for general qualification of U_3Si_2 fuel, however. Additional U_3Si_2 elements have been irradiated in other reactors (DR 3 in Denmark, FRG-2 in Germany, and SAPHIR in Switzerland) without the involvement of the RERTR Program, as part of the conversion studies for those reactors.

5.1.2 Reactors and Test Conditions

As stated in the previous section, irradiations of U_3Si_2 miniplates, full-sized plates, and full-sized elements have been carried out in two medium-power materials testing reactors, the ORR and SILOE. The ORR and SILOE normally operate at powers of 30 and 35 MW, respectively. Power densities in the fuel meat are similar in these reactors. In the ORR the pH and electrical resistivity of the primary coolant ranged between 5.0 and 6.3 and 0.7×10^4 and 2.5×10^4 $\Omega \cdot m$, respectively, during the irradiations.

The miniature fuel plates were irradiated in five stacked modules assembled in an irradiation device which could be loaded into any of the normal fuel positions of the ORR.[29] When assembled, the irradiation device resembled an ORR element with narrow fuel plates. The miniplates were irradiated in relatively high-flux positions in the core. At the end of each irradiation cycle, typically two to three weeks in length, channel gap thicknesses were measured with an ultrasonic probe to detect the onset of rapid swelling of any plate. During the course of its irradiation, each miniplate experienced many thermal cycles owing to normal startups and shutdowns and power setbacks required by other experiments. Fuel meat centerline temperatures are estimated to have been between 75 and 125°C during irradiation.

The ORR conditions for the full-sized elements were basically the same as for the miniplates. Although the elements were not cycled through the core in a normal pattern, they did experience irradiation in a variety of typical core positions. It is estimated that each element produced ~1.3 MW during its first cycle of irradiation, with a peak-to-average power density and heat flux factor of no more than 1.5. It is estimated that the peak fuel meat temperatures were between 110 and 130°C during the early cycles of irradiation. Average fuel meat temperatures are estimated to have been ~20 to 25°C less. The accessible channel gaps were measured at various times during the irradiation of the elements (following each cycle beyond 50% burnup). Conditions in SILOE were similar to those in the ORR.

5.2 Test Results

The miniplates and elements irradiated in the ORR were subjected to an extensive series of postirradiation examinations following suitable periods of cooling. The key examinations were thickness and volume measurements to assess the swelling of the fuel meat, metallography to assess the condition of the fuel meat, and blister threshold temperature measurements. Gamma scans were performed to provide fission density profiles and plate-to-plate fission density normalization, and uranium and plutonium isotopic analyses of selected samples were performed to provide absolute burnup information. As described

in Appendix G of Ref. 30, calculated ^{235}U fission fractions were used to convert ^{235}U fission densities to the total fission densities reported below.

5.2.1 General

The irradiations of all miniplates and elements proceeded without incident in the ORR. No indications of fission product leaks from the plates were detected. Profiles of channel gaps of the elements remained essentially unchanged during the course of the irradiations, indicating no abnormal swelling or warping of the plates. The miniplates which have been examined thus far, and for which results will be presented below, ranged in ^{235}U burnup from 39 to 96%. Most of the miniplates were irradiated to high burnups in order to establish failure thresholds. Three of the six ORR elements were irradiated to burnups in the normal range for the ORR. The other three, one from each fabricator, were irradiated to ~80% average burnup. Peak burnups in these elements were ~98%. The SILOE element had reached an average burnup of 54%, also without incident, before an extended outage interrupted its irradiation.[32] Except when specifically noted, the data discussed below are from the miniplates and the six elements irradiated in the ORR.

Visual examinations in the hot cells showed the ORR elements to be in excellent condition. No abnormal conditions were observed. Within the accuracy of the in-cell measurements, the dimensions were within the envelope of tolerances allowed for as-fabricated dimensions. In-cell coolant channel gap thickness measurements confirmed the results of the in-pool measurements. Visual examination of the plates following element disassembly revealed no evidence of blisters, excessive swelling, or any other unusual condition.

5.2.2 Fuel Meat Swelling and Microstructure

5.2.2.1 Miniplates

Fuel meat swelling data obtained from immersion density measurements on the uranium silicide miniplates which have been examined to date are summarized in Table IV. These data indicate that the swelling as a function of fission density increases from USi to U_3Si_2 to U_3Si. Data for each of the U_3Si_2 miniplates irradiated are listed in Table V. Four of these miniplates (A87, A89, A90, and A93) have now experienced an estimated 7.5% additional burnup following their initial examinations and are currently being reexamined. Thickness measurements indicate that swelling has remained stable.

A much clearer picture of the swelling behaviors of the various uranium silicides is obtained by calculating the swelling of the fuel particles themselves, assuming that the as-fabricated porosity has been completely filled.

Table IV. Summary of Swelling Data for Uranium Silicide Dispersion Fuels (From PIE of Miniature Fuel Plates)

Fuel Type	Fabricator*	Density Range, Mg/m^3 Low	Density Range, Mg/m^3 High	Enrichment	No. of Plates	Fission Density Range, $10^{27}/m^3$ Low	Fission Density Range, $10^{27}/m^3$ High	Fuel Meat Swelling Range, % $\Delta V/V_m$ Low	Fuel Meat Swelling Range, % $\Delta V/V_m$ High
USi	A	3.86		19.8	1		0.8	0.3	
USi	A	3.81	3.90	40.1	3	2.7	2.8	3.2	6.0
U_3Si_2	A	3.72	3.76	19.9	4	1.6		3.7	4.9
U_3Si_2	A	3.72	3.75	19.9	2†	1.8		6.8	7.1
U_3Si_2	A	5.10	5.20	19.8	5	1.0	2.1	0.0	3.3
U_3Si_2	A	5.60	5.67	19.8	6	2.3		0.1	2.9
U_3Si_2	A	3.94	3.95	40.1	2	1.5	2.5	0.7	11.6
U_3Si_2	A	5.13	5.18	40.1	2	1.8		1.1	2.1
U_3Si_2	A	1.66		93.0	2	1.4	2.3	4.9	11.6
U_3Si	A	4.79	4.83	19.9	5	0.7		0.1	0.8
U_3Si	A	4.77	4.81	19.9	6	2.0	2.2	8.9	11.8
U_3Si	C	5.18	5.20	19.8	2	2.2		10.3	11.4
U_3Si	A	5.65	5.72	19.9	4	1.9		0.7	7.6
U_3Si	A,C	6.10	6.33	19.8	5	2.5	2.6	20.4	38.8**
U_3Si	N	6.89	6.93	19.4	6	2.5		13.3	21.7
U_3Si	A	7.10	7.16	19.8	3	2.6		38.9**	39.1**
U_3Si	A	4.51		40.1	1	2.0		10.3	
U_3Si	A	6.23	6.40	40.1	3	2.4	2.6	9.6	39.6**
U_3Si	A	1.98		92.6	2	1.7		8.8	9.7

*Fabricators: ANL, NUKEM, CNEA.
**Indicates that plates were in various stages of breakaway swelling.
†These two plates, part of the preceding group of plates, were irradiated further following initial postirradiation examination.

Table V. U_3Si_2 Miniplate Swelling Data Summary

Plate No.*	U Dens., Mg/m^3	Fuel Vol. Fraction, %	Fuel Meat Porosity, %	^{235}U Burnup, %	Fuel Meat Fission Dens., $10^{27}/m^3$	Fuel Particle Fission Dens., $10^{27}/m^3$	Fuel Meat Swelling, vol%	Fuel Particle Swelling, vol%
A32	3.8	33.3	4.5	90	1.6	4.8	3.8	25
A34	3.8	33.4	4.3	90	1.6	4.8	4.1	25
A36	3.8	33.3	4.5	90	1.6	4.8	4.3	26
				96	1.8	5.5	7.1	35
A46	3.7	33.1	5.2	90	1.6	4.8	3.7	27
				96	1.8	5.5	6.8	36
A100	5.2	46.2	8.5	42	1.0	2.1	0.0	≤18
A85	5.0	45.4	10.3	79	1.8	4.2	1.6	26
A99	5.2	45.9	9.1	79	1.9	4.2	2.0	24
A87	5.1	45.6	9.8	85	2.1	4.6	3.3	29
A88	5.2	45.8	9.5	85	2.1	4.6	2.6	26
A89	5.6	49.8	13.4	85	2.3	4.6	0.9	29
A90	5.6	49.9	13.3	85	2.3	4.6	0.2	27
A91	5.6	49.7	13.5	85	2.3	4.6	0.1	27
A92	5.6	50.0	12.9	85	2.3	4.6	1.5	29
A93	5.6	50.0	13.0	85	2.3	4.6	0.4	26
A94	5.7	50.4	12.4	85	2.3	4.6	2.9	30
A123M	4.0	35.1	4.2	42	1.5	4.2	0.7	≤14
A124M	3.9	35.0	4.3	69	2.5	7.1	11.6	45
A125M	5.1	45.6	11.8	39	1.8	3.9	2.1	30
A126M	5.2	46.0	11.0	39	1.8	3.9	1.1	26
A121H	1.7	14.7	0.8	41	1.4	9.3	4.9	38
A122H	1.7	14.7	0.8	69	2.3	15.7	11.6	84

*All plates LEU except those with plate number ending in M (MEU) or H (HEU).

The general trends of these data and, for comparison, data for UAl_x,[33] are shown in Fig. 9. The swelling of UAl_x, USi, and U_3Si_2 fuel particles is very stable, being a linear function of the fission density to fission densities well beyond those which can be achieved in LEU fuel (2.4, 5.0, and 5.8 × 10^{27} f/m^3 in the fuel particles of UAl_x, USi, and U_3Si_2, respectively). On the other hand, U_3Si fuel particles in highly loaded fuel plates exhibit an unstable behavior, called breakaway swelling, for fission densities greater than ~4.5 × 10^{27} f/m^3 (~65% ^{235}U burnup for LEU).* The swelling rates per unit fission density of U_3Si_2 and UAl_x fuel particles are the same within the accuracy of the data. The slopes of the linear swelling curves are 4.8%, 6.0%, and 6.2% per 10^{27} f/m^3 for USi, UAl_x, and U_3Si_2, respectively. These data were derived for 40 vol% loadings of USi, 28 to 36 vol% loadings of UAl_x, and 45 to 50 vol% loadings of U_3Si_2. The UAl_x was fully enriched, and the uranium silicides were low enriched. The data of Table V indicate that the slope of the U_3Si_2 swelling curve may be marginally lower for lower fuel volume loadings. Given the fuel particle swelling rate, the fuel volume fraction, and the as-fabricated porosity, the meat swelling for a given fission density can be reliably predicted.

An example of the meat microstructure of a U_3Si_2 miniplate after >90% burnup is shown in Fig. 10. Some of the noteworthy features in this optical micrograph are the absence of fission gas bubbles and the fact that all of the as-fabricated porosity has been consumed by fuel particle swelling. Fuel-aluminum interaction was limited to a narrow zone around the U_3Si_2 particles with a thickness about equal to the range of fission product recoils in aluminum. SEM examination of fractured fuel particles reveals a gas bubble morphology typical of pure U_3Si_2, as shown in Fig. 11. The very uniform distribution of small gas bubbles that show no tendency to interlink is the reason for the stable swelling behavior of U_3Si_2.

---

*The fuel particle swelling curve for another fuel commonly used in aluminum-matrix dispersions today, U_3O_8, is quite similar to the U_3Si curve for highly loaded fuel plates. (Note that the maximum fission density achievable in low-enriched U_3O_8 is 3.6 × 10^{27} f/m^3.) Although the swelling mechanism in U_3O_8 is different than that in U_3Si,[34] the occurrence of breakaway swelling in either requires fission gas bubble growth and interlinkage across extended areas of the fuel meat. If enough aluminum matrix surrounds the fuel particles (i.e., if the fuel volume loading is low enough) to restrain the expansion of fission gas bubbles and/or to prevent bubble linkage from particle to particle, breakaway swelling does not occur. Data for such low-loaded plates lie well to the right of the U_3Si curve shown in Fig. 9.

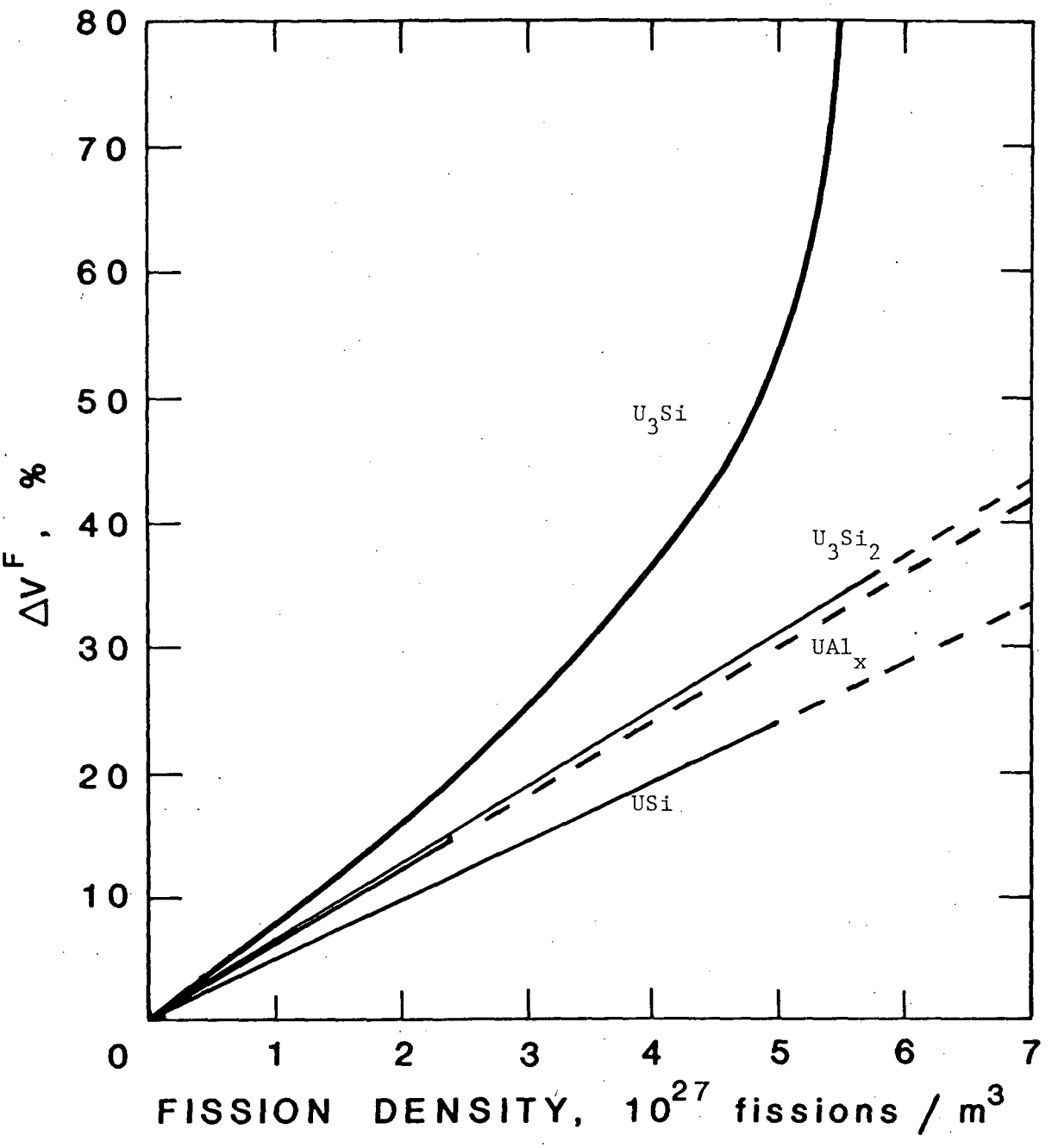

Fig. 9. Swelling of Uranium Silicide and UAl_x Fuel Particles vs. Fission Density in the Particle. Dashed Lines Indicate Fission Densities Not Attainable in LEU Fuel.

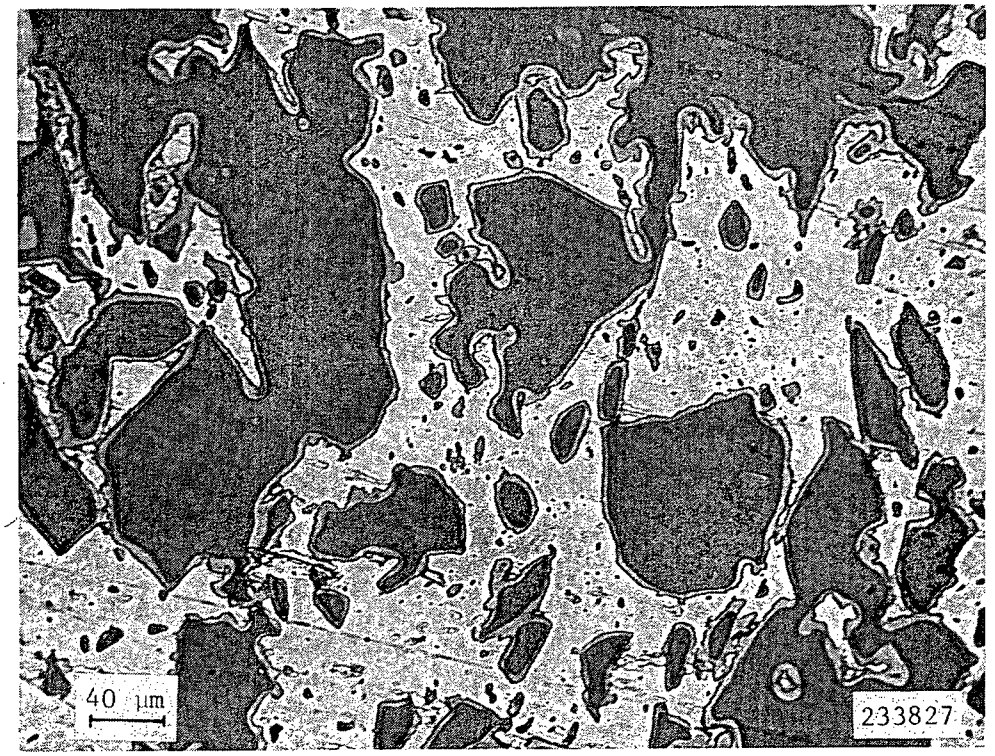

Fig. 10. Meat Microstructure of U_3Si_2 Miniplate After 90% Burnup (Bu).

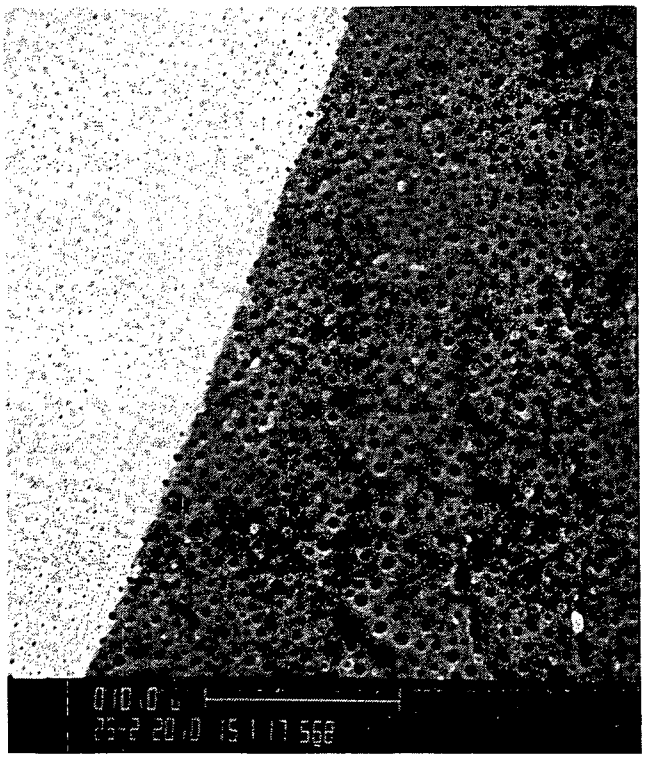

Fig. 11. Fission Gas Bubble Morphology in U_3Si_2 After 90% Bu.

The microstructural changes in U_3Si miniplates resulting from irradiation to high burnups are quite different, as shown in Fig. 12. Fission gas bubbles are clearly visible in the optical micrograph. The bubble morphology, more clearly shown in the SEM images in Fig. 13, reveals a basic difference in fission gas behavior between U_3Si and U_3Si_2. The fission gas bubbles in U_3Si are not uniformly distributed and vary widely in size. The large bubbles are growing rapidly and interlinking, resulting in a much larger fuel swelling rate than that of U_3Si_2. As will be shown in the next section, the fuel in the full-sized U_3Si_2 plates exhibits characteristics of both U_3Si_2 and U_3Si.

5.2.2.2 Full-Sized Plates and Elements

Average thickness changes of plates from the U_3Si_2 elements irradiated in the ORR are shown in Table VI. Although not nearly as accurate a measure of the fuel meat swelling as the volume measurements performed on the miniplates, thickness measurements do show the general trends of the swelling. Note that thickness changes always overestimate the actual volume swelling of the fuel meat because thicknesses between high points of the cladding surfaces are measured. Any warping or twisting of the plate tends to increase the apparent thickness. At 98% burnup ($\sim 2.4 \times 10^{27}$ f/m^3) the thickness increases are small compared to tolerances for the as-fabricated channel gap thicknesses. Similar results were obtained for the individual U_3Si_2 plates irradiated in SILOE. For example, plates with 5.2 Mg U/m^3 had swelled 25 μm at a fission density of 1.4×10^{27} f/m^3 and 45 μm at 2.2×10^{27} f/m^3.

Fuel meat microstructures of plates from the two B&W elements are shown in Figs. 14-16. At 31% burnup a large amount of as-fabricated porosity remains, and no fission gas bubbles are visible in the fuel particles. At 71% burnup most of the porosity has been filled, and fission gas bubbles are visible in scattered fuel particles. These fission gas bubbles have grown considerably by 97% burnup, where the measured thickness increase was 46 μm. The SEM images in Figs. 17-20 show examples of the fission gas behavior in three distinct fuel phases. The major phase has a bubble morphology characteristic of pure U_3Si_2 (Fig. 20), while parts of several fuel particles have either a characteristic U_3Si bubble morphology (Figs. 17 and 18) or, as shown in Fig. 19, a total absence of bubbles and apparent brittle properties reminiscent of UAl_4.

The different fission gas behavior in parts of the ostensibly pure U_3Si_2 fuel grains was understood through the results of a detailed microscopic examination of an unirradiated fuel plate. The fuel particles were found to contain both U_3Si and U_{ss}. The B&W fuel had not been heat treated, so U_{ss} resulting from inhomogeneities in the as-cast ingot was not converted to U_3Si. The small amount of U_3Si in the unirradiated fuel meat was undoubtedly formed

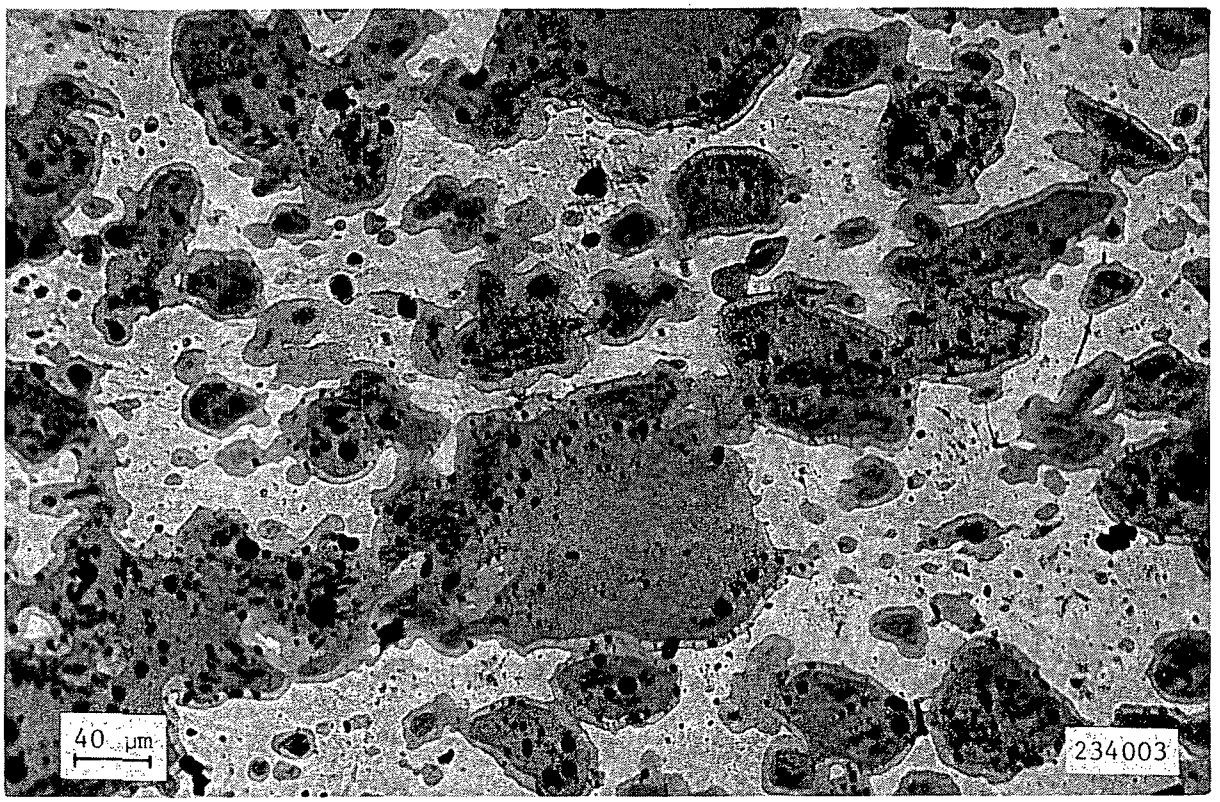

Fig. 12. Meat Microstructure of U_3Si Miniplate After 90% Bu.

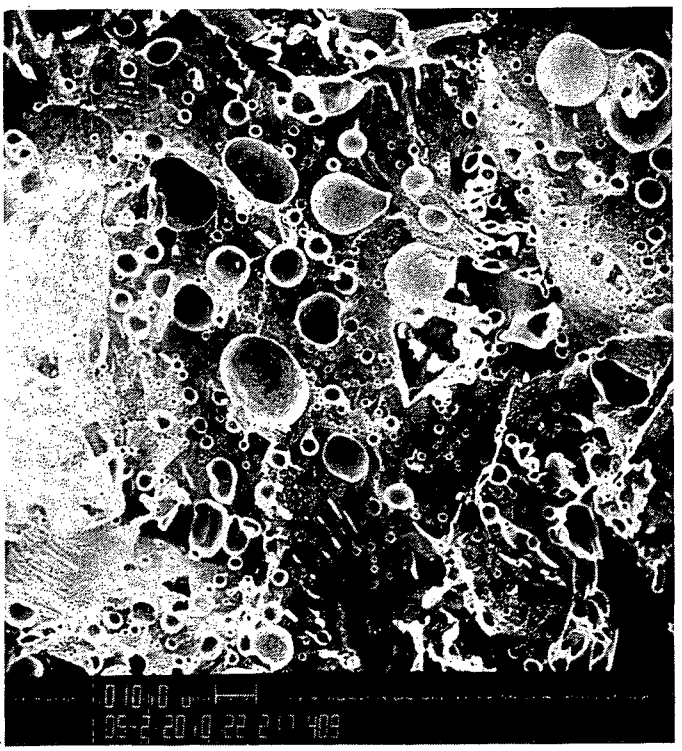

Fig. 13. Fission Gas Bubble Morphology in U_3Si After 90% Bu.

Table VI. Average Thickness Increase and Burnup of ORR U_3Si_2 Test Elements

Element No.	Low-Burnup End			Peak-Burnup Region			Element-Average Burnup, %
	Burnup, %	Thickness Increase, mils	μm	Burnup, %	Thickness Increase, mils	μm	
BSI-201	28	0	0	69	1.5	38	54
BSI-202	53	0	0	97	1.8	46	77
CSI-201	32	0.1	3	66	1.7	43	52
CSI-202	55	0.9	23	98	4.4	112	82
NSI-201	19	0.7	18	46	1.0	25	35
NSI-202	53	1.2	30	97	4.1	104	82

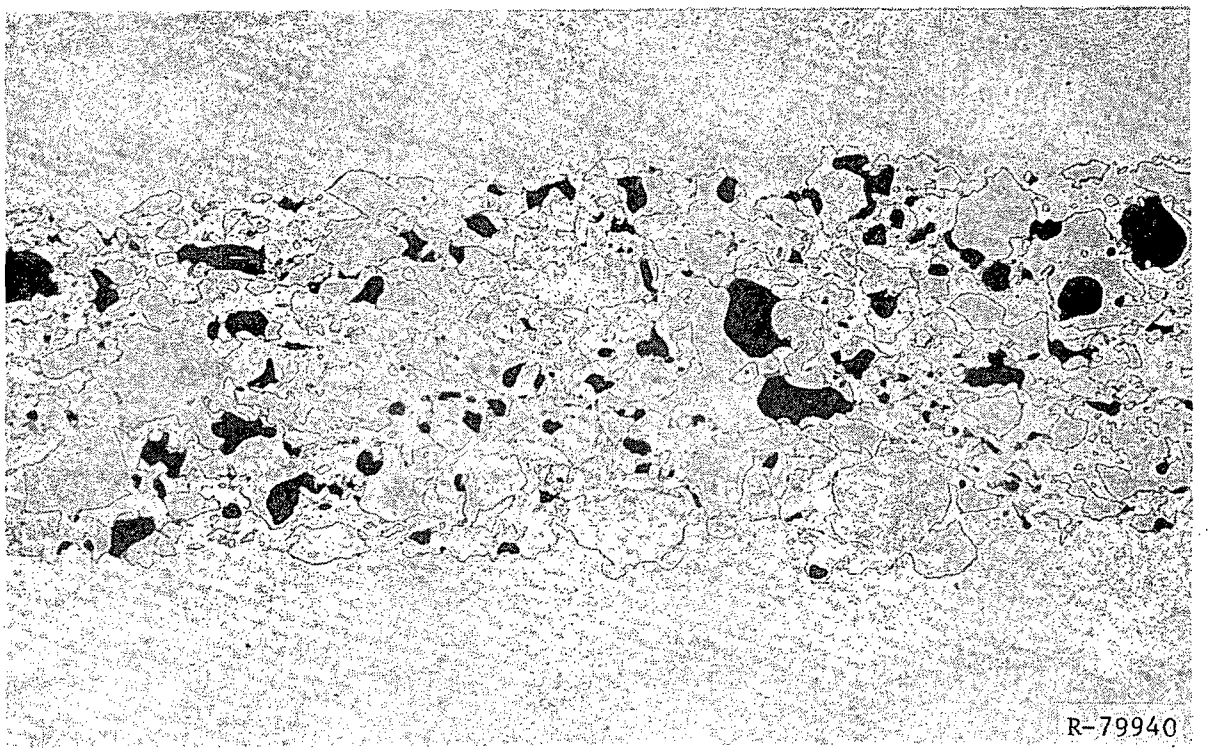

Fig. 14. Meat Microstructure of Plate BSI-201, at 31% Bu.

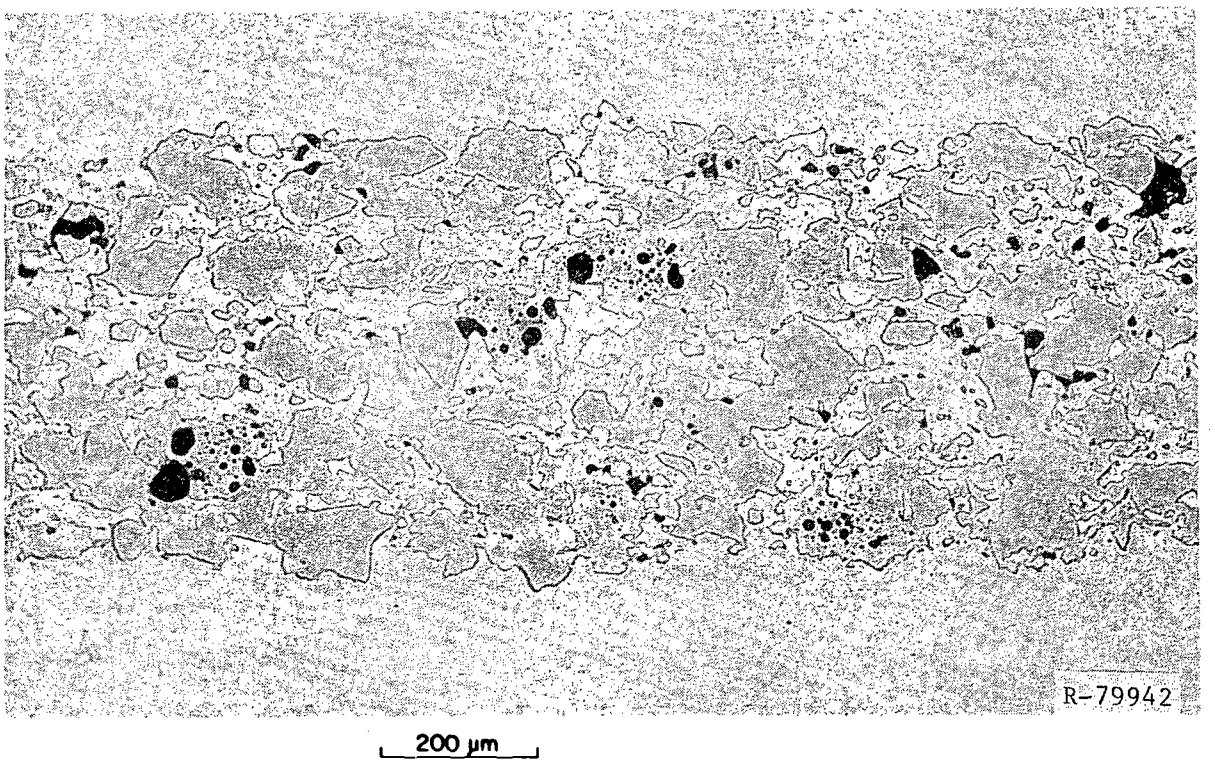

Fig. 15. Meat Microstructure of Plate BSI-201, at 71% Bu.

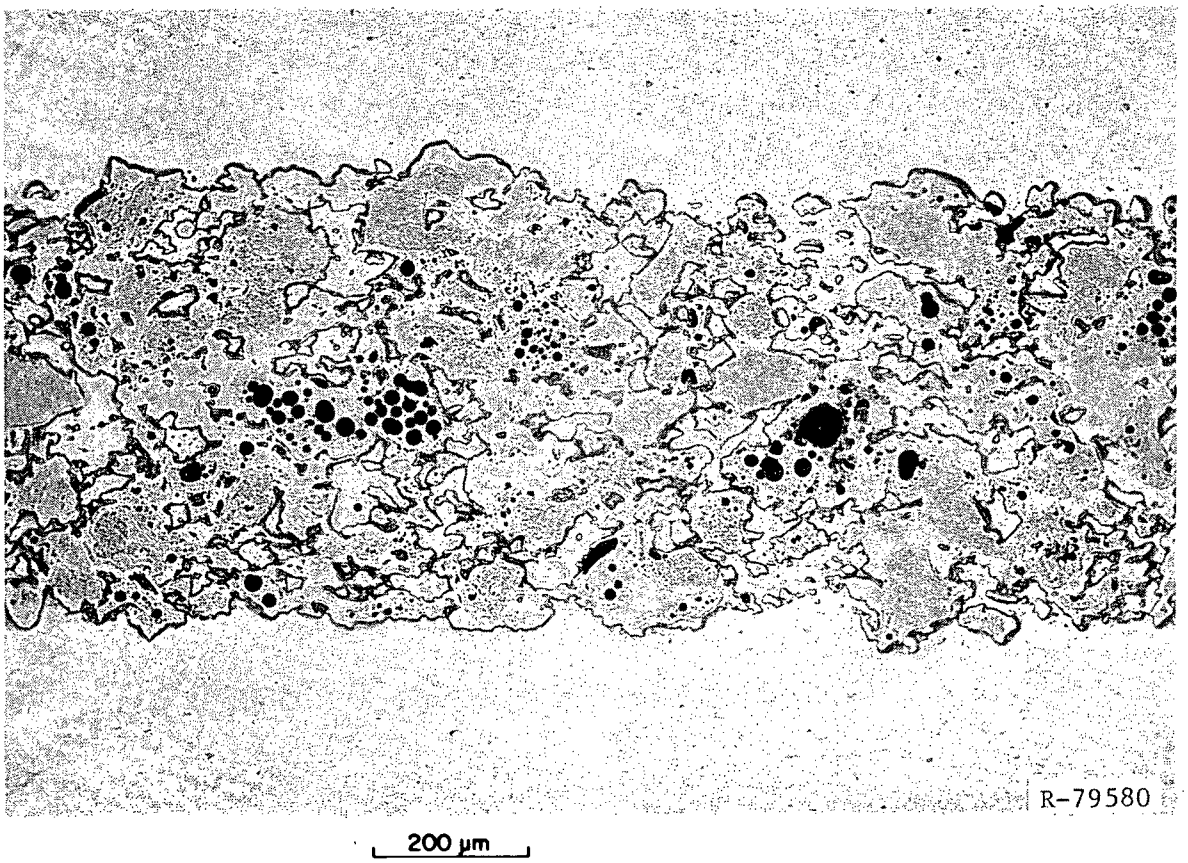

Fig. 16. Meat Microstructure of Plate BSI-202, at 97% Bu.

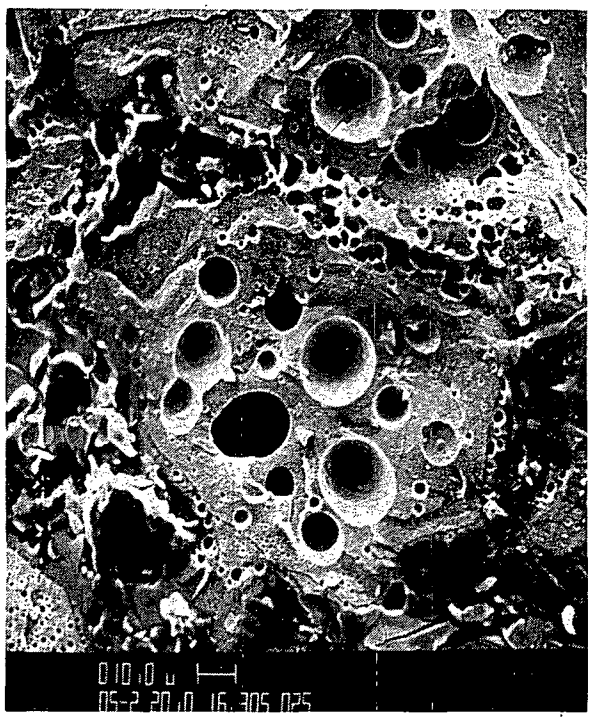

Fig. 17. SEM Image of Fuel Meat of Plate BSI-202, at 97% Bu, Showing Various Bubble Morphologies.

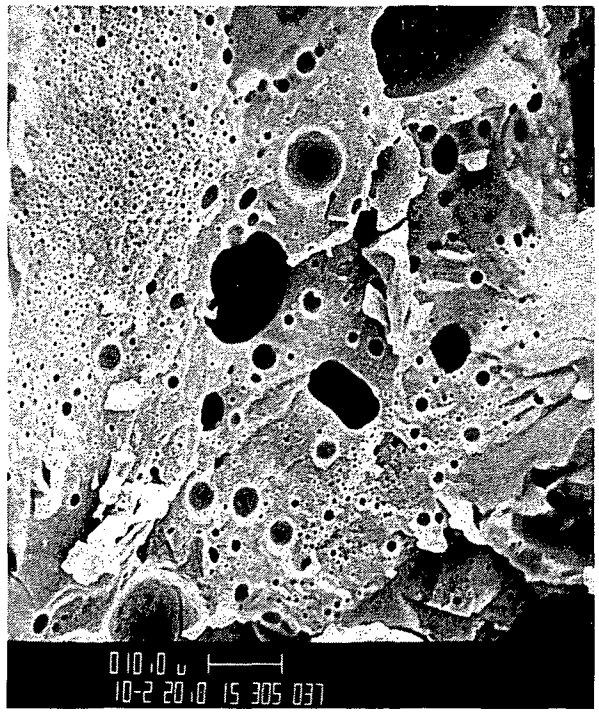

Fig. 18. Idem Fig. 17.

Fig. 19. Idem Fig. 17.

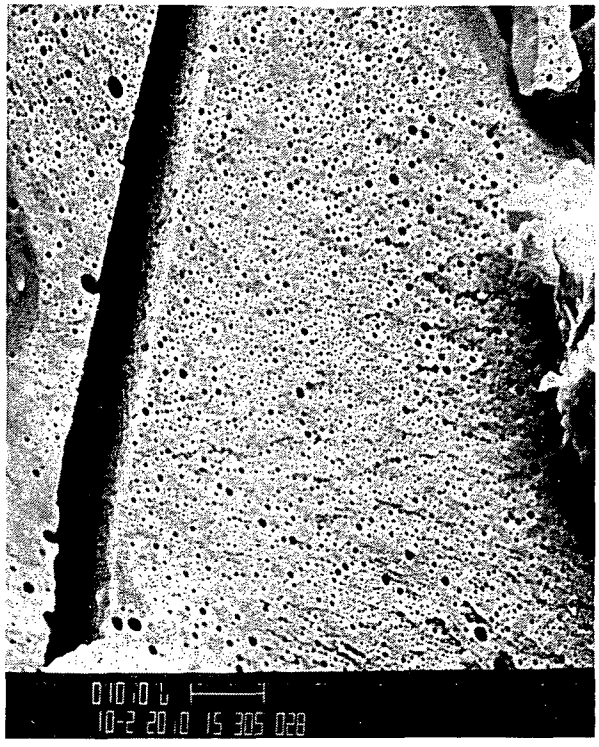

Fig. 20. Idem Fig. 17.

during hot rolling and blister testing. Therefore, the U_3Si and U_3Si_2 show their characteristic irradiation behaviors, and the U_{ss} presumably reacts with Al during irradiation to form the stable UAl_4 compound, in which fission gas bubbles have never been observed. Therefore, the presence of U_{ss} in the as-fabricated fuel does not appear to be detrimental to the performance of the fuel plate. Even though the U_3Si was found to contain all the larger bubbles, its amount was such that no continuous network of large bubbles could develop, even at the very high burnup attained in these plates. It has been established in miniplate irradiations that interparticle linkup of larger bubbles is a prerequisite for possible large swelling in U_3Si.

Fuel meat microstructures of plates from the two CERCA elements are shown in Figs. 21-23, at burnups similar to those of the B&W plates. The much lower residual porosity seen in Fig. 21 reflects the 4% porosity in the unirradiated CERCA plates compared to 9 to 10% in the B&W plates. The high-burnup (97%) end of plate CSI-202 had a measured thickness increase of 112 μm, more than twice that of the B&W plate. The fuel microstructure shows basically the same two-phase fission gas morphology seen in plate BSI-202 with the U_3Si-type bubbles more evenly distributed throughout the fuel. The total fission gas bubble volume appears to be significantly larger than that seen in the B&W plates, as would be expected from the much larger thickness increase experienced by the CERCA plates. Some of this larger thickness increase is attributable to the smaller porosity of the CERCA fuel meat relative to the B&W fuel meat, but the largest part of the difference undoubtedly owes to a larger amount of U_3Si in the CERCA plates.

The fission gas bubble behavior is, in fact, consistent with the as-fabricated fuel microstructure. The CERCA fuel did contain more U_3Si than did the B&W fuel; however, it was more finely distributed than in the B&W fuel. The CERCA fuel did not contain U_{ss} because it had been heat treated, hence the absence of the UAl_4-like phase in the irradiated plate.

Fuel meat microstructures at three different burnups in plates from the NUKEM elements are shown in Figs. 24-26. The appearance is very similar to that of the CERCA fuel meat. The fuel consisted of U_3Si_2 with a somewhat coarsely distributed (compared to the CERCA fuel) second phase. The amount of this second phase, identified as U_3Si, appeared to be the highest of the three, albeit still minor. The high-burnup (96%) end of plate NSI-202, shown in Fig. 26, had a measured thickness change of 104 μm. The fission gas bubble morphology is rather similar to that of the other high-burnup plates, exhibiting a two-phase behavior. The SEM images of a U_3Si_2 fuel particle with low (24%) burnup, shown in Figs. 27 and 28, show that at this burnup the U_3Si_2 particles appear very similar to UAl_4 particles.

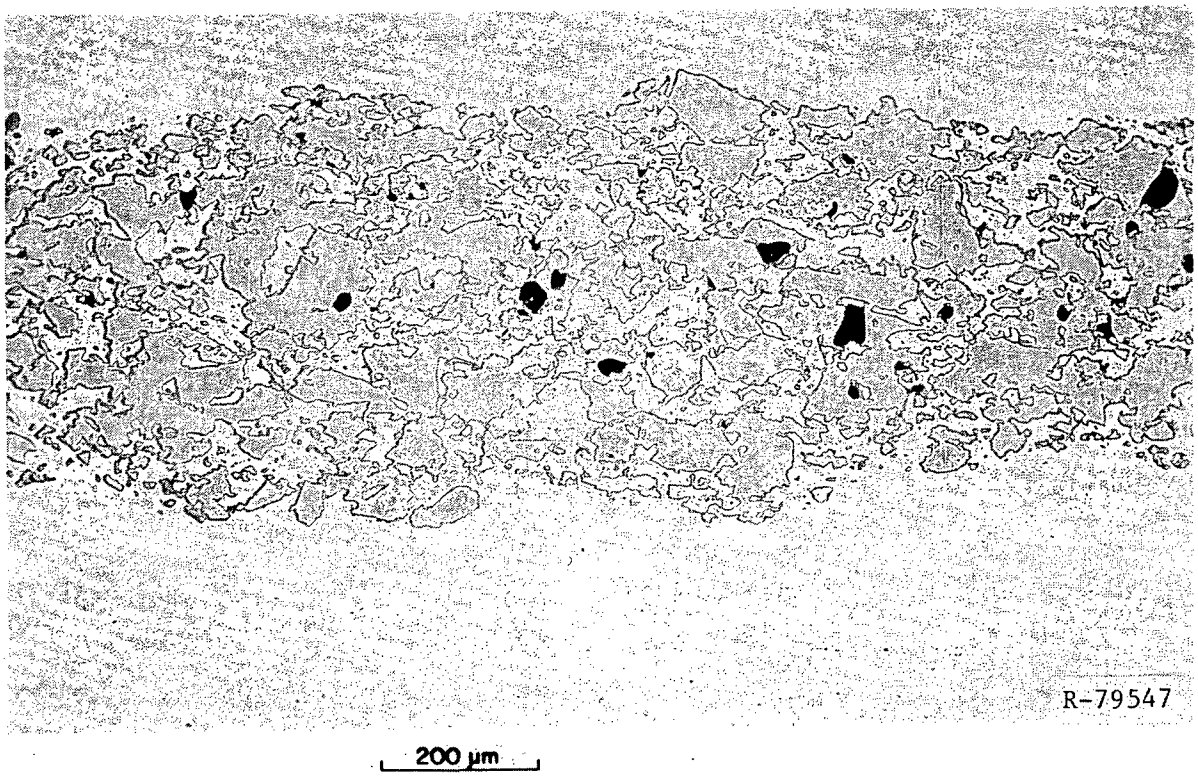

Fig. 21. Meat Microstructure of Plate CSI-201, at 33% Bu.

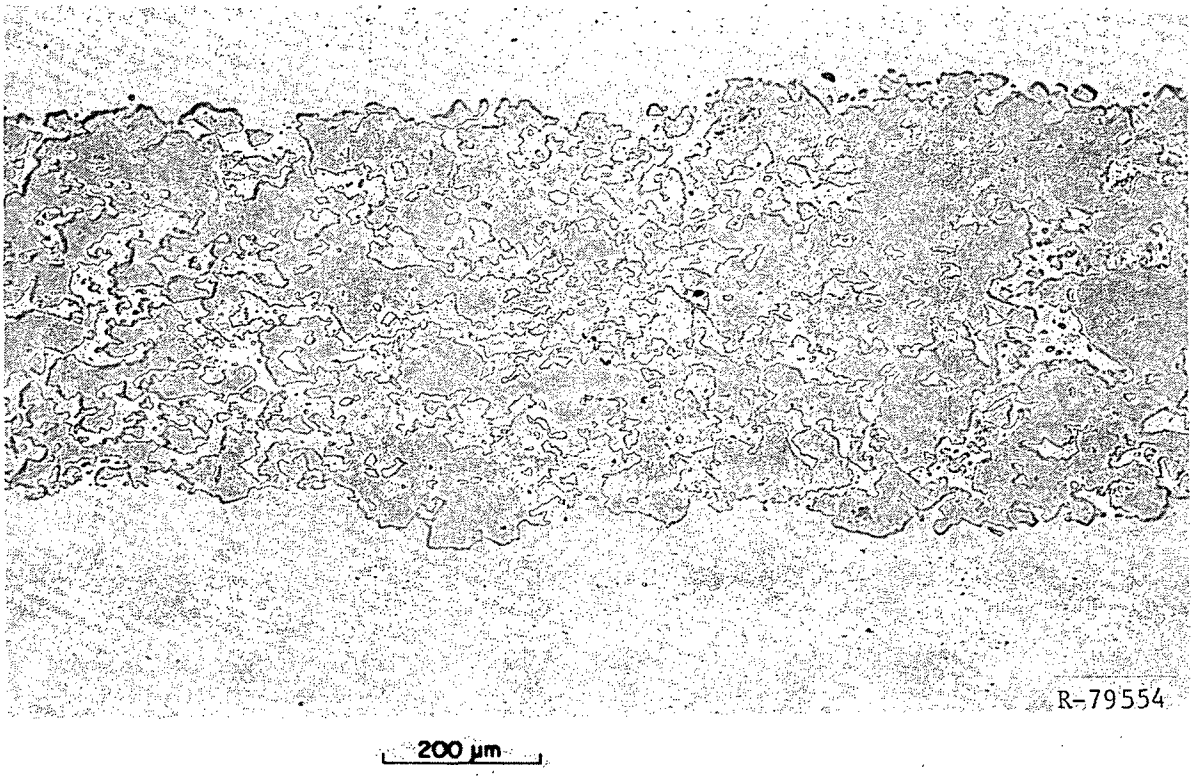

Fig. 22. Meat Microstructure of Plate CSI-201, at 67% Bu.

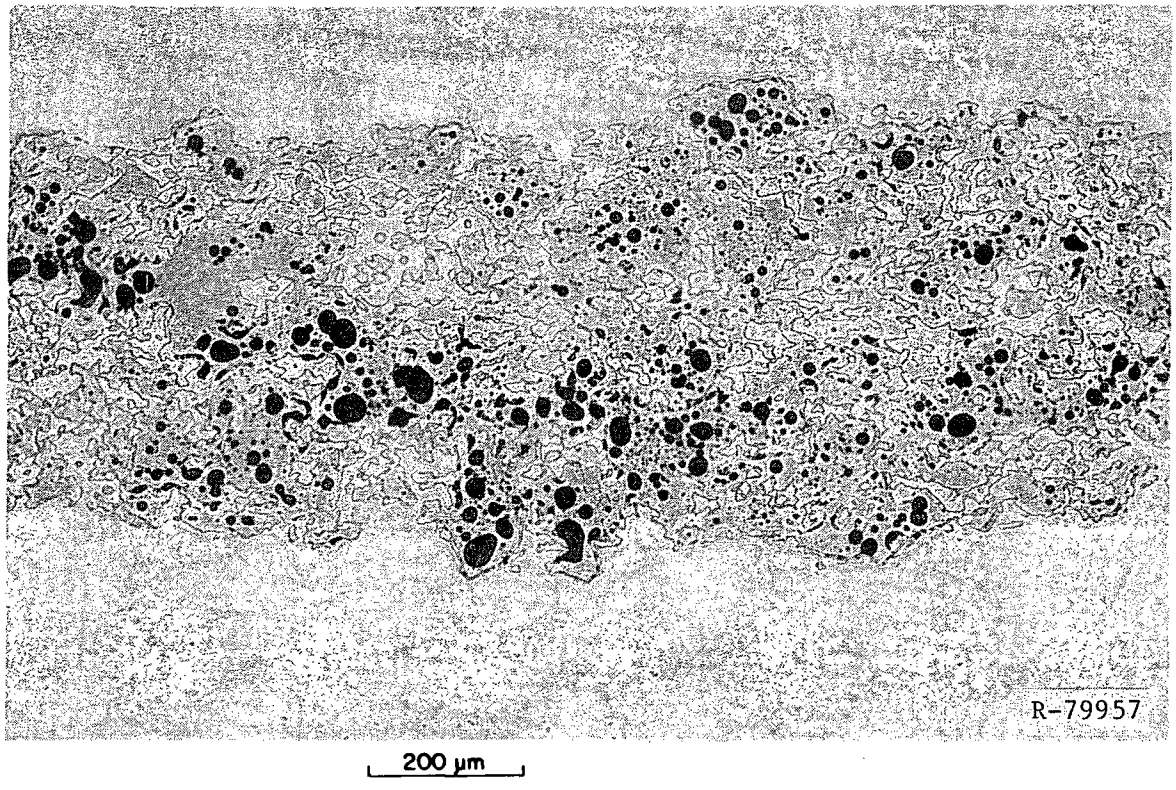

Fig. 23. Meat Microstructure of Plate CSI-202, at 97% Bu.

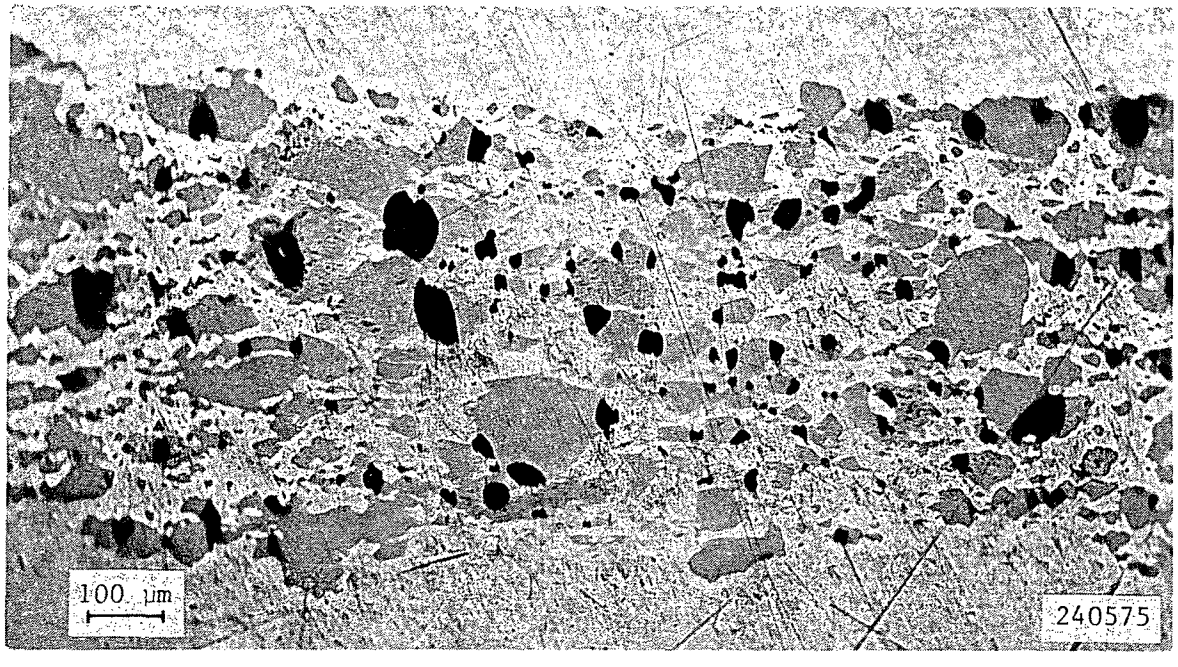

Fig. 24. Meat Microstructure of Plate NSI-201, at 24% Bu.

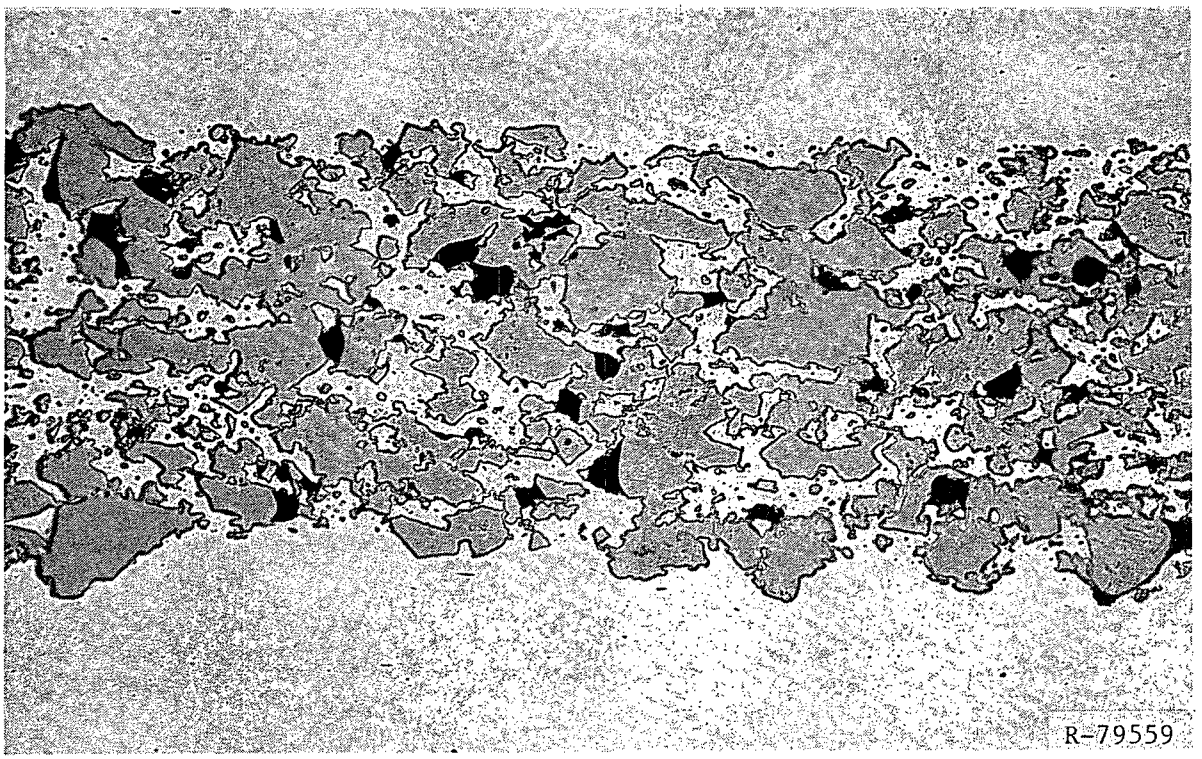

Fig. 25. Meat Microstructure of Plate NSI-202, at 54% Bu.

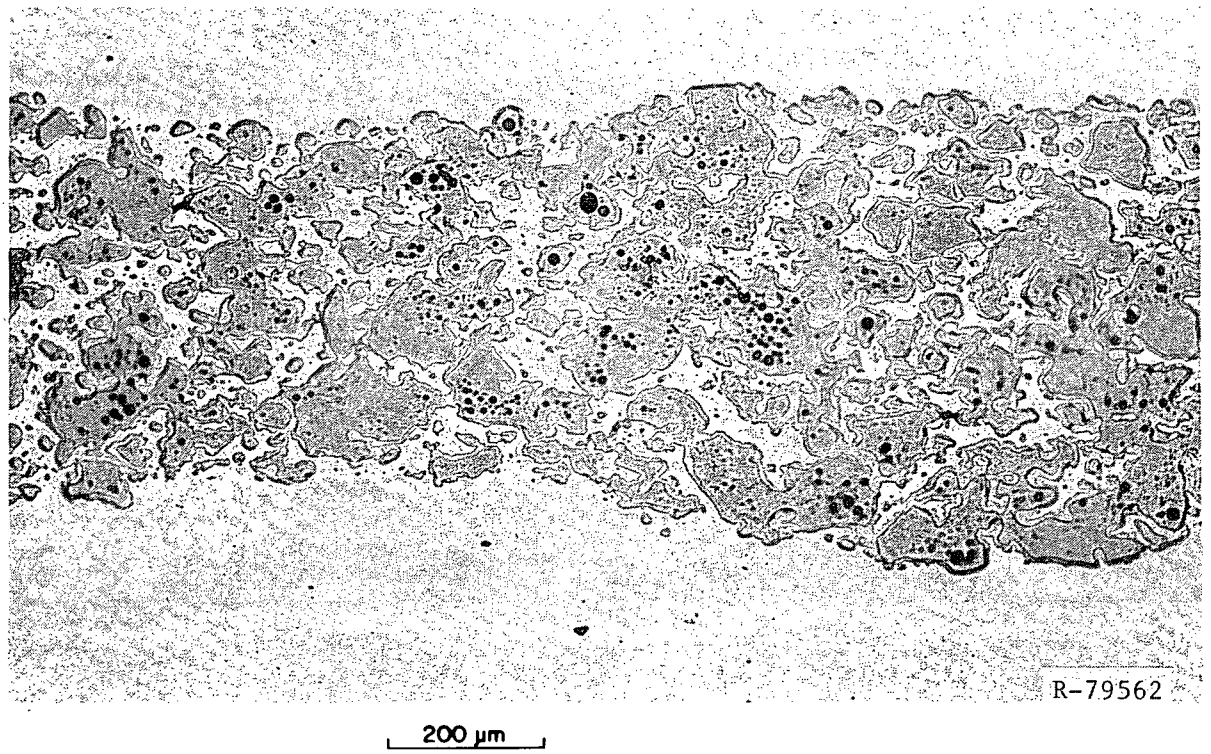

Fig. 26. Meat Microstructure of Plate NSI-202, at 96% Bu.

Fig. 27. SEM Image of Fuel Meat of Plate NSI-201, at 24% Bu.

Fig. 28. Detail of Fig. 27.

In conclusion, the metallographic observations are consistent with the relatively small plate thickness increases experienced during irradiation. The swelling is primarily caused by formation of two distinct fission gas bubble morphologies. The by-far-major phase, U_3Si_2, developed a very uniform and dense distribution of submicron-sized bubbles, characteristic of this fuel. The second silicide phase, U_3Si, which occurred in different amounts in the three fuels, developed its characteristic coarse, nonuniform bubble morphology. The amount of U_3Si and its larger swelling account, with the as-fabricated porosity, for the variability in overall plate swelling between plates of the different fabricators. The similarity of the average thickness changes in the high-burnup regions of elements CSI-202 and NSI-202 suggest that differences in bubble morphology may not be as great as comparison of Figs. 23 and 26 seems to indicate. Since only one section from the high-burnup region of CSI-202 was examined, there is a possibility that the section was atypical.

The non-U_3Si_2 phases present in the fuels are a result of fabrication practices. It is not possible, on a commercial scale, to produce a perfectly homogeneous alloy with the exact composition of a line compound such as U_3Si_2. Heat treatment of the ingots employed by CERCA and NUKEM but not by B&W would explain the absence of U_{ss} in the CERCA and NUKEM fuel. However, the U_{ss} phase found in B&W plates evidently reacted with aluminum during irradiation and had no deleterious effect on the swelling behavior of the fuel.

The minor differences in postirradiation microstructure of the fuel meat of the six ORR test elements reflect differences in fabrication practices of the manufacturers at the various times of fabrication. For example, when NUKEM fabricated the first two U_3Si_2 elements, it was not known that U_3Si behaved differently under irradiation than U_3Si_2 and that it might be desirable to control the amount of U_3Si in the fuel powder. Procedures developed during the course of U_3Si_2 development should result in a more uniform product now and in the future.

The discussion of this section has concentrated on differences in irradiation behavior in order to foster an understanding of the processes at work. However, the completely satisfactory behavior of the six U_3Si_2 test elements in the ORR, three of which were operated to ~80% burnup, must be emphasized.

5.2.3 Blister Threshold Temperature

The postirradiation blister threshold temperature has been used traditionally as an indicator of the relative failure resistance of plate-type dispersion fuels. The U_3Si_2 (and U_3Si) miniplates blistered at temperatures in the range of 515 to 530°C, except for very highly loaded U_3Si miniplates

which, at the threshold of breakaway swelling, blistered at 450 to 475°C. Thirteen plates from the full-sized elements were blister tested. Blister temperatures were in the range of 550 to 575°C. The blister threshold temperature appears to be insensitive both to burnup and to fuel volume loading. These temperatures are at least as high as those measured for highly enriched UAl_x and U_3O_8 dispersion fuels in use today.[33,35]

5.2.4 Fission Product Release

Over the years several studies of fission product release from plate-type reactor fuels have been done, first for plates with U-Al alloy meat and later for plates with UAl_x and U_3O_8 dispersion meats. Results of these experiments have been summarized in Refs. 36 and 37. As part of the development of high-density fuels under the RERTR Program, some fission product release measurements of limited scope have been performed.

Measurements using UAl_x miniplates were performed at ORNL in collaboration with the Kyoto University Research Reactor Institute primarily to determine the threshold temperature for fission product release and to measure release rates above that temperature.[38] These tests showed that the first significant release of gaseous fission products occurred when the fuel plate blistered. Another significant release occurred at about the solidus temperature of the cladding, and a third significant release occurred at about the UAl_4-Al eutectic temperature. Only very small releases of ^{131}I and ^{137}Cs were detected; however, since the system was designed primarily for the measurement of gaseous fission products, it is likely that only a small fraction of the total quantity released was detected.

Similar measurements, using the same equipment, were made using U_3O_8 and U_3Si miniplates, with similar results.[39] The first release of gaseous fission products was detected when the plates blistered, at 500°C for the U_3Si plate and at 550°C for the U_3O_8 plates. Essentially all of the gaseous fission products had been released by the end of the test at 650°C. From the amounts of Cs detected in the traps and from visual observations of deposits on the sample holder following the 650°C test, it was determined that much more Cs was released from the U_3Si plate than from the U_3O_8 plate.

It is expected that the fission product release characteristics of U_3Si_2 dispersed in aluminum are similar to those of U_3Si. The major release of fission gas occurred at about the aluminum melting temperature, where it is known from the DTA studies discussed in Section 4.5 that both U_3Si_2 and U_3Si fully react with the aluminum. The disruption of the fuel structure during the reaction undoubtedly enhances the release of the volatile and solid fission products. Release fractions in U_3Si_2 fuel might be less than those in U_3Si

fuel because the exothermic energy release in the U_3Si_2-Al reaction is less than that in the U_3Si-Al reaction. It is also possible that release rates of fission gas below the threshold of the exothermic reaction might be less for U_3Si_2 than for U_3Si, since the bubble morphologies of the irradiated fuel particles indicate that fission gas mobilities in U_3Si_2 are considerably less than in U_3Si.

Although no quantitative release data were obtained for I and Cs, the data for U-Al alloy and U_3O_8 dispersions[37,40] provide guidance in arriving at release fractions for safety analyses. These data indicate that up to 25% of the Cs and 70% of the I are released at 700°C in air. The presence of steam lowers the release fraction somewhat. There is certainly no reason to think that release fractions would be smaller in the uranium silicides, and for Cs, there is evidence that the release fraction could be considerably larger. Therefore, reasonable bounds for the release fractions of Cs and I are 25 to 100%. The uncertainty in this quantity is quite small compared to the uncertainty in the attenuation factor for transport of these fission products from the molten fuel to the containment or confinement boundary.

5.3 Demonstration of Commercially Fabricated U_3Si_2 Fuel Elements in the ORR

Following successful irradiation testing of the six fuel elements in the ORR described above, a whole-core demonstration of U_3Si_2 fuel was conducted in the ORR to provide both reactor physics data and proof that commercially fabricated elements would perform well. The fuel elements for the demonstration were essentially identical to the test elements and were fabricated by B&W, CERCA, and NUKEM. In addition the shim rods contained fuel followers with 15 fuel plates loaded to 3.5 Mg U/m^3. The fuel elements and shim rods were moved about the core in the normal ORR pattern.

At the end of the demonstration in March 1987, 68 fuel elements and eight fuel followers had been irradiated, with average burnups (estimated from calculations) as shown in Table VII. All elements and followers appear to have performed flawlessly. Channel gap measurements, made periodically on a few elements from each fabricator, indicated no significant changes.

5.4 Reprocessing of Uranium Silicide Fuels

Currently, most spent plate-type research reactor fuel elements from the free world are reprocessed in the U.S. to recover unburned ^{235}U. In order to demonstrate the reprocessability of uranium silicide fuels, studies were conducted at the Savannah River Laboratory for the RERTR Program.[41] Both unirradiated and irradiated fuel samples were tested. The studies demonstrated that uranium silicide fuels can be successfully reprocessed at the

Table VII. ^{235}U Burnup of ORR U_3Si_2 Demonstration Fuel Elements*

Range, %	Number of 19-Plate Standard Fuel Elements			
	CERCA	NUKEM	Babcock & Wilcox	Total
>50	2	2	2	6
45-50	6	3	2	11
40-45	2	6	4	12
35-40	1	1	4	6
30-35	0	1	3	4
25-30	1	2	0	3
20-25	5	1	0	6
15-20	1	2	2	5
10-15	0	1	7	8
5-10	2	1	4	7
Total:	20	20	28	68

Range, %	Number of 15-Plate B&W Fuel Followers
70-75	2
55-60	2
35-40	2
10-15	2
Total:	8

*Based on REBUS-3 calculations performed by M. M. Bretscher and R. J. Cornella.

Savannah River Plant. Subsequently the U.S. Department of Energy agreed to accept spent LEU silicide fuels for disposition on essentially the same terms as for the current HEU fuels.[42]

6. FABRICATION SPECIFICATIONS

A number of the findings from the tests of U_3Si_2 dispersion fuels discussed above have direct bearing on requirements of fabrication specifications. Some of these, related directly to the fuel powder or to general properties of high-density fuels, are discussed briefly below, with recommendations.

6.1 U_3Si_2 Powder

6.1.1 Composition

As indicated in Table I, the silicon content of the U_3Si_2 in the miniplates and test elements ranged from 7.2 to 7.7 wt%. For the U_3Si_2 elements procured for the ORR demonstration, the silicon content ranged from 7.4 to 7.9 wt%. Based upon the results from the test elements, it appears that there is no detrimental effect of up to a few vol% of U_{ss}.

It is recommended that U_3Si_2 fuel be specified at its stoichiometric composition, with a suitable tolerance range: 7.3 ± 0.2 wt%. At 7.1 wt% Si there would be only 1.9 vol% (2.9 wt%) of U_{ss} in homogeneous fuel at equilibrium. At the upper end of the range, there would be 6.5 vol% (5.9 wt%) of USi in the fuel. The use of a slightly higher silicon content, e.g. 7.5 wt%, would considerably reduce the potential amount of U_{ss} in the fuel. However, there appears to be no practical improvement in fuel performance, and the volume loading of fuel required for a given ^{235}U loading would be slightly increased.

It is also recommended that the fuel not be heat treated. Having small amounts of U_{ss} present, which converts primarily to UAl_4, is preferable to having U_3Si present.

It does not appear necessary to have a requirement limiting the amounts of constituent phases per se. Commercial production practices are capable of achieving adequate homogeneity. Therefore, only a test of the average U, Si, and impurity contents is needed to assure a fuel with an acceptably low content of minor phases once the melting process has been qualified.

6.1.2 Impurities

Principal impurities in the fuel for the miniplates and test elements were Al (400 ppm), C (400 ppm), Fe (550 ppm), N (1672 ppm), and O (1290 ppm). No detrimental effects of these impurities were found. In fact, allowing a reasonable amount of surface oxidation to passivate the fuel particles appears prudent. Based upon experience obtained from the ORR demonstration, it recommended that the following impurity levels be accepted: Al (600 ppm), C (1000 ppm), Fe + Ni (1000 ppm), N (1700 ppm), and O (7000 ppm).

6.1.3 Particle Size Distribution

The fines content of the fuels tested ranged between 15 and 40 wt%. There appears to be no detrimental effect of the higher fines content. It is recommended that up to 50 wt% fines be allowed.

The upper limit of particle size in current specifications ranges between 125 and 150 μm. There is no reason based on fuel performance to change this limit. However, a fabricator may find it advantageous to further limit the maximum particle size in order to more easily meet minimum cladding and homogeneity requirements. A 90-μm upper limit is acceptable, based on experience with the CERCA test elements.

6.2 Stray Fuel Particles

It is anticipated that as the use of high-density fuels becomes prevalent, all fabricators will adopt methods to eliminate the possiblity of stray fuel particles. In the meantime, however, it is important not to be overly restrictive in the number of stray fuel particles allowed by the specifications. A fuel-free zone of 0.4- to 0.5-mm width is recommended for the edges and ends of the plates to preclude fission product leaks from the particles. Filing to eliminate particles close to the edges or ends appears to be a viable means of saving a plate which would otherwise be rejected. Fuel particles should not be allowed in the plate identification number area since the cladding thickness is reduced by the numbering process. Smears of very fine fuel particles covering significant areas should be avoided since it is possible that cover-frame bonding might be poor in such areas.

6.3 Fuel Meat Porosity

As discussed previously, the as-fabricated porosity of the fuel meat varies from fabricator to fabricator, probably because of differences in materials and fabrication parameters. For U_3Si_2 at the upper range of fabricability, the porosity varied from 4 to 10 vol% for the ORR test elements. However, the 6% difference in thickness change (~30 μm) attributable to this

difference in porosity is not significant for U_3Si_2 fuel. It is recommended that there be no specific requirement for as-fabricated porosity. If the amount of porosity should be required to be reported as information, only a small sample is needed because the amount of porosity will remain quite constant for a given set of materials and process parameters.

7. SUMMARY AND CONCLUSIONS

As discussed in the preceding sections, extensive tests of the properties of U_3Si_2 dispersion fuel and its irradiation behavior have been performed under the auspices of the RERTR Program. In summary, it has been found that:

1. U_3Si_2 is compatible with the aluminum matrix and cladding. Very little reaction between U_3Si_2 and Al occurs at or below fabrication temperatures. During irradiation this reaction occurs only in the fission fragment recoil zone. The fuel is also compatible with water. No dissolution of the fuel occurred in water boiling at 100°C. U_3Si_2 dispersion fuel can be successfully fabricated with the cladding materials currently used for HEU dispersion fuels, so no question regarding cladding-coolant compatibility is raised.

2. The thermal conductivity of U_3Si_2 dispersion fuel has been measured and found to be similar to those of UAl_x and U_3O_8 dispersion fuels at similar volume loadings of fuel.

3. An exothermic reaction between U_3Si_2 and Al occurs at about the Al melting temperature. The magnitude of the energy release is low enough to be compensated by the Al melting endotherm. The reaction occurs slowly enough (over a period of minutes) to mitigate its consequences in an accident.

4. U_3Si_2 swells very stably under irradiation, at almost the same rate as a function of fission density as UAl_x. Fission gas is contained within the particles in submicron-sized bubbles. Fuel particle swelling is a linear function of the fission density to well beyond the maximum fission density possible in LEU fuel. Test samples containing ~45 vol% fuel showed no evidence of incipient failure at 98% burnup (~2.5×10^{27} f/m^3 in the fuel meat). The presence of minor amounts of other phases which might be present in nominal U_3Si_2 (U_3Si, U_{ss}, and USi) are acceptable. Full burnup of LEU fuel appears feasible.

5. Blister threshold temperatures (515 to >550°C) are at least as high as those of the HEU fuels now being used.

6. Fuel elements irradiated to well beyond normal burnup were dimensionally stable, indicating that the mechanical properties of Al-clad U_3Si_2 dispersion fuel are acceptable.

7. Release fractions of volatile fission products were not measured for uranium silicide fuels, but major releases would occur during the exothermic reaction. Release fractions could not be significantly above the 25 to 70% values measured for U-Al alloy or U_3O_8 dispersion fuels, being limited, of course, to 100%.

It is concluded, therefore, that U_3Si_2 dispersion fuel with uranium densities up to at least 4.8 Mg/m^3 is a suitable LEU fuel for typical plate-type research and test reactors.

ACKNOWLEDGMENTS

The talents and dedicated efforts of many persons have resulted in the successful development and testing of U_3Si_2 dispersion fuel. The contributions of personnel associated with the Materials Processing Group and the Alpha-Gamma Hot Cells at ANL and with the ORR and the HRLEL at ORNL are gratefully acknowledged. We especially thank F. J. Karasek and D. R. Schmitt for their unique contributions to fuel fabrication and E. D. Clemmer for performing hundreds of channel gap scans throughout the irradiation program. Finally, the guidance of H. R. Thresh, L. A. Neimark, and D. Stahl (during early stages of development and testing) has been very much appreciated.

REFERENCES

1. A. Travelli, "The RERTR Program: A Progress Report," Proc. 1986 Int. Mtg. on Reduced Enrichment for Research and Test Reactors, Gatlinburg, Tennessee, November 3-6, 1986, Argonne National Laboratory Report ANL/RERTR/TM-9 (in press).

2. G. B. West, M. T. Simnad, and G. L. Copeland, "Final Results from TRIGA LEU Fuel Post-Irradiation Examination and Evaluation Following Long Term Irradiation Testing in the ORR," Proc. 1986 Int. Mtg. on Reduced Enrichment for Research and Test Reactors, Gatlinburg, Tennessee, November 3-6, 1986, Argonne National Laboratory Report ANL/RERTR/TM-9 (in press).

3. D. F. Sears, L. C. Berthiaume, and L. N. Herbert, "Fabrication and Irradiation Testing of Reduced Enrichment Fuels in Canadian Research Reactors," Proc. 1986 Int. Mtg. on Reduced Enrichment for Research and Test Reactors, Gatlinburg, Tennessee, November 3-6, 1986, Argonne National Laboratory Report ANL/RERTR/TM-9 (in press).

4. F. Cherruau, "The Caramel Fuel in OSIRIS: The Complete Conversion of a High Flux Research Reactor to a Low Enriched Fuel," Proc. Int. Mtg. on Development, Fabrication and Application of Reduced Enrichment Fuels for Research and Test Reactors, Argonne, Illinois, November 12-14, 1980, Argonne National Laboratory Report ANL/RERTR/TM-3 (CONF-801144), pp. 310-318 (August 1983).

5. M. Barnier and J. P. Beylot, "OSIRIS, A MTR Adapted and Well Fitted to LEU Utilization Qualification and Development," Proc. Int. Mtg. on Reduced Enrichment for Research and Test Reactors, Tokai, Japan, October 24-27, 1983, Japan Atomic Energy Research Institute Report JAERI-M 84-073, pp. 256-267 (May 1984).

6. R. F. Domagala, "Phases in U-Si Alloys," Proc. 1986 Int. Mtg. on Reduced Enrichment for Research and Test Reactors, Gatlinburg, Tennessee, November 3-6, 1986, Argonne National Laboratory Report ANL/RERTR/TM-9, in press.

7. R. F. Domagala, T. C. Wiencek, and H. R. Thresh, "Some Properties of U-Si Alloys in the Composition Range U_3Si to U_3Si_2," Proc. 1984 Int. Mtg. on Reduced Enrichment for Research and Test Reactors, Argonne, Illinois, October 15-18, 1984, Argonne National Laboratory Report ANL/RERTR/TM-6 (CONF-8410173), pp. 47-60 (July 1985).

8. A. G. Samoilov, A. I. Kashtanov, and V. S. Volkov, *Dispersion-Fuel Nuclear Reactor Elements*, (1965), translated from the Russian by A. Aladjem, Israel Program for Scientific Translations Ltd., Jerusalem, pp. 54-57 (1968).

9. A. E. Dwight, "A Study of the Uranium-Aluminum-Silicon System," Argonne National Laboratory Report ANL-82-14, p. 29 (September 1982).

10. H. Shimizu, "The Properties and Irradiation Behavior of U_3Si_2," Atomics International Report NAA-SR-10621, p. 14 (July 25, 1965).

11. R. F. Domagala, T. C. Wiencek, and H. R. Thresh, "U-Si and U-Si-Al Dispersion Fuel Alloy Development for Research and Test Reactors," Nucl. Tech. 62, 353-360 (September 1983).

12. T. Görgenyi and U. Huth, "Determination of Cladding Thickness in Fuel Plates for Material Test and Research Reactors (MTR)," presented at Seminar on Research Reactor Operation and Use, Jülich, Fed. Rep. of Germany, September 14-18, 1981.

13. H. W. Hassel and E. Wehner, NUKEM, personal communication (April 1986).

14. G. Thamm, "The German AF-Program Status and Final Activities," Proc. 1986 Int. Mtg. on Reduced Enrichment for Research and Test Reactors, Gatlinburg, TN, November 3-6, 1986, Argonne National Laboratory Report ANL/RERTR/TM-9, in press.

15. K. Bogacik, "Status of LEU Programs at Babcock & Wilcox," *Reduced Enrichment for Research and Test Reactors--Proceedings of an International Meeting, Petten, The Netherlands, October 14-16, 1985*, P. von der Hardt and A. Travelli, Eds., D. Reidel Publishing Company, Dordrecht, pp. 165-173 (1986).

16. S. Nazaré, "Low Enrichment Dispersion Fuels for Research and Test Reactors," J. of Nucl. Materials 124, 14-24 (1984).

17. P. Toft and A. Jensen, "Differential Thermal Analysis and Metallographic Examinations of U_3Si_2 Powder and U_3Si_2/Al (38 w/o) Miniplates," *Reduced Enrichment for Research and Test Reactors--Proceedings of an International Meeting, Petten, The Netherlands, October 14-16, 1985*, P. von der Hardt and A. Travelli, Eds., D. Reidel Publishing Company, Dordrecht, pp. 373-381 (1986).

18. T. C. Wiencek, "A Study of the Effect of Fabrication Variables on the Quality of Fuel Plates," Proc. 1986 Int. Mtg. on Reduced Enrichment for Research and Test Reactors, Gatlinburg, Tennessee, November 3-6, 1986, Argonne National Laboratory Report ANL/RERTR/TM-9, in press.

19. *CRC Handbook of Chemistry and Physics*, 64th Edition, R. C. Weast, Ed., CRC Press, Boca Raton, pp. D-43 and D-44 (1983).

20. R. K. Williams, R. S. Graves, R. F. Domagala, and T. C. Wiencek, "Thermal Conductivities of U_3Si and U_3Si_2-Al Dispersion Fuels," Proc. 19th Int. Conf. on Thermal Conductivity, Cookeville, Tennessee, October 21-23, 1985, in press.

21. R. R. Hobbins, EG&G Idaho, unpublished information (1973).

22. G. L. Copeland and M. M. Martin, "Development of High-Uranium-Loaded U_3O_8-Al Fuel Plates," Nucl. Tech. 56, 547 (1982).

23. T. C. Wiencek, R. F. Domagala, and H. R. Thresh, "Thermal Compatibility Studies of Unirradiated Uranium Silicide Dispersed in Aluminum," Nucl. Tech. 71, 608-616 (1985).

24. C. E. Weber, "Progress on Dispersion Elements," *Progress in Nuclear Energy*, Ser. V, 2, Pergamon Press, N.Y. (1959).

25. R. F. Domagala, T. C. Wiencek, J. L. Snelgrove, M. I. Homa, and R. R. Heinrich, "Differential Thermal Analysis of U_3Si-Al and U_3Si_2-Al Reactions," Argonne National Laboratory Report ANL/RERTR/TM-7 (October 1984) and Am. Cer. Soc. Bull. 65(8), 1164-70 (1986).

26. S. Nazaré, "Reaction Behavior of U_xSi_y- and U_6Fe-Al Dispersions," Proc. 1984 Int. Mtg. on Reduced Enrichment for Research and Test Reactors, Argonne, Illinois, October 15-18, 1984, Argonne National Laboratory Report ANL/RERTR/TM-6 (Conf-8410173), pp. 39-46 (July 1985).

27. A. E. Pasto, G. L. Copeland, and M. M. Martin, "Quantitative Differential Thermal Analysis Study of the U_3O_8-Al Thermite Reaction," Am. Cer. Soc. Bull., 61(4), 491-496 (1982).

28. J. D. Fleming and J. W. Johnson, "Aluminum-U_3O_8 Exothermic Reactions," Nucleonics, 21(5), 84-87 (May 1963).

29. R. L. Senn and M. M. Martin, "Irradiation Testing of Miniature Fuel Plates for the RERTR Program," Oak Ridge National Laboratory Report ORNL/TM-7761 (July 1981).

30. G. L. Copeland, R. W. Hobbs, G. L. Hofman, and J. L. Snelgrove, "Performance of Low-Enriched U_3Si_2-Aluminum Dispersion Fuel Elements in the Oak Ridge Research Reactor," Argonne National Laboratory Report ANL/RERTR/TM-10 (October 1987).

31. C. Baas, M. Barnier, J. P. Beylot, P. Martel, and F. Merchie, "Progress Report on LEU Fuel Testing in CEA Reactors," Proc. 1986 Int. Mtg. on Reduced Enrichment for Research and Test Reactors, Gatlinburg, Tennessee, November 3-6, 1986, Argonne National Laboratory Report ANL/RERTR/TM-9, in press.

32. F. Merchie, CEN-G, personal communication (July 1987).

33. J. M. Beeston, R. R. Hobbins, G. W. Gibson, and W. C. Francis, "Development and Irradiation Performance of Uranium Aluminide Fuels in Test Reactors," Nucl. Tech. 49, 136-149 (June 1980).

34. G. L. Hofman, G. L. Copeland, and J. E. Sanecki, "Microscopic Investigation into the Irradiation Behavior of U_3O_8-Al Dispersion Fuel," Nucl. Tech. 72, 338-344 (1986).

35. A. E. Richt, R. W. Knight, and G. M. Adamson, Jr., "Postirradiation Examination and Evaluation of the Performance of HFIR Fuel Elements," Oak Ridge National Laboratory Report ORNL-4714 (December 1968).

36. D. Stahl, "Fuels for Research and Test Reactors, Status Review: July 1982," Argonne National Laboratory Report ANL-83-5, pp. 37-39 (December 1982).

37. R. E. Woodley, "The Release of Fission Products from Irradiated SRP Fuels at Elevated Temperature," Hanford Engineering Development Laboratory Report HEDL-7598 (June 1986).

38. T. Shibata, T. Tamai, M. Hayashi, J. C. Posey, and J. L. Snelgrove, "Release of Fission Products from Irradiated Aluminide Fuel at High Temperatures," Nucl. Sci. and Eng. 87, 405-417 (1984).

39. J. C. Posey, "Release of Fission Products from Miniature Fuel Plates at Elevated Temperatures," Proc. Int. Mtg. on Research and Test Reactor Core Conversions from HEU to LEU Fuels, Argonne, Illinois, November 8-10, 1982, Argonne National Laboratory Report ANL/RERTR/TM-4 (CONF-821155), pp. 117-133 (September 1983).

40. G. W. Parker, G. E. Creek, C. J. Barton, W. J. Martin, and R. A. Lorenz, "Out-of-Pile Studies of Fission-Product Release from Overheated Reactor Fuels at ORNL, 1955-1965," Oak Ridge National Laboratory Report ORNL-3981 (July 1967).

41. G. C. Rodrigues and A. P. Gouge, "Reprocessing RERTR Silicide Fuels," Savannah River Laboratory Report DP-1657 (May 1983).

42. U.S. Department of Energy, "Receipt and Financial Settlement Provisions for Nuclear Research Reactor Fuels," Federal Register 51(32), 5754-5756 (February 18, 1986) and Federal Register 51(42), 7487 (March 4, 1986).

APPENDIX B

PERFORMANCE OF LOW-ENRICHED U_3SI_2-ALUMINUM DISPERSION FUEL ELEMENTS IN THE OAK RIDGE RESEARCH REACTOR ANL/RERTR/TM-10

Distribution Category:
Nuclear Converter Reactor Fuel Cycle
Technology: Base Technology (UC-83)

ANL/RERTR/TM-10

ARGONNE NATIONAL LABORATORY
9700 South Cass Avenue
Argonne, Illinois 60439

PERFORMANCE OF LOW-ENRICHED U_3Si_2-ALUMINUM DISPERSION FUEL ELEMENTS IN THE OAK RIDGE RESEARCH REACTOR

by

G. L. Copeland and R. W. Hobbs

Oak Ridge National Laboratory

and

G. L. Hofman and J. L. Snelgrove

Argonne National Laboratory

October 1987

Performance of Low-Enriched U_3Si_2-Aluminum Dispersion Fuel Elements in the Oak Ridge Research Reactor

G. L. Copeland and R. W. Hobbs

Oak Ridge National Laboratory
Oak Ridge, Tennessee 37831

and

G. L. Hofman and J. L. Snelgrove

Argonne National Laboratory
Argonne, Illinois 60439

ABSTRACT

Six high-density, low-enriched U_3Si_2-Al dispersion fuel elements have been tested in the Oak Ridge Research Reactor (ORR). The elements were geometrically identical to standard ORR elements. The uranium density in the fuel meat ranged between 4.6 and 5.2 Mg/m^3. The elements were fabricated by B&W, CERCA, and NUKEM using their normal materials and fabrication practices, with minor modifications necessitated by the new fuel. The U_3Si_2 contained minor amounts of USi, U_3Si and/or uranium solid solution. The elements were irradiated in a variety of typical core positions. Three elements were irradiated to approximately normal ORR burnup, and three elements were irradiated twice as long, to average burnups of ~80% of the initially contained ^{235}U, well above the burnups normally achieved in research and test reactors. Peak burnups of 98% were achieved.

Following suitable cooling periods, the elements were subjected to a series of nondestructive and destructive examinations, including visual inspection and dimensional measurements, channel gap thickness measurements, gamma scans, plate thickness measurements, blister threshold temperature tests, metallography, and isotopic burnup analyses. Externally, the elements were essentially unchanged from their as-fabricated condition. The behavior of the fuel was found to be entirely consistent with the known irradiation behavior of the constituent phases. The extremely stable swelling behavior of the U_3Si_2 phase dominated in all cases. The plates showed small, uniform thickness changes, ranging up to 112 μm in regions of ~98% burnup. Blister threshold temperatures were ≥550°C, at the upper end of the the range of those of current fuels.

It is concluded that low-enriched U_3Si_2-Al dispersion fuel elements will perform at least as well in research and test reactors with power densities up to that of the ORR as the highly enriched UAl_x-Al and U_3O_8-Al dispersion fuels currently being used. There were no indications that use of this fuel under substantially more stringent conditions might be precluded.

Table of Contents

Table of Contents (Cont.)

List of Tables

List of Figures

List of Figures (Cont.)

List of Figures (Cont.)

List of Figures (Cont.)

Performance of Low-Enriched U_3Si_2-Aluminum Dispersion Fuel Elements in the Oak Ridge Research Reactor

1. INTRODUCTION

Since its inception in 1978, the U.S. Reduced Enrichment Research and Test Reactor (RERTR) Program[1] has pursued the development of high-density dispersion fuels as one means of making feasible the conversion of research and test reactors from the use of highly enriched uranium (HEU) fuel to the use of low-enriched uranium (LEU) fuel. At that time the highest density fuels in common use in plate-type research reactor fuel elements were dispersions of uranium aluminide (UAl_x) and uranium oxide (U_3O_8) in aluminum with fuel meat densities of 1.7 Mg U/m^3 and 1.3 Mg U/m^3, respectively. These two types of dispersion fuels have now been developed and tested for LEU applications up to their practical fabrication limits--2.4 Mg U/m^3 for UAl_x and 3.2 Mg U/m^3 for U_3O_8.[2]

Although 3.2 Mg U/m^3 is significantly higher than the densities available in 1978, even higher density fuels are needed for the higher performance research and test reactors. To this end the development of fuels consisting of uranium silicide compounds dispersed in aluminum has been pursued. The two highest density uranium silicides are U_3Si and U_3Si_2, with bulk densities of 15.4 and 12.2 Mg/m^3 and uranium densities of 14.8 and 11.3 Mg U/m^3, respectively. There is general agreement among the developers and fabricators of aluminum-matrix dispersion fuels that yields of acceptable plates drop rapidly as dispersant loadings are increased beyond 43 to 45 vol%, or 4.8 to 5.1 Mg U/m^3 for U_3Si_2 and 6.3 to 6.7 Mg U/m^3 for U_3Si.

Irradiation testing of the various fuels began with miniature plates (miniplates) to determine basic irradiation behaviors. All miniplate irradiations were performed in the Oak Ridge Research Reactor (ORR) at Oak Ridge National Laboratory (ORNL).[3] Successful candidate fuels were then tested in full-sized fuel elements to confirm their good behavior under typical reactor conditions. Early indications of acceptable performance of uranium silicide dispersion fuels led to a decision in 1981 to proceed with the fabrication and irradiation of full-sized, low-enriched uranium silicide fuel elements in the ORR.[4] At that time U_3Si_2 was chosen because it was much more brittle and, therefore, could be more easily comminuted than U_3Si. That was a fortunate choice because, subsequently, U_3Si_2 was shown to be much more stable under irradiation than U_3Si.[5,6]

NUKEM,* CERCA,† and B&W** each fabricated two U_3Si_2 fuel elements for testing in the ORR under cooperative arrangements in which the RERTR Program provided the low-enriched uranium and the testing and the fabricators provided

*NUKEM GmbH, Hanau, Fed. Rep. of Germany.
†Compagnie pour l'Etude et la Réalisation de Combustibles Atomiques, Romans-sur-Isere, France.
**Babcock & Wilcox Company, Lynchburg, Virginia, U.S.A.

the fuel elements, each without cost to the other. Fabrication of the elements was completed in January 1982 by NUKEM, in March 1983 by CERCA, and in October 1983 by B&W. Irradiation of the first element began in May 1982, the final element was removed from the core in December 1984, and the examinations were completed in September 1986.

The elements, their irradiation history, and the results of detailed post-irradiation examinations are described and discussed in this report.

2. DESCRIPTION OF FUEL ELEMENTS

2.1 General Description

The LEU U_3Si_2 test elements were essentially identical to the HEU elements routinely used in the ORR, except for the composition of the fuel meat and, for CERCA and NUKEM, the aluminum alloy compositions of the cladding and side plates. The ORR element is a standard box-type element containing 19 curved fuel plates. A cross section of the fuel box is shown in Fig. 1. The nominal fuel meat thickness is 0.51 mm (0.020 in.), giving nominal cladding thicknesses of 0.38 mm (0.015 in.) and 0.57 mm (0.0225 in.) for the inner and outer plates, respectively.

The ^{235}U loading of the test elements was nominally 340 g, a 19% increase over the 285-g loading of the HEU elements. The fuel meat consisted of uranium silicide particles with the nominal composition of U_3Si_2 dispersed in an aluminum matrix. Based on the nominal fuel meat dimensions, the uranium density of the fuel meat was 4.75 Mg U/m^3 (42 vol% U_3Si_2).* By comparison, the nominal uranium density of the HEU elements is 0.85 Mg U/m^3 (12 vol% U_3O_8).

2.2 Specifications

Each of the three fabricators developed a set of specifications for the U_3Si_2 test elements based upon ORNL specifications for ORR HEU fuel elements. For the most part, each fabricator was allowed to use its standard materials and fabrication and inspection procedures. The materials used in the test elements are listed in Table I. The compositions and properties of the principal aluminum alloys used in the elements are listed in Table II. The greatly increased volume loading of fuel particles in the LEU fuel plates necessitated changes in, or in the interpretation of, several specifications related to the fuel meat.

The specifications for fuel plates for the ORR HEU elements required minimum cladding thicknesses of 0.33 mm (0.013 in.) and 0.46 mm (0.018 in.) for

*The 340-g loading for the test elements was chosen to remain below the 350-g maximum loading approved for the ORR in order to avoid possible delays in the irradiation schedule. It is only coincidental that the chosen uranium density is near the practical upper limit for U_3Si_2 fuel.

Table I. Materials Used in U_3Si_2 Test Elements

Part Name	Fabricators		
	B&W	CERCA	NUKEM
Fuel Plate			
Frame	6061	AG 3 NE	AlMg2
Cover	6061	AG 3 NE	AlMg2
Fuel Core			
Fuel	U_3Si_2	U_3Si_2	U_3Si_2
Matrix	MD X75	A5 NE or AL 405	Al-Powder 99.8
Side Plate	6061-T6	AG 3 NE	AlMgSil, F32
Comb	6061-T6	6061-T6[a]	AlMgSil, F32
Pin (Rivet)	4043 or 5356	4043 or 5356[a]	AlMgSil, F21
End Adapter	356 Al	356 Al[a]	356 Al[a]
Welding Wire	N/A	AG 3 NE	S-AlSi5

[a]Supplied by ORNL/ANL.

Table II. Properties of Aluminum Alloys Specified for ORR LEU Fuel Elements

Alloy[a]	AlMg2	AG 3 NE	6061	6061-T6	AlMGSi1, F32
Composition, wt%[b]					
Al[c]	97.6	96.7	97.6	97.6	97.2
Mg	2.0	2.7	1.0	1.0	0.9
Si	<0.3	<0.3	0.6	0.6	1.0
Cu	<0.05	<0.008	0.28	0.28	<0.05
Cr	<0.3	<0.3	0.2	0.2	<0.25
Mn	<0.05	<0.7	<0.15	<0.15	0.7
Tensile Strength, MPa	>147	235	124	310	>314
Yield Strength, MPa	>59	127	55	276	>255
Hardness (HB)	40	42	30	95	95
Thermal Conductivity, W/m•K	150	130	180	167	170
Heat Capacity, J/kg•K	---	960	896	896	---
Solidus Temperature, °C	620	---	582	582	585
Liquidus Temperature, °C	650	650	652	652	650

[a]All properties are for O-temper anneal unless listed otherwise.
[b]Average value of composition limit range used.
[c]Typical Al contents are provided for comparison purposes only. The specification is for Al to constitute the remainder after accounting for additions and impurities.

the inner and outer plates, respectively. Surface defects with depths up to 0.127 mm (0.005 in.) were allowed, leaving a minimum of 0.20 mm (0.008 in.) of cladding over the fuel meat at any point. With only 12 vol% of fuel in the fuel meat of the HEU plates, it was relatively easy to meet these requirements. At the 42-vol% fuel loading required for the LEU plates, however, the rolling process tends to leave the fuel meat thicker at the ends than in the middle (commonly referred to as a dogbone). This, of course, results in thinner cladding over the dogbones. In addition the large concentration of fuel particles results in an increased probability that several fuel particles will come into contact with each other and that one of them will be pushed into the cladding. Both of these phenomena would have resulted in a reduced yield of plates meeting the original ORR minimum cladding thickness specification. ORNL agreed to a minimum cladding thickness specification of 0.267 mm (0.0105 in.) for the inner fuel plates and 0.40 mm (0.016 in.) for the outer plates. They also agreed to allow a 0.25-mm (0.010-in.) minimum at up to six points in the sections to be examined from any one fuel plate. If the plates exhibited dogbones, the depth of surface defects was limited to 0.076 mm (0.003 in.) in the dogbone region in order to maintain approximately the same absolute minimum cladding thickness as for the HEU fuel plates.

Also related to the high volume loading of fuel in the meat is an increased number of fuel particles at the surface of the fuel compact and, consequently, an increased probability for fuel particles to become dislodged and spread into nominally fuel-free zones during the rolling process. This phenomenon, referred to as fuel flaking or fuel out of zone, is identified by the occurrence of white spots on an x-radiograph of the fuel plate. Although the specifications approved for the LEU elements did not specifically address this new problem, ORNL used realistic criteria in judging the acceptability of plates with fuel out of zone. Since the amount of fission energy liberated in these relatively isolated particles is so small as to preclude any cooling problem, the only concern is the isolation of fission products. In general, it was required that no particle be within 0.5 mm (0.020 in.) of the edges or ends of fuel plates.

Another consequence of the high volume loading of fuel particles in the fuel meat and of the high uranium loading in each fuel particle was a difficulty in achieving as homogeneous a uranium loading as was possible in the HEU fuel meat. In addition, it was necessary to accept the spot size normally associated with each fabricator's scanning equipment since it was impractical to request that special collimators be installed for such limited work under a cooperative arrangement. The homogeneity tolerances to which each fabricator agreed are shown in Table III. It is apparent that the different sets of requirements yield different degrees of homogeneity. All were acceptable to ORNL, however.

Finally, the HEU element specifications required a metallographic grain growth test to verify a metallurgical bond between covers (cladding) and frame. The fabricators were allowed to substitute a bending (delamination) test of a strip of material trimmed from the end of the plate. In addition, it was required that each fuel plate be ultrasonically scanned to detect the

Table III. Comparison of Homogeneity Tolerances for U_3Si_2 Test Elements

	Spot Size		Tolerance	
	Linear, mm	Area, mm^2	Dogbone Region	Non-Dogbone Region[a]
HEU Element	2.0 diam	3.1	+27%/-100%	+27%/-100%
	2.0 × 12.7	25.4	+12%/-100%	±12%
B&W LEU Element	2.0 diam	3.1	+30%/-100%	---
	20 × 2.0 diam[b]	62.8	---	±10%
CERCA LEU Element	3.0 diam	7.1	+27%/-100%	±27%
	5.0 diam	19.6	---	±12%
NUKEM LEU Element	5.6 diam	24.6	+27%/-100%	±12%

[a]In the area between the maximum and minimum core outlines a tolerance of -100% was used in place of the listed negative tolerance.
[b]Twenty spots distributed along a 25.4-mm (1.0-in.) line.

presence of non-bond areas in the fuel zone. It was recognized that false non-bond indications might occur from reflections at the fuel-frame interface, so the fabricators were given considerable latitude in interpreting the ultrasonic records in this region. Primary reliance was placed on the blister test to detect non-bonds at the fuel-frame interface.

2.3 As-Fabricated Attributes

The stoichiometric composition of U_3Si_2, 7.3 wt% Si, was chosen by each fabricator as the nominal composition of the fuel compound. Metallic uranium and silicon were combined by arc-melting to form the fuel alloy. Since it is a practical impossibility to produce a perfectly homogeneous ingot by arc melting, the as-cast ingots consisted of U_3Si_2 as the major phase with minor amounts of USi and uranium solid solution (U_{ss}, also called free uranium). Both CERCA and NUKEM heat treated the ingots for approximately three days at 800°C, as had been the practice at ANL for the U_3Si_2 used in the miniplates. During this heat treatment, most or all of the U_{ss} was converted to U_3Si through the peritectoid reaction. By the time B&W began production, however, it had been decided at ANL that no advantage was to be gained by heat treating U_3Si_2. Therefore, the B&W fuel was not heat treated. As will be discussed later, a knowledge of the differences in the compositions of the fuel powders used in the elements from the different fabricators was important in understanding the details of the irradiation behavior of the different elements.

The results of chemical and spectroscopic analyses of the fuel powders produced by the three fabricators are given in Table IV. The maximum U_3Si_2 particle size was 150 μm for B&W and NUKEM and 90 μm for CERCA. The quantity of fines (particles smaller than 40 μm for CERCA and NUKEM or 44 μm for B&W) in the powder was 17% for NUKEM, 18% for B&W, and 40% for CERCA.

The minimum cladding thickness specification was discussed in Section 2.2. Smaller values of this parameter were discovered during metallographic examination of plates during fabrication. The following minima were accepted: 0.22 mm (0.0087 in.) for B&W, 0.23 mm (0.0091 in.) for NUKEM, and 0.25 mm (0.0098 in.) for CERCA. One must understand, of course, that the penetration of fuel particles into the cladding is a random process and that the actual minima for the fuel plates assembled into elements are not necessarily the same as those measured in the sections of the plates destructively examined.

Another parameter of importance in understanding the swelling characteristics of the fuel plates is the volume of void in the as-fabricated fuel plates. Void volumes were measured by the fabricators and/or by ANL using the immersion density technique. The results for inner plates were 4.0 vol% for CERCA and 6.8 vol% for NUKEM. The results for outer plates were 7.8 vol% for NUKEM and 9.9 vol% for B&W.

The immersion density measurements mentioned above yield the fuel meat volume of each plate measured. Based upon these measurements, the calculated

Table IV. Reported Average U_3Si_2 Powder Compositions and Impurities

Major Constituent, wt%	Fabricator		
	B&W	CERCA	NUKEM
U	91.8 (91.2-92.3)	92.1	---
Si	7.4 (7.2- 7.7)	---	7.3
Impurity, ppm			
Al	4	---	400
B	5	<10	0.9
C	607	337	400
Cd	<0.5	<10	<5
Co	---	---	<5
Cu	7	---	96
Fe	6	---	550
H	---	13	---
Li	---	<5	<5
N	---	1672	---
Ni	5	---	---
O	806	1290	---
Zn	<2	---	<10

average uranium densities for the fuel plates from each fabricator are 5.2 Mg U/m^3 for the CERCA elements, 4.9 Mg U/m^3 for the NUKEM elements, and 4.6 Mg U/m^3 for the B&W elements, compared to the 4.75 Mg U/m^3 nominal uranium density. The as-fabricated uranium densities correspond to fuel volume fractions of 46, 43, and 41 vol% for the CERCA, NUKEM, and B&W fuel, respectively. These density data are consistent with average fuel meat thicknesses determined from metallographic studies by CERCA and B&W--0.49 mm and 0.53 mm, respectively.

3. IRRADIATION HISTORY

The irradiation history of the U_3Si_2 test elements is summarized in Table V. One element of each pair was irradiated to approximately normal (~50% average) burnup in the ORR. The second element was irradiated until more than 75% average burnup was achieved. Element No. NSI-201, one of the first pair of elements to be irradiated, was removed from the core earlier than planned in order to take advantage of two months of cooling during a major maintenance outage so that the postirradiation examination of the element would not be delayed.

The two basic core configurations employed during the irradiation of the U_3Si_2 test elements are shown in Fig. 2. At various times, experiments were replaced with filler pieces or with fuel elements. Although the test elements were not cycled through the core in a normal pattern, they did experience irradiation in a variety of typical core positions.

Although fluxes were measured for only a few of the cores containing these elements, results of calculations of similar cores have been used to estimate the maximum powers and associated heat fluxes and temperatures of the test elements during irradiation. It is estimated that each element produced ~1.3 MW during its first cycle of irradiation, with a peak-to-average power density and heat flux factor of no more than 1.5. The average heat transfer area of the element is 1.39 m^2, giving average and peak heat fluxes of 0.94 and 1.4 MW/m^2, respectively. Estimated temperature drops from the center of the fuel meat to the bulk coolant are given in Table VI for various materials and assumptions. The maximum temperature drops given in the table are overestimates since it took several cycles for the boehmite film to build up to its maximum thickness, by which time the element power had decreased owing to burnup. With an average bulk coolant temperature in the ORR core of ~53°C, it is estimated that peak fuel meat temperatures were between 110 and 130°C during the early cycles of irradiation. Average fuel meat temperatures are estimated to have been ~20 to 25°C less.

The pH and electrical resistivity of the primary coolant during the irradiation of the elements ranged between 5.0 and 6.3 and 0.7×10^4 and 2.5×10^4 $\Omega \cdot m$, respectively.

Table V. Irradiation History Summary for U_3Si_2 Test Elements

Core Position	Irradiation Time, fpd					
	BSI-201	BSI-202	CSI-201	CSI-202	NSI-201	NSI-202
B-3	24.8		25.7	43.1		12.6
B-7		24.8	43.1	25.7		
C-2	27.1	12.5	42.7	9.4		
C-4		174.9	12.6	54.9		29.0
C-5		24.9				70.3
C-6	24.9			112.0		54.9
C-8	12.5	27.1	9.4	42.7		
D-2		12.7			57.0	60.8
D-3		30.0				
D-7	30.0					
D-8	12.7				53.2	57.0
E-2				11.5		
E-8			11.5			
Total	132.0	306.9	145.0	299.3	110.2	284.6
Begin Irrad.	11/23/83	11/23/83	4/28/83	4/28/83	5/27/82	5/27/82
End Irrad.	4/22/84	12/19/84	9/29/83	8/14/84	1/14/83	8/14/84
Total No. of Cycles	8	26	11	26	8	24
Ave. Burnup,[a] % 235U	54	77	52	82	35	82
Ave. Burnup,[b] MWd	150	217	144	228	95	231
Ave. Power, MW	1.13	0.71	0.99	0.76	0.86	0.81

[a] See Table VIII.

[b] Based on the following calculated ^{235}U burnup rate correlation:

$$\text{Burnup rate (g/MWd)} = 1.2608 - 0.0004103 \cdot \text{Burnup (MWd)}.$$

Table VI. Estimated Average and Peak Fuel Temperature Drops

	Thickness, mm	Thermal Conductivity, W/m•K
Fuel Meat	0.25[a]	30 - 60[b]
Cladding	0.38	130 - 180[c]
Boehmite Layer	0 - 0.025	2.25

	Temperature Drops, °C	
	Average (0.94 MW/m^2)	Peak (1.4 MW/m^2)
Fuel Meat		
30 W/m•K	7.8	11.7
60 W/m•K	15.7	23.3
Cladding		
130 W/m•K	2.7	4.1
180 W/m•K	3.8	5.7
Boehmite		
13 μm thick	5.4	8.1
25 μm thick	10.4	15.6
Water Film[d]	27.6	41.2
Total		
Minimum (no Boehmite)	38.1	57.0
Maximum	57.5	85.8

[a] Half-thickness.

[b] R. K. Williams, R. S. Graves, R. F. Domagala, and T. C. Wiencek, "Thermal Conductivities of U_3Si and U_3Si-Al Dispersion Fuels," Proc. 19th International Conference on Thermal Conductivity, Cookeville, Tennessee, USA, October 21-23, 1985, in press.

[c] See Table II.

[d] Film coefficient calculated using the Dittus-Boelter correlation for a bulk water temperature of 53.3°C.

The accessible channel gaps of the elements were measured at various times during the irradiation of the elements (following each cycle beyond 50% burnup) using the ultrasonic probe described in Ref. 3. In all cases the channel profiles remained essentially unchanged during the course of the irradiations, indicating no abnormal swelling or warping of the plates.

4. POSTIRRADIATION EXAMINATION OF FUEL ELEMENTS

After suitable periods of cooling in the ORR pool following completion of irradiation, the elements were transported to the ORNL High-Radiation-Level Examination Laboratory (HRLEL). All six elements were given the complete nondestructive and destructive examinations outlined in Appendix A. The nondestructive portion consisted of visual examination, dimensional inspection, gamma scanning, and coolant channel measurements. Then, the elements were dismantled, and the plates were visually inspected. Selected plates were measured for thickness and were gamma scanned. Two plates from each element were tested for blister threshold temperature, and one plate from each element was sectioned for microstructural and burnup analyses.

4.1 Visual Examination

The elements were examined visually through the cell windows and through the Kollmorgan periscope. All six of the elements appeared to be in excellent condition. With the exception of the oxide film and some handling scratches, the elements appeared to be as fabricated. No abnormal conditions were observed. Photographs obtained of the exterior of the elements and through the coolant channels are contained in Appendix B.

4.2 Dimensional Inspection

The width (between side plate outer surfaces) and stack height (between outer fuel plate outer surfaces) of each element were measured at six axial locations along a central line and along parallel lines near the edges of the element. The measurements were made by positioning the element between opposing dial micrometers at the desired point of measurement and comparing the readings to a standard. By comparing readings from the upper and lower micrometers, bow or twist could be detected. The length of each element was determined by comparison to a standard using a fixture and a dial indicator. No unusual bow, twist, or swelling was observed for any of the elements. Within the accuracy of the in-cell measurements, the dimensions were within the envelope of tolerances allowed for as-fabricated dimensions. A summary of the dimensional measurement result is given in Table VII. Individual measurement results for each element are presented in Appendix C.

Table VII. Results of Dimensional Inspection of Irradiated Elements

	Width,		Stack Height,		Length,	
	mm	in.	mm	in.	mm	in.
Fabrication Tolerance						
Max	76.10	2.996	78.18	3.078	975.1	38.390
Min	75.84	2.986	77.67	3.058	973.5	38.328
Element No.						
BSI-201	76.17	2.999	77.83	3.064	975.0	38.386
	75.72	2.981	78.31	3.083		
BSI-202	76.20	3.000	77.85	3.065	974.8	38.378
	76.05	2.994	77.75	3.061		
CSI-201	76.07	2.995	78.05	3.073	---	---
	75.82	2.985	77.09	3.035		
CSI-202	75.69	2.980	78.10	3.075	974.5	38.367
	75.56	2.975	77.50	3.051		
NSI-201	75.95	2.990	78.10	3.075	974.5	38.365
	75.84	2.986	77.93	3.068		
NSI-202	76.23	3.001	78.26	3.081	975.7	38.413
	76.02	2.993	78.00	3.071		

4.3 Gamma Scanning of Elements

The elements were passed in front of a 432-mm (17-in.)-long collimator with a 0.25 mm × 25.4 mm (0.010 in. × 1.0 in.) aperture, and the gamma spectrum was measured. The detector was either a NaI or a Ge(Li) crystal. During the course of the work, several methods of recording the data were used. Profiles of gamma intensity versus axial position were obtained for integrated energies greater than 0.5 MeV and for a narrow energy window containing the ^{137}Cs peak at 662 keV. At certain positions, complete multichannel energy spectra were obtained using the Ge(Li) crystal.

The primary purpose of these measurements was, in conjunction with the results of the destructive burnup analyses discussed in Section 5.3, to provide data for determining burnups of similar elements not scheduled to be destructively examined. Since all of the present elements were destructively examined, including burnup analysis, these data will not be discussed in detail. The ^{137}Cs profiles are presented in Appendix D.

4.4 Coolant Channel Gap Thickness Measurements

Following removal of the end adapters from the elements, the coolant channel gap thicknesses were measured on either side of the comb along the entire length of each channel. For element NSI-201 the measuring probe was a spring-loaded device containing a linear voltage differential transformer (LVDT). Channel gaps of elements CSI-202, BSI-201, and BSI-202 were measured using a capacitance probe. For elements NSI-202 and CSI-201 neither device was available, and a 2.64-mm (0.104-in.)-diameter wire was rolled between the plates to assure that the channels exceeded the 2.64-mm minimum gap allowed by the specifications.

Tabulated results of the coolant channel measurements are contained in Appendix E. These data indicate that the gaps of all but a few channels everywhere exceeded the as-fabricated minimum dimension. In these few channels, the gap thicknesses at a few isolated points were slightly below this value (but greater than 2.62 mm). No comparable preirradiation data are available to determine changes. The uniformity of the channels indicates that no excessive swelling or warping of the plates occurred during irradiation.

5. EXAMINATION OF FUEL PLATES

The individual plates were removed from the element by cutting through the side plates into the coolant channels using a milling machine. The strips of aluminum clinging to the plate were then easily pulled off without damaging the plate.

5.1 Visual Inspection of Plates

The first examination of the plates following their removal from the element was verification of the plate numbers and a thorough visual inspection. The plates in all elements exhibited some warping and bowing after removal from the element. This is typical of all irradiated elements of this configuration. All of the plates from the six elements appeared to be in good condition with no evidence of blisters, excessive swelling, or any other unusual condition.

5.2 Plate Thickness Measurements

Plate thickness measurements were made by positioning the plate between opposing dial micrometers at the desired point of measurement and comparing the readings to a standard. The indicator tip for the top (convex) surface was a 6.35-mm (1/4-in.)-diam flat and for the bottom (concave) surface was a 3.18-mm (1/8-in.)-diam ball. Measurements were made along tracks at the center and near the sides of the plate. No attempt was made to remove the oxide film from the plates, so its thickness is included in the overall plate thickness. Near the end of the examinations, a new device based on capacitance became available to measure the plate thickness. This device was used to remeasure the thickness of several plates as an overcheck of the micrometer measurements and to supplement some incomplete data. Thicknesses determined with the new device were consistent with the data obtained using the micrometers.

All plates of NSI-201 and NSI-202 were measured at NUKEM's request, since they were the first U_3Si_2 elements to be irradiated. Five plates (in positions 2, 6, 10, 14, and 18) from each of the other four elements were selected for measurement. Plate thickness increases were determined from the thicknesses measured at each position by subtracting the plate thickness measured outside the fuel zone, near the end of the plate. This method at least partially corrects for the oxide film buildup, since the normalization region also has an oxide film, though probably not as thick a one as in the fuel zone, where the heat flux was higher. The average fuel plate thickness increases in the peak- and minimum-burnup regions (based upon the plates in positions 2, 6, 10, 14, and 18) are listed in Table VIII. Swelling profiles for the five plates used for the averages are presented in Appendix F.

Apart from the contribution from the oxide film, plate thickness changes result only from swelling of the fuel meat. Since the fuel meat is well constrained by the frame in the transverse directions, it swells almost exclusively in the thickness direction. The fractional change in fuel meat thickness is, then, equal to the fractional change in fuel meat volume, the number most commonly reported as the fuel meat swelling. Experience with well over 100 miniplates, where both fuel plate thickness changes and fuel meat volume changes were accurately measured, has shown that swelling estimates based on thickness changes are always greater than the actual fuel meat volume changes since the thicknesses are measured between the "high" points on the

Table VIII. Average Thickness Increase and Burnup[a]

Element No.	Low-Burnup End			Peak-Burnup Region			Element-Average Burnup, %
	Burnup, %	Thickness Increase, mils	μm	Burnup, %	Thickness Increase, mils	μm	
BSI-201	28	0	0	69	1.5	38	54
BSI-202	53	0	0	97	1.8	46	77
CSI-201	32	0.1	3	66	1.7	43	52
CSI-202	55[b]	0.9	23	98	4.4	112	82
NSI-201	19	0.7	18	46	1.0	25	35
NSI-202	53	1.2	30	97	4.1	104	82

[a]Average thickness increases and burnups at the low-burnup end and in the peak-burnup region are average values for the plates in positions 2, 6, 10, 14, and 18. Data from all 19 plates were used in calculating the element-average burnup.

[b]Based on analyzed burnup and comparison to other elements because of discrepant data at the low-burnup end.

fuel plate surfaces. The curvature of the ORR fuel plates increases this problem. Therefore, no attempt has been made to calculate volume swelling from the thickness change data. Nevertheless, significant differences in measured thickness change do represent significant differences in the volume swelling of the fuel meat. However, from the point of view of fuel element performance, the overall thickness changes were small compared to the allowed tolerance in the channel gap thickness. This is consistent with the results from the channel gap thickness measurements discussed in Sections 3 and 4.4.

5.3 Plate Gamma Scanning and Burnup Analysis

Five plates from each element (including the one from which burnup samples were taken) were selected for determining the axial burnup profile by gamma scanning. The setup and techniques described in Section 4.3 for full-element scanning were also used for the plates. Complete multichannel energy spectra were obtained with the Ge(Li) crystal at the peak-burnup points of all nineteen plates of each element, with the exception of NSI-201.

Samples for burnup analysis were obtained at the positions of peak and minimum burnup, as determined by the gamma profiles. Following dissolution of the sample, the relative uranium and plutonium isotopic abundances were determined by mass spectrometry. The ^{235}U isotopic abundances before and after irradiation were used, with calculated correlations for changes in the ^{238}U and ^{236}U abundances, to derive the ^{235}U burnup.

Relative plate-average burnups were determined from the individual axial profiles, and the relative plate-to-plate burnup profile in the element was determined from the areas of the 662 keV peak of ^{137}Cs in the multichannel spectra (NaI gamma intensity data used for NSI-201) at the peak-burnup point of each plate. These data were normalized to the results of the destructive burnup analysis to determine the element-average burnup. The results are summarized in Table VIII. Typical profiles are shown in Fig. 3. Typical examples of the gamma scanning data and the complete burnup analysis data and correlations are in Appendix G.

As was mentioned in Section 3, the average burnup of one element from each fabricator was intentionally pushed well beyond the ~50% level normally achieved in reactors using this type of fuel. This resulted in peak burnups of ~98% in each case. Accounting for non-^{235}U fissions, the fission density in the high-burnup elements ranged between $\sim 1.1 \times 10^{27}$ and $\sim 2.5 \times 10^{27}$ f/m^3.

5.4 Blister Threshold Testing

A method which has been used historically to compare the relative irradiation performance of dispersion plate-type research reactor fuels is their resistance to blistering during heating after irradiation. This test, termed the "blister threshold test," is performed by sequentially heating the plate (or portions thereof) to higher and higher temperatures and visually examining the plate after each heating for evidence of blisters. Two plates from each

element were blister threshold tested. The entire plate rather than a plate section was heated to preclude the possibility of fission gas diffusing out of the cut edges rather than causing blisters at these relatively high volume fractions of fuel. The plates were held at the following temperatures for 30 minutes; removed from the furnace, cooled and examined; then heated to the next higher temperature (or removed from testing if blistering was observed): 400, 450, 475, 500, 525, 550, and 575°C. This procedure corresponds closely to the test procedure used previously for the highly enriched, low-volume-fraction uranium aluminide and uranium oxide fuels.

Typical blister threshold temperatures for the highly enriched dispersion fuels in use today range from 480 to >565°C for the uranium aluminide[7] and from 400 to >550°C for the uranium oxide[8] fuels. Blister threshold temperatures measured during miniplate tests of high-density, low-enriched uranium aluminide and uranium oxide dispersion fuels developed by the RERTR Program ranged from 550 to >550°C and from 450 to >550°C, respectively.[9] The same type of tests on uranium silicide miniplates yielded blister threshold temperatures of 530°C for U_3Si_2 fuel and 500 to 525°C for U_3Si fuel.[9]

The results of the present tests are presented in Table IX. The blister threshold temperature in each case was in the upper range of that which could have been expected with the established fuels. The appearance of the blisters was similar to that of the small blisters between the cladding and meat which were observed during testing of uranium silicide miniplates. The blister threshold temperatures of these full-sized plates are consistent with the results of the miniplate tests cited above. Photographs of the plates after blistering are contained in Appendix H.

These tests have shown that blister threshold temperatures of low-enriched, high-density uranium silicide fuels are about the same or higher than those of the highly enriched, lower-density uranium aluminide and uranium oxide fuels they are proposed to replace. Therefore, the propensity for blistering in-reactor will be no worse for these new fuels than for those presently in use.

5.5 Toughness of Irradiated Fuel Plates

Owing to the very high volume fraction of fuel particles in the meat following irradiation, some concern was expressed about the brittleness of the fuel and whether the fuel plates might be subject to breaking during handling and shipping. Even though one would expect the cladding and frame, which were fabricated from the same alloys used for HEU fuel plates for many years with no problems, and not the fuel meat to be the major determinant of the toughness of the fuel plate, it was considered prudent to devise a simple test to address this concern in a very qualitative manner.

Therefore, several high-burnup plates were bent to determine their ductility and toughness. The center of a plate was positioned under a mandrel

Table IX. Results of Blister Anneals of Full-Sized Plates

Element No.	Plate Position	Plate No.	Maximum Temperature, °C	Description of Blisters[a]
BSI-201	3	S-3-211-13	575	None
	8	S-3-210-23	575	Typical PI
BSI-202	3	S-3-213-15	550	Typical PI
	8	S-3-212-19	550	Typical PI
CSI-201	4	OSIIW-065	550	Typical PI
	8	OSIIW-054	550	Typical PI
CSI-202	3	OSIIW-044	550	Typical PI[b]
	8	CSIIW-026	550	Typical PI[c]
NSI-201	2	ORR-092	550	None
	8	ORR-100	550	None
	19	ORR-144	550	None
NSI-202	3	ORR-114	550	Typical PI
	9	ORR-123	550	Typical PI

[a]Typical PI--typical of postirradiation blisters observed previously in low-volume-fraction fuels (i.e., appear to be discrete blisters between meat and cladding with no "pillowing").
[b]Small blisters off of fuel formed at 500°C.
[c]Small blisters off of fuel formed at 525°C.

(~2.5 mm diam), and, with one end fixed, the plate was bent around the mandrel with the concave surface inward. A plate from CSI-202 broke at about 160° of bend. One plate from BSI-202 broke at about 90° of bend. Another plate from BSI-202 was bent 80° and straightened out completely when the force was removed. A plate from BSI-201, which had experienced significantly less neutron fluence, was bent 80° and straightened out when the force was removed. The same plate was the bent again to 90° and recovered to a bend of about 10° when the force was removed. The bent plates are shown in Fig. 4.

Therefore, it can be concluded that U_3Si_2 fuel plates in irradiated elements have more than adequate toughness to maintain their integrity during handling and shipping. The differences in the characteristics of the B&W and CERCA fuel plates demonstrated by the bending test are believed to be related primarily to differences in the cladding.

5.6 Metallography

The outermost of the inner plates on the concave side of each element was sectioned for destructive examination according to the diagram in Fig. 5. The burnup analysis sections were cut from the minimum- and maximum-burnup areas of the plate as determined by the gamma scan profile. Sections were cut immedi-ately adjacent to the burnup analysis sections for optical metallography, Scanning Electron Microscopy (SEM), and Scanning Auger Microscopy (SAM). In order to characterize the unirradiated fuel, a section from one plate produced by each fabricator during the fabrication run for the test elements was also examined.

The metallographic sections were prepared for viewing (transverse to the length direction of the plate) using conventional techniques. The section was mounted in epoxy, ground on progressively finer silicon carbide paper through 600 grit, then vibratorily polished. The vibratory polishing was a three step process. The first and second steps were on a Texmet* cloth with a water medium and 3-μm and 1-μm diamond paste respectively. The final polish was on Microcloth* with a thick water slurry of Magomet* for 12 minutes.

The SEM and SAM samples were small discs, approximately 1.5 mm in diameter, punched from the irradiated plates. These discs were split parallel to the cladding surface, yielding two samples of a fracture surface through the fuel meat. The small sample size was needed to reduce gamma activity enough to allow examination outside the hot cell. SEM and SAM examinations of the unirradiated plates were performed on polished metallography samples.

Before proceeding with a discussion of the results of the metallographic examinations, some data obtained from miniplate irradiations that preceded the present full-sized fuel element experiments will be briefly reviewed. An example of the meat microstructure of a U_3Si_2 miniplate after >90% burnup is

*Texmet, Microcloth, and Magomet are trademarks of Buehler, Ltd.

shown in Fig. 6M.* Some of the noteworthy features in this optical micrograph are the absence of fission gas bubbles and the fact that all of the as-fabricated porosity has been consumed by fuel particle swelling. Fuel-aluminum interaction was limited to a narrow zone around the U_3Si_2 particles with a thickness about equal to the range of fission product recoils in aluminum. SEM examination of fractured fuel particles reveals a gas bubble morphology typical of pure U_3Si_2, as shown in Fig. 7M. The very uniform distribution of small gas bubbles that show no tendency to interlink is the reason for the stable swelling behavior of U_3Si_2.

The microstructural changes in U_3Si miniplates resulting from irradiation to high burnups are quite different, as shown in Fig. 8M. Fission gas bubbles are clearly visible in the optical micrograph. The bubble morphology, more clearly shown in the SEM images in Fig. 9M, reveals a basic difference in fission gas behavior between U_3Si and U_3Si_2. The fission gas bubbles in U_3Si are clearly not uniformly distributed and vary widely in size. The large bubbles are growing rapidly and linking up, resulting in a much larger fuel swelling rate than that of U_3Si_2. As will be shown further on in this report, the fuel in the full-sized U_3Si_2 plates exhibits characteristics of both U_3Si_2 and U_3Si.

Several uranium silicide miniplates fabricated with depleted uranium were irradiated to determine the effects of neutrons, as opposed to fission fragments, on the fuel. Figs. 10M and 11M clearly show that irradiation-enhanced diffusion has occurred.

The microstructure of the fuel as it changes during irradiation is discussed in alphabetical order for the three fabricators, beginning with the low-burnup plate in each case, followed by the high-burnup plate, and concluding with some observations on unirradiated fuel. The micrographs used in the discussion represent the typical fuel condition observed under the microscope. The serial number of the fuel element rather than that of the specific fuel plate from which the sample came is used for simplicity; plate numbers are the same as those from which burnup samples were taken (See Appendix G, Table G.8). Burnups are those measured for samples taken adjacent to the metallographic sections. Thickness changes are averaged for five plates from the element in order to reduce the considerable scatter in the data.

The B&W fuel meat microstructure at the low-burnup (31%) end of plate BSI-201 is shown in Figs. 12B-16B. A large fraction of the as-fabricated porosity is still present, and the fuel swelling that has taken place is easily accommodated by these pores. This is consistent with the fact that no

*A large number of photomicrographs are presented in this section, grouped by fabricator. So that each figure can easily be associated with the fabricator in the discussions to follow, a letter designating the fabricator has been appended to the remaining figure numbers, as follows: M - Miniplates (fabricated by ANL); B - B&W; C - CERCA; N - NUKEM.

thickness increase has occurred at this end of the plate. A narrow interaction zone between fuel particles and aluminum, as well as the rounding of the pores by radiation-enhanced diffusion, can be seen in Fig. 13B. Except for the somewhat-more-extensive Al-fuel interaction inside some of the particles, the structure is similar to that of irradiated depleted U_3Si_2 miniplates shown in Figs. 10M-11M. Figure 14B is a typical SEM image taken at the low-burnup end of the plate. The fuel appears free of fission gas bubbles at this magnification and the smoothed as-fabricated porosity is clearly evident. However, at higher magnification, areas containing small fission gas bubble populations were found in a few fuel particles, as shown in Figs. 15B and 16B. Figure 16B was taken using the backscatter electron (BSE) detector in order to show the different phases in the fuel more clearly. In this figure, as well as in the backscatter images to follow, the image intensity is proportional to the atomic number of the material. The light phase containing the small bubbles is, therefore, the highest U-Si phase present whereas the other extreme shading, black, represents matrix aluminum.

A considerably larger number of fission gas bubbles have formed in the fuel at the high-burnup (71%) end of plate BSI-201, and the fuel swelling has nearly consumed all as-fabricated porosity; only a few pores (the irregularly shaped ones in Figs. 17B and 18B) remain. Fuel swelling has resulted in a plate thickness increase of 38 μm at this location. The fuel has essentially three different phases with regards to gas bubble morphology: (1) the lighter phase that appears to be bubble free; (2) a light grey phase containing many very small bubbles; and (3) isolated irregular clusters of larger bubbles. SEM images, shown in Figs. 19B-22B, more clearly distinguish two very different bubble morphologies. The areas containing irregular, larger-sized bubbles look similar to U_3Si fuel observed in the miniplates, while areas containing dense and uniform small bubbles appear identical to U_3Si_2.

The low-burnup end of plate BSI-202 reached a burnup of 51%. No thickness increase was measured at the this location, and the fuel microstructure is not much different from that of the low-burnup end of plate BSI-201, as shown in Figs. 23B and 24B.

The high-burnup (97%) end of plate BSI-202 had a measured thickness increase of 46 μm, and, indeed, the fuel microstructure has somewhat-more-developed fission gas bubbles. As was the case at 71% burnup in plate BSI-201, three distinct phases exist in the fuel (see Figs. 25B-27B). The SEM images in Figs. 28B-33B show examples of the fission gas behavior in these three fuel phases. The major phase has a bubble morphology characteristic of pure U_3Si_2 (Fig. 33B), while parts of several fuel particles have either a characteristic U_3Si bubble morphology (Figs. 30B and 31B) or, as shown in Fig. 32B, a total absence of bubbles and apparent brittle properties reminiscent of UAl_4.

The different fission gas behavior in parts of the ostensibly pure U_3Si_2 fuel grains can be understood through the results of a detailed microscopic examination of an unirradiated fuel plate. As shown in Figs. 34B-36B, the

fuel particles are not single-phase U_3Si_2; rather, they contain both U_3Si and U, as determined by energy dispersive x-ray analysis (Fig. 37B). The Si-to-U ratios of phases A and B identify them as, respectively, U_3Si_2 and U_3Si, while the absence of Si in phase C indicates U_{ss}. Therefore, the U_3Si and U_3Si_2 show their characteristic irradiation behaviors, and the U_{ss} presumably reacts with Al during irradiation to form the stable UAl_4 compound. UAl_4 is indeed very stable and has never been found to contain fission gas bubbles. Therefore, the presence of U_{ss} in the as-fabricated fuel appears not to be detrimental to the performance of the fuel plate. This is consistent with the results of miniplate tests of UAl_2 fuel containing U_{ss} in the as-fabricated condition.[10] Even though the U_3Si was found to contain all the larger bubbles, its amount is such that no continuous network of large bubbles can develop, even at the very high burnup attained in these plates. It has been established in miniplate irradiations that interparticle linkup of larger bubbles is a prerequisite for possible large swelling in U_3Si.

The low-burnup (33%) end of plate CSI-201 may have just begun to show a thickness increase (3 μm was measured at this location). This may owe to the lower as-fabricated porosity of the CERCA plates (4%) than for the B&W plates (9 to 10%). Indeed the microstructure shown in Figs. 38C and 39C illustrates the rather low residual porosity at this burnup compared to that in the B&W plates discussed before (cf. Figs. 12B and 13B). The narrow interaction zone at the fuel particle surface is also seen in this fuel, but no significant amount of fuel-Al reaction phase inside the fuel particles is present.

The high-burnup (67%) end of plate CSI-201, with a thickness increase of 43 μm, has a fuel microstructure in which the fuel swelling has completely consumed the as-fabricated porosity and in which the fuel particles have begun to develop fission gas bubbles (see Figs. 40C and 41C). This is shown in more detail in the SEM images in Figs. 42C-45C. The phase in which larger bubbles occur (presumably U_3Si) is more dispersed, in a stringy or lacy manner, than in the B&W fuel.

The fuel microstructure at the low-burnup end (55%) of plate CSI-202 is very similar to that of plate CSI-201 (see Figs. 46C-51C). The thickness increase at this location is 23 μm.

The high-burnup (97%) end of plate CSI-202 has a measured thickness increase of 112 μm, more than twice that of the B&W plate. The fuel microstructure shows basically the same two-phase fission gas morphology seen in plate BSI-202, with the U_3Si-type bubbles more evenly distributed throughout the fuel (see Figs. 52C-57C). The total fission gas bubble volume appears to be significantly larger than that seen in the B&W plates, as would be expected from the much larger thickness increase experienced by the CERCA plates. Some of this larger thickness increase is attributable to the 4% porosity of the CERCA fuel meat compared to the 9-10% porosity of the B&W fuel meat, but the largest part of the difference undoubtedly owes to a larger amount of U_3Si in the CERCA plates.

The fission gas bubble behavior is, in fact, consistent with the as-fabricated fuel microstructure. The CERCA fuel did contain more U_3Si than did the B&W fuel (compare, for example, Figs. 58C and 34B), and it was more finely distributed than in the B&W fuel. The CERCA fuel did not contain U_{ss} because it had been heat treated, hence the absence of the UAl_4-like phase in the irradiated plate. It did, however, contain a powdery, grey phase (see Fig. 59C) which, by means of Auger Electron Spectroscopy, was found to contain oxygen and carbon in addition to U, Si, and Al. No trace of this material was found in the irradiated plates and it is assumed that it reacted in-pile to form a compound not distinguishable from the common fuel phases.

The fuel microstructure of the low-burnup (24%) end of NUKEM plate NSI-201 (shown in Figs. 61N-66N) was essentially the same as that of the low-burnup plates discussed before. The fuel consisted of U_3Si_2 with a somewhat coarsely distributed (compared to the CERCA fuel) second phase. The amount of second phase in this fuel appeared to be the highest of the three, albeit still minor. The second phase, and the tendency for gas bubbles to occur first in this phase, is more clearly illustrated in the microstructure at the high-burnup (51%) end of plate NSI-201, shown in Figs. 67N-72N. SAM analysis of the irradiated fuel positively identified the light phase containing the irregular bubbles in Fig. 72N as U_3Si, while the remainder of the fuel was identified as U_3Si_2.

The fuel at the low-burnup (54%) end of plate NSI-202, shown in Figs. 73N-78N, had the expected microstructure, with the beginning of small uniform bubble formation in U_3Si_2 (see Figs. 77N-78N) and continued irregular bubble development in U_3Si (see Fig. 76N). The high-burnup (96%) end of plate NSI-202, shown in Figs. 79N and 80N, had a measured thickness change of 104 μm. The fission gas bubble morphology is rather similar to that of the other high-burnup plates with a two-phase behavior, as clearly illustrated in Figs. 81N-83N.

As was the case for the B&W and CERCA fuels, the fission gas behavior can be traced to the microstructure of the as-fabricated fuel. The SEM images in Figs. 84N-87N show a major, dark grey, brittle phase, identified by energy dispersive x-ray analysis as U_3Si_2, interlaced with a more ductile light phase, U_3Si. The light phase occurs primarily in the largest fuel particles, acting as a bond during grinding, due to its more ductile properties. As indicated before, the NUKEM fuel appears to contain slightly more U_3Si than the CERCA fuel, and because this fuel was heat treated, it does not contain U_{ss}. It also does not contain the powdery oxy-carbide-like phase found in the CERCA fuel.

In conclusion, the metallographic observations are consistent with the relatively small plate thickness increases experienced during irradiation. The swelling is primarily caused by formation of two distinct fission gas bubble morphologies. The by-far-major phase, U_3Si_2, developed a very uniform and dense distribution of submicron-sized bubbles, characteristic of this

fuel. The second silicide phase, U_3Si, which occurred in different amounts in the three fuels, developed its characteristic coarse, non-uniform bubble morphology. The amount of U_3Si and its larger swelling account, with the as-fabricated porosity, for the variability in overall plate swelling between plates of the different fabricators.

The similarity of the average thickness changes in the high-burnup regions of elements CSI-202 and NSI-202 suggest that differences in bubble morphology may not be as great as comparison of Figs. 52C and 79N seem to indicate. Since only one section from the high-burnup region of CSI-202 was examined, there is a possibility that the section was atypical.

The non-U_3Si_2 phases present in the fuels are a result of fabrication practices. It is not possible, on a commercial scale, to produce a perfectly homogeneous alloy with the exact composition of a line compound such as U_3Si_2. Heat treatment of the ingots employed by CERCA and NUKEM and not by B&W would explain the absence of U_{ss} in their fuel. The oxy-carbide-like phase present in the CERCA fuel could be related to the larger amount of fuel fines (with much larger surface-to-volume ratio) used by CERCA. However, the U_{ss} phase found in the B&W plates and the oxy-carbide-like phase in the CERCA plates evidently react with aluminum during irradiation and have no deleterious effects on the swelling behavior of the fuel.

6. SUMMARY AND DISCUSSION OF RESULTS

The postirradiation examination of these low-enriched U_3Si_2 fuel elements confirmed the excellent behavior experienced during their irradiation and expected from previous miniplate tests. The dimensional examinations, visual examinations, coolant channel measurements, and destructive examinations revealed no abnormalities or evidence of undesirable behavior.

In general, the microstructures were as expected from previous miniplate irradiations, revealed no abnormal conditions, and were consistent with the measured thickness increases. No, or very little, swelling was measured for the areas where fabrication porosity remained. The CERCA and NUKEM plates, which contained more of the U_3Si phase, showed more areas where large gas bubbles were beginning to form and more thickness change. The B&W plates, which contained some U_{ss} as fabricated and less U_3Si, showed fewer areas with large bubbles forming and less thickness change. The U_{ss} apparently converted to UAl_4 during irradiation and retained the gas.

These minor differences in postirradiation microstructure reflect the differences in fabrication practices of the manufacturers at the various times of fabrication. For example, when NUKEM fabricated the first two U_3Si_2 elements, it was not known that U_3Si behaved differently under irradiation than U_3Si_2 and that it might be desirable to control the amount of U_3Si in the fuel powder. The results of the metallographic examinations presented and

discussed in Section 5.6 have concentrated on these differences because, through their explanations, the overall understanding of the effects of the different phases on irradiation behavior has been confirmed.

The completely satisfactory behavior of these six U_3Si_2 fuel elements in the ORR, three of which were operated to >75% burnup, must be emphasized. The swelling of the fuel plates was stable and small in comparison to allowed fabrication tolerances for coolant channel gap thicknesses, even at 98% burnup of the ^{235}U and 2.5×10^{27} f/m^3. The variety of as-fabricated attributes of the fuel meat--most importantly, the different fuel phases present and the different fuel meat porosities and densities--appear to cover the range of attributes to be expected in U_3Si_2 fuel elements fabricated in the future.

7. CONCLUSION

Postirradiation evaluations of low-enriched U_3Si_2 fuel elements irradiated in the ORR have confirmed their expected satisfactory performance. Peak burnups ranged up to 98%--far above that expected from normal reactor operation. Externally, the elements were essentially unchanged from their as-fabricated condition, both dimensionally and visually. The plates showed small, uniform thickness changes. Blister threshold temperatures were at the upper end of the range of those typical of current fuels.

It is concluded from the results of these tests that low-enriched U_3Si_2-aluminum dispersion fuel elements will perform at least as well in research and test reactors with power densities up to that of the ORR as the highly enriched UAl_x-aluminum and U_3O_8-aluminum dispersion fuels currently being used. There were no indications that use of this fuel under substantially more stringent conditions might be precluded.

ACKNOWLEDGMENTS

Many persons made important contributions to the work reported here during the approximately seven years required to plan, perform, and analyze the results. The authors especially acknowledge the contributions of personnel associated with ORR operations, the HRLEL at ORNL, and the Alpha-Gamma Hot Cells at ANL. Particular thanks are extended to E. D. Clemmer for performing the in-pool channel gap scans and to L. G. Shrader for assistance in following the progress of the examinations.

REFERENCES

1. A. Travelli, "Current Status of the RERTR Program," Proc. Int. Mtg. on Development, Fabrication and Application of Reduced Enrichment Fuels for Research and Test Reactors, Argonne, Illinois, November 12-14, 1980, ANL/RERTR/TM-3, CONF-801144, pp. 3-13 (1983).

2. J. L. Snelgrove, G. L. Hofman, and G. L. Copeland, "Irradiation Performance of Reduced-Enrichment Fuels Tested Under the U.S. RERTR Program," Reduced Enrichment for Research and Test Reactors--Proceedings of an International Meeting, Petten, The Netherlands, October 14-16, 1985, P. von der Hardt and A. Travelli, Eds., D. Reidel Publishing Company, Dordrecht, pp. 59-68 (1986).

3. R. L. Senn and M. M. Martin, "Irradiation Testing of Miniature Fuel Plates for the RERTR Program," Oak Ridge National Laboratory Report ORNL/TM-7761 (July 1981).

4. D. Stahl, "Status of U.S. Development Program for High-Uranium Density Reduced-Enrichment Plate-Type Fuels," presented at the Seminar on Research Reactor Operation and Use, Jülich, Fed. Rep. of Germany, September 14-18, 1981.

5. G. L. Hofman and L. A. Neimark, "Irradiation Behavior of Uranium Silicide Dispersion Fuels," Proc. Int. Mtg. on Reduced Enrichment for Research and Test Reactors, October 24-27, 1983, Tokai, Japan, JAERI-M 84-073, pp. 43-53 (May 1984).

6. G. L. Hofman and L. A. Neimark, "Postirradiation Examination of Experimental Uranium Silicide Dispersion Fuel Plates," Proc. 1984 Int. Mtg. on Reduced Enrichment for Research and Test Reactors, October 15-18, 1984, Argonne, Illinois, ANL/RERTR/TM-6, CONF-8410173, pp. 75-85 (July 1985).

7. J. M. Beeston, R. R. Hobbins, G. W. Gibson, and W. C. Francis, "Development and Irradiation Performance of Uranium Aluminide Fuels in Test Reactors," Nucl. Tech. 49, 136-149 (June 1980).

8. A. E. Richt, R. W. Knight, and G. M. Adamson, Jr., "Postirradiation Examination and Evaluation of the Performance of HFIR Fuel Elements," Oak Ridge National Laboratory Report ORNL-4714 (Dec. 1971).

9. J. L. Snelgrove, "RERTR Program Fuel Testing and Demonstration - An Update," Proc. 1984 Int. Mtg. on Reduced Enrichment for Research and Test Reactors, October 15-18, 1984, Argonne, Illinois, ANL/RERTR/TM-6, CONF-8410173, pp. 137-145 (July 1985).

10. J. Gómez, R. Morando, E. E. Pérez, D. R. Giorsetti, G. L. Copeland, G. L. Hofman and J. L. Snelgrove, "Postirradiation Examination of High-U-Loaded, Low-Enriched U_3O_8, UAl_2, and U_3Si Test Fuel Plates," Proc. 1984 Int. Mtg. on Reduced Enrichment for Research and Test Reactors, October 15-18, 1984, Argonne, Illinois, ANL/RERTR/TM-6, CONF-8410173, pp. 86-102 (July 1985).

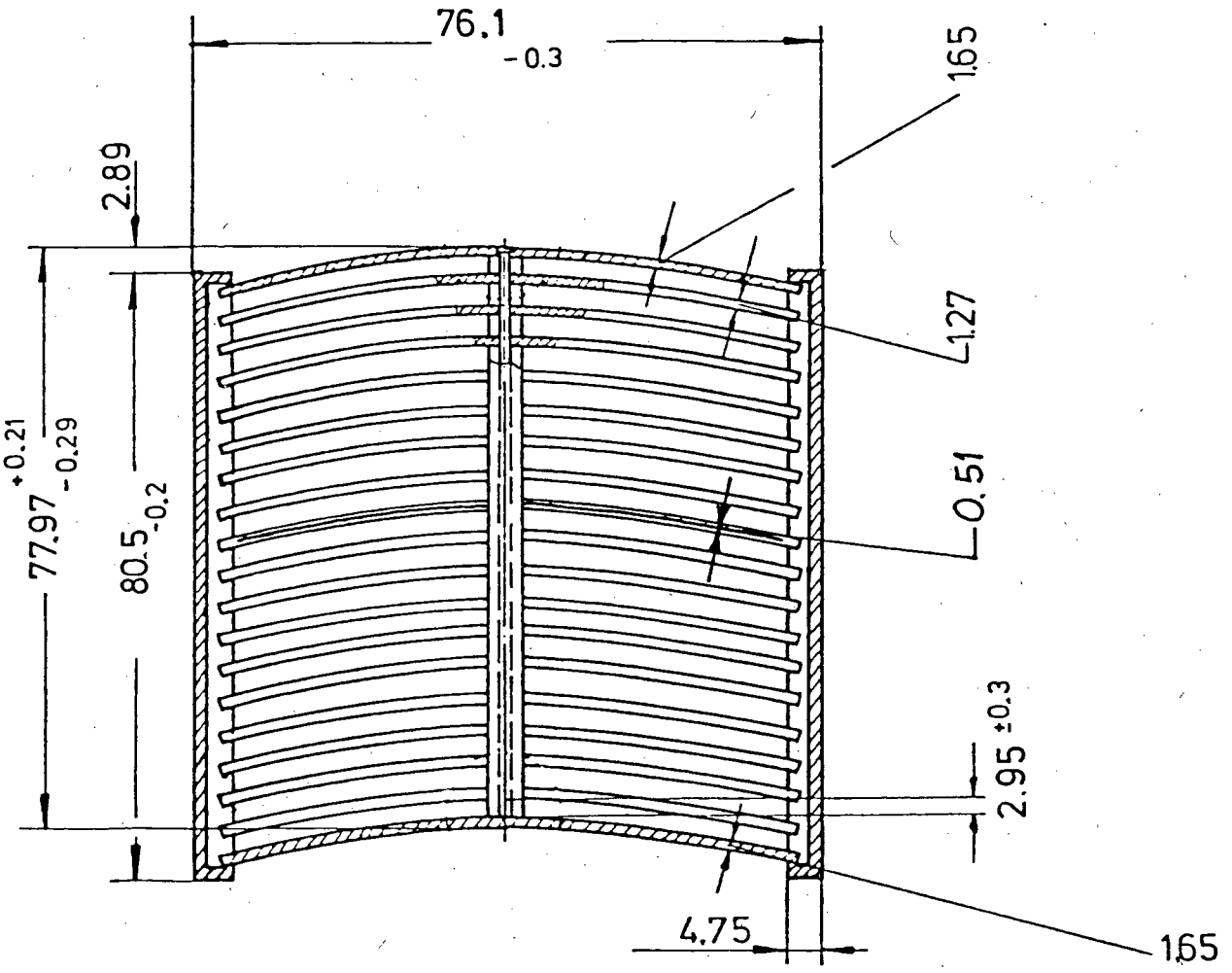

Fig. 1. Cross Section of Standard 19-Curved-Plate ORR Fuel Element.

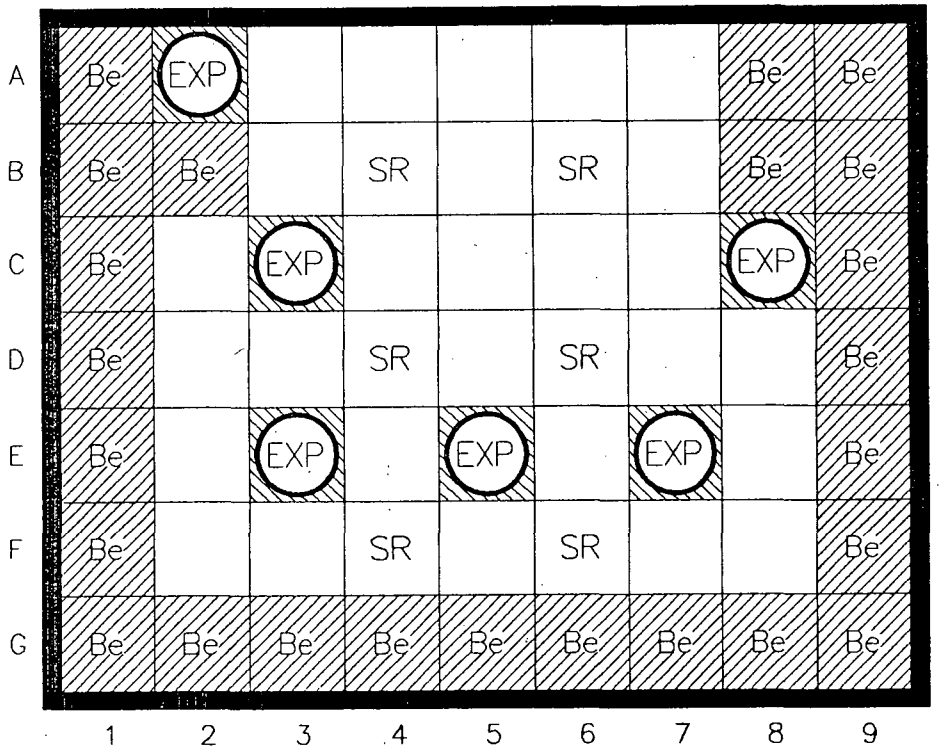

Configurations 161-C Through 167-A, 5/27/82 Through 2/23/84

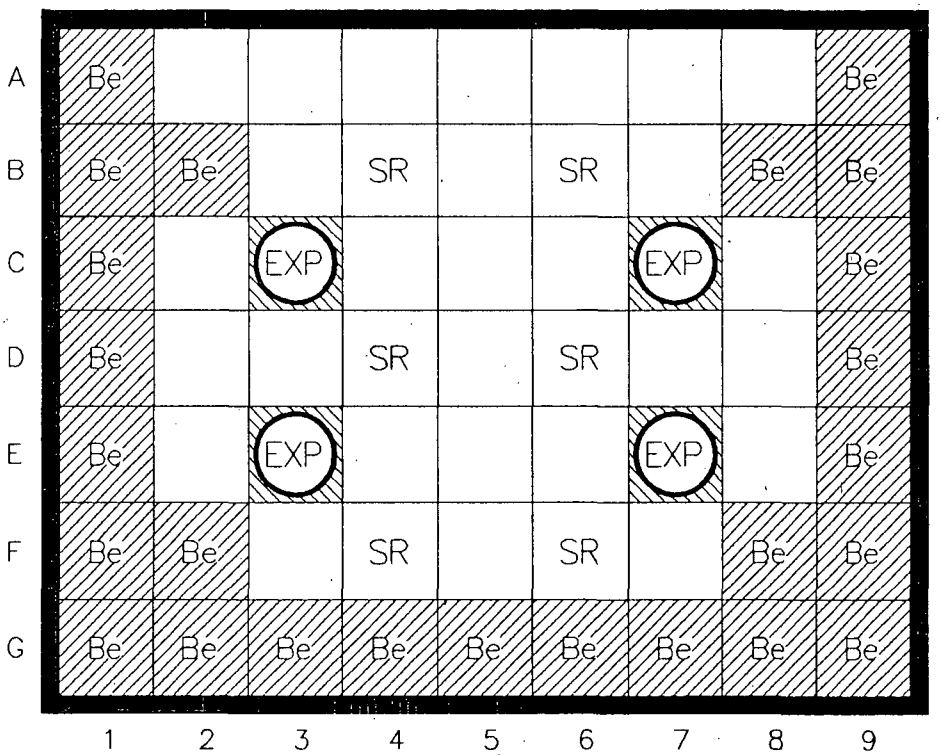

Configurations 167-C Through 170-C, 3/07/84 Through 12/19/84

Fig. 2. Basic Core Configurations During Irradiation of U_3Si_2 Elements.

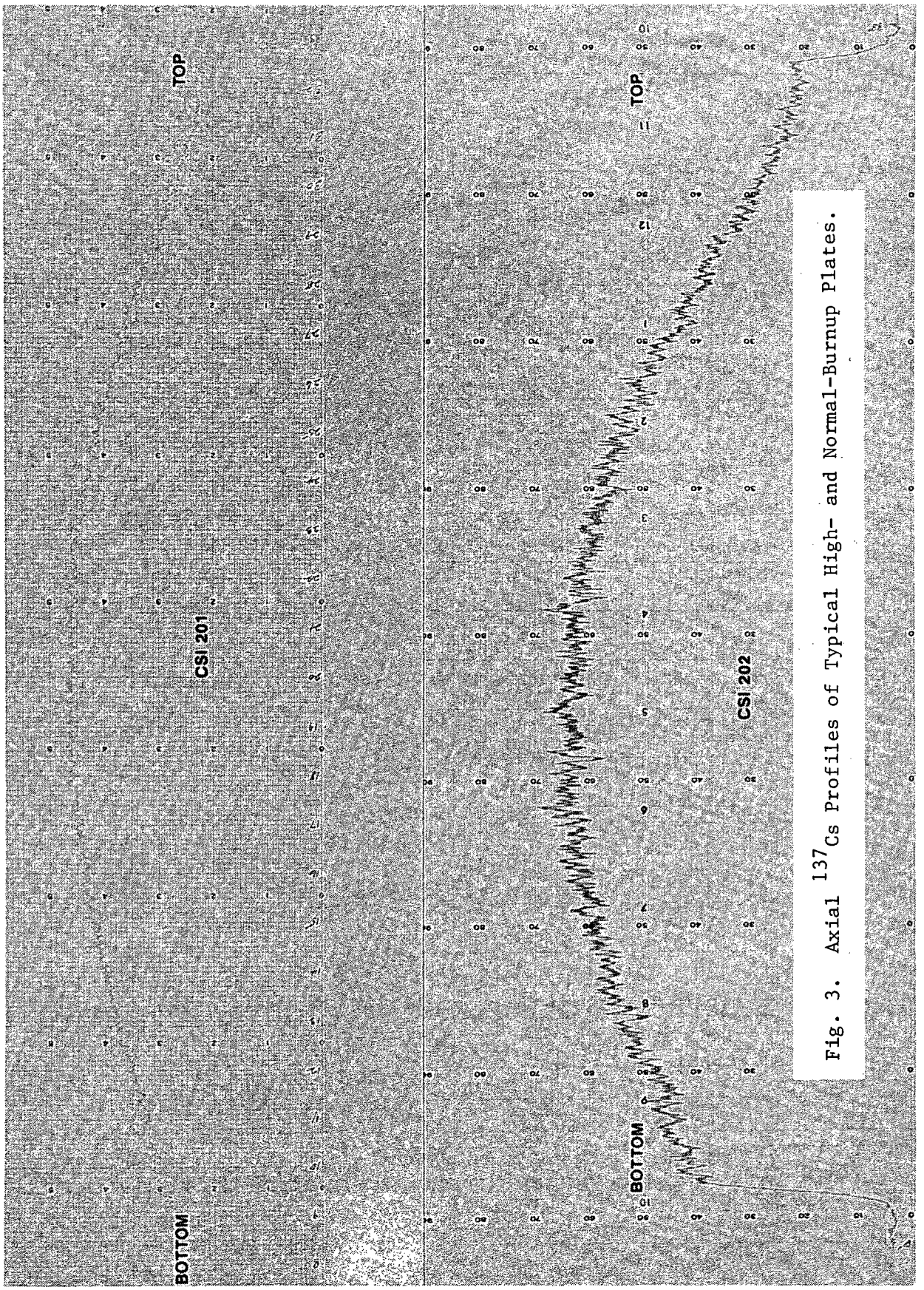

Fig. 3. Axial ^{137}Cs Profiles of Typical High- and Normal-Burnup Plates.

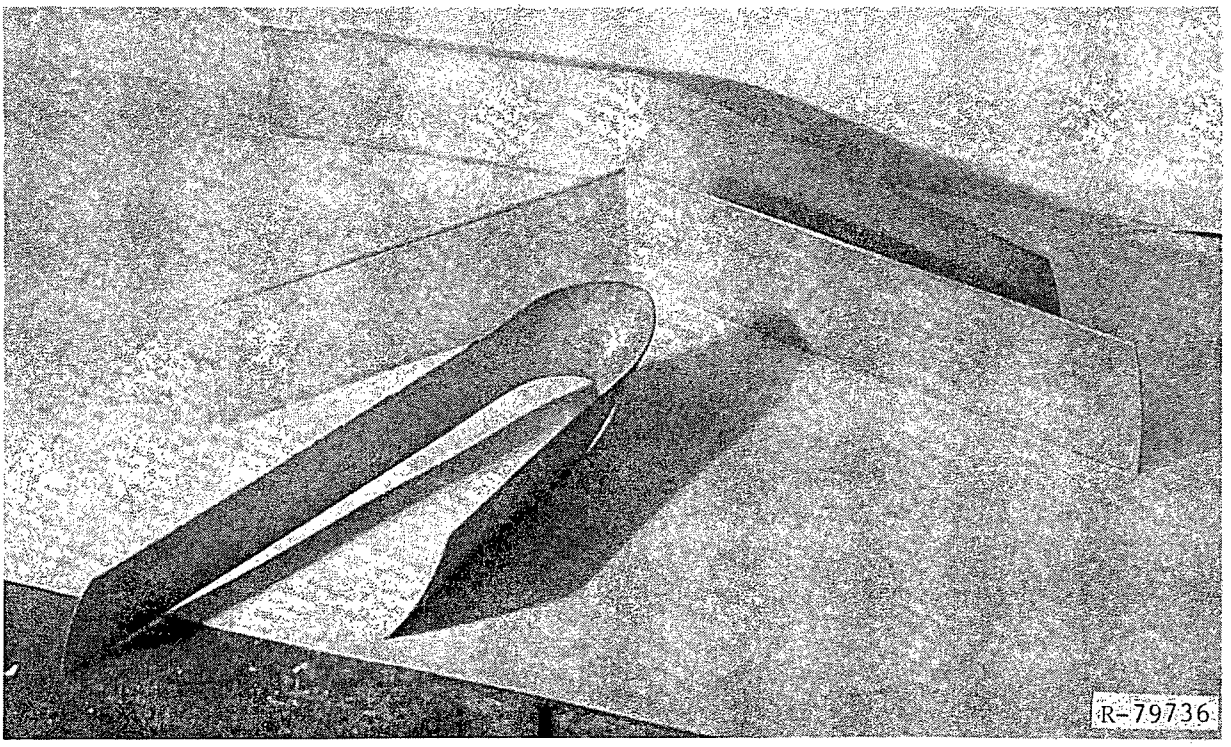

Fig. 4. Photograph of Three Plates After Bending to Evaluate Toughness.

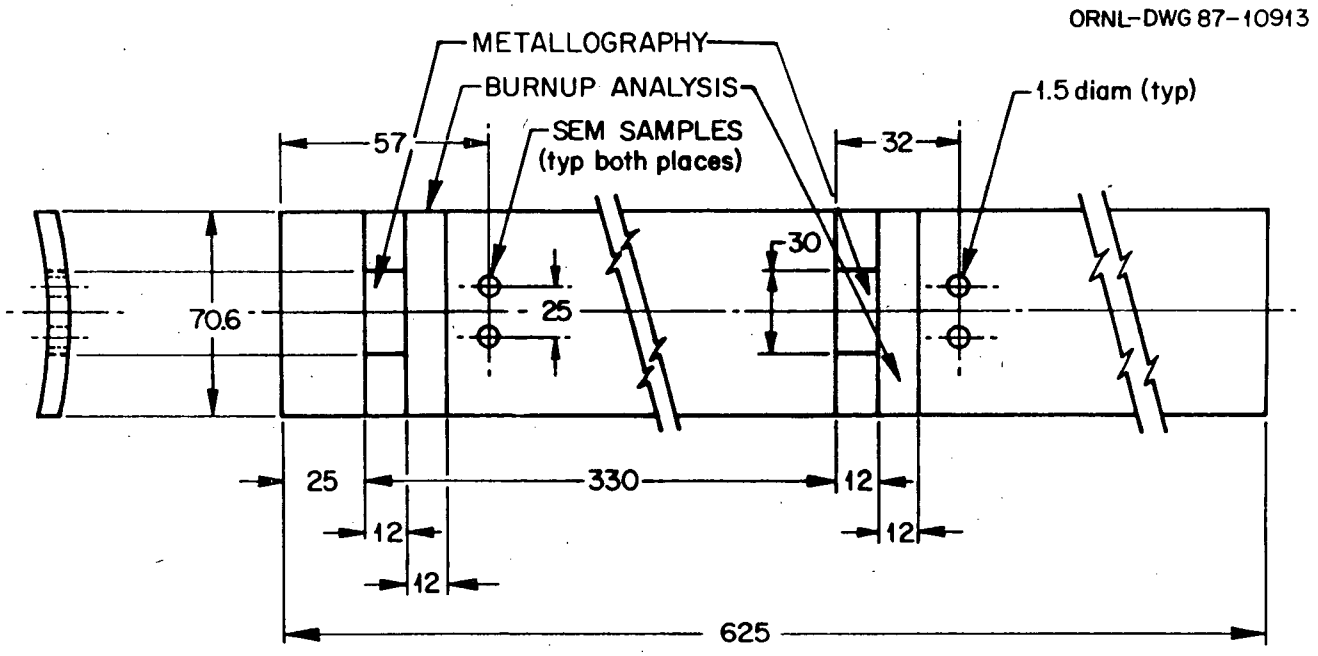

Fig. 5. Sectioning Diagram for Destructive Evaluation of Plates.

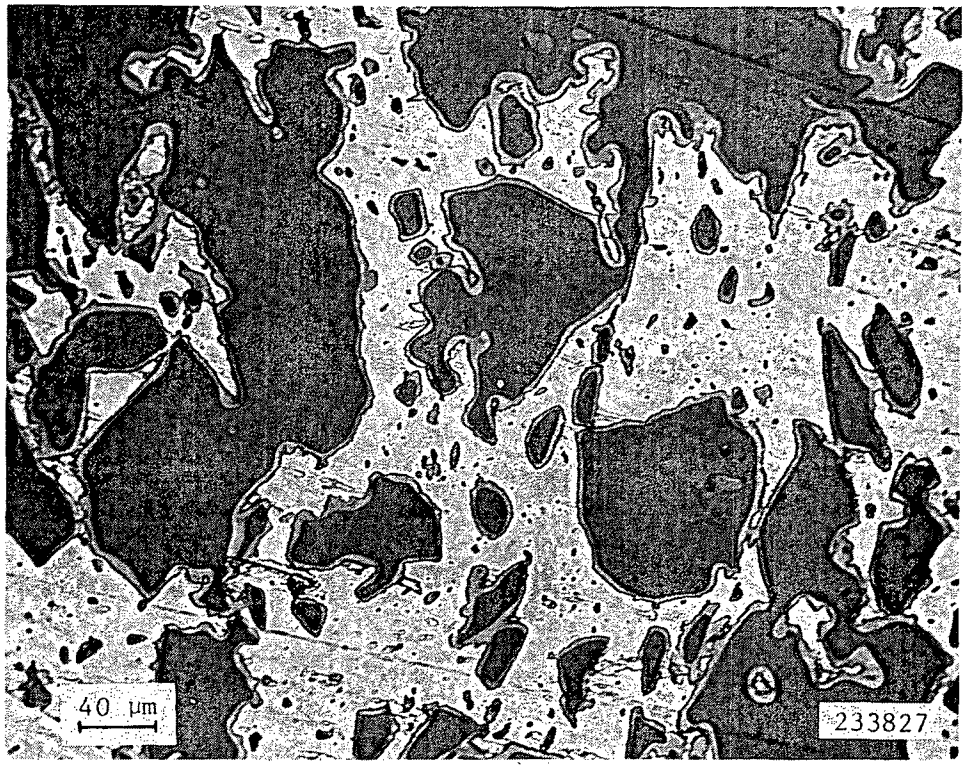

Fig. 6M. Meat Microstructure of U_3Si_2 Miniplate After 90% Burnup (Bu).

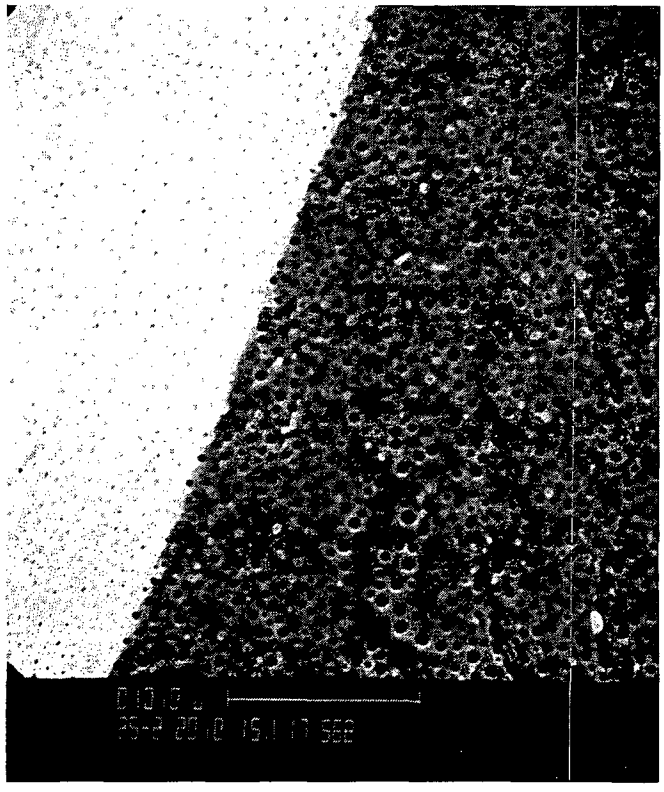

Fig. 7M. Fission Gas Bubble Morphology in U_3Si_2 After 90% Bu.

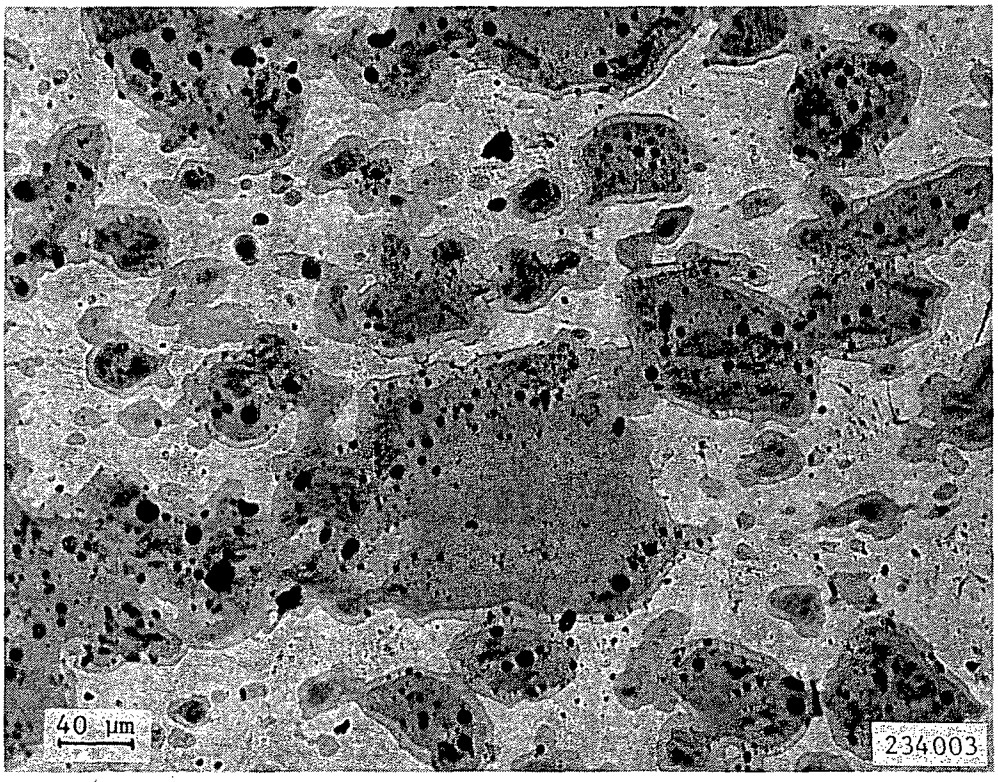

Fig. 8M. Meat Microstructure of U_3Si Miniplate After 90% Bu.

Fig. 9M. Fission Gas Bubble Morphology in U_3Si After 90% Bu.

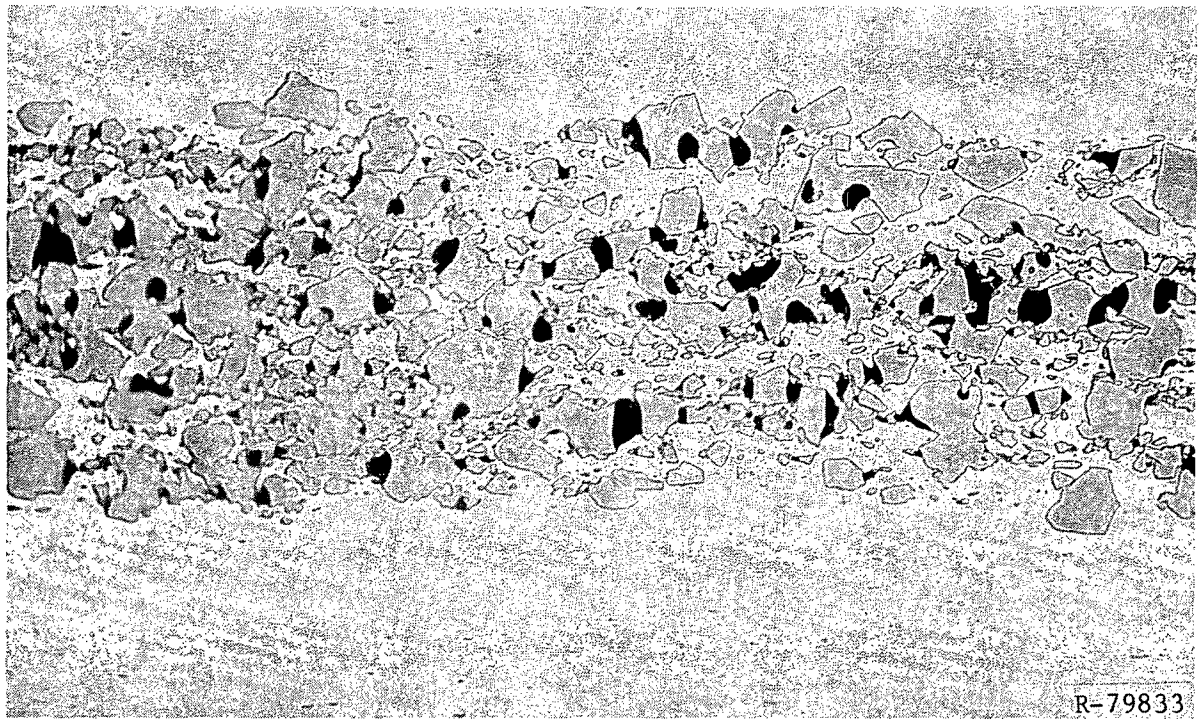

200 μm

Fig. 10M. Meat Microstructure of Irradiated Depleted U_3Si_2 Miniplate.

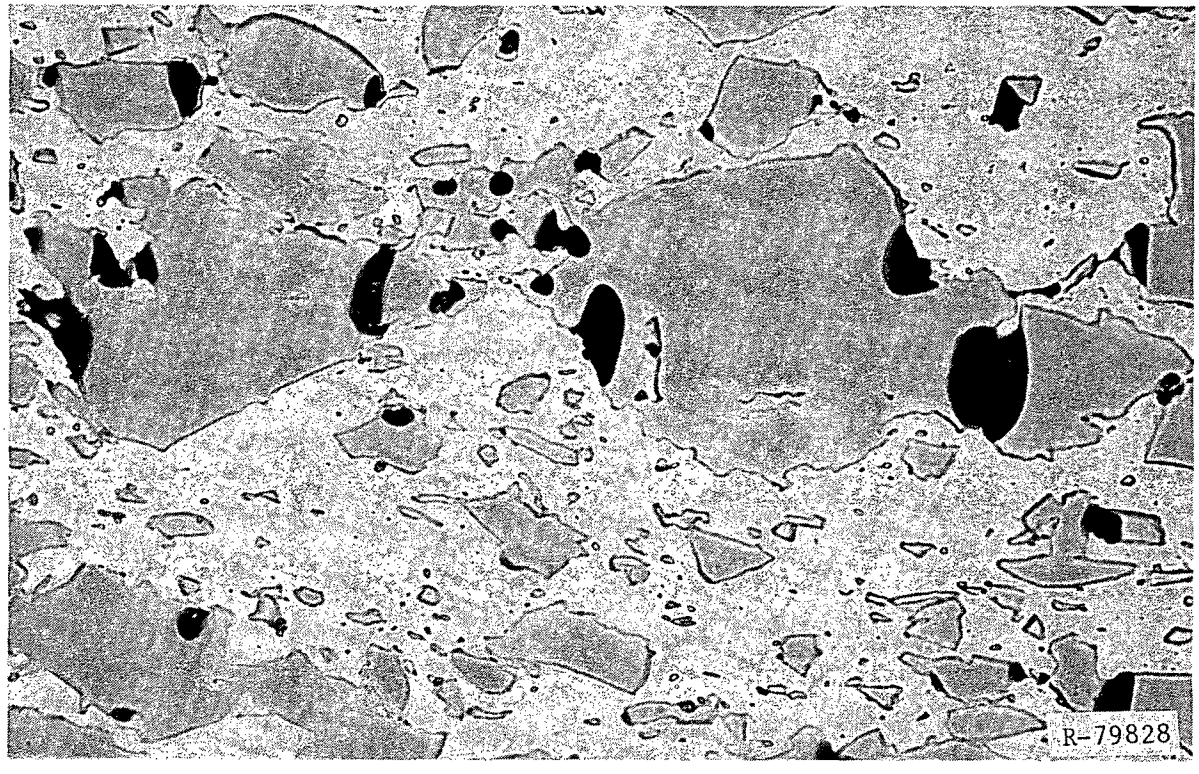

40 μm

Fig. 11M. Detail of Fig. 10M.

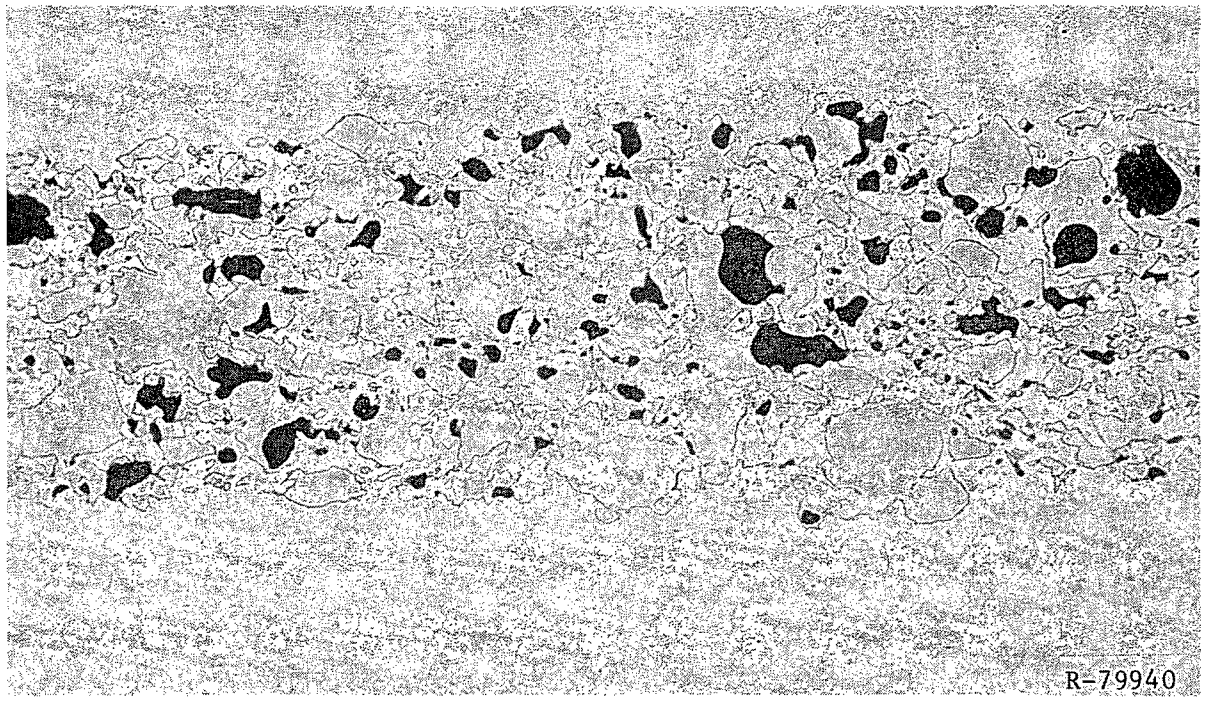

Fig. 12B. Meat Microstructure of Plate BSI-201, at 31% Bu.

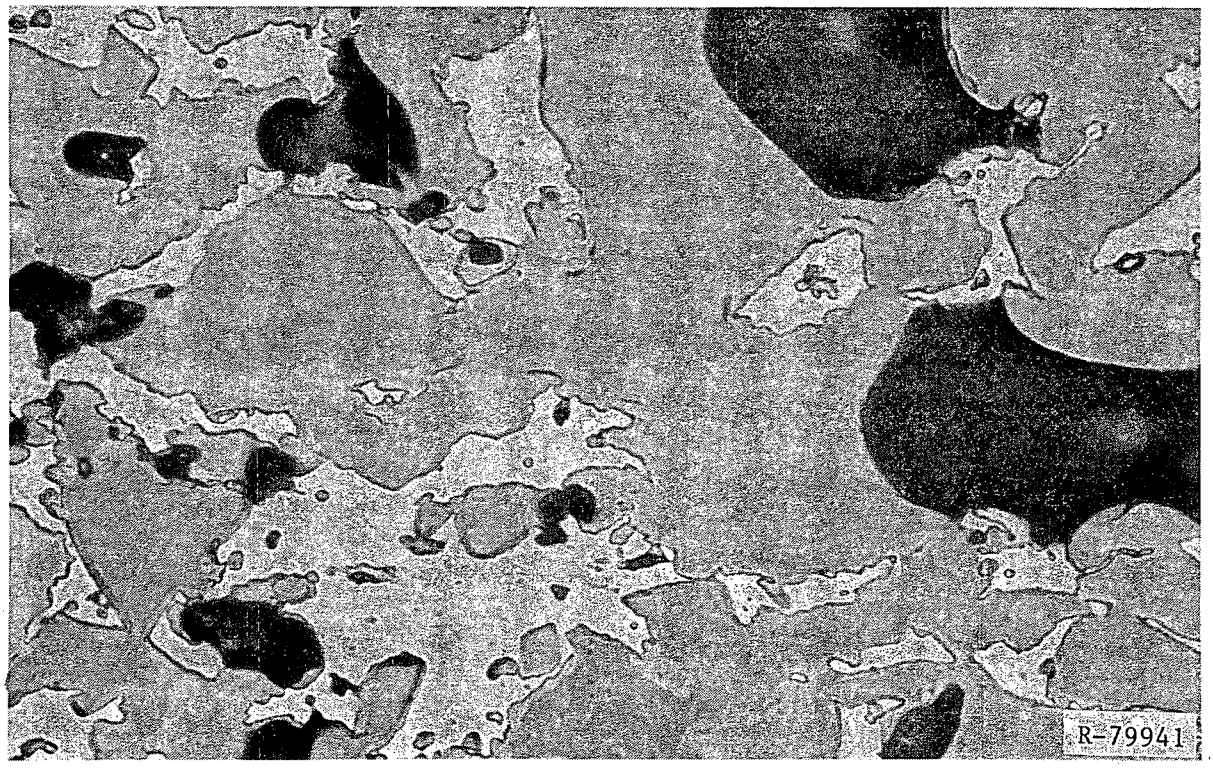

Fig. 13B. Detail of Fig. 12B.

Fig. 14B. SEM Image of Fuel Meat of Plate BSI-201, at 31% Bu.

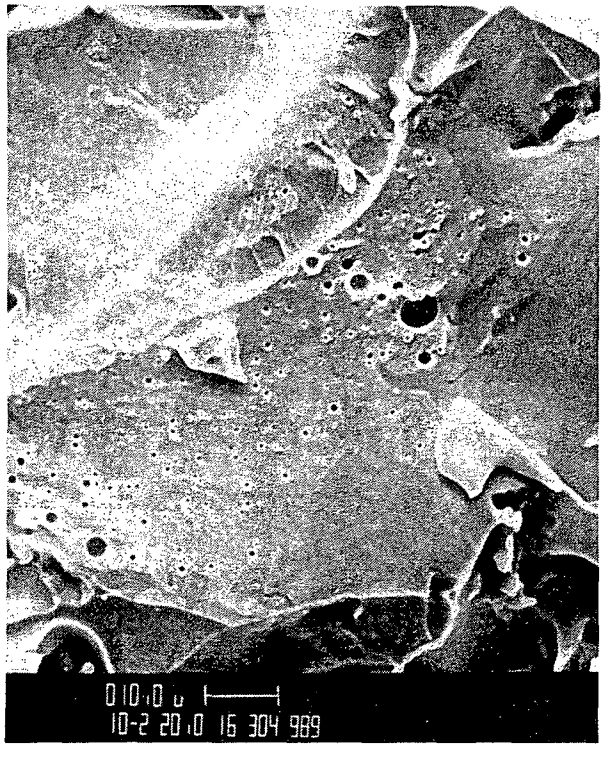

Fig. 15B. Detail of Fig. 14B.

Fig. 16B. Idem Fig. 15B, BSE Mode.

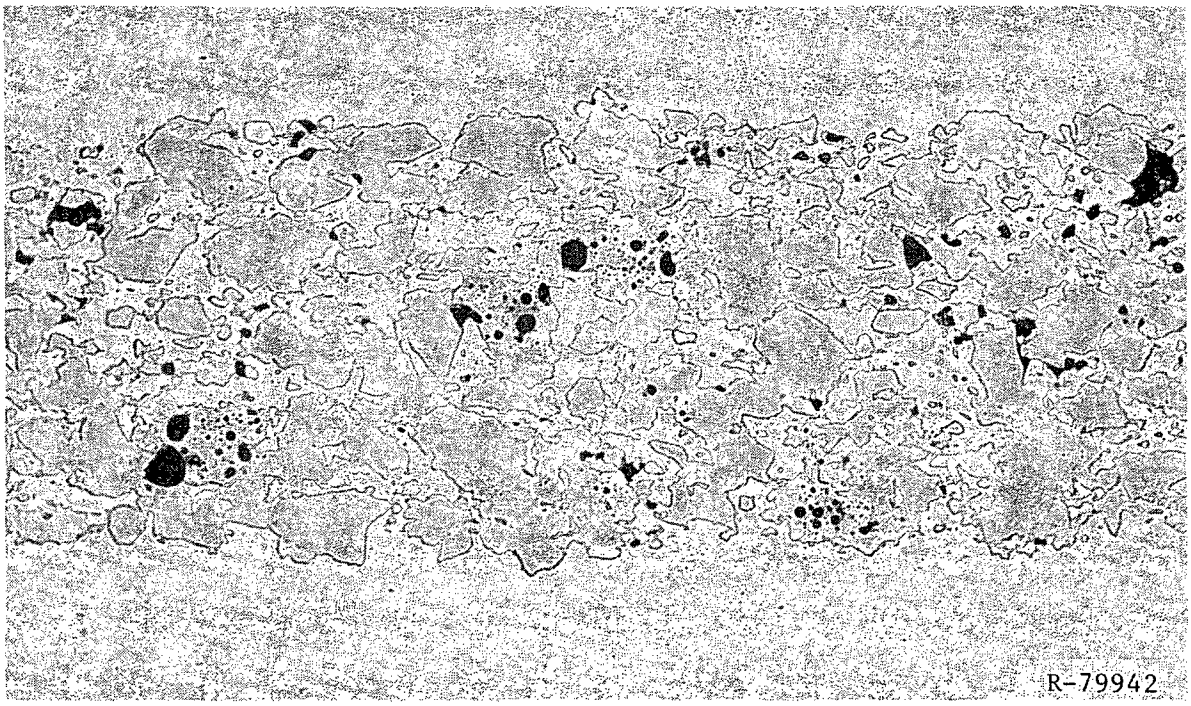

Fig. 17B. Meat Microstructure of Plate BSI-201, at 71% Bu.

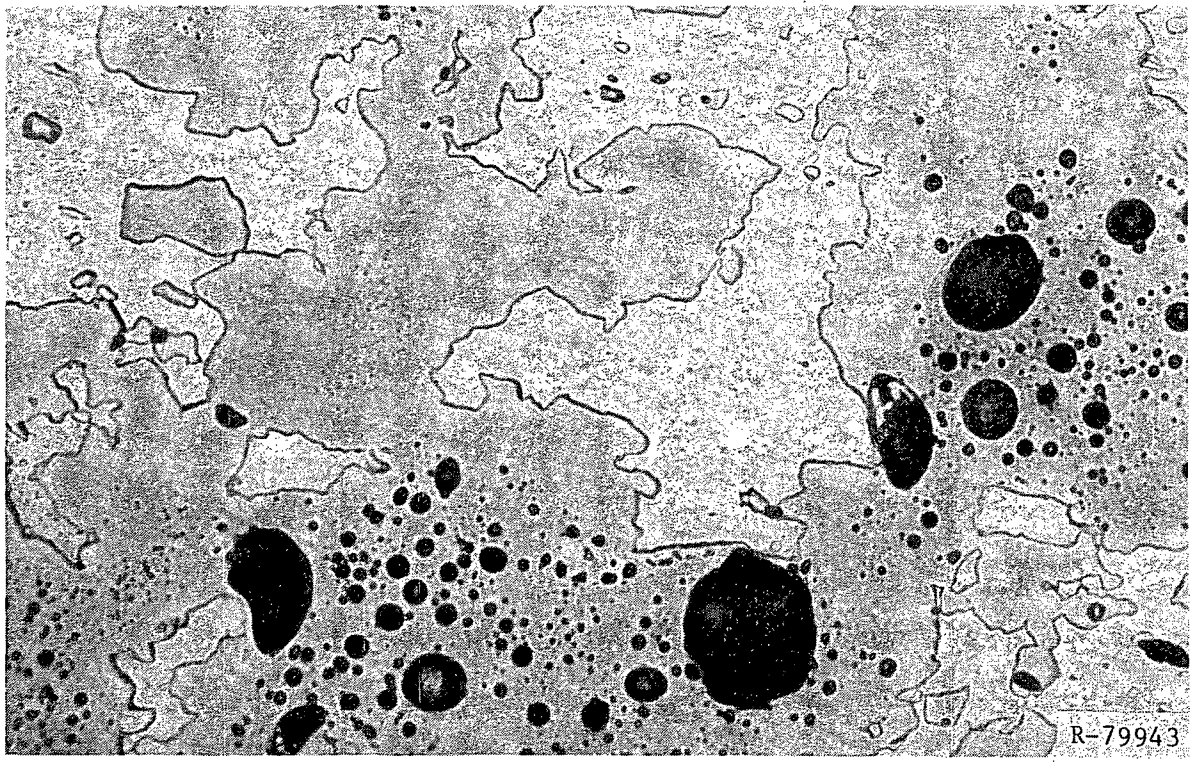

Fig. 18B. Detail of Fig. 17B.

Fig. 19B. SEM Image of Fuel Meat of Plate BSI-201, at 71% Bu.

Fig. 20B. Detail of Fig. 19B.

Fig. 21B. Detail of Fig. 19B.

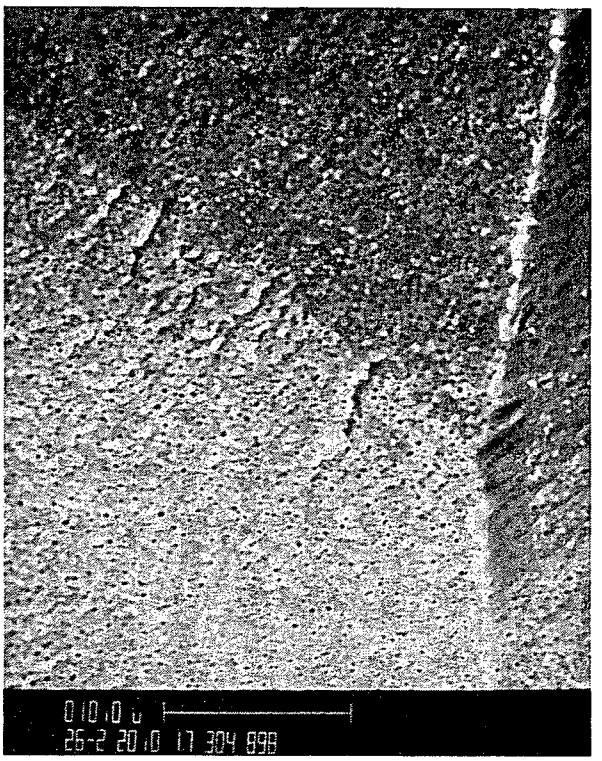

Fig. 22B. Detail of Fig. 19B.

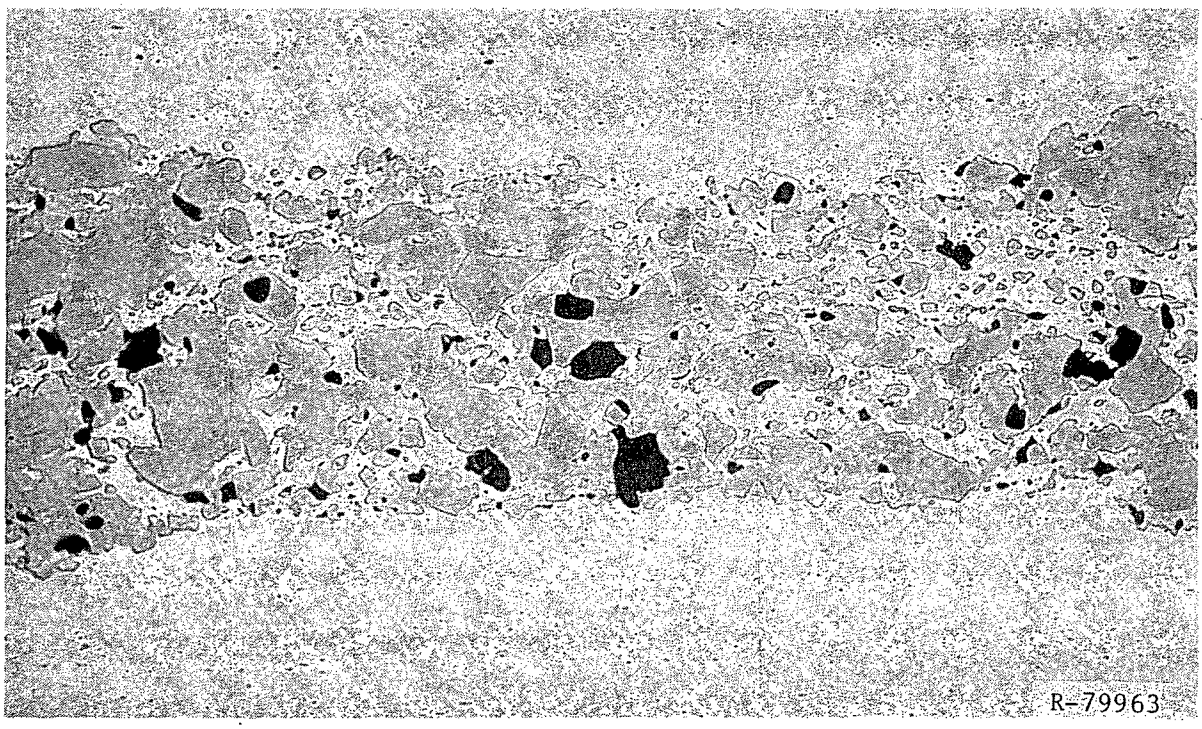

Fig. 23B. Meat Microstructure of Plate BSI-202, at 51% Bu.

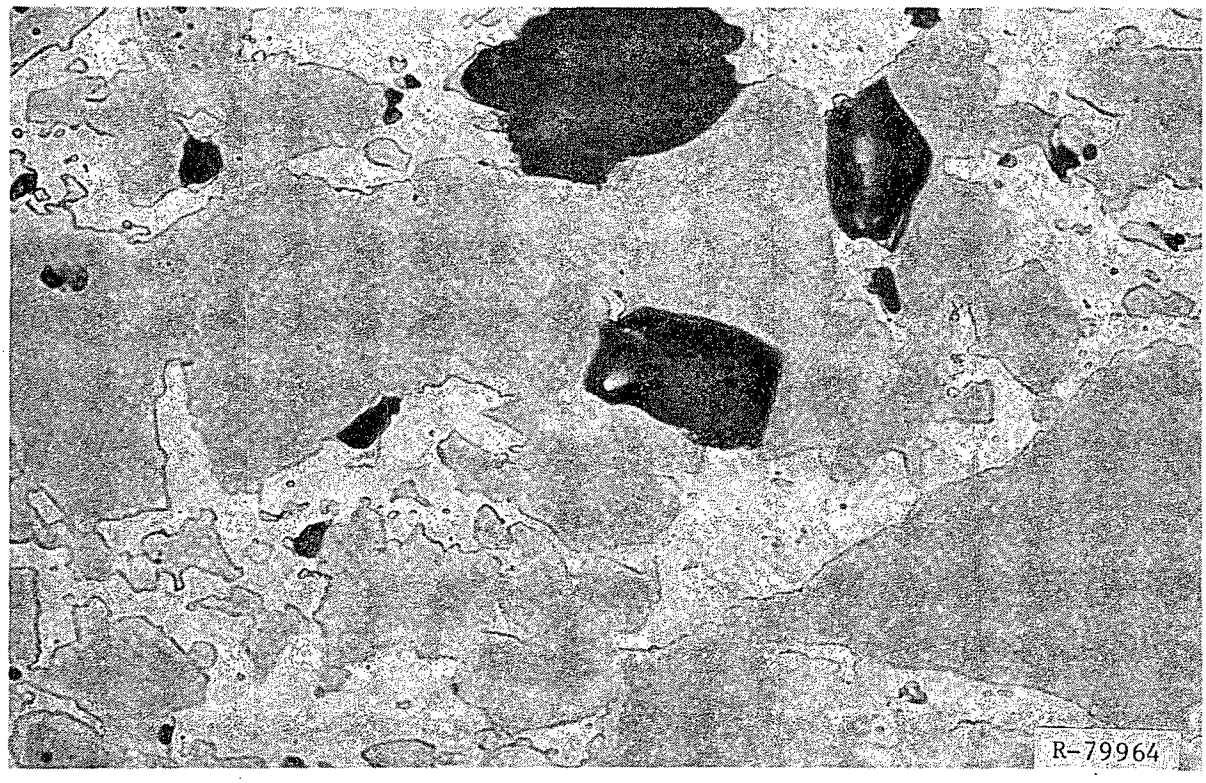

Fig. 24B. Detail of Fig. 23B.

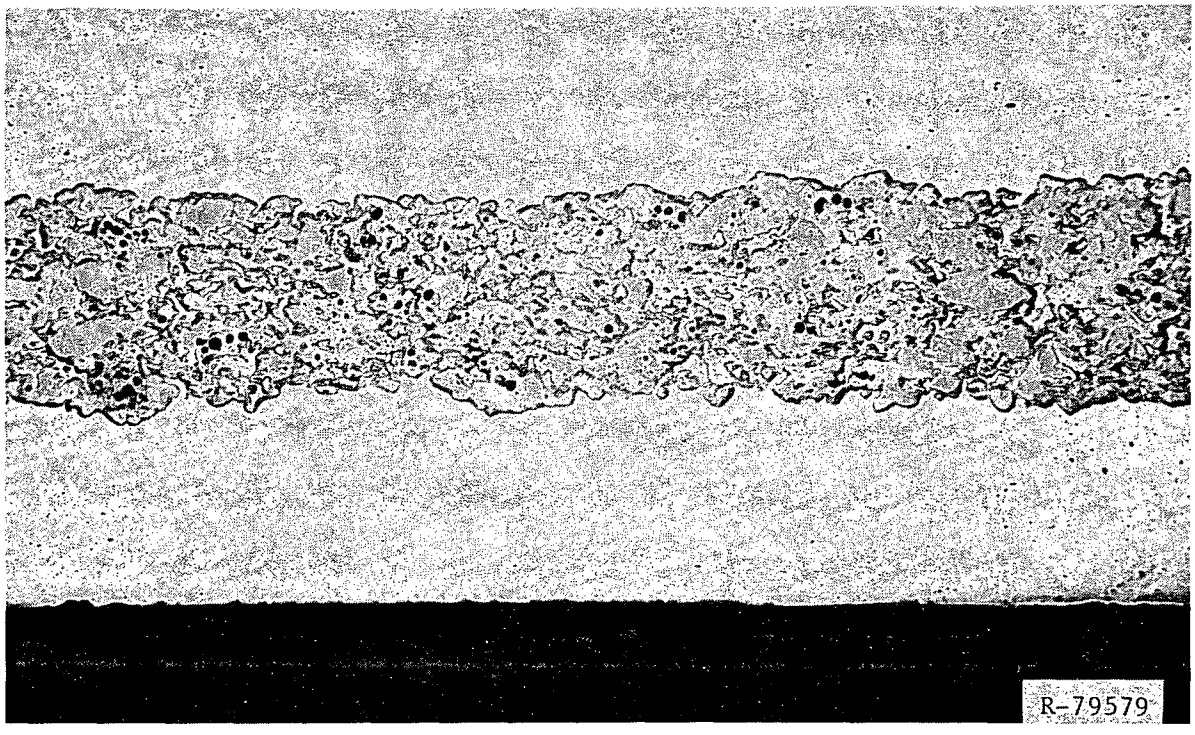

Fig. 25B. Meat Microstructure of Plate BSI-202, at 97% Bu.

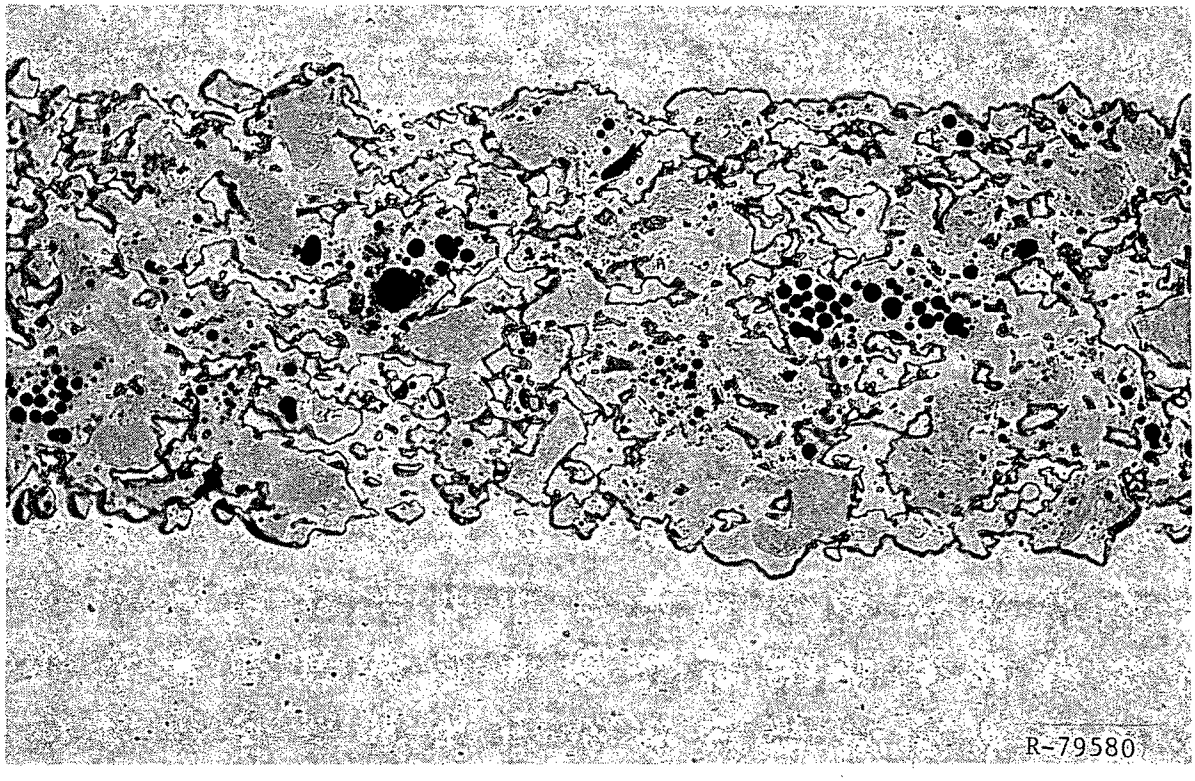

Fig. 26B. Detail of Fig. 25B.

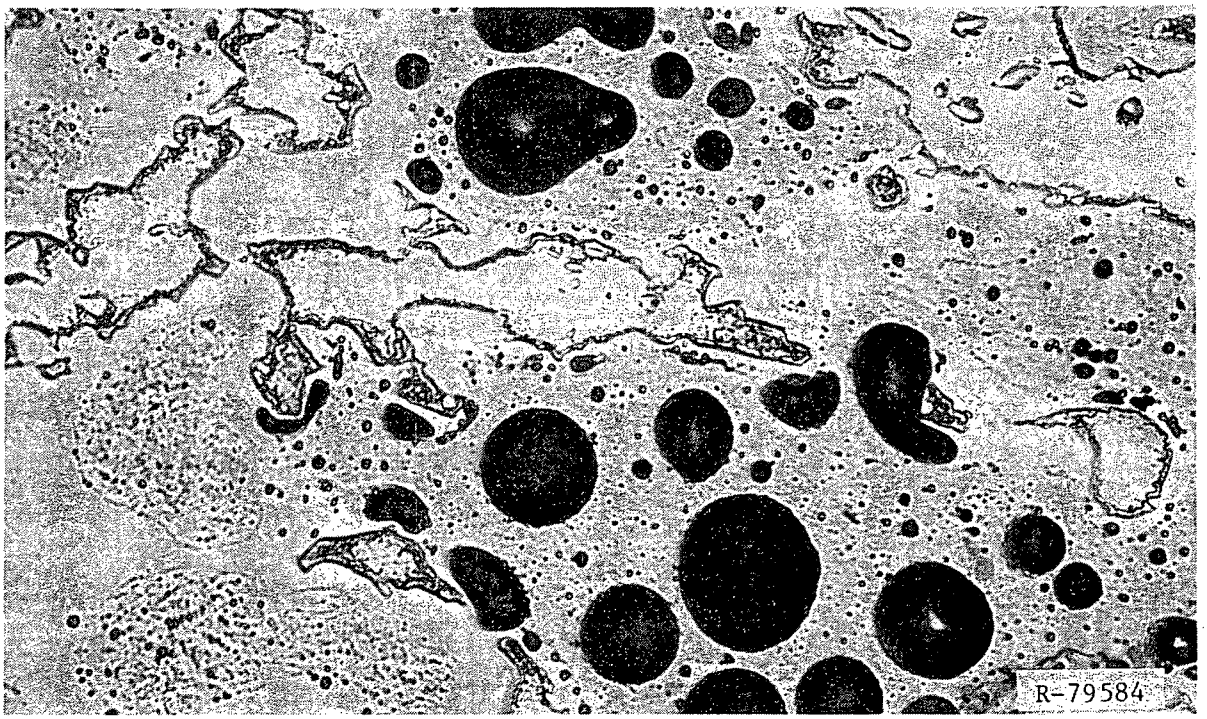

Fig. 27B. Detail of Fig. 26B.

Fig. 28B. SEM Image of Fuel Meat of Plate BSI-202, at 97% Bu.

Fig. 29B. Idem Fig. 28B, BSE Mode

Fig. 30B. SEM Image of Fuel Meat of Plate BSI-202, at 97% Bu, Showing Various Bubble Morphologies.

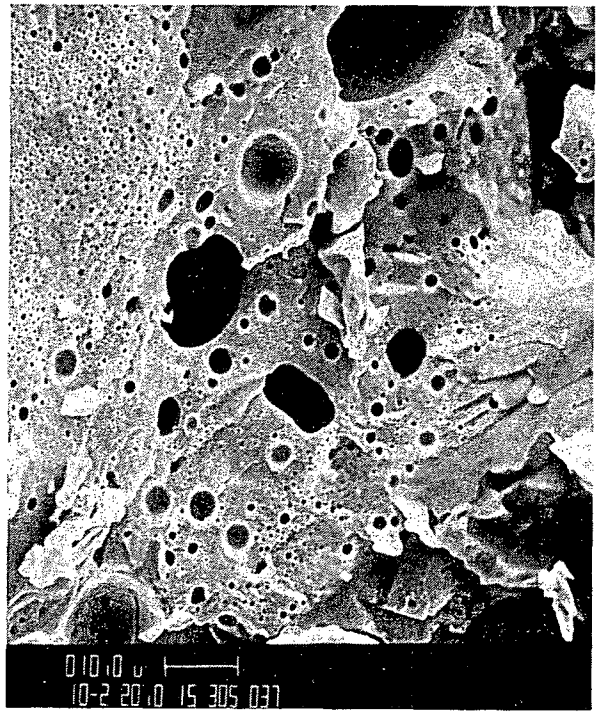

Fig. 31B. Idem Fig. 30B.

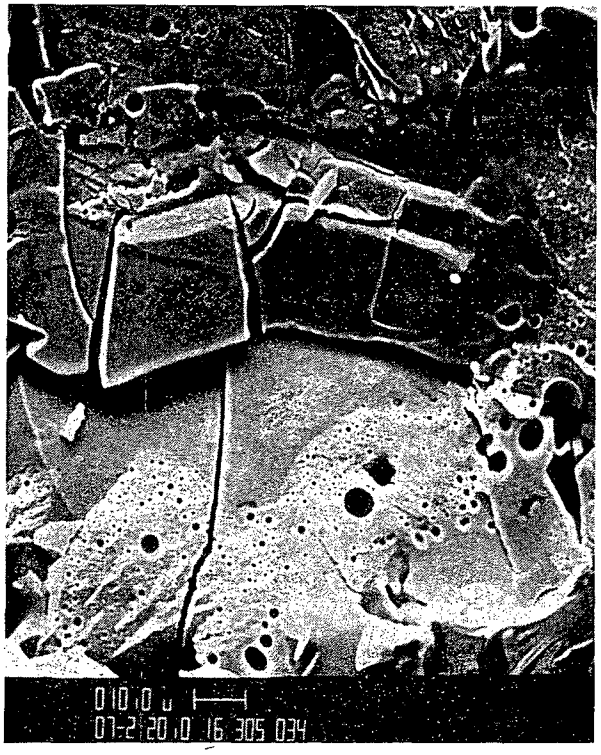

Fig. 32B. Idem Fig. 30B.

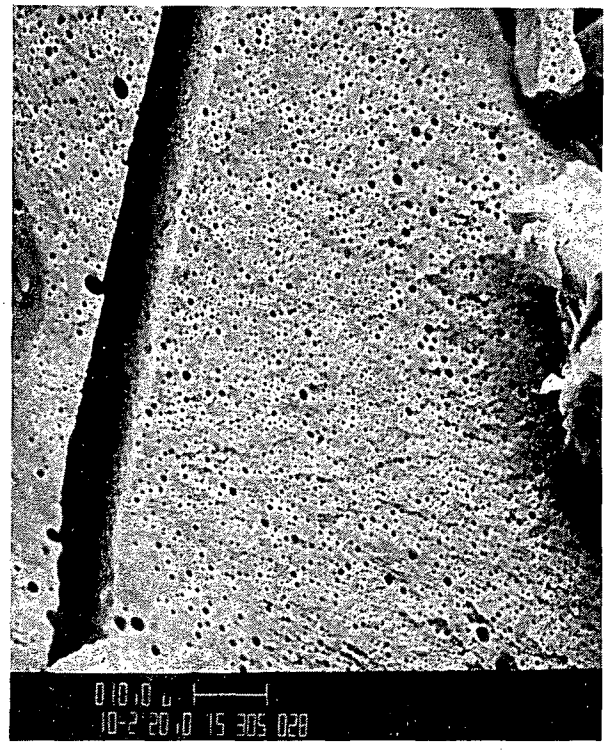

Fig. 33B. Idem Fig. 30B.

Fig. 34B. SEM Image of Fuel Meat in Unirradiated BSI Plate, Showing U_3Si_2 and U_3Si, BSE Mode.

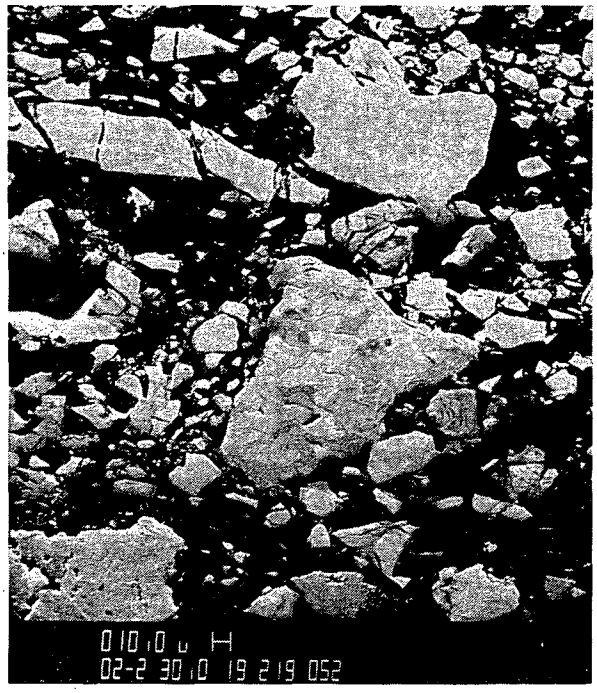

Fig. 35B. Idem Fig. 34B, Showing U_3Si_2 and U.

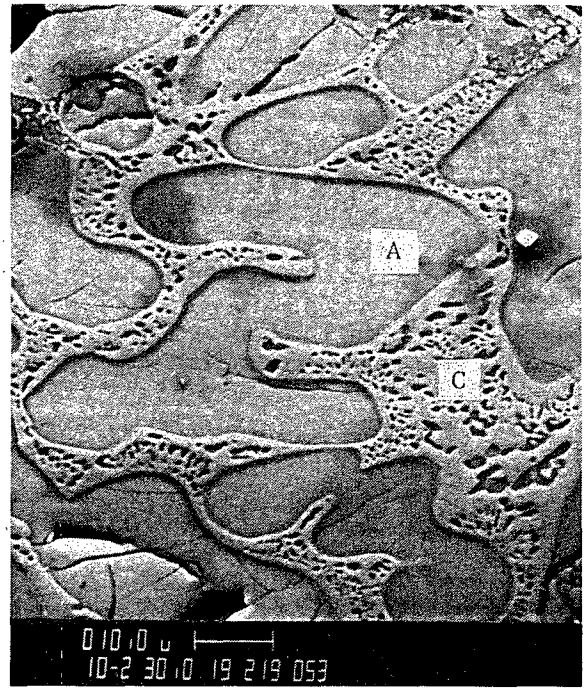

Fig. 36B. Detail of Fig. 35B.

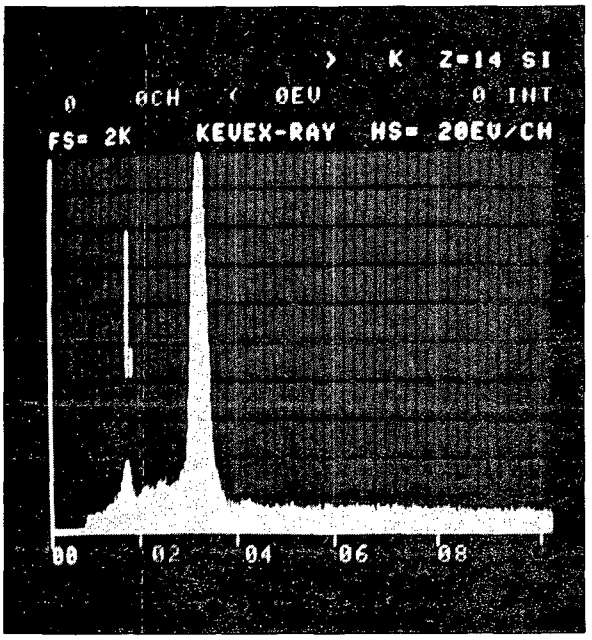

(A, U_3Si_2)

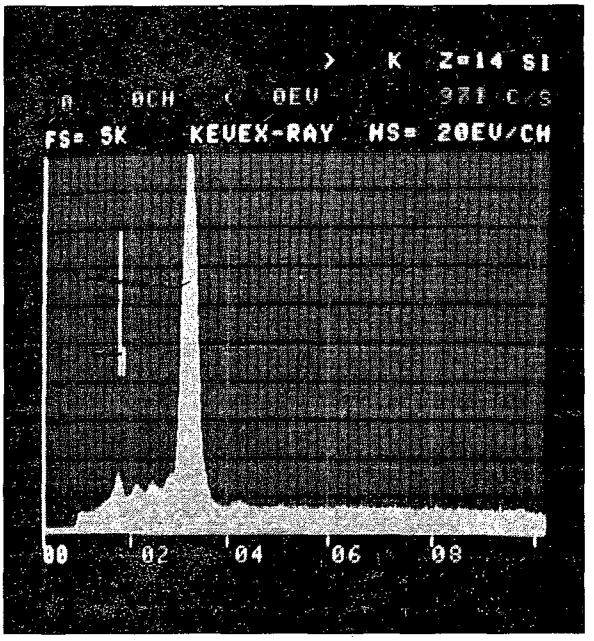

(B, U_3Si)

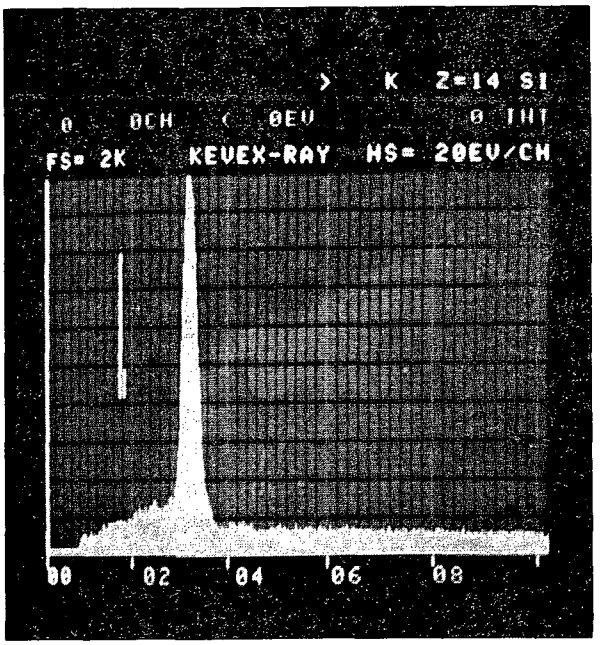

(C, U)

Fig. 37B. Energy Dispersive X-Ray Spectra Identifying Various Phases in Unirradiated BSI Plate.

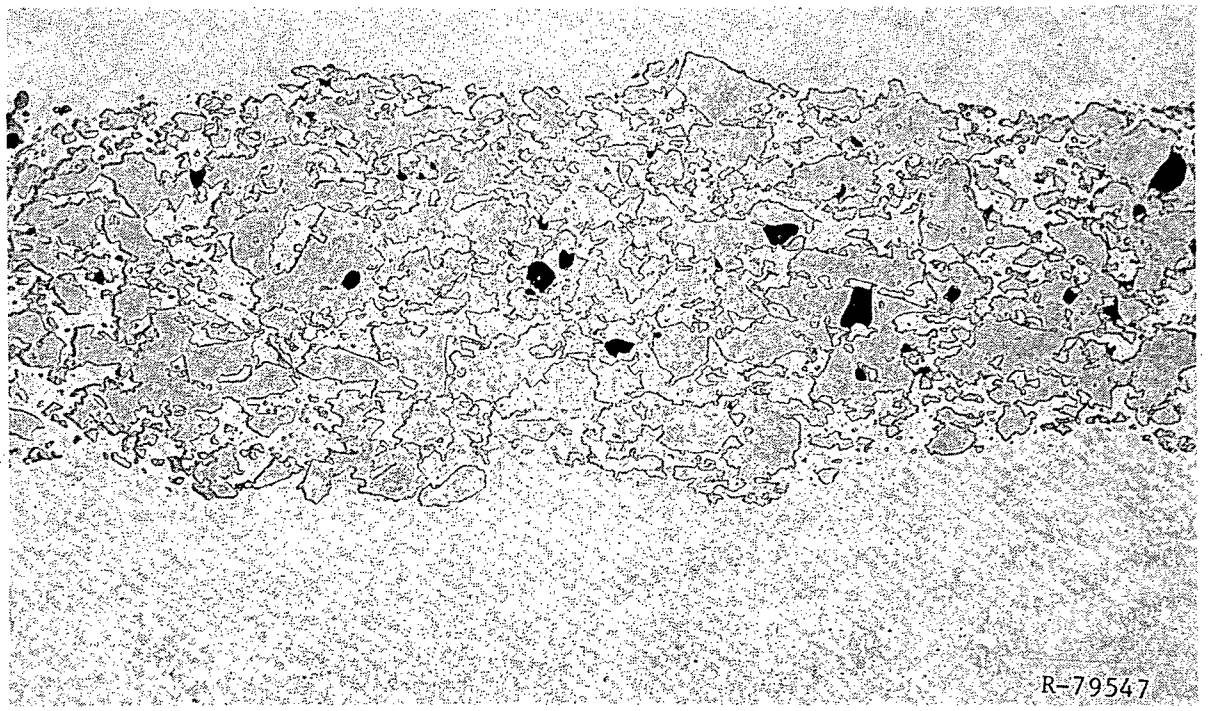

Fig. 38C. Meat Microstructure of Plate CSI-201, at 33% Bu.

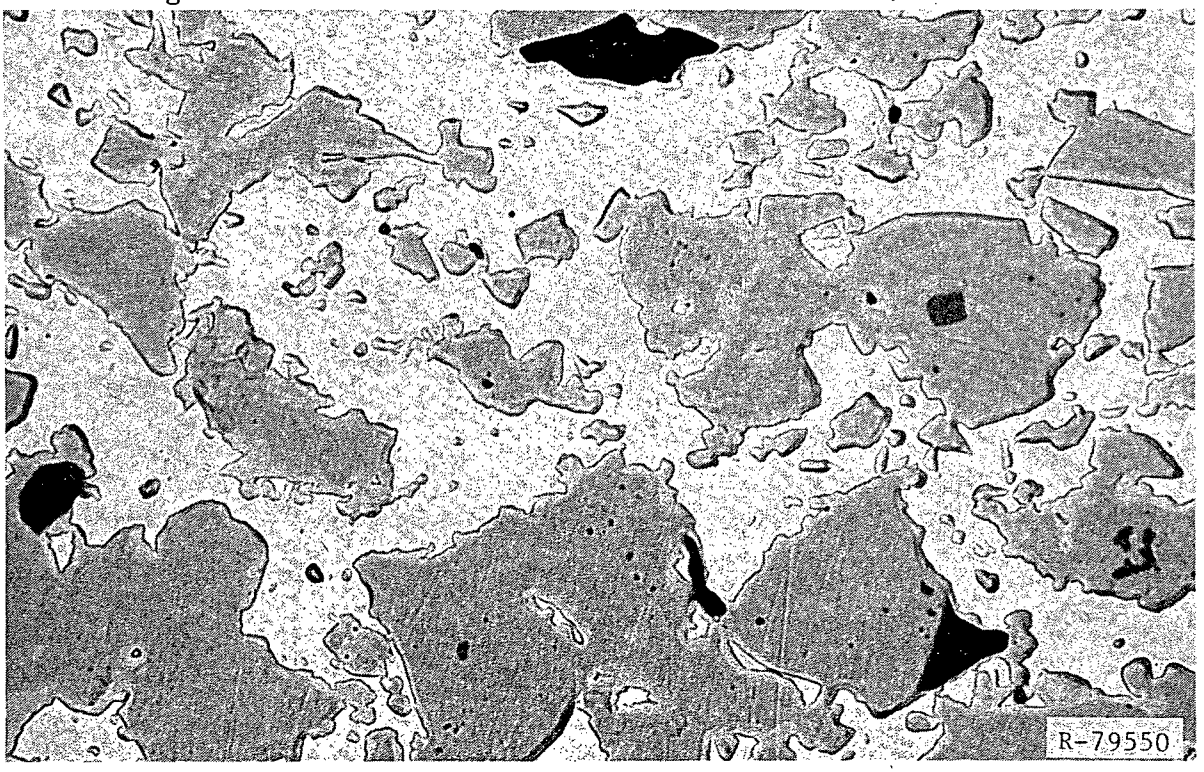

Fig. 39C. Detail of Fig. 38C.

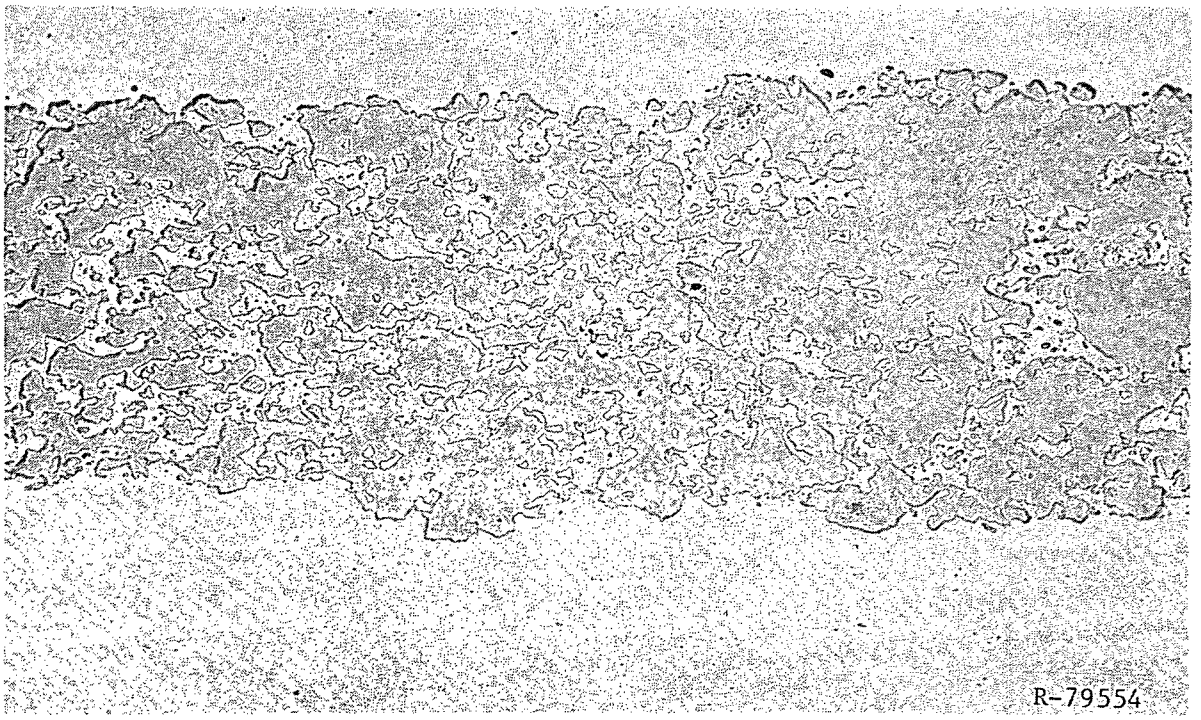

Fig. 40C. Meat Microstructure of Plate CSI-201, at 67% Bu.

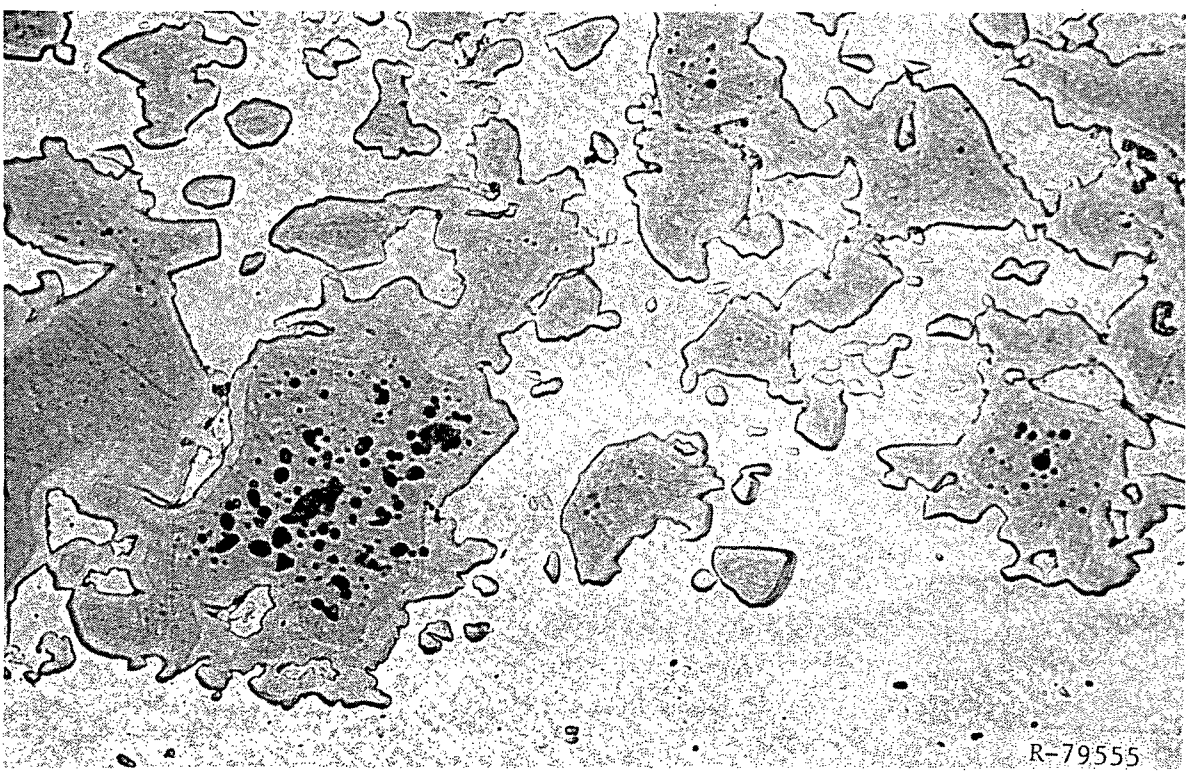

Fig. 41C. Detail of Fig. 40C.

Fig. 42C. SEM Image of Fuel Meat of Plate CSI-201, at 67% Bu.

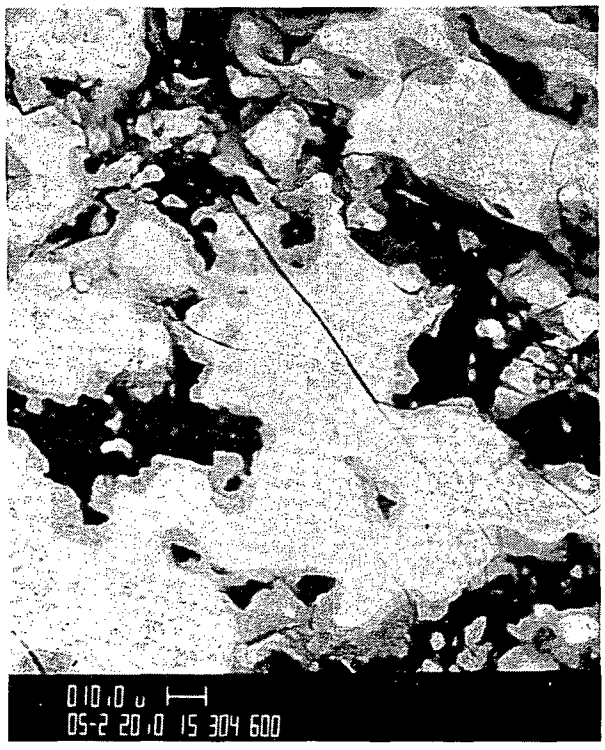

Fig. 43C. Idem Fig. 42C, BSE Mode.

Fig. 44C. Detail of Fig. 42C.

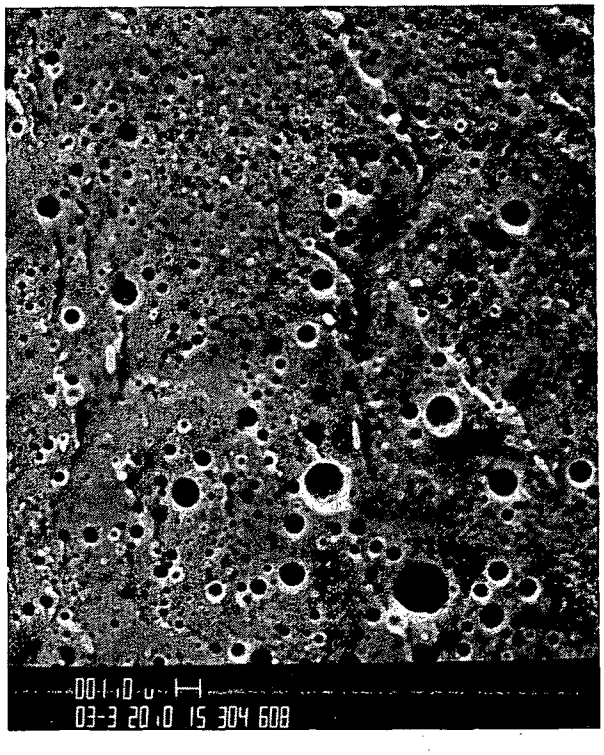

Fig. 45C. Detail of Fig. 42C.

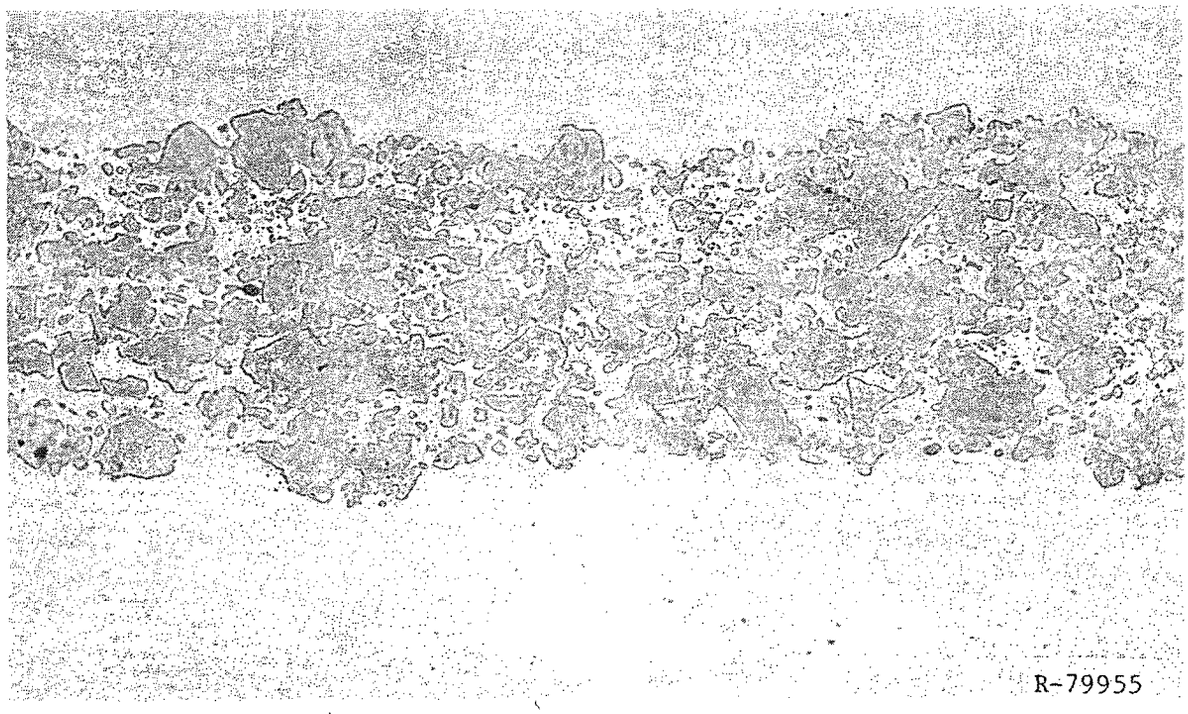

Fig. 46C. Meat Microstructure of Plate CSI-202, at 55% Bu.

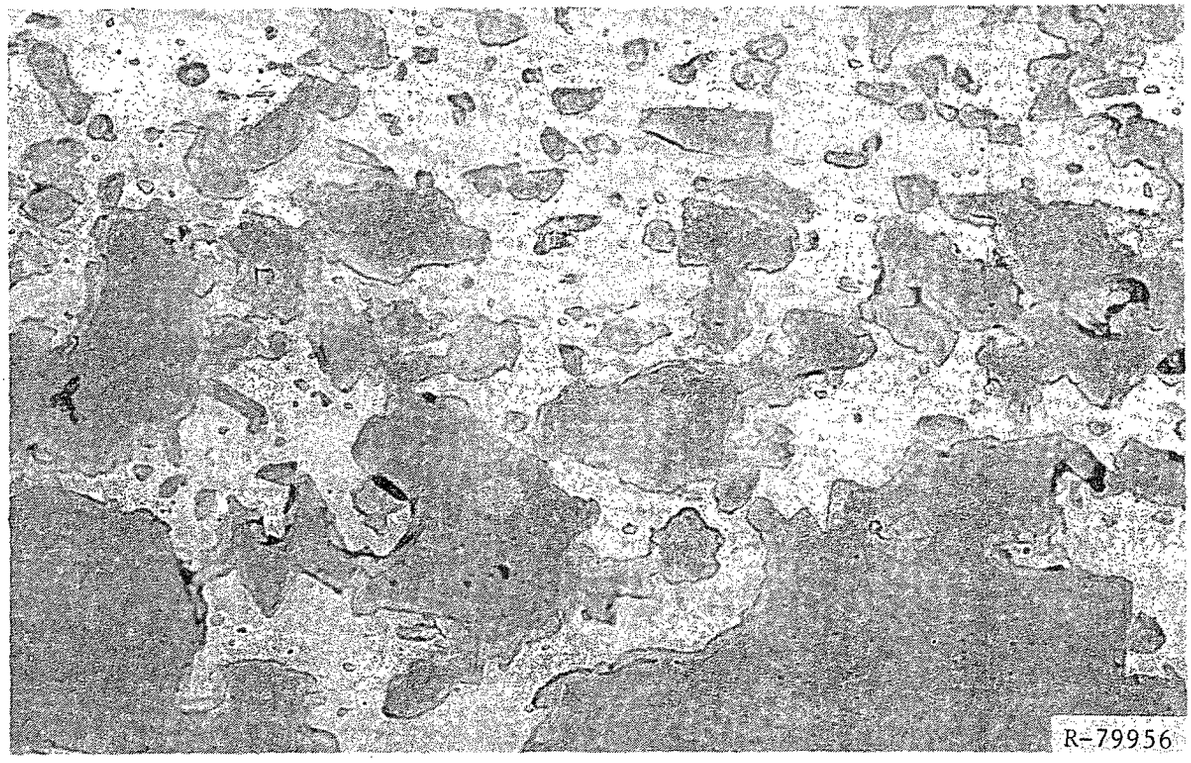

Fig. 47C. Detail of Fig. 46C.

Fig. 48C. SEM Image of Fuel Meat of Plate CSI-202, at 55% Bu.

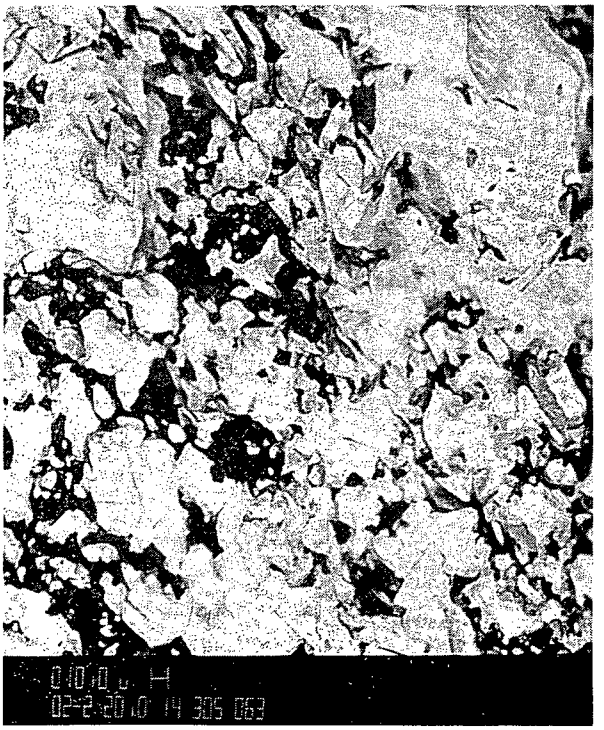

Fig. 49C. Idem Fig. 48C, BSE Mode.

Fig. 50C. Detail of Fig. 48C.

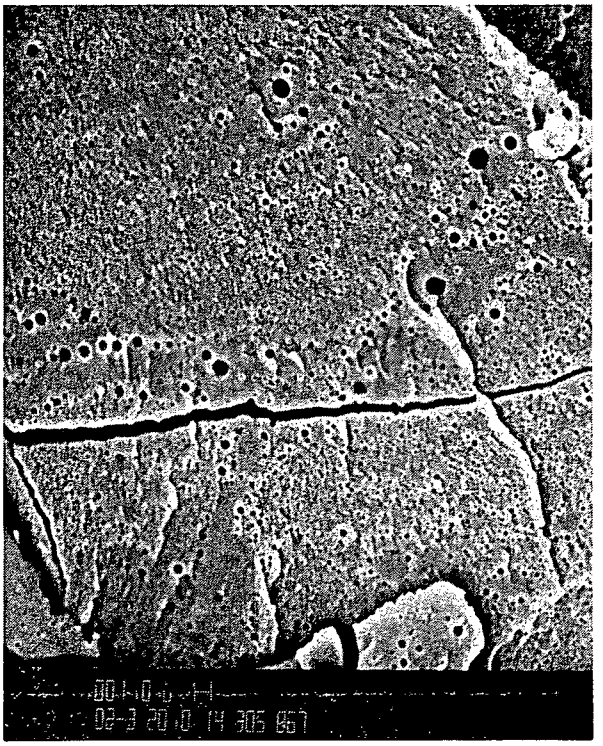

Fig. 51C. Detail of Fig. 48C.

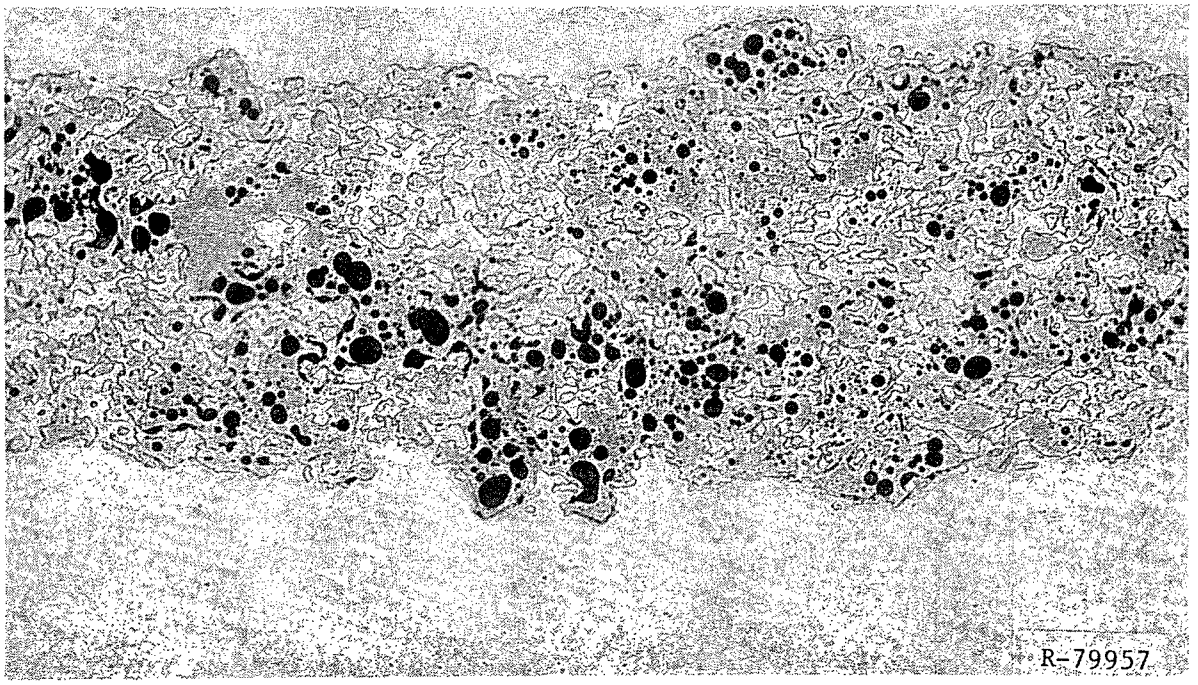

Fig. 52C. Meat Microstructure of Plate CSI-202, at 97% Bu.

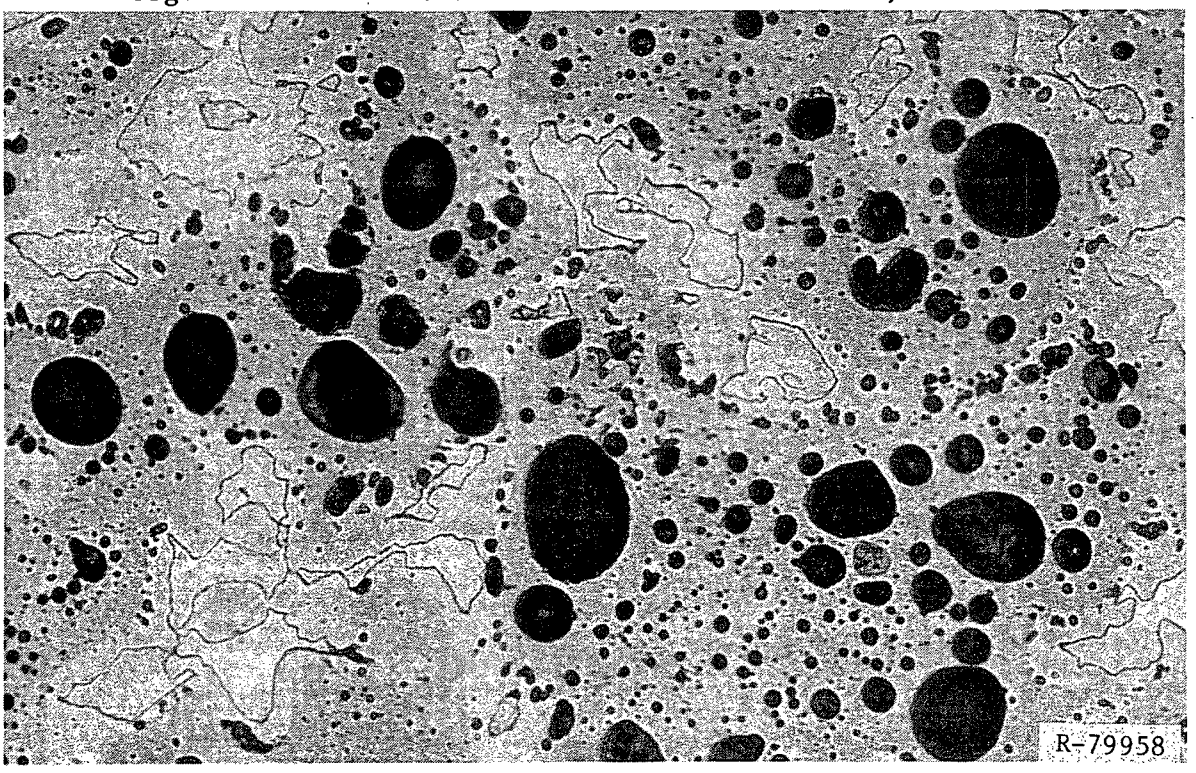

Fig. 53C. Detail of Fig. 52C.

Fig. 54C. SEM Image of Fuel Meat of Plate CSI-202, at 97% Bu.

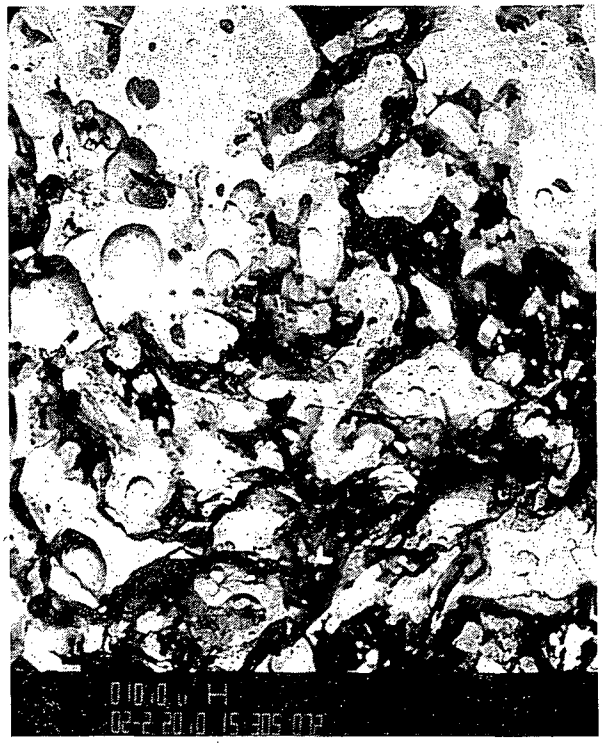

Fig. 55C. Idem Fig. 54C, BSE Mode.

Fig. 56C. Detail of Fig. 54C.

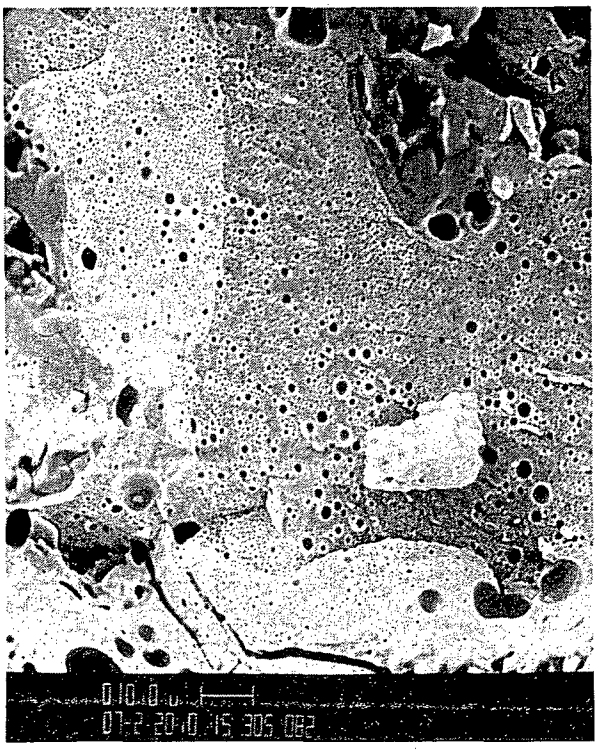

Fig. 57C. Detail of Fig. 54C.

Fig. 58C. SEM Image of Fuel Meat in Unirradiated CSI Plate, Showing U_3Si in U_3Si_2 Grain, BSE Mode.

Fig. 59C. SEM Image of Fuel Meat in Unirradiated CSI Plate, Showing Oxy-Carbide Phase (C).

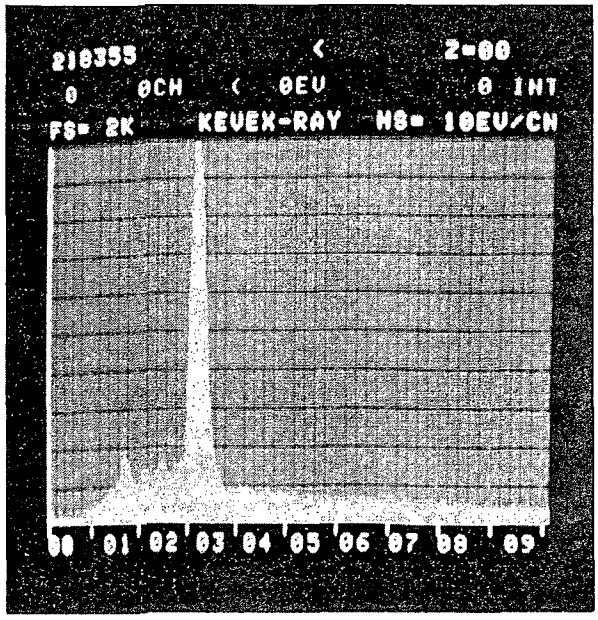

(A, U_3Si)

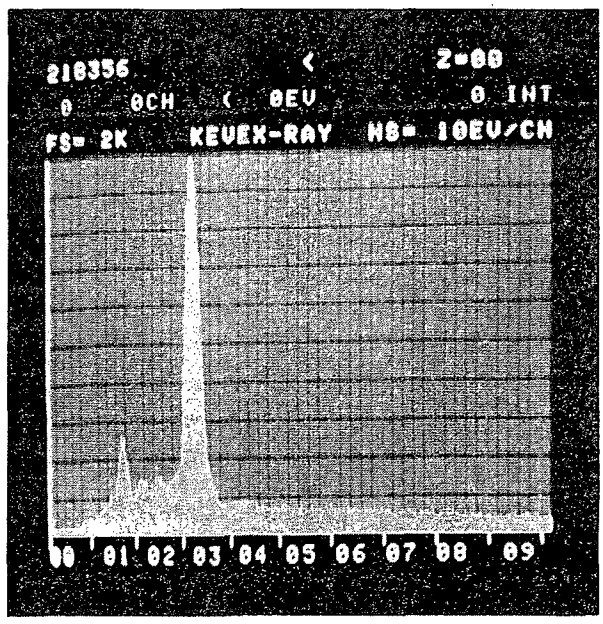

(B, U_3Si_2)

Fig. 60C. Energy Dispersive X-Ray Spectra Identifying U_3Si and U_3Si_2 in Unirradiated CSI Plate.

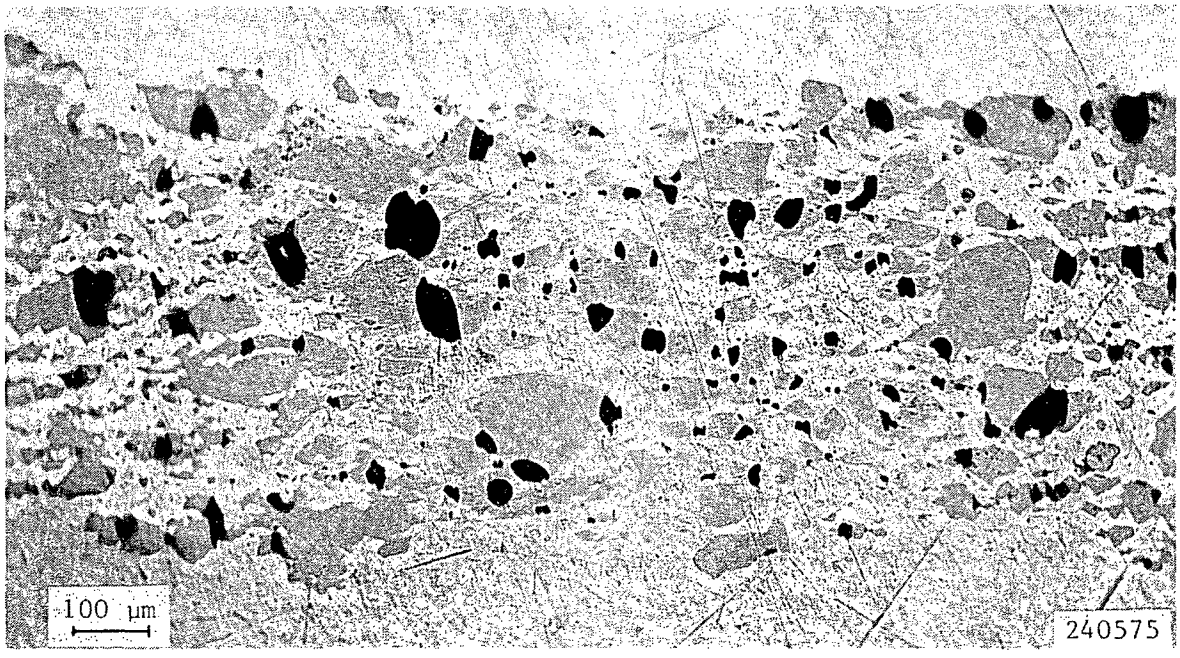

Fig. 61N. Meat Microstructure of Plate NSI-201, at 24% Bu.

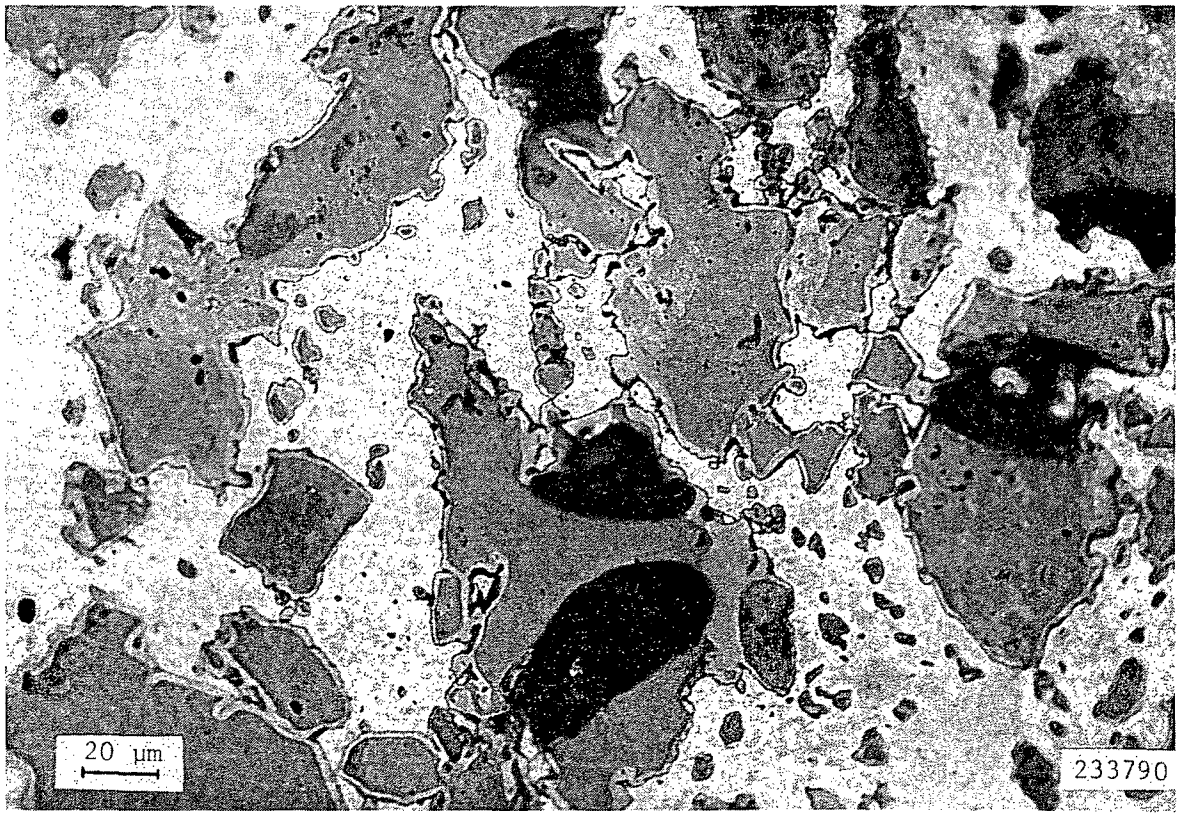

Fig. 62N. Detail of Fig. 61N.

Fig. 63N. SEM Image of Fuel Meat of Plate NSI-201, at 24% Bu.

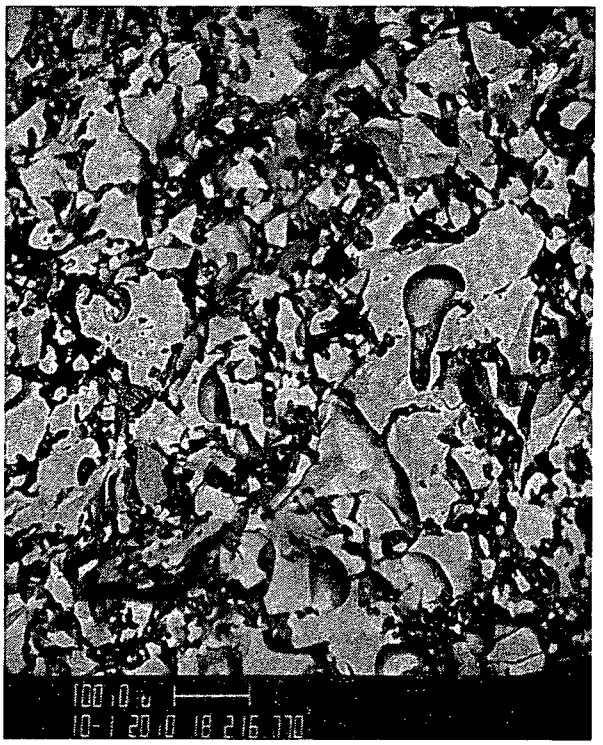

Fig. 64N. Idem Fig. 63N, BSE Mode.

Fig. 65N. Detail of Fig. 63N.

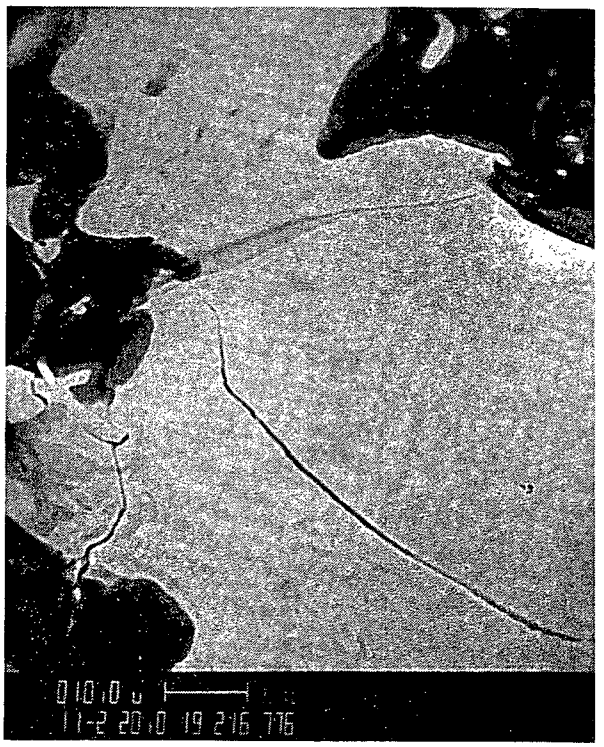

Fig. 66N. Detail of Fig. 64N.

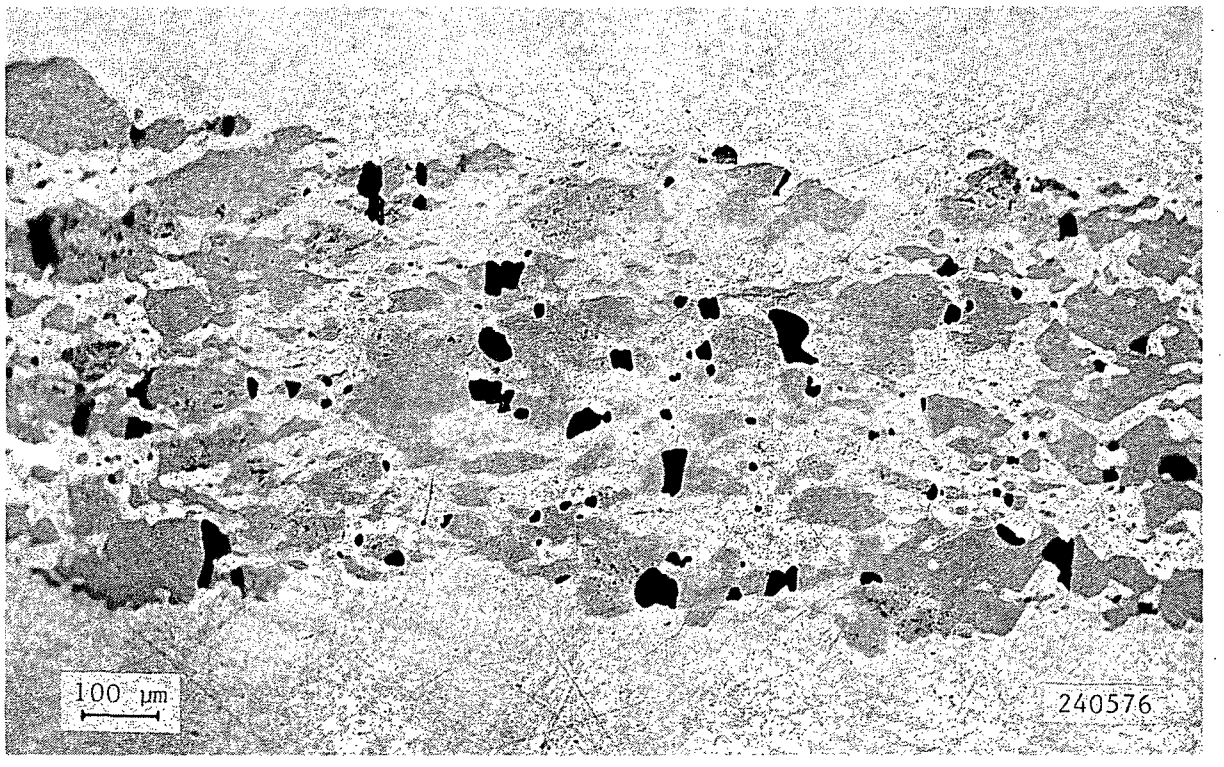

Fig. 67N. Meat Microstructure of Plate NSI-201, at 51% Bu.

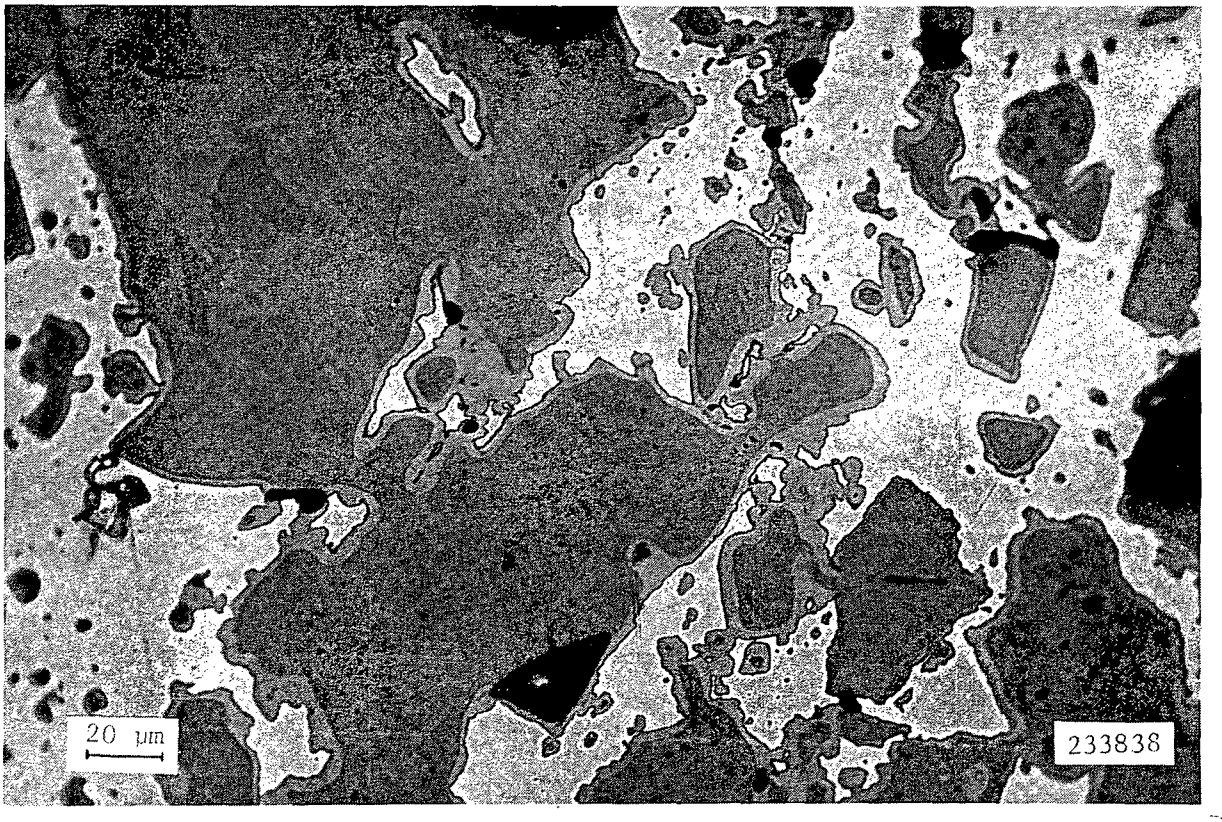

Fig. 68N. Detail of 67N.

Fig. 69N. SEM Image of Fuel Meat of Plate NSI-201, at 51% Bu.

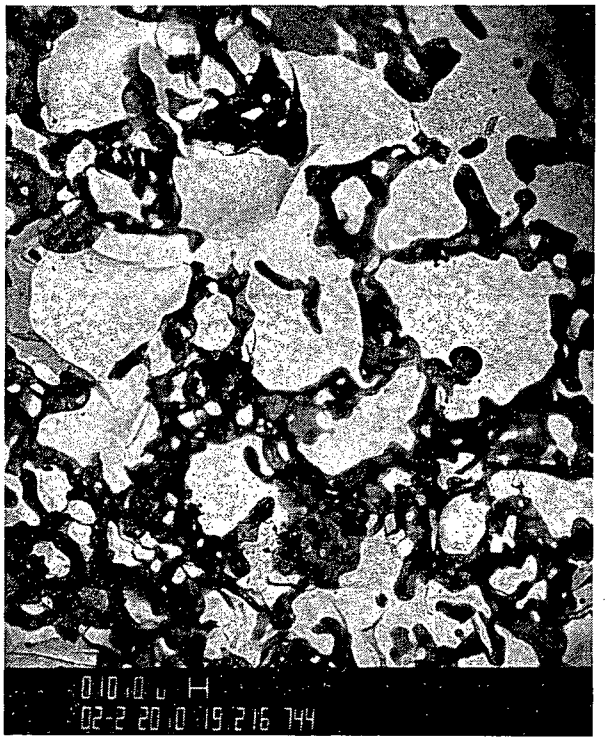

Fig. 70N. Idem Fig. 69N, BSE Mode.

Fig. 71N. Detail of Fig. 69N.

Fig. 72N. Detail of Fig. 71N, BSE Mode.

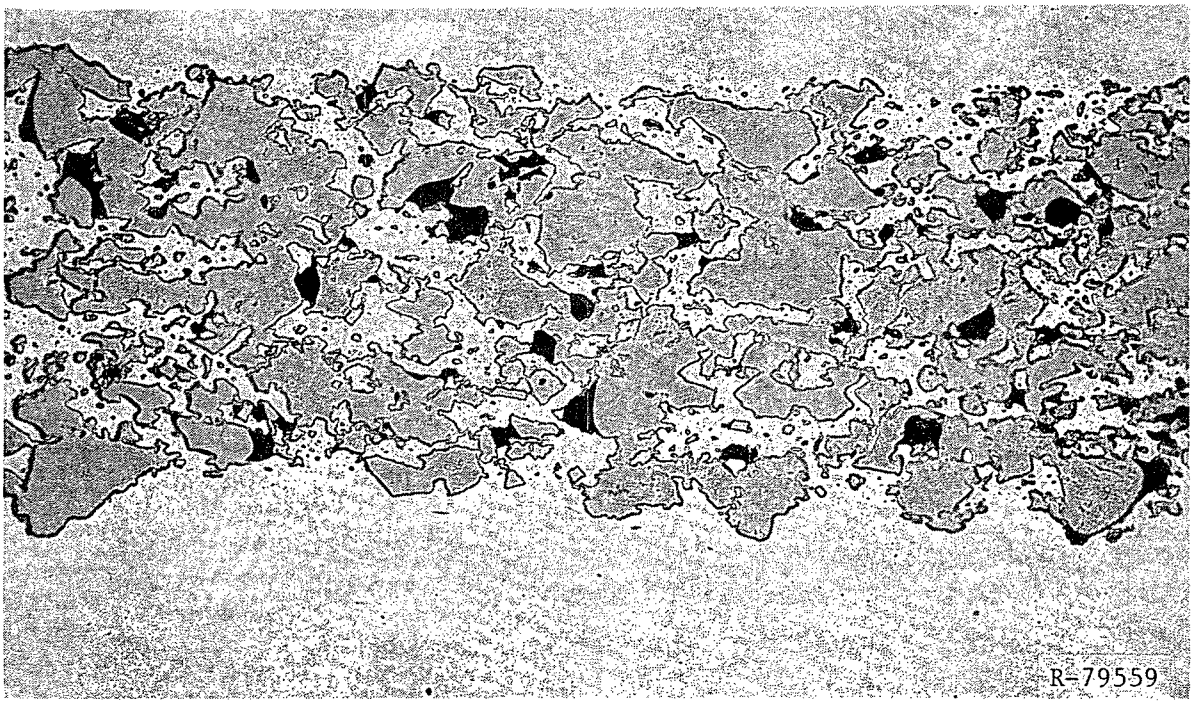

Fig. 73N. Meat Microstructure of Plate NSI-202, at 54% Bu.

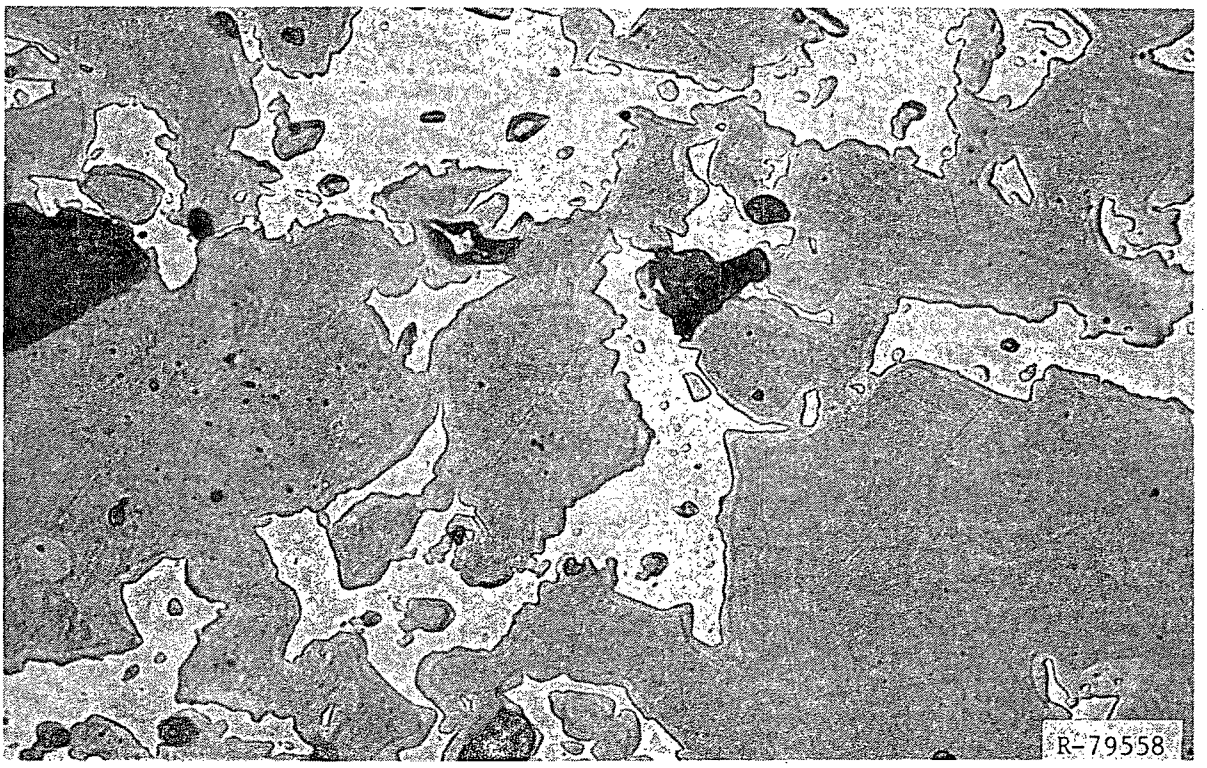

Fig. 74N. Detail of Fig. 73N.

Fig. 75N. SEM Image of Fuel Meat of Plate NSI-202, at 54% Bu.

Fig. 76N. Detail of Fig. 75N.

Fig. 77N. Detail of Fig. 75N.

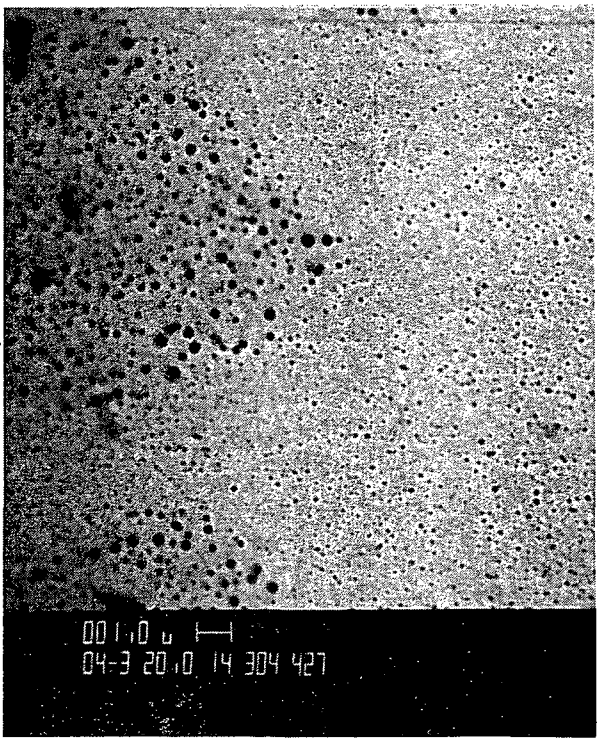

Fig. 78N. Idem Fig. 77N.

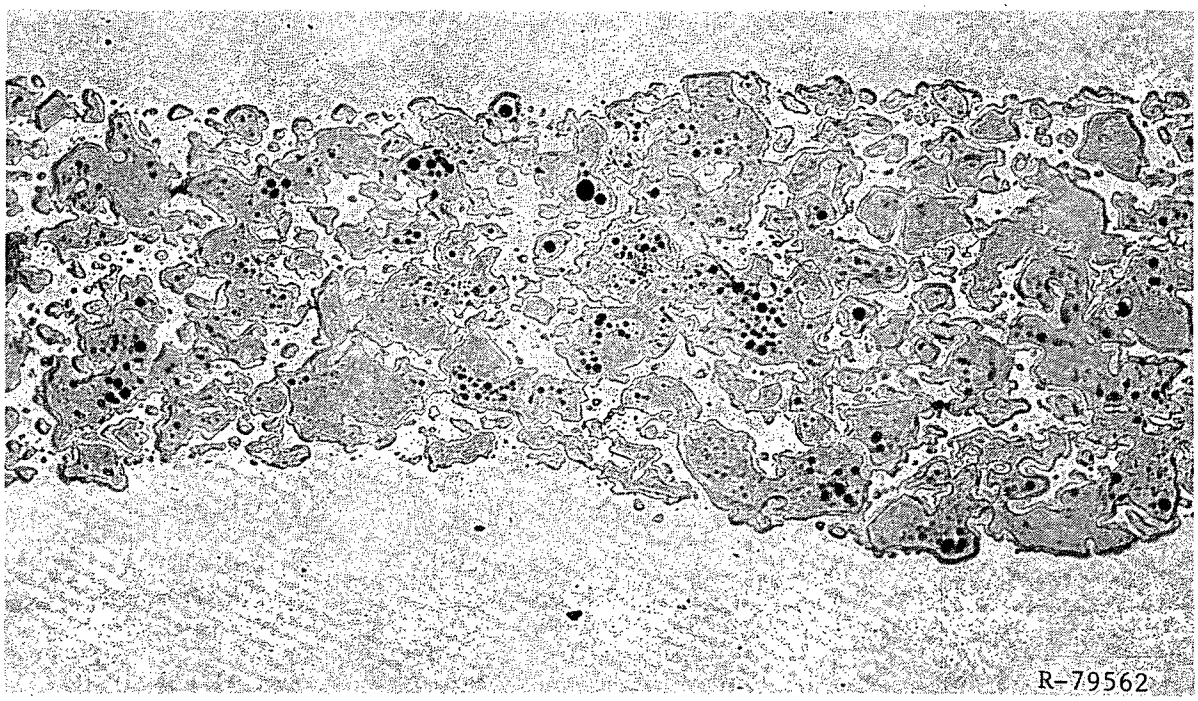

Fig. 79N. Meat Microstructure of Plate NSI-202, at 96% Bu.

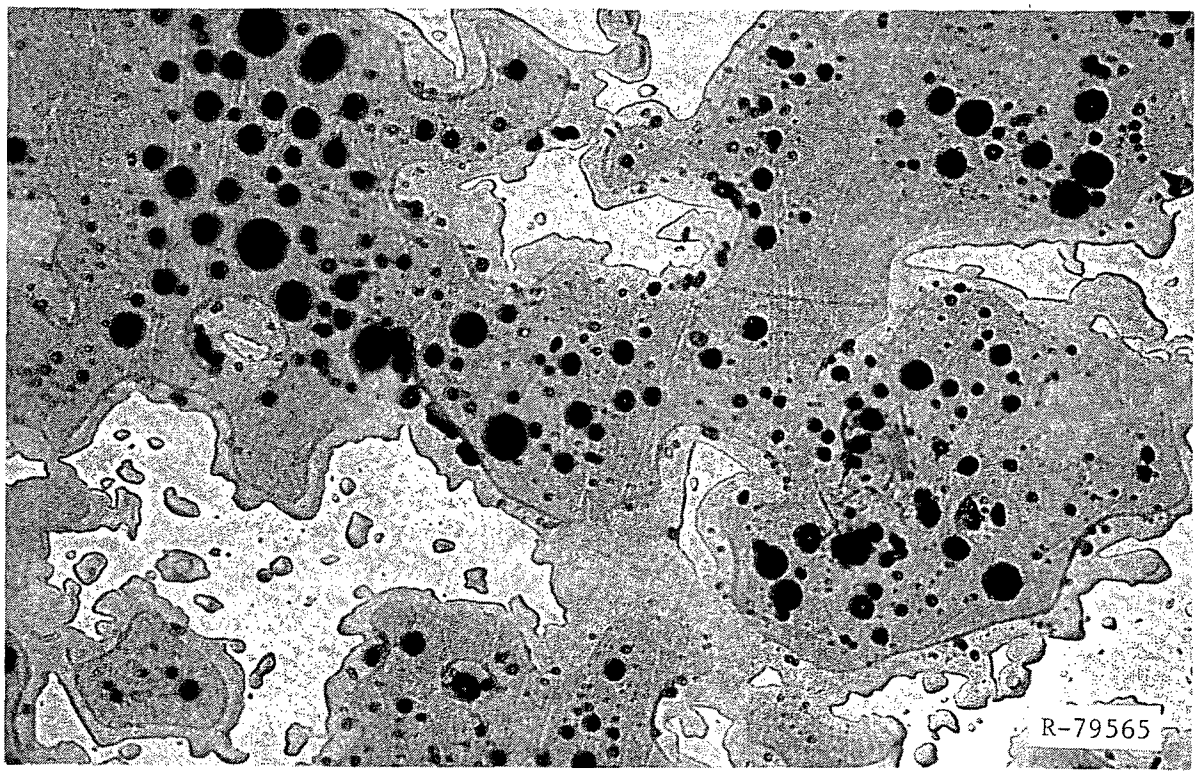

Fig. 80N. Detail of Fig. 79N.

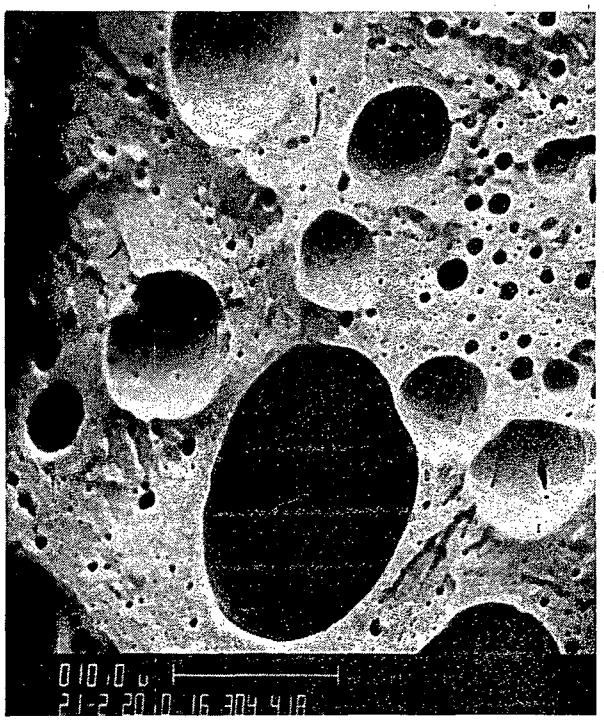

Fig. 81N. SEM Image of Fuel Meat of Plate NSI-202, at 96% Bu, Showing Various Bubble Morphologies.

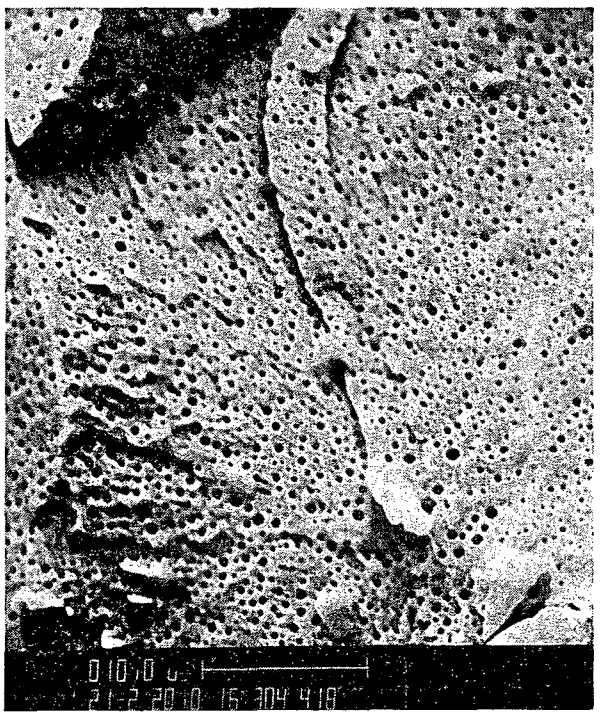

Fig. 82. Idem Fig. 81N.

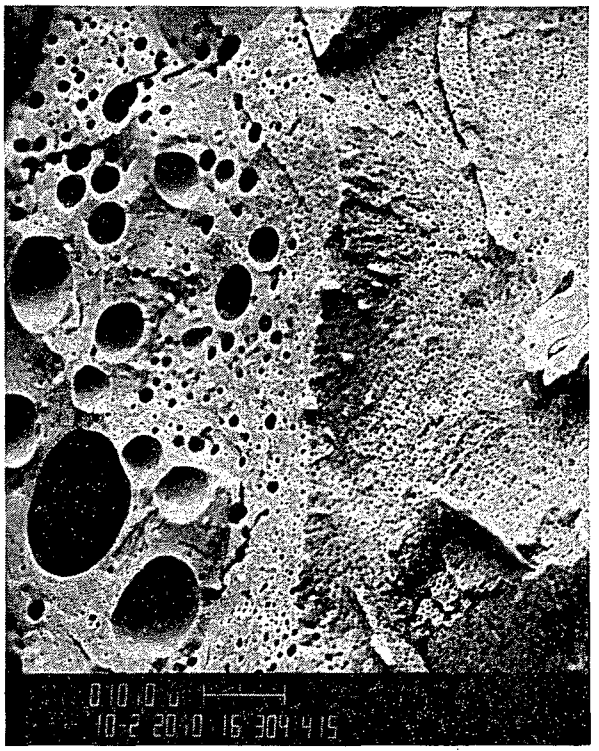

Fig. 83N. Idem Fig. 81N.

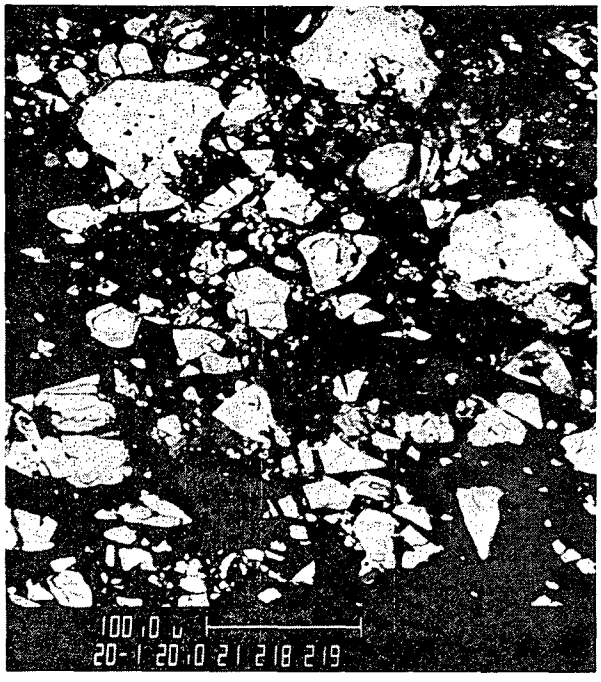

Fig. 84N. SEM Image of Fuel Meat of Unirradiated NSI Plate, BSE Mode.

Fig. 85N. Idem Fig. 84N.

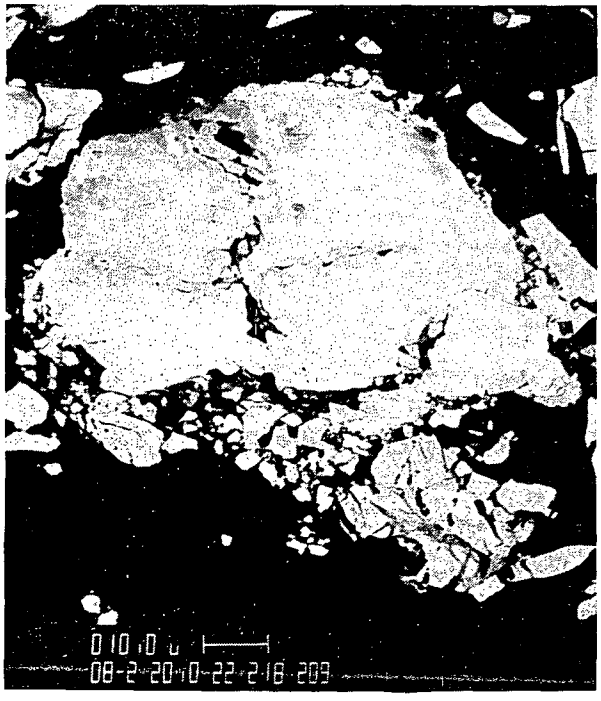

Fig. 86N. Detail of Fig. 84N Showing U_3Si_2 and U_3Si.

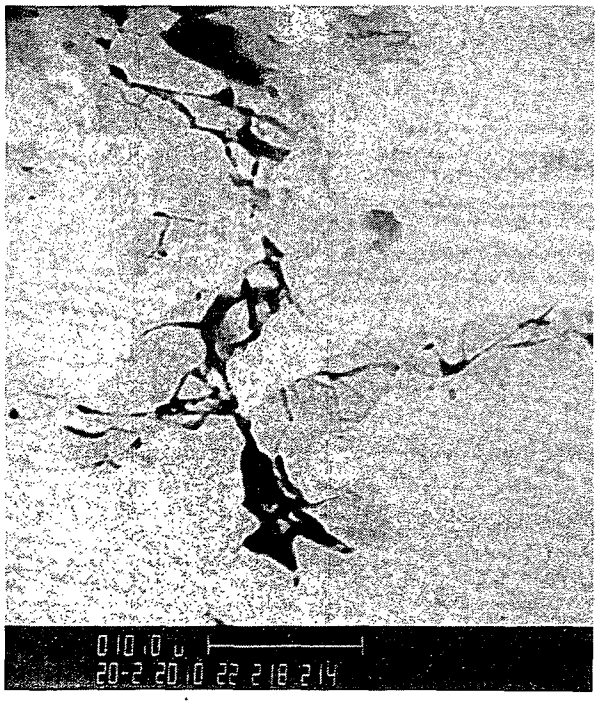

Fig. 87N. Idem Fig. 86N.

APPENDIX A

POSTIRRADIATION EXAMINATION STEPS

NONDESTRUCTIVE PIE

1. Visual Inspection

   Purpose: To observe general appearance and photograph.

   a. Observe general external appearance.
   b. Note any unusual features.
   c. Photograph element exterior with close-ups of unusual features.
   d. Photograph through channels with element backlighted.

2. External Dimensions

   Purpose: To determine dimensional changes during irradiation.

   a. Measure major external dimensions (length, width, depth).
   b. Determine amount of warp, twist, or bow.

3. Gamma Scanning of Full Element

   Purpose: To determine relative longitudinal burnup (fission product) distribution for entire element and to determine relative burnup from element to element.

   a. Scan using Ge(Li) detector and multichannel analyzer for fission-product peaks in the energy range 100 to 1400 keV, including ^{106}Ru and ^{137}Cs.

   b. Scan longitudinally in 1.0-in. increments along centerline of element.

4. Measure Channel Gaps

   Purpose: To detect unusual amounts of plate swelling or warping.

   a. Remove end fittings.
   b. Measure channel gaps on both sides of comb.

1-4. Same as above.

5. Dismantling of Element

Purpose: To prepare plates for individual examination.

a. Separate individual fuel plates from side plates.

6. Visual Inspection of Plate

Purpose: To detect blisters or other unusual features.

a. Observe general external appearance of each plate and note any unusual features.

b. Photograph typical plates (2 or 3) and any areas of unusual features.

7. Thickness Measurements

Purpose: To provide data for estimation of plate swelling. Since measured thickness changes always overestimate the volume change (only the "high" points on the surface are measured), these measurements will serve mainly to show that no unexpected swelling has occurred.

a. Measure thickness at ~24 points on plates Nos. 1, 5, 9, 13, and 17, including at least two points outside the fuel meat zone.

b. Measure thickness at conspicuous spots.

8. Gamma Scanning

Purpose: To Determine relative longitudinal and transverse burnup (fission-product) distributions.

a. Perform analog scan longitudinally along centerline for all plates, for both integral above 0.5 MeV and ^{137}Cs.

b. Perform multichannel spectrum measurements along centerline at peak, as determined from analog scan, at 6 in. below peak, and at 10 in. above peak for plates Nos. 1, 5, 9, 13, and 17.

c. Perform analog scan transversely at peak of longitudinal scan, at 6 in. below peak, and at 10 in. above peak for plates Nos. 1 and 9, for both integral above 0.5 MeV and ^{137}Cs.

9. Blister Testing

Purpose: To determine the threshold temperature for the formation of blisters. The threshold temperature will be measured by the standard technique of heating the entire plate in a furnace to a specified temperature, holding at that temperature for approximately 30 minutes and removing the plate for visual examination. The sequence is repeated for successively higher temperatures until blistering is observed.

a. Blister test two plates (Nos. 2 and 8).

b. If results are not consistent, test also plate No. 18.

10. Metallography

Purpose: To confirm that the behavior of the fuel is as expected, based upon previous examinations of miniplates.

a. Obtain two sections (high- and low-burnup) from the plate (other than No. 1) showing the highest burnup.

b. Perform optical metallographic examination.

11. Burnup Analysis

Purpose: To determine the absolute number of fissions (burnup). These data will be used with gamma scanning data to assign absolute burnups to each element.

a. Obtain burnup samples from high- and low-burnup regions of plate sectioned for metallography.

b. Perform U and Pu isotopic analyses.

c. Determine burnup and fission density based on ^{235}U isotopic abundance.

APPENDIX B

VISUAL EXAMINATION AND PHOTOGRAPHS

All elements were visually examined for damage and evidence of swelling or distortion. All of the elements appeared to be in good condition. All showed a corrosion film and some handling marks. Looking through the coolant channels with backlighting showed the coolant channels to be uniform with no evidence of plate swelling or distortion. Photographs through the coolant channels vary in quality due to varying lighting, whether or not the end boxes had been removed, and differing reflectivities of the oxide film. However, all the elements were judged to be in excellent condition based on the visual examinations. Photographs of the elements are presented below.

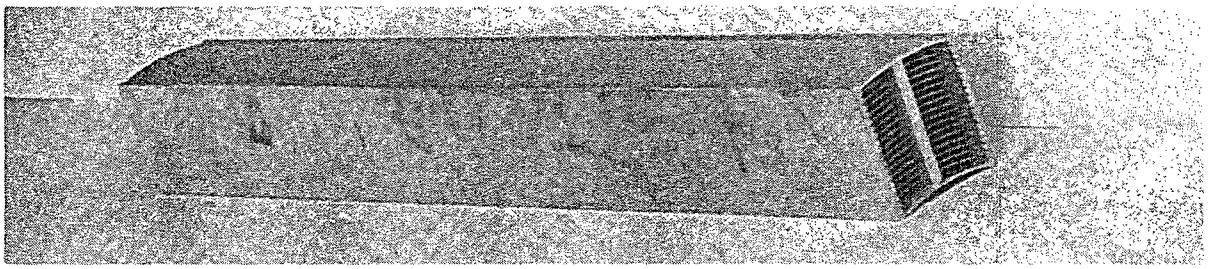

Figure B.1. Element BSI-201 After Removing End Boxes. (R-79655)

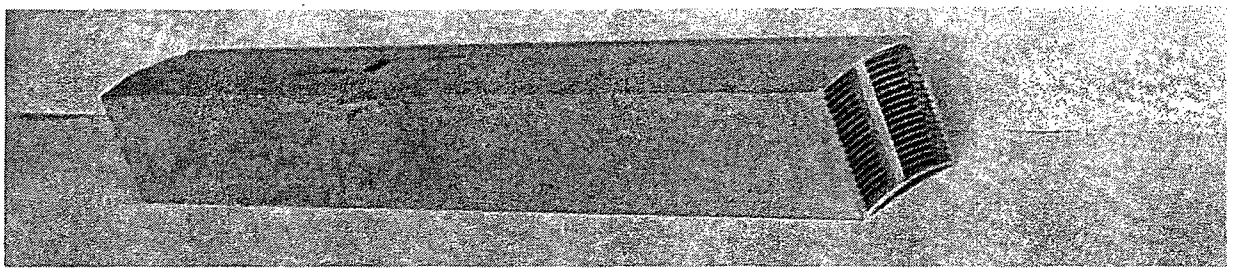

Figure B.2. Element BSI-202 After Removing End Boxes. (R-79657)

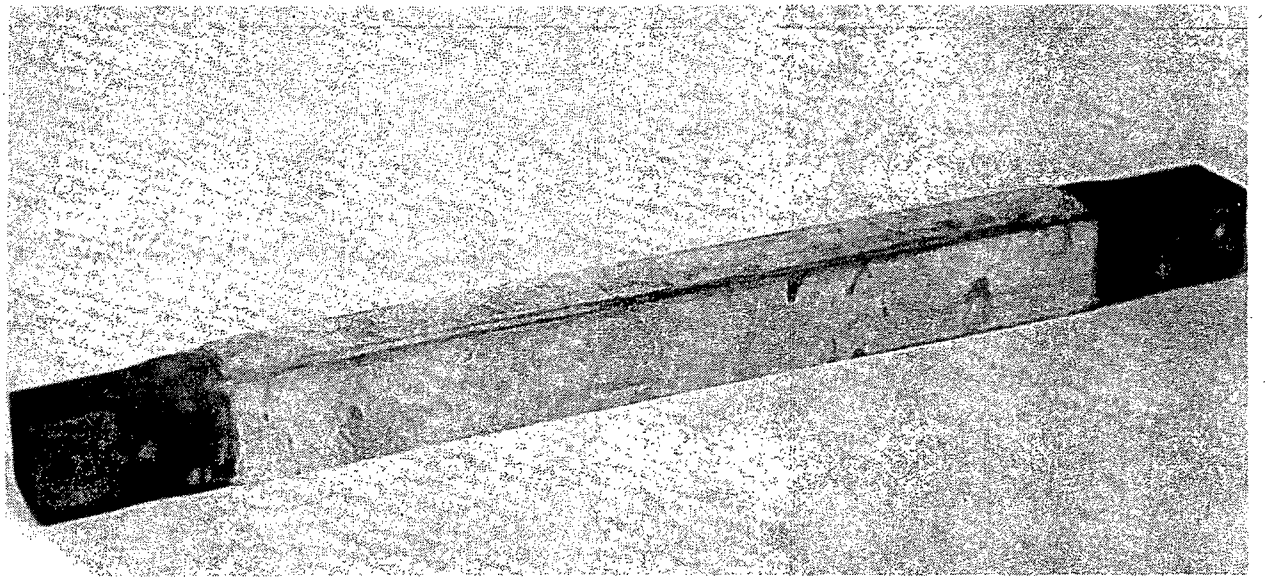

Figure B.3. Element CSI-201 with End Boxes Attached. (Y-197349)

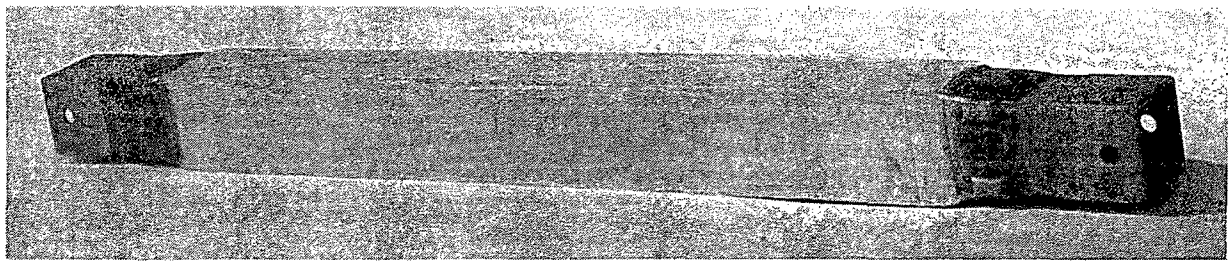

Figure B.4. Element CSI-202 with End Boxes Attached. (R-79659)

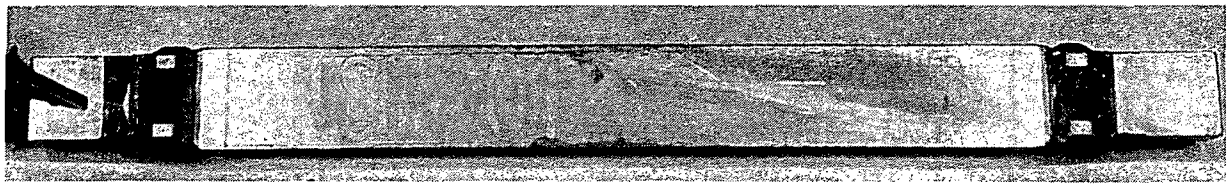

Figure B.5. Element NSI-201 with End Boxes Attached. (Y-193260)

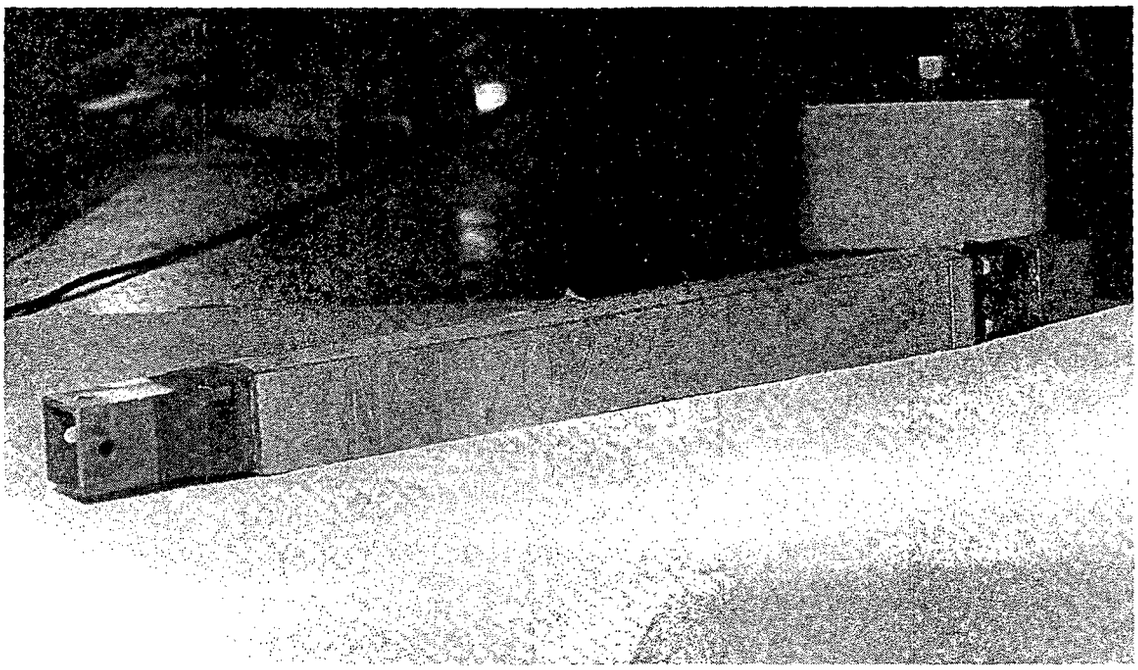

Figure B.6. Element NSI-202 with End Boxes Attached. (Y-200764)

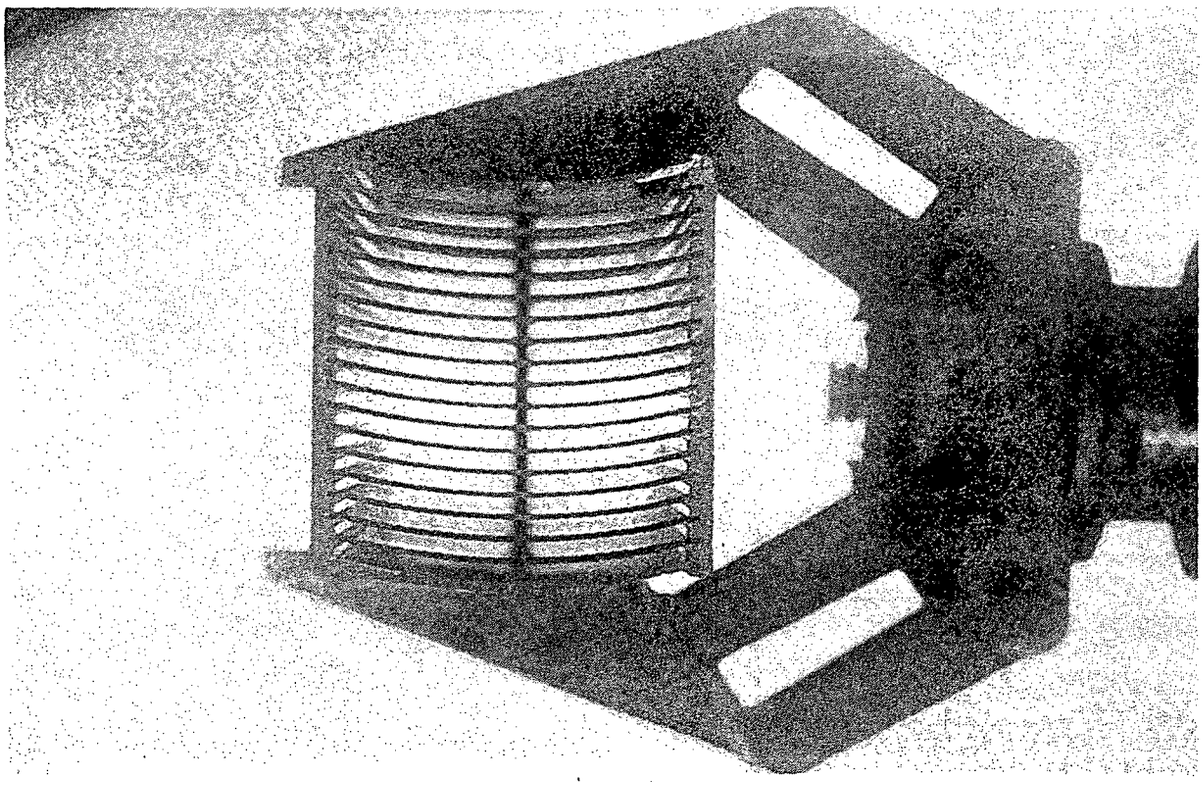

Figure B.7. View Through Coolant Channels of Element BSI-201 After Removal of End Boxes. (R-79656)

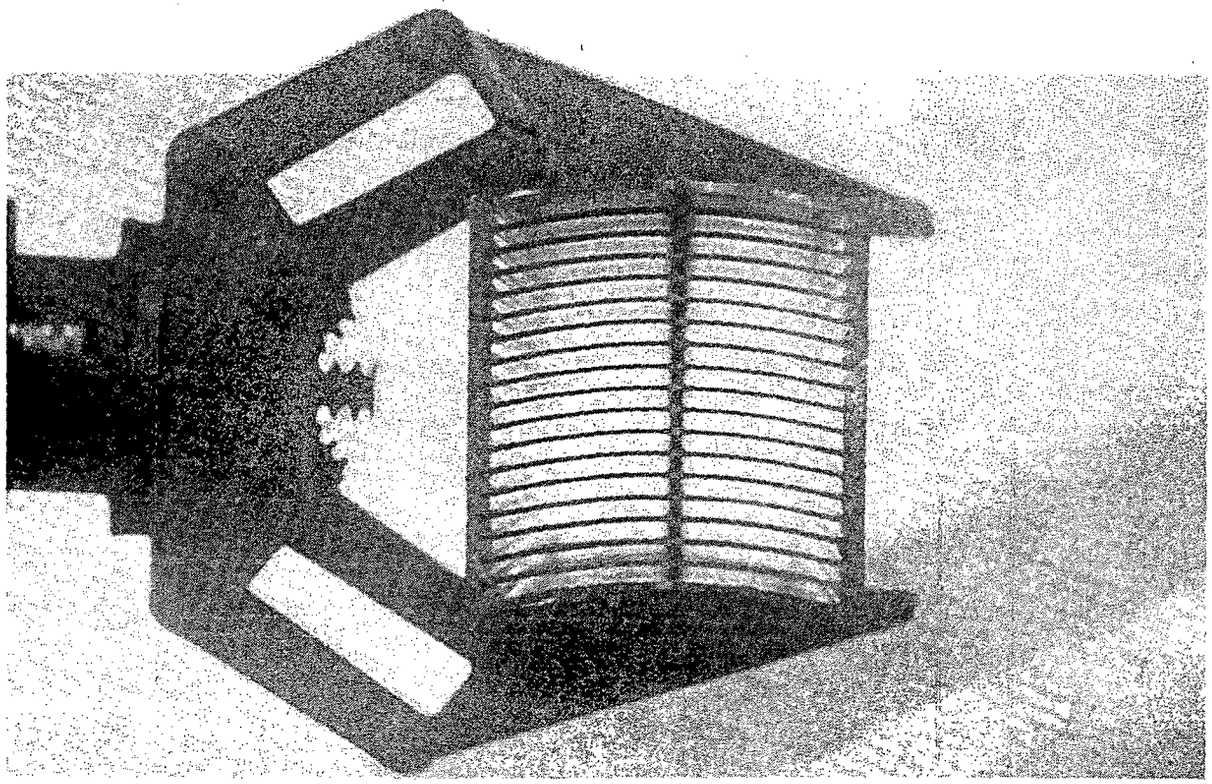

Figure B.8. View Through Coolant Channels of Element BSI-202 After Removal of End Boxes. (R-79658)

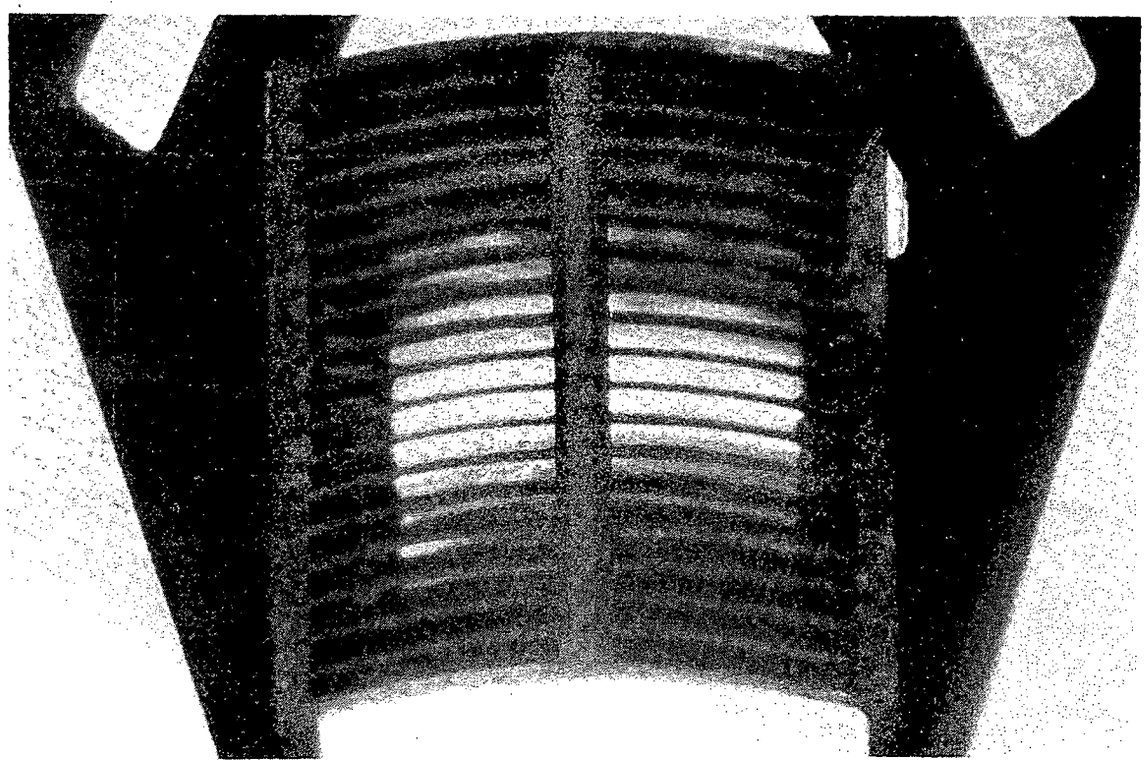

Figure B.9. View Through Coolant Channels of Element CSI-201 After Removal of End Boxes. (Y-197813)

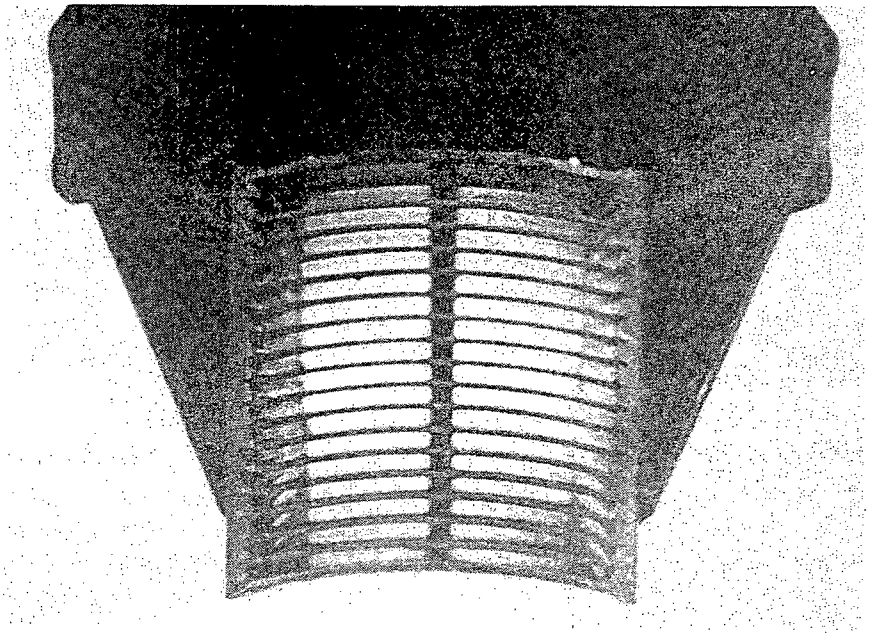

Figure B.10. View Through Coolant Channels of Element CSI-202 After Removal of End Boxes. (R-79660)

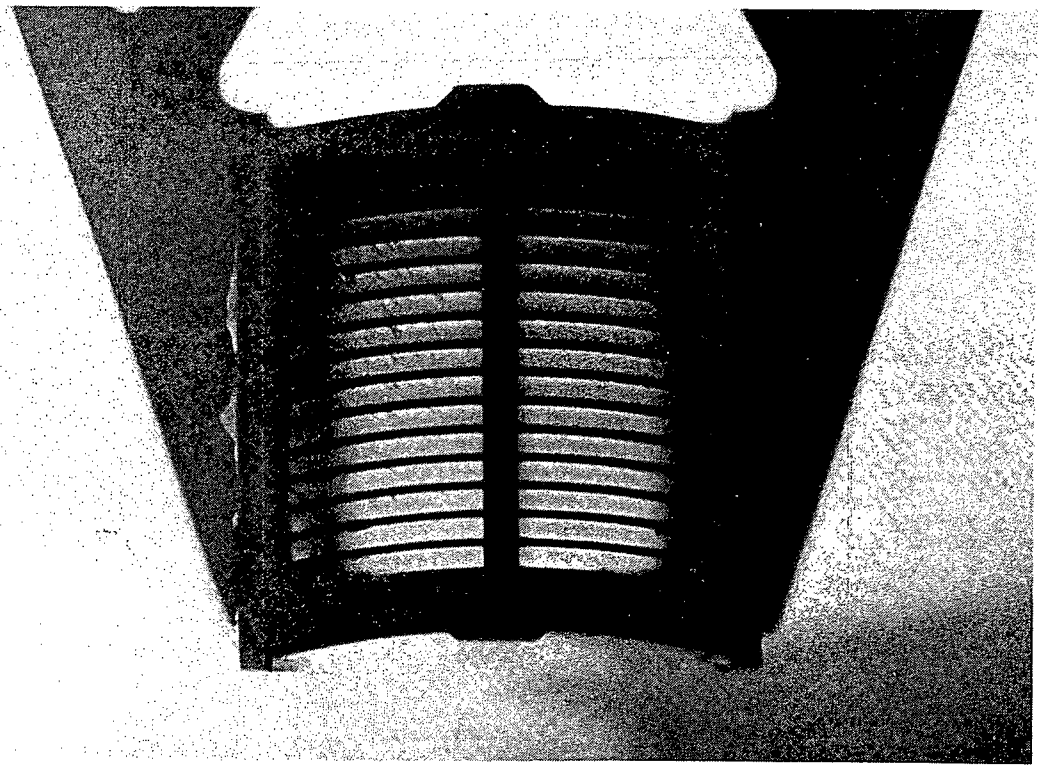

Figure B.11. View Through Coolant Channels of Element NSI-202 Before Removal of End Boxes. (Y-200765)

APPENDIX C

ELEMENT DIMENSIONAL MEASUREMENT DATA

This appendix presents the backup data for the element dimensions reported in Table VII. The method of measuring the elements is discussed in the text. The maximum and minimum reading for stack height and width are reported in Table VII. To determine if the element was bowed, the upper and lower dial indicator readings were plotted as a function of length and examined for nonlinearity. To determine twist, the upper and lower dial indicator readings were plotted and examined to see the departure from parallel of the front, back, and center tracks from top to bottom.

Table C.1. Dimensional Measurements -- Element BSI-201

Location (In. from top)	Stack Height (In.)	Width (In.)		FOR TWIST Indicator Readings Upper (In.)	Lower (In.)	Total (In.)	Width (In.)
Back 5	3.0738	2.9918	AT TOP				
10	3.0813	2.9882					
15	3.0788	2.9897	BACK	0.1370	0.2845	0.4215	2.9955
20	3.0770	2.9906	CENTER	0.1381	0.2864	0.4245	2.9985
25	3.0746	2.9909	FRONT	0.1348	0.2860	0.4208	2.9948
30	3.0744	2.9916					
Center 5	3.0638	2.9954	AT BOTTOM				
10	3.0683	2.9889					
15	3.0667	2.9913	BACK	0.1652	0.2530	0.4182	2.9822
20	3.0671	2.9917	CENTER	0.1614	0.2574	0.4188	2.9828
25	3.0645	2.9913	FRONT	0.1561	0.2619	0.4180	2.9820
30	3.0834	2.9924					
Front 5	3.0765	2.9950		LENGTH			
10	3.0838	2.9895		(In.)			
15	3.0827	2.9812					
20	3.0852	2.9821		38.386			
25	3.0841	2.9818					
30	3.0839	2.9824					

Table C.2. Dimensional Measurements -- Element BSI-202

Location (in. from top)	Stack Height (in.)	Width (in.)		FOR TWIST: Indicator Readings Upper (in.)	Lower (in.)	Total (in.)	Width (in.)
Back 5	3.0699	3.0003	AT TOP				
10	3.0772	2.9932					
15	3.0742	2.9952	BACK	0.1408	0.2830	0.4238	2.9968
20	3.0737	2.9944	CENTER	0.1419	0.2836	0.4255	2.9985
25	3.0706	2.9945	FRONT	0.1432	0.2812	0.4244	2.9974
30	3.0679	2.9948					
Center 5	3.0648	2.9972	AT BOTTOM				
10	3.0628	2.9944					
15	3.0608	2.9958	BACK	0.1859	0.2359	0.4218	2.9948
20	3.0647	2.9949	CENTER	0.1853	0.2369	0.4222	2.9952
25	3.0612	2.9950	FRONT	0.1834	0.2384	0.4218	2.9948
30	3.0626	2.9954					
Front 5	3.0824	2.9968		LENGTH			
10	3.0849	2.9934		(in.)			
15	3.0855	2.9959					
20	3.0879	2.9952		38.378			
25	3.0863	2.9951					
30	3.0856	2.9948					

Table C.3. Dimensional Measurements -- Element CSI-201

Location (in. from top)	Stack Height (in.)	Width (in.)		FOR TWIST Indicator Readings Upper (in.)	Lower (in.)	Total (in.)	Width (in.)
Back 5	3.0703	a	AT TOP				
10	3.0832						
15	3.0835		BACK	0.2252	0.3005	0.5257	2.9914
20	3.0784		CENTER	0.2278	0.2970	0.5248	2.9905
25	3.0778		FRONT	0.2295	0.2942	0.5237	2.9894
30	3.0715						
Center 5	3.0616		AT BOTTOM				
10	3.0734						
15	3.0731		BACK	0.2455	0.2841	0.5296	2.9953
20	3.0531		CENTER	0.2468	0.2756	0.5224	2.9881
25	3.0349		FRONT	0.2459	0.2738	0.5197	2.9854
30	3.0615						
Front 5	3.0531			LENGTH			
10	3.0698			(in.)			
15	3.0708						
20	3.0675			a			
25	3.0576						
30	3.0614						

[a]Width and length data unusable because of faulty calibration. Width data from twist measurements used.

Table C.4. Dimensional Measurements Element CSI-202

Location (in. from top)	Stack Height (in.)	Width (in.)		FOR TWIST Indicator Readings Upper (in.)	Lower (in.)	Total (in.)	Width (in.)
Back 5	3.0567	2.9793	AT TOP				
10	3.0732	2.9795					
15	3.0786	2.9783	BACK	0.1616	0.2718	0.4334	2.9794
20	3.0799	2.9777	CENTER	0.1588	0.2776	0.4364	2.9824
25	3.0738	2.9779	FRONT	0.1515	0.2840	0.4355	2.9815
30	3.0579	2.9802					
Center 5	3.0511	2.9790	AT BOTTOM				
10	3.0636	2.9784					
15	3.0726	2.9773	BACK	0.1723	0.2622	0.4345	2.9805
20	3.0750	2.9751	CENTER	0.1611	0.2729	0.4340	2.9800
25	3.0658	2.9760	FRONT	0.1493	0.2829	0.4322	2.9782
30	3.0694	2.9798					
Front 5	3.0645	2.9790		LENGTH			
10	3.0771	2.9788		(in.)			
15	3.0829	2.9790					
20	3.0842	2.9761		38.367			
25	3.0799	2.9765					
30	3.0684	2.9782					

Table C.5. Dimensional Measurements -- Element NSI-201

Location (in. from top)	Stack Height (in.)	Width (in.)		FOR TWIST Indicator Readings Upper (in.)	Lower (in.)	Total (in.)	Width (in.)
Back 5	-	-	AT TOP				
10	-	-					
15	-	-	BACK	0.2151	0.1609	0.3760	2.9870
20	-	-	CENTER	0.2155	0.1598	0.3753	2.9863
25	-	-	FRONT	0.2162	0.1589	0.3751	2.9861
30	-	-					
Center 5	3.0681	2.9865	AT BOTTOM				
10	3.0736	2.9876					
15	3.0726	2.9844	BACK	0.2150	0.1641	0.3791	2.9901
20	3.0741	2.9843	CENTER	0.2134	0.1654	0.3788	2.9898
25	3.0754	2.9843	FRONT	0.2116	0.1672	0.3788	2.9898
30	3.0734	2.9898					
Front 5	-	-		LENGTH			
10	-	-		(in.)			
15	-	-					
20	-	-		38.365			
25	-	-					
30	-	-					

Table C.6. Dimensional Measurements -- Element NSI-202

Location (in. from top)	Stack Height (in.)	Width (in.)		FOR TWIST Indicator Readings Upper (in.)	Lower (in.)	Total (in.)	Width (in.)
Back 5	-	-	AT TOP				
10	-	-					
15	-	-	BACK	0.2365	0.3004	0.5369	2.9930
20	-	-	CENTER	0.2461	0.2992	0.5453	3.0014
25	-	-	FRONT	0.2382	0.2982	0.5364	2.9925
30	-	-					
Center 5	3.0709	3.0014	AT BOTTOM				
10	3.0751	2.9940					
15	3.0796	2.9938	BACK	0.2521	0.2860	0.5381	2.9942
20	3.0815	2.9940	CENTER	0.2488	0.2888	0.5376	2.9937
25	3.0809	2.9933	FRONT	0.2455	0.2821	0.5276	2.9837
30	3.0746	2.9937					
Front 5	-	-		LENGTH			
10	-	-		(in.)			
15	-	-					
20	-	-		38.413			
25	-	-					
30	-	-					

APPENDIX D

ELEMENT GAMMA SCANS

Figures D.1 through D.3 show the strip chart records produced when scanning the fuel elements using a NaI detector and a narrow energy window containing the ^{137}Cs 662-keV peak. The gamma intensity is in relative units for each element separately.

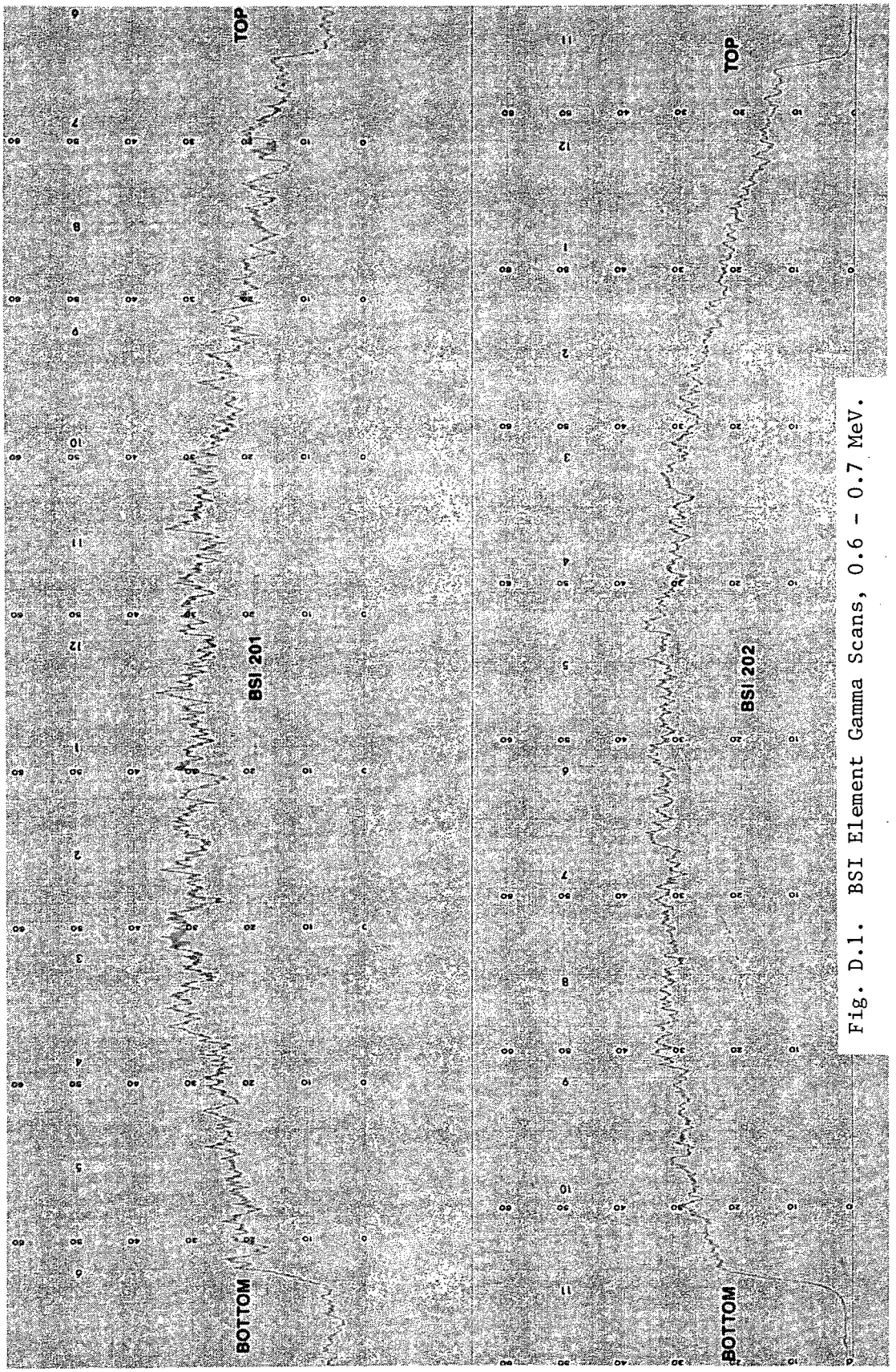

Fig. D.1. BSI Element Gamma Scans, 0.6 - 0.7 MeV.

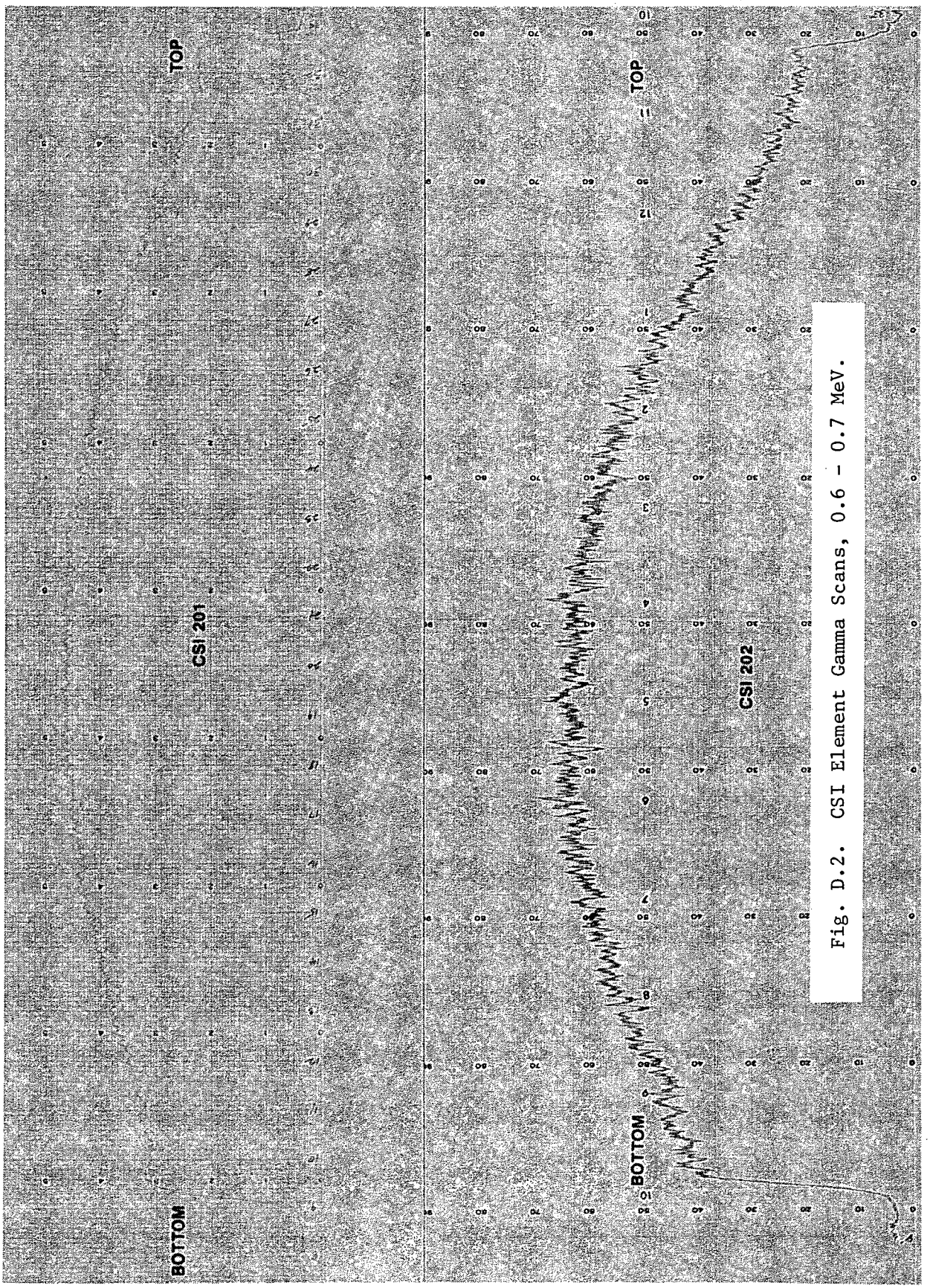

Fig. D.2. CSI Element Gamma Scans, 0.6 - 0.7 MeV.

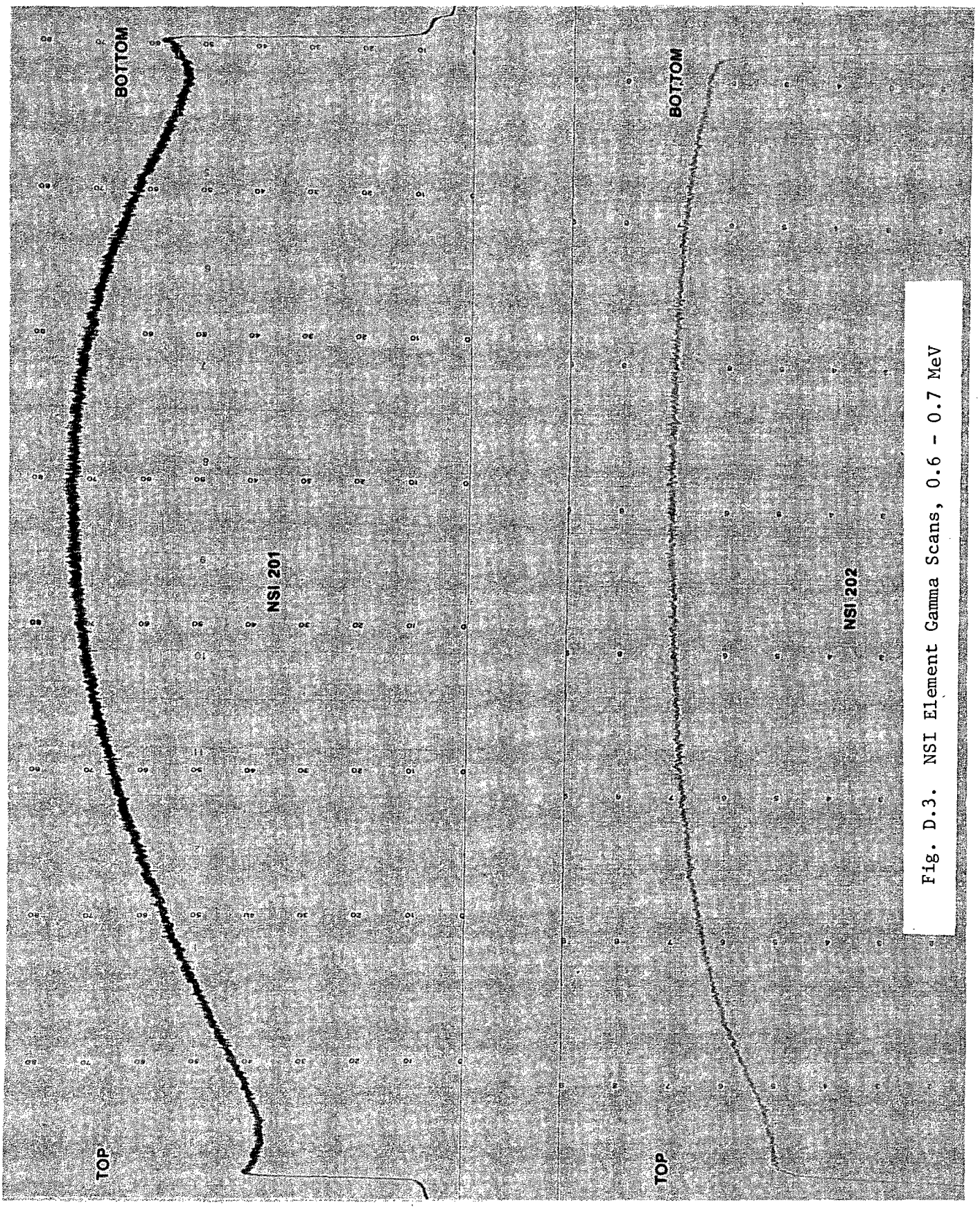

Fig. D.3. NSI Element Gamma Scans, 0.6 - 0.7 MeV

APPENDIX E

COOLANT CHANNEL GAP THICKNESS MEASUREMENTS

Table E-1. BSI-201 Coolant Channel Measurements

	Bottom Side (mils)				Top Side (mils)			
Channel	Max.	Min.	Avg.	At Peak Burnup	Max.	Min.	Avg.	At Peak Burnup
1	121.0	114.1	116.2	116.1	121.0	114.2	116.5	117.1
2	120.0	114.5	116.2	116.5	121.0	114.5	116.2	116.4
3	117.0	114.2	115.8	115.5	118.1	115.0	116.8	117.2
4	114.0	110.0	111.2	111.0	115.1	109.0	111.0	109.9
5	118.0	115.1	116.8	117.6	118.9	113.3	117.7	118.0
6	115.0	109.8	111.2	110.3	116.2	109.5	111.0	110.2
7	117.0	113.4	115.0	114.3	118.8	113.5	115.8	114.5
8	118.8	116.5	118.0	118.8	119.7	115.2	118.0	119.0
9	113.1	110.5	112.0	111.5	114.0	111.5	112.6	111.6
10	117.5	112.8	115.2	116.0	114.8	112.0	113.2	113.0
11	116.0	109.7	114.0	113.6	116.0	111.7	113.6	113.1
12	118.0	112.4	113.9	113.3	114.5	110.7	112.5	112.4
13	115.7	108.7	113.6	115.4	115.1	110.3	113.0	113.7
14	125.0	121.5	123.4	122.7	111.1	105.6	109.6	111.0
15	123.2	114.6	119.3	120.5	115.0	108.8	111.3	109.1
16	120.3	106.3	113.4	114.7	118.4	115.1	117.2	116.9
17	116.0	107.8	111.6	110.3	117.3	113.0	114.8	113.4
18	116.5	105.0	112.0	111.7	117.8	109.8	114.3	114.4
			Average	115.0			Average	113.9

Table E-2. BSI-202 Coolant Channel Measurements

	Bottom Side (mils)				Top Side (mils)			
Channel	Max.	Min.	Avg.	At Peak Burnup	Max.	Min.	Avg.	At Peak Burnup
1	120.0	114.3	116.0	117.5	120.0	112.7	115.2	115.4
2	117.0	111.5	113.5	114.0	115.0	110.0	113.0	112.9
3	114.8	111.4	112.6	113.3	114.0	111.0	112.2	112.9
4	115.3	111.0	112.3	112.3	117.0	111.0	112.0	111.9
5	120.4	114.9	115.9	115.7	115.4	112.0	112.8	113.2
6	113.4	111.0	112.2	113.2	115.0	110.9	112.0	112.2
7	119.7	116.0	116.6	116.5	115.2	113.3	114.4	115.2
8	116.0	111.9	114.1	114.3	115.0	112.1	113.1	113.5
9	116.0	113.3	114.2	114.2	115.6	112.8	113.7	114.1
10	115.6	113.0	113.7	114.3	115.4	112.9	114.0	113.3
11	116.0	110.8	112.5	112.0	115.6	112.0	112.7	112.5
12	116.3	113.7	114.8	115.0	116.5	114.2	115.4	114.5
13	111.6	107.5	109.0	108.8	112.3	107.6	109.1	108.9
14	119.0	113.2	117.5	117.7	121.0	113.7	118.0	115.9
15	121.1	116.3	117.4	117.7	119.8	115.1	117.0	116.7
16	110.0	106.7	108.6	108.1	110.5	105.3	108.1	107.7
17	116.5	115.3	116.9	118.1	117.0	112.2	114.6	115.8
18	113.7	109.6	112.4	111.9	114.4	106.4	110.8	112.5
			Average	114.1			Average	113.3

Table E-3. CSI-202 Coolant Channel Measurements

Channel	Bottom Side (mils)				Top Side (mils)			
	Max.	Min.	Avg.	At Peak Burnup	Max.	Min.	Avg.	At Peak Burnup
1	115.0	104.0	112.3	111.9	120.0	112.8	115.2	113.6
2	111.6	103.3	108.0	108.6	112.5	106.2	108.8	108.9
3	112.0	104.8	107.4	107.5	112.0	103.8	107.0	106.2
4	115.0	106.6	110.0	108.8	114.0	105.4	108.0	107.1
5	113.0	105.7	108.7	108.9	112.5	106.4	108.8	109.1
6	112.9	110.4	111.9	111.4	112.0	106.1	108.6	108.4
7	113.8	107.3	110.7	111.0	111.6	106.3	108.1	107.8
8	113.6	107.4	110.2	111.0	111.4	105.8	108.4	108.4
9	114.6	110.2	113.1	113.6	113.3	106.5	109.5	109.6
10	111.3	107.4	109.4	109.2	112.7	108.1	110.5	111.2
11	110.2	106.2	108.6	108.2	112.2	108.8	109.6	109.7
12	112.8	109.4	112.0	111.8	115.0	108.2	111.3	111.3
13	111.4	107.9	109.6	109.4	110.3	106.2	109.2	110.3
14	114.2	110.6	112.1	112.0	113.0	109.2	111.2	110.0
15	115.1	111.0	113.0	113.6	113.1	111.7	112.4	112.5
16	120.0	117.7	119.1	120.0	115.3	113.0	114.6	115.2
17	119.0	113.6	117.6	116.2	115.1	111.8	113.6	114.2
18	123.4	120.0	122.1	123.0	116.8	109.4	115.8	116.6
			Average	112.0			Average	110.6

Table E-4. NSI-201 Coolant Channel Measurements

Channel	Bottom Side (mils)				Top Side (mils)			
	Max.	Min.	Avg.	At Peak Burnup	Max.	Min.	Avg.	At Peak Burnup
1	116.0	108.0	109.2	109.2	117.0	108.0	114.6	109.5
2	106.4	103.0	104.7	104.5	108.7	104.2	107.2	106.7
3	112.0	104.0	106.0	104.6	109.0	103.2	105.2	104.1
4	110.0	108.0	109.3	109.1	109.8	107.2	108.7	108.8
5	110.0	105.0	107.6	107.3	109.7	105.3	107.5	107.1
6	109.2	107.2	108.6	108.1	109.1	107.0	108.2	107.5
7	109.0	105.0	107.0	106.5	109.0	105.0	107.0	105.9
8	111.0	108.3	109.1	109.3	111.0	108.2	109.6	109.8
9	108.0	105.0	105.2	105.3	107.5	104.3	105.5	104.7
10	109.6	107.5	108.9	108.8	109.8	107.8	109.2	109.2
11	109.3	106.7	108.2	107.7	110.0	107.0	108.4	107.1
12	110.2	108.1	109.5	108.9	110.4	108.5	109.5	108.8
13	109.8	106.9	108.3	108.3	105.5	104.0	104.7	105.6
14	112.2	109.3	111.0	110.6	108.7	106.8	107.8	107.7
15	111.6	108.5	110.0	109.5	124.0	105.9	107.0	106.0
16	115.5	110.0	114.3	114.7	124.0	108.0	109.7	109.8
17	113.2	108.8	112.0	112.3	124.0	106.5	107.0	106.1
18	107.3	101.8	103.2	102.7	106.0	102.5	103.9	104.0
			Average	108.2			Average	107.1

APPENDIX F

PLATE THICKNESS MEASUREMENTS

This appendix presents the backup data for the plate thickness increases reported in Table VIII. The methods of measuring plate thickness are discussed in the text. In general, the plate thickness was measured at 26 locations on the plate. Along the length of the plate in eight locations, the thickness was measured in the center of the plate and near both edges. Two measurements were taken 1/4-inch from the top of the plates over the unfueled region. In calculating average thickness change for plate swelling, only the center measurements were used because of the additional uncertainties in the measurements near the edges due to the angle of the plate between the dial indicator tips. Since burnup is not uniform, thickness increases are compared at two locations--the maximum- and minimum-burnup locations. The minimum-burnup location is near the top of the plate and only the measurment at the 1-inch point was included. The peak-burnup region is larger and the 13- and 16-inch measurements were averaged. Although all plates of NSI-201 and NSI-202 were measured, only those plates in positions 2, 6, 10, 14, and 18 were included in the averages since only the plates in those positions were measured for the other four elements.

Table F.1
Element BSI-201
Plate Thickness and Incremental Thickness Compared to Ends (mils)

Distance From Top of Plate in.	Plate S-3-211-15 Position 2		Plate S-3-211-3 Position 6		Plate S-3-210-19 Position 10		Plate S-3-210-9 Position 14		Plate S-3-210-1 Position 18	
	t*	Δt	t*	Δt	t*	Δt	t*	Δt	t*	Δt
1/4	50.7	-	49.9	-	50.3	-	49.1**	-	49.9	-
1	50.7	0	49.9	0	50.3	0	49.8**	0.7	49.9	0
4	50.6	-0.1	49.7	-0.2	50.4	0.1	49.8	0.7	50.8	0.9
7	50.6	-0.1	49.8	-0.1	51.1	0.8	50.0	0.9	51.6	1.7
10	50.9	0.2	49.7	-0.2	51.8	1.5	50.5	1.4	52.7	2.8
13	50.6	-0.1	49.7	-0.2	52.0	1.7	51.0	1.9	53.2	3.3
16	50.9	0.2	50.3	0.4	52.1	1.8	51.0	1.9	53.7	3.8
19	50.7	0	49.6	-0.3	52.2	1.9	51.1	2.0	54.3	4.4
22	-	-	-	-	51.0	0.7	50.8	1.8	54.2	4.3

Average at 1 inch (low-burnup end) 0.1 mil

Average at 13 to 16 inches (peak-burnup region) 1.5 mils

*Plate thickness calculated by adding thickness change from plate end to preirradiation end tab thickness.

**Values determined by capacitance measuring device. Preirradiation end tab measured 50.3.

Table F.2
Element BSI-202
Plate Thickness and Incremental Thickness Compared to Ends (mils)

Distance From Top of Plate in.	Plate S-3-212-3 Position 2		Plate S-3-213-3 Position 6		Plate S-3-212-15 Position 10		Plate S-3-212-7 Position 14		Plate S-3-211-19 Position 18	
	t*	Δt	t*	Δt	t*	Δt	t*	Δt	t*	Δt
1/4	50.8	-	49.9**	-	50.1**	-	50.1	0	50.4	-
1	50.8	0	49.9**	0	50.1**	0	50.1	0	50.4	0
4	51.3	0.5	49.9	0	50.4	0.3	51.2	1.1	51.2	0.8
7	52.1	1.3	50.2	0.3	50.9	0.8	52.7	2.6	51.8	1.4
10	52.6	1.8	50.5	0.6	51.4	1.3	52.1	2.0	51.4	1.0
13	52.7	1.9	50.8	0.9	51.5	1.4	53.3	3.2	51.6	1.2
16	53.3	2.5	50.8**	0.9	51.5**	1.4	53.5	3.4	51.5	1.1
19	53.3	2.5	50.6	0.7	51.8	1.7	53.5	3.4	51.5	1.1
22	53.0	2.2	50.6	0.7	51.9	1.8	52.0	1.9	52.2	1.8

Average at 1 inch (low-burnup end) 0

Average at 13 to 16 inches (peak-burnup region) 1.8 mils

*Plate thickness calculated by adding thickness change from plate end to preirradiation end tab thickness.

**Plate thickness corroborated by new capacitance measuring device.

Table F.3
Element CSI-201
Plate Thickness and Incremental Thickness Compared to Ends (mils)

Distance From Top of Plate in.	Plate OSIEW-087 Position 1		Plate OSIIW-061 Position 5		Plate OSIIW-047 Position 9		Plate OSIIW-052 Position 13		Plate OSIIW-083 Position 17	
	t	Δt	t	Δt	t	Δt	t	Δt	t	Δt
1/4	*	-	*	-	*	-	*	-	*	-
1		0.5		1.2		-0.9		-0.6		0.5
4		1.3		0.6		0.5		1.0		0.5
7		1.6		0.6		0.5		1.2		1.4
10		2.3		0		1.1		2.1		1.0
13		2.8		0.7		1.3		2.7		0.9
16		2.8		0.4		1.5		3.0		1.3
19		2.7		1.7		2.2		2.6		0.9
22		2.9		0.6		1.4		2.2		1.4

Average at 1 inch (low-burnup end) 0.1 mil

Average at 13 to 16 inches (peak-burnup region) 1.7 mils

*Actual plate thicknesses are not calculated due to erroneous standard readings. Thickness changes are measured relative to the plate thickness at 1/4" over the unfueled region.

Table F.4
Element CSI-202
Plate Thickness and Incremental Thickness Compared to Ends (mils)

Distance From Top of Plate in.	Plate OSIIW-085 Position 2		Plate OSIIW-079 Position 6		Plate OSIIW-063 Position 10		Plate OSIIW-039 Position 14		Plate OSIIW-075 Position 18	
	t*	Δt	t*	Δt	t*	Δt	t*	Δt	t*	Δt
1/4	50.0	-	50.0	-	50.4	-	49.2	-	49.4	-
1	51.0	1.0	50.5	0.5	50.9	0.5	49.7	0.5	49.6	0.2
4	51.4	1.4	52.6	2.6	52.6	2.2	50.5	1.3	51.6	2.2
7	52.9	2.9	52.6	2.6	53.1	2.7	51.7	2.5	53.3	3.9
10	53.6	3.6	53.9	3.9	53.5	3.1	52.2	3.0	54.4	5.0
13	55.8	5.8	55.2	5.2	53.6	3.2	53.3	4.1	54.9	5.5
16	52.8	2.8	55.2	5.2	53.8	3.4	53.0	3.8	54.1	4.7
19	52.2	2.2	54.4	4.4	53.6	3.2	52.4	3.2	53.7	4.3
22	50.5	0.5	53.3	3.3	54.6	4.2	50.9	1.7	53.6	4.2

Average at 1 inch (low-burnup end) 0.5 mil

Average at 13 to 16 inches (peak-burnup region) 4.4 mils

*Plate thickness calculated by adding thickness change from plate end to preirradiation end tab thickness.

Table F.5
Element NSI-201
Plate Thickness and Incremental Thickness Compared to Ends (mils)

Distance From Top of Plate in.	Plate ORR-92 Position 2		Plate ORR-97 Position 6		Plate ORR-102 Position 10		Plate ORR-106 Position 14		Plate ORR-110 Position 18	
	t*	Δt	t*	Δt	t*	Δt	t*	Δt	t*	Δt
1/4	49.2	-	48.7	-	49.0	-	49.0	-	49.2	-
1	48.8	-0.4	49.8	1.1	50.1	1.1	49.8	0.8	50.2	1.0
4	48.9	-0.3	50.0	1.3	50.1	1.1	50.1	1.1	50.0	0.8
7	48.7	-0.5	50.0	1.3	50.0	1.0	50.0	1.0	50.2	1.0
10	48.8	-0.4	50.1	1.4	50.0	1.0	50.3	1.3	50.3	1.1
13	49.4	0.2	50.2	1.5	50.1	1.1	50.2	1.2	50.2	1.0
16	49.2	0	50.0	1.3	50.1	1.1	50.0	1.0	50.3	1.1
19	49.2	0	49.9	1.2	50.1	1.1	50.3	1.3	50.4	1.2
22	49.7	0.5	50.1	1.4	50.0	1.0	50.3	1.3	50.5	1.3

Δt average at 1 inch (low-burnup end) 0.7 mil

Δt average at 13 to 16 inches (peak-burnup region) 1.0 mils

*Plate thickness based on comparison to standard with thickness change calculated from plate end tabs postirradiation measurement.

Table F.6
Element NSI-202
Plate Thickness and Incremental Thickness Compared to Ends (mils)

Distance From Top of Plate in.	Plate ORR-120 Position 7		Plate ORR-121 Position 8		Plate ORR-131 Position 15		Plate ORR-139 Position 17		Plate ORR-140 Position 18	
	t*	Δt	t*	Δt	t*	Δt	t*	Δt	t*	Δt
1/4	50.6	-	50.0	-	51.1	-	50.7	-	51.2	-
1	51.8	1.2	51.6	1.6	51.7	0.6	52.0	1.3	51.7	0.5
4	52.8	2.2	53.4	3.4	52.4	1.3	52.4	1.7	53.2	2.0
7	53.0	2.4	57.8	2.8	53.0	1.9	52.9	2.2	54.4	3.2
10	53.6	3.0	53.4	3.4	54.0	2.9	53.5	2.8	55.5	4.1
13	54.3	3.7	54.2	4.2	54.5	3.4	53.9	3.2	56.2	5.0
16	55.0	4.4	54.7	4.7	54.5	3.4	54.6	3.9	56.7	5.5
19	55.1	4.5	54.5	4.5	55.0	3.9	54.5	3.8	56.6	5.4
22	55.6	5.0	54.1	4.1	54.2	3.1	54.0	3.3	56.8	5.6

Average at 1 inch (low-burnup end) 1.0 mil

Average at 13 to 16 inches (peak-burnup region) 4.1 mils

*Plate thickness based on comparison to standard with thickness change calculated from plate end tabs postirradiation measurement.

APPENDIX G

PLATE GAMMA SCANNING DATA AND BURNUP ANALYSIS

Correlation of Gamma Scanning and Burnup Data - As discussed in the text, several methods of taking and recording gamma scanning data were used over the course of this work. The gamma scan profile was used to select the axial minimum- and maximum-burnup locations for the burnup analysis samples. Full width sections were removed from one plate of each element at these locations and analyzed by mass spectrometry to determine the burnup (see below). To obtain the average burnup at the low- and maximum-burnup positions, the ^{137}Cs peak as measured by the NaI crystal and strip chart was used. The chart readings at the minimum were averaged and the ratio of the average to the reading of the analyzed plate was multiplied by the analyzed burnup value. The same method was used for finding the average burnup at the axial maximum. To find the average burnup along the length of the plates (and hence elements), the chart readings were averaged along the length of the charts at one-inch intervals (about 35 readings per chart). This gives a bias toward a low average since the minimum-to-maximum ratios of the readings are consistently lower than those of the analyzed burnups. Such a discrepancy could result if a plate had different transverse burnup profiles at the minimum- and maximum-burnup positions since only the central part of the plate was scanned while the entire width of the plate was averaged in the burnup analyses. The same five plates were used for the minimum- and maximum-burnup location averages as were used for the thickness measurements.

The data obtained using the Ge(Li) detector and the multichannel analyzer are believed to be more accurate than the analog data obtained using the NaI crystal for determining the burnup profile through an element. Therefore, these data were used for elements BSI-201, BSI-202, CSI-201, and NSI-202. As explained in Table G.4, the multichannel data appeared to be discrepant for the plate in position 18 of CSI-202. Multichannel data were not obtained for all plates of NSI-201. The analog data were used for these two elements. The element was assumed to have the axial profile of the plate from which the burnup analysis sample was taken, and the analyzed maximum burnup was used. The data and correlation calculations are presented in Tables G.1 through G.6. Examples of the analog gamma scan charts are shown in Figs. G.1 through G.6.

Burnup Calculation from Isotopic Analysis - The isotopic composition of the uranium and plutonium after irradiation can be used to calculate the burnup or percentage depletion of the original ^{235}U in the elements. The isotopic abundance data as determined by mass spectrographic analysis are presented in Table G.7.

The burnup can be expressed in terms of the pre- and postirradiation ^{235}U isotopic abundances, as shown in the following. Let

B = fractional ^{235}U depletion (burnup),
A_o = fractional ^{235}U atomic abundance prior to irradiation,
A = fractional ^{235}U atomic abundance after irradiation,
C = $^{238}U/^{235}U$ atomic depletion ratio during irradiation,
and D = $^{236}U/^{235}U$ atomic depletion ratio during irradiation (negative quantity).

Now,
$$B = 1 - \frac{AN}{A_o N_o} ,$$

where N_o and N represent the pre- and postirradiation uranium atom densities. If ΔN^5 represents the change in ^{235}U atom density during irradiation,

$$N = N_o - (1 + C + D)\Delta N^5$$

and
$$B = 1 - \frac{AN_o - (1 + C + D)A\Delta N^5}{A_o N_o}$$

$$= 1 - A/A_o + (1 + C + D)AB.$$

Therefore,
$$B = \frac{1 - A/A_o}{1 - (1 + C + D)A} \qquad (1)$$

The parameters C and D have been derived from the results of integral transport cell calculations performed at ANL by M. M. Bretscher and R. J. Cornella. They behave as follows:

	LEU		MEU	
B	C	D	C	D
0.54	0.13	-0.16	0.06	-0.16
0.76	0.15	-0.15	0.07	-0.16
0.89	0.18	-0.15	0.08	-0.15
0.96	0.22	-0.14	0.10	-0.15
0.98	0.26	-0.14	0.10	-0.14

It appears that C and D are not particularly sensitive to the uranium density. There is obviously a dependence of C on the enrichment; however, there is a very weak dependence of B on either C or D, as indicated by Eq. 2, since A is small ($\leq$0.20 for LEU).

$$\frac{\partial B}{\partial C} = \frac{\partial B}{\partial D} = \frac{AB}{1 - (1 + C + D)A} \qquad (2)$$

Therefore, the calculations from which C and D are derived do not have to be extremely accurate.

As used in Eq. 1, A and A_o are atomic ratios while the enrichment, e, is a weight ratio. The relationship between A_o and e_o is

$$A_o = \frac{1}{1 + 0.98736(1/e_o - 1)} \qquad (3)$$

The fission density due to ^{235}U fission alone (F_{DU}) can be derived as follows:

$$B = \frac{N_F + N_C}{N}$$

where N_F, N_C, and N are the densities of ^{235}U fissions, ^{235}U captures, and originally contained ^{235}U atoms, respectively.

$$N_F + N_C = N_F(1 + \alpha)$$

where α = the ^{235}U capture-to-fission ratio.

$$N = \frac{6.022 \times 10^{21}\ \rho_U e}{235.04}$$

Therefore, substituting the symbol F_{DU} for N_F,

$$F_{DU} = \frac{2.562 \times 10^{21}\ \rho_U eB}{1 + \alpha}$$

Assuming an average value of 0.19 for α over the burnup of the fuel,

$$F_{DU} = 2.15 \times 10^{21}\ \rho_U eB \qquad \text{(fissions/cm}^3\text{)}. \qquad (4)$$

Integral transport cell depletion calculations, performed at ANL by R. J. Cornella, provided the ^{235}U fission fraction as a function of ^{235}U depletion. The cumulative fission fraction is plotted as a function of ^{235}U burnup in Fig. G.8 for 20%-enriched (LEU) and 45%-enriched (MEU) fuel. The result of Eq. (4), divided by the appropriate fission fraction, gives the absolute fission density. Burnups, fission fractions, and fission densities of the analyzed samples are given in Table G.8.

It was the intent early in the RERTR Program to determine absolute fission densities based upon ^{148}Nd measurements. The results of such determinations were found to be unreliable, for undetermined reasons. Therefore, acquisition and use of ^{148}Nd data were abandoned.

Table G.1.
Element BSI-201
Burnup Analysis Plate S-3-210-1, Position 18

Calculation of Plate Average

	^{137}Cs, 10^3 Cts/s	Burnup % ^{235}U Depletion
Minimum	22.5	$\frac{22.5}{24.0} \times 31.5 = 29.5$
At Top Analysis Point	24.0	31.5
Maximum (Bottom Analysis Point)	62.5	70.9
Average	48.4	$\frac{48.4}{62.5} \times 70.9 = 54.9$

Calculation of Element Average

Plate Position	^{137}Cs, 10^3 Cts/s		
	Minimum	Maximum	Average
2	21.0	62.5	48.3
6	21.0	57.0	44.9
10	20.5	60.0	45.5
14	21.5	61.5	47.3
18	22.5	62.5	48.4
Average	21.3	60.7	46.9
Correlated Average Burnup	$\frac{21.3}{22.5} \times 29.5 =$ 28.0	$\frac{60.7}{62.5} \times 70.9 =$ 68.9	$\frac{46.9}{48.4} \times 54.9 =$ 53.2

^{137}Cs peak measured by multichannel analyzer gave the following counts/s at the maximum-burnup position for plates 1 through 19: 141.8, 156.1, 157.9, 150.0, 148.9, 146.3, 154.5, 152.1, 146.9, 149.0, 154.2, 150.9, 155.0, 150.7, 154.6, 152.5, 162.9, 154.3, and 151.9. The average of 152.1 correlates to an element average burnup of 54.1% using all 19 plates.

Table G.2.

Element BSI-202

Burnup Analysis Plate S-3-211-19, Position 18

Calculation of Plate Average

	^{137}Cs, 10^3 Cts/s	Burnup % ^{235}U Depletion
Minimum	115	$\frac{115}{115} \times 50.5 = 50.5$
At Top Analysis Point	115	50.5
Maximum (Bottom Analysis Point)	315	97.3
Average	259	$\frac{259}{315} \times 97.3 = 80.0$

Calculation of Element Average

Plate Position	^{137}Cs, 10^3 Cts/s Minimum	Maximum	Average
2	115	320	269
6	130	310	265
10	125	310	262
14	120	310	260
18	115	315	259
Average	121	313	263
Correlated Average Burnup	$\frac{121}{115} \times 50.5 =$ 53.1	$\frac{313}{315} \times 97.3 =$ 96.7	$\frac{263}{259} \times 80.0$ 81.2

^{137}Cs peak measured by multichannel analyzer gave the following counts/s at the maximum-burnup position for plates 1 through 19: 239.2, 250.2, 237.5, 264.2, 252.5, 239.5, 231.4, 253.0, 226.1, 235.4, 248.8, 240.1, 233.3, 245.9, 228.4, 233.3, 243.8, 250.3, and 252.1. The average of 242.4 correlates to an element average burnup of 77.5% using all 19 plates.

Table G.3.

Element CSI-201

Burnup Analysis Plate OSIIW-084, Position 18

Calculation of Plate Average

	^{137}Cs, 10^3 Cts/s	Burnup % ^{235}U Depletion
Minimum	17.0	$\frac{17.0}{17.5} \times 32.7 = 31.8$
At Top Analysis Point	17.5	32.7
Maximum (Bottom Analysis Point)	45.5	66.9
Average	36.7	$\frac{36.7}{45.5} \times 66.8 = 54.0$

Calculation of Element Average

Plate Position	^{137}Cs, 10^3 Cts/s		
	Minimum	Maximum	Average
2	17.0	46.0	38.0
6	17.0	43.5	34.7
10	16.5	45.0	36.0
14	17.0	44.0	34.6
18	17.0	45.5	36.7
Average	16.9	44.8	36.0
Correlated Average Burnup	$\frac{16.9}{17.0} \times 31.8 =$ 31.6	$\frac{44.8}{45.5} \times 66.8 =$ 65.8	$\frac{36.0}{36.7} \times 54.0 =$ 53.0

^{137}Cs peak measured by multichannel analyzer gave the following counts/s at the maximum-burnup position for plates 1 through 19: 714.2, 575.8, 662.1, 646.8, 568.6, 541.5, 545.9, 610.9, 584.9, 608.4, 602.0, 615.6, 594.2, 600.7, 604.2, 607.2, 611.1, 627.4, and 656.5. The average of 609.4 correlates to an element average burnup of 52.4% using all 19 plates.

Table G.4.

Element CSI-202

Burnup Analysis Plate OSIIW-075, Position 18

Calculation of Plate Average

	^{137}Cs, 10^3 Cts/s	Burnup % ^{235}U Depletion
Minimum	105	$\frac{105}{105} \times 55.0 = 55.0$
At Top Analysis Point	105	55.0
Maximum (Bottom Analysis Point)	290	96.6
Average	245	$\frac{245}{290} \times 96.6 = 81.6$

Calculation of Element Average

Plate Position	^{137}Cs, 10^3 Cts/s Minimum	Maximum	Average
2	115	300	251
6	130	300	246
10	135	290	240
14	130	295	241
18	105	290	245
Average	123	295	245
Correlated Average Burnup	$\frac{123}{105} \times 55.0 =$ 64.4	$\frac{295}{290} \times 96.6 =$ 98.3	$\frac{245}{245} \times 81.7 =$ 81.7

^{137}Cs peak measured by multichannel analyzer gave the following counts/s at the maximum-burnup position for plates 1 through 19: 259.6, 232.6, 239.8, 235.8, 251.7, 248.4, 249.0, 235.6, 257.5, 240.1, 242.9, 236.0, 237.4, 234.9, 235.8, 232.2, 237.7, 228.8, and 239.9. The average of 240.8 was not used to correlate to an average element burnup because the value for plate 18 is obviously low and results in unphysically high burnups for many of the plates.

Table G.5.
Element NSI-201
Burnup Analysis Plate ORR-93, Position 3

Calculation of Plate Average

	^{137}Cs, 10^3 Cts/s	Burnup % ^{235}U Depletion
Minimum	21.5	$\frac{21.5}{23.0} \times 24.1 = 22.5$
At Top Analysis Point	23.0	24.1
Maximum (Bottom Analysis Point)	55.0	50.9
Average	43.0	$\frac{43}{55} \times 50.9 = 39.8$

Calculation of Element Average

Plate Position	^{137}Cs, 10^3 Cts/s		
	Minimum	Maximum	Average
1	21.0	51.0	40.1
2	20.0	53.5	41.5
3	21.5	55.0	43.0
4	19.0	52.0	39.6
5	18.5	50.5	38.5
6	17.0	47.0	35.9
7	16.5	47.0	35.7
8	21.5	54.0	42.0
9	16.5	46.0	34.6
10	19.0	52.0	39.6
11	15.5	45.0	33.8
12	16.0	45.5	34.5
13	17.0	48.5	37.2
14	16.0	46.0	34.8
15	17.0	48.5	36.5
16	16.5	46.5	35.5
17	16.5	47.0	35.7
18	16.5	47.5	35.8
19	21.0	54.5	41.9
Average	18.0	49.3	37.7
(Plates 2, 6, 10, 14, 18)	17.7	49.2	37.5
Correlated Average Burnup	$\frac{18.0}{21.5} \times 22.5 =$	$\frac{49.3}{55.0} \times 50.9 =$	$\frac{37.7}{43.0} \times 39.8 =$
(19 Plates)	18.9	45.6	34.9
(Plates 2, 6, 10, 14, 18)	18.5	45.5	34.7

Table G.6.

Element NSI-202

Burnup Analysis Plate ORR-140, Position 18

Calculation of Plate Average

	^{137}Cs, 10^3 Cts/s	Burnup % ^{235}U Depletion
Minimum	22.0	$\frac{22.0}{22.5} \times 54.2 = 53.0$
At Top Analysis Point	22.5	54.2
Maximum (Bottom Analysis Point)	49.0	96.4
Average	43.4	$\frac{43.4}{49.0} \times 96.4 = 85.4$

Calculation of Element Average

Plate Position	^{137}Cs, 10^3 Cts/s		
	Minimum	Maximum	Average
2	20.0	48.5	41.9
6	22.0	50.0	43.3
10	22.5	50.0	44.1
14	22.5	50.0	43.7
18	22.0	49.0	43.4
Average	21.8	49.5	43.3
Correlated Average Burnup	$\frac{21.8}{22.0} \times 53.0 =$ 52.5	$\frac{49.5}{49.0} \times 96.4 =$ 97.4	$\frac{43.3}{43.4} \times 85.5 =$ 85.3

^{137}Cs peak measured by multichannel analyzer gave the following counts/s at the maximum-burnup position for plates 1 through 19: 102.5, 97.4, 100.4, 98.0, 98.5, 100.0, 93.5,, 95.6, 97.8, 97.0, 95.4, 94.5, 92.9, 92.8, 95.4, 96.5,. 99.3, 100.9, and 100.0. The average of 97.3 correlates to an element average burnup of 82.4% using all 19 plates.

Table G.7. Final Isotopic Composition of Uranium and Plutonium

Element Number	BSI-201		BSI-202	
Plate Number	S-3-210-1		S-3-211-19	
	Top	Bottom	Top	Bottom
^{234}U	0.111	0.097	0.104	0.068
^{235}U	14.62	6.81	11.01	0.700
^{236}U	1.254	2.73	1.962	3.737
^{238}U	84.01	90.37	86.92	95.495
^{238}Pu	0.240	1.46	0.833	5.86
^{239}Pu	86.91	66.41	77.28	45.53
^{240}Pu	10.18	20.09	14.42	22.74
^{241}Pu	2.48	9.05	6.49	10.70
^{242}Pu	0.187	3.00	0.973	15.16

Element Number	CSI-201		CSI-202	
Plate Number	OSIIW-084		OSIIW-075	
	Top	Bottom	Top	Bottom
^{234}U	0.110	0.100	0.107	0.068
^{235}U	14.400	7.644	10.11	0.852
^{235}U	1.253	2.537	2.092	3.67
^{238}U	84.237	89.718	87.69	95.41
^{238}Pu	0.236	1.271	0.889	5.41
^{239}Pu	86.566	68.216	75.81	47.19
^{240}Pu	10.472	19.638	15.53	22.72
^{241}Pu	2.530	8.427	6.63	10.71
^{242}Pu	0.196	2.448	1.135	13.97

Element Number	NSI-201		NSI-202		NSI-202
Plate Number	ORR-093		ORR-140		ORR-145
	Top	Bottom	Top	Bottom	Outside Plate, #1 Near Peak
^{234}U	0.111	0.104	0.107	0.068	0.078
^{235}U	15.820	10.830	10.168	0.893	1.238
^{235}U	0.932	1.935	2.031	3.626	3.580
^{238}U	83.138	87.131	87.694	95.413	95.104
^{238}Pu	0.134	0.701	0.894	5.423	4.792
^{239}Pu	90.276	76.659	75.386	47.211	49.442
^{240}Pu	8.086	15.362	15.841	22.574	20.773
^{241}Pu	1.432	6.308	6.753	11.191	12.567
^{242}Pu	0.071	0.969	1.126	13.601	12.424

Table G.8. Burnups and Fission Densities of Analyzed Sample

Element	BSI-201		BSI-202	
Plate	S-3-210-1		S-3-211-19	
Pos.	Top	Bottom	Top	Bottom
ρ_U	4.60	4.60	4.60	4.60
e	0.1987	0.1987	0.1987	0.1987
A_0	0.2007	0.2007	0.2007	0.2007
A	0.1462	0.0681	0.1101	0.0070
C	0.12	0.14	0.13	0.25
D	-0.17	-0.15	-0.16	-0.14
B	0.315	0.709	0.505	0.973
FD_U	0.6	1.4	1.0	1.9
FF	0.966	0.920	0.947	0.851
FD	0.6	1.5	1.0	2.2

Element	CSI-201		CSI-202	
Plate	OSIIW-084		OSIIW-075	
Pos.	Top	Bottom	Top	Bottom
ρ_U	5.20	5.20	5.20	5.20
e	0.1986	0.1986	0.1986	0.1986
A_0	0.2006	0.2006	0.2006	0.2006
A	0.1440	0.0764	0.1011	0.0085
C	0.12	0.14	0.13	0.23
D	-0.17	-0.16	-0.16	-0.14
B	0.327	0.669	0.550	0.966
FD_U	0.7	1.5	1.2	2.1
FF	0.965	0.926	0.942	0.856
FD	0.8	1.6	1.3	2.5

Element	NSI-201		NSI-202		NSI-202
Plate	ORR-93		ORR-140		ORR-145 Outside Plate,
Pos.	Top	Bottom	Top	Bottom	Near Peak
ρ_U	4.90	4.90	4.90	4.90	4.90
e	0.1969	0.1969	0.1969	0.1969	0.1969
A_0	0.1989	0.1989	0.1989	0.1989	0.1989
A	0.1582	0.1083	0.1017	0.0089	0.0124
C	0.12	0.13	0.13	0.23	0.21
D	-0.17	-0.16	-0.16	-0.14	-0.14
B	0.241	0.509	0.542	0.964	0.950
FD_U	0.5	1.1	1.1	2.0	2.0
FF	0.965	0.926	0.942	0.856	0.856
FD	0.5	1.1	1.2	2.3	2.3

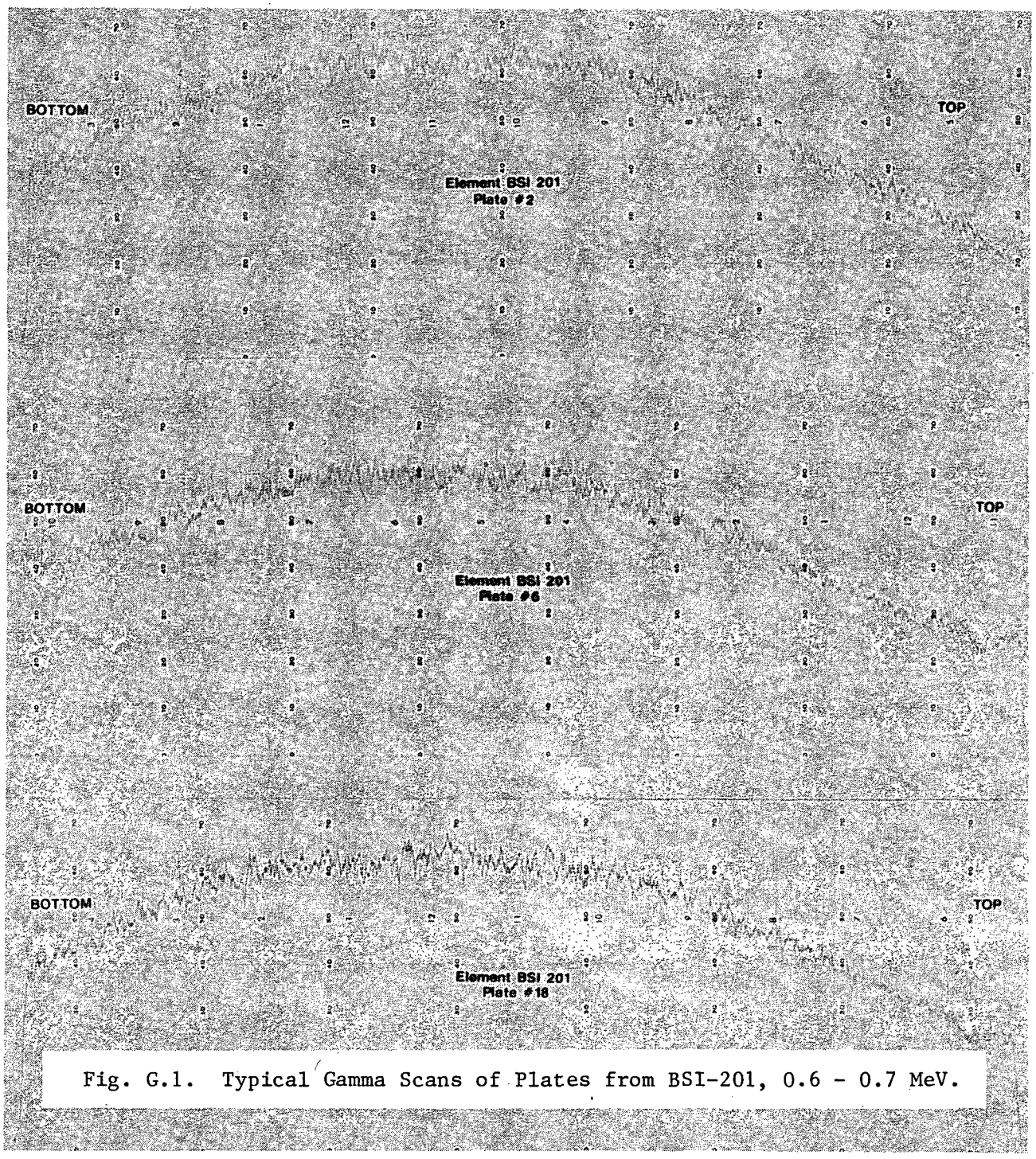

Fig. G.1. Typical Gamma Scans of Plates from BSI-201, 0.6 - 0.7 MeV.

Fig. G.2. Typical Gamma Scans of Plates from BSI-202, 0.6 - 0.7 MeV.

Fig. G.3. Typical Gamma Scans of Plates from CSI-201, 0.6 - 0.7 MeV.

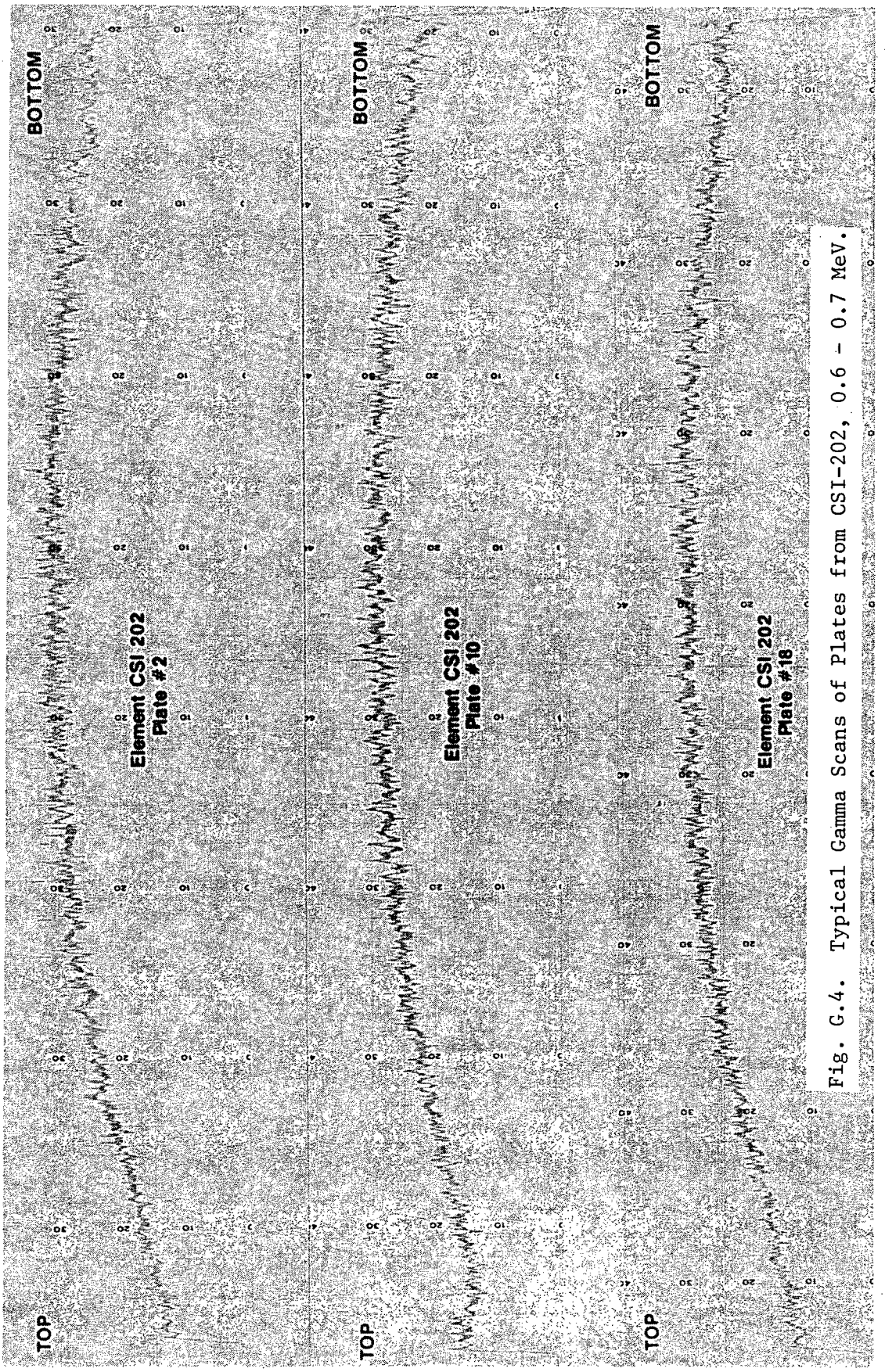

Fig. G.4. Typical Gamma Scans of Plates from CSI-202, 0.6 - 0.7 MeV.

Fig. G.5. Typical Gamma Scans of Plates from NSI-201, 0.6 - 0.7 MeV.

Fig. G.6. Typical Gamma Scans of Plates from NSI-202, 0.6 - 0.7 MeV.

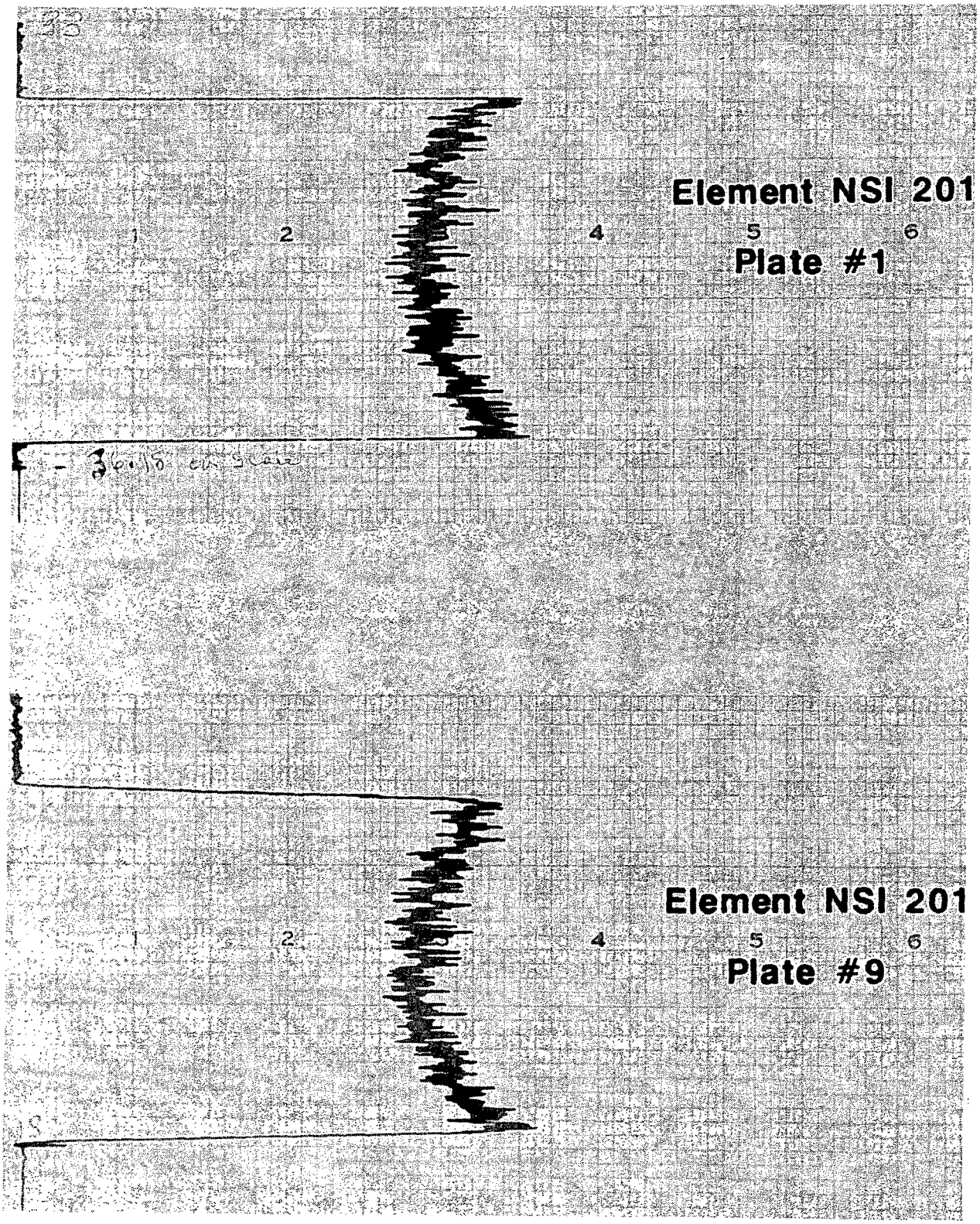

Fig. G.7. Transverse Gamma Scans of Plates from NSI-201, 0.6 - 0.7 MeV.

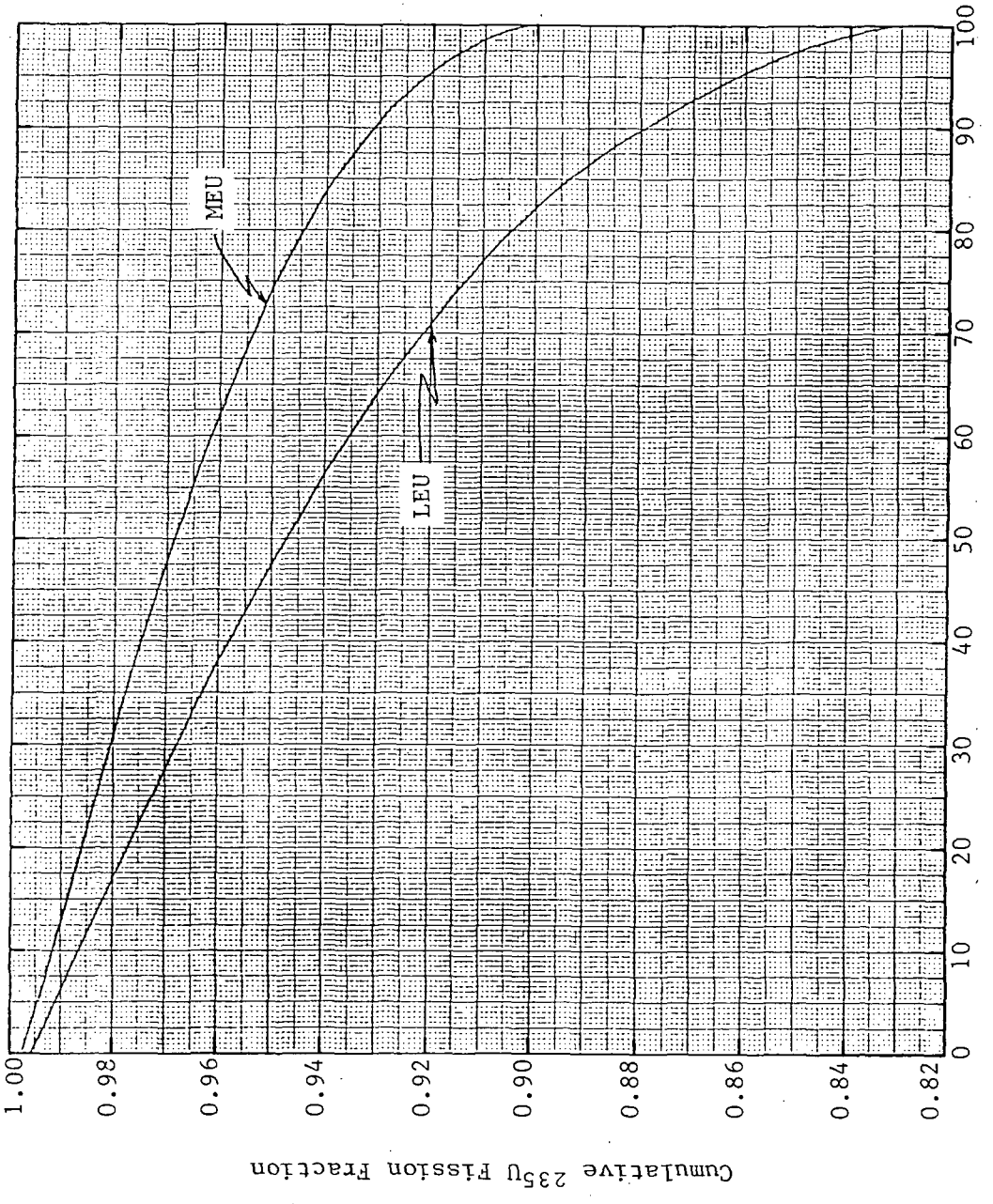

Fig. G.8. Calculated Cumulative ^{235}U Fission Fraction as a Function of ^{235}U Burnup.

APPENDIX H

PHOTOGRAPHS OF PLATES AFTER BLISTER TESTING

Figure H.1. Blister on Plate S-3-201-23 from Element BSI-201 After Heating to 575°C. (R-79721)

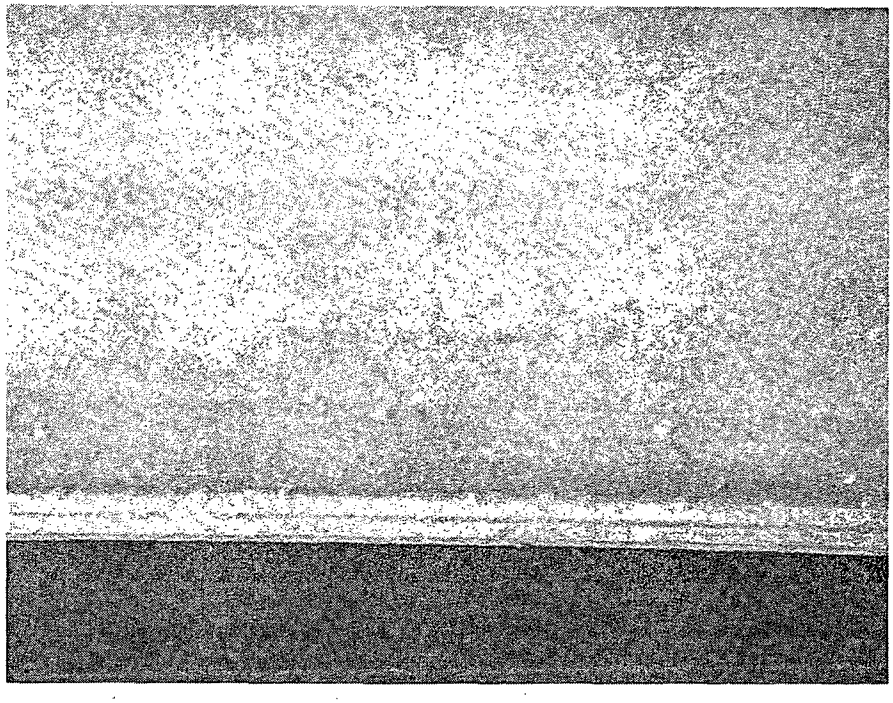

Figure H.2. Blisters on Plate S-3-213-15 from Element BSI-202 After Heating to 550°C. (R-79722)

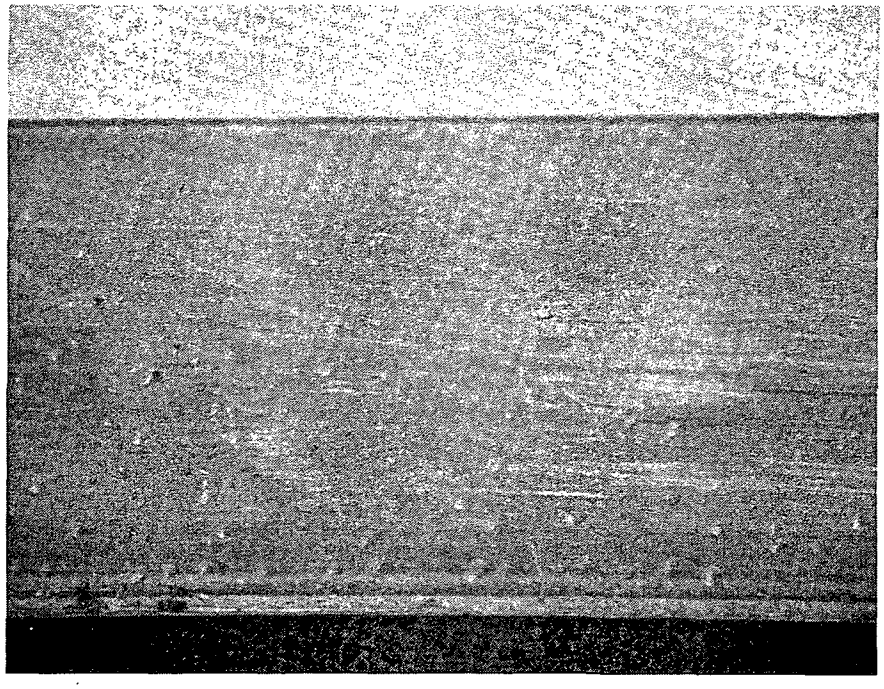

Figure H.3. Blisters on Plate S-3-212-19 from Element BSI-202 After Heating to 550°C. (R-79729)

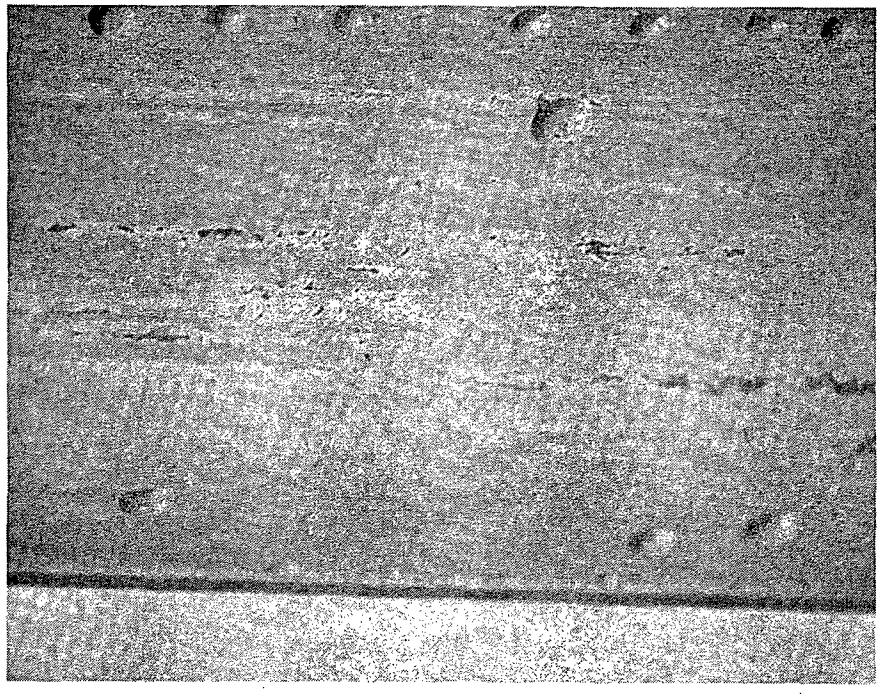

Figure H.4. Blisters on Plate OSIIW-054 from Element CSI-201 After Heating to 550°C. (R-79727)

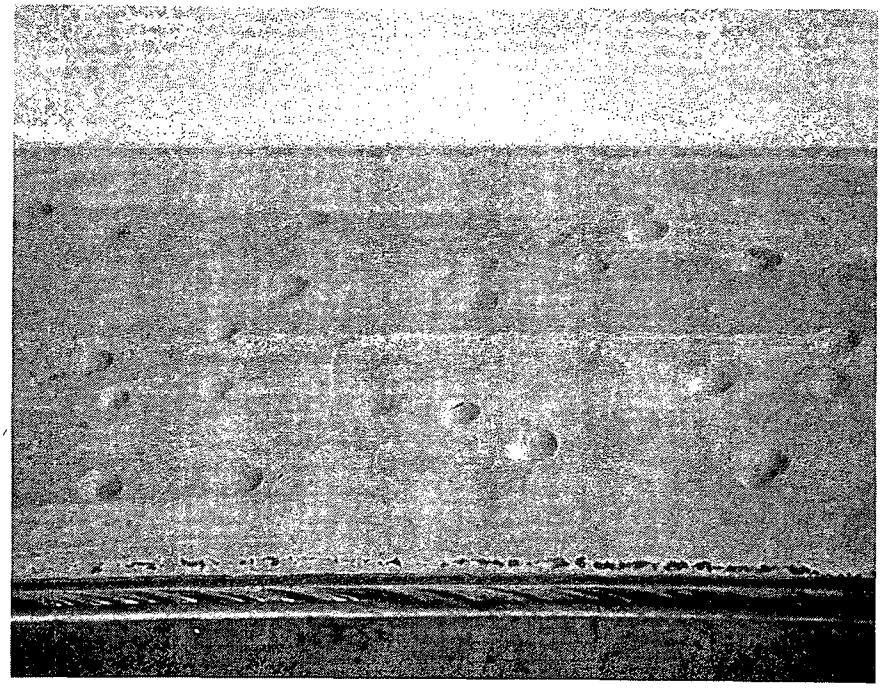

Figure H.5. Blisters on Plate OSIIW-065 from Element CSI-201 After Heating to 550°C. (R-79728)

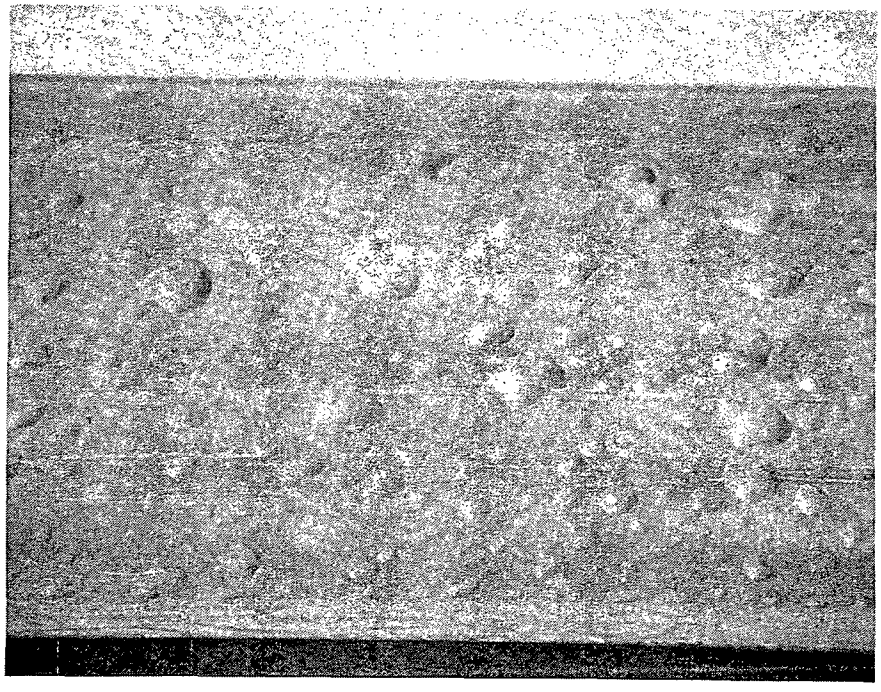

Figure H.6. Blisters on Plate OSIIW-044 from Element CSI-202 After Heating to 550°C. (R-79731)

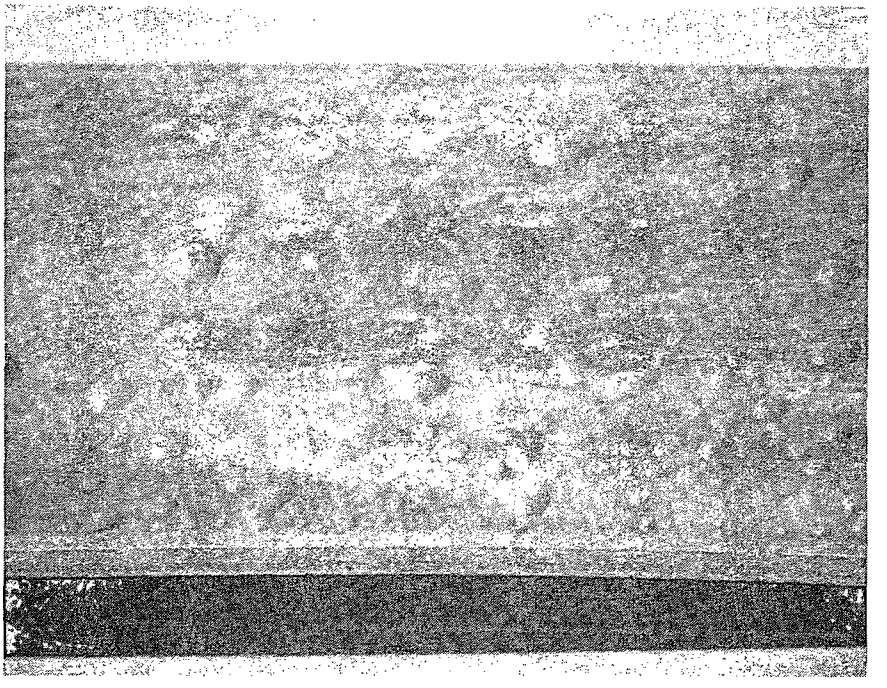

Figure H.7. Blisters on Plate OSIIW-026 from Element CSI-202 After Heating to 550°C. (R-79730)

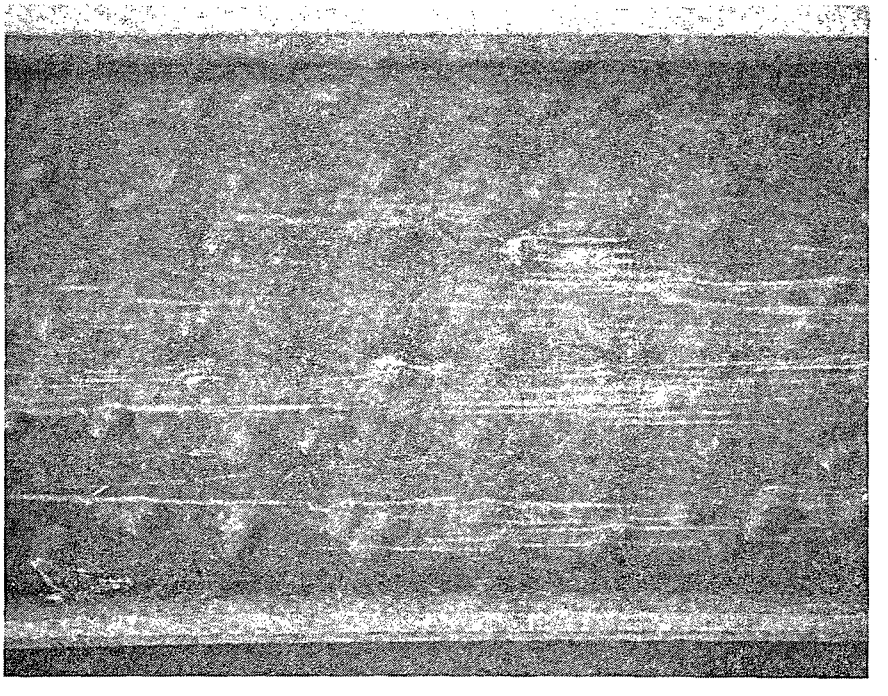

Figure H.8. Blisters on Plate ORR-114 from Element NSI-202 After Heating to 550°C. (R-79735)

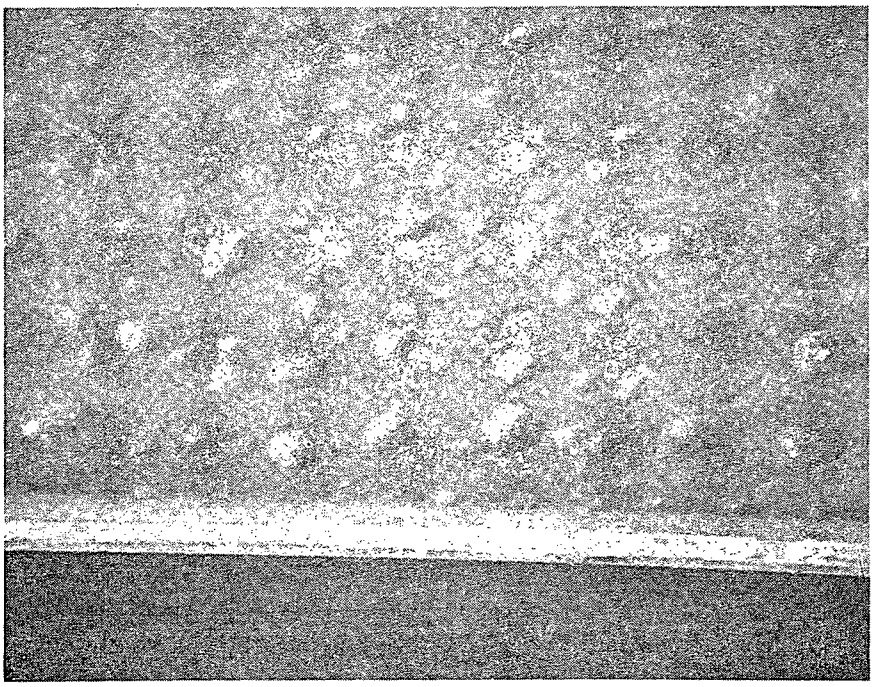

Figure H.9. Blisters on Plate ORR-123 from Element NSI-202 After Heating to 550°C. (R-79734)

NRC FORM 335 (2-84) NRCM 1102, 3201, 3202

U.S. NUCLEAR REGULATORY COMMISSION

BIBLIOGRAPHIC DATA SHEET

SEE INSTRUCTIONS ON THE REVERSE.

1. REPORT NUMBER (Assigned by TIDC, add Vol. No., if any)
NUREG-1313

2. TITLE AND SUBTITLE
Safety Evaluation Report related to the Evaluation of Low-Enriched Uranium Silicide-Aluminum Dispersion Fuel for Use in Non-Power Reactors

3. LEAVE BLANK

4. DATE REPORT COMPLETED
MONTH: July YEAR: 1988

5. AUTHOR(S)

6. DATE REPORT ISSUED
MONTH: July YEAR: 1988

7. PERFORMING ORGANIZATION NAME AND MAILING ADDRESS (Include Zip Code)
Standardization and Non-Power Reactor Project Directorate
Office of Nuclear Reactor Regulation
U. S. Nuclear Regulatory Commission
Washington, D. C. 20555

8. PROJECT/TASK/WORK UNIT NUMBER

9. FIN OR GRANT NUMBER

10. SPONSORING ORGANIZATION NAME AND MAILING ADDRESS (Include Zip Code)

11a. TYPE OF REPORT
Safety Evaluation Report

b. PERIOD COVERED (Inclusive dates)

12. SUPPLEMENTARY NOTES

13. ABSTRACT (200 words or less)

Low-enriched uranium silicide-aluminum dispersion plate-type fuels have been extensively researched and developed under the international program, Reduced Enrichment in Research and Test Reactors. The international effort was led by Argonne National Laboratory (ANL) in the United States. This evaluation is based primarily on reports issued by ANL that discuss and summarize the developmental tests and experiments, including postirradiation examinations, of both miniature and full-sized plates of prototypical fuel compositions. This evaluation concludes that plate-type fuels suitable and acceptable for use in research and test reactors can be fabricated with U_3Si_2-Al dispersion compacts with uranium densities up to 4.8 g/cm^3.

14. DOCUMENT ANALYSIS - a. KEYWORDS/DESCRIPTORS
low-enriched uranium
silicide-uranium dispersion fuel
research and test reactors

b. IDENTIFIERS/OPEN-ENDED TERMS

15. AVAILABILITY STATEMENT
Unlimited

16. SECURITY CLASSIFICATION
(This page) Unclassified
(This report) Unclassified

17. NUMBER OF PAGES

18. PRICE

* U.S. G.P.O. 1988-202-292:80145

UNITED STATES
NUCLEAR REGULATORY COMMISSION
WASHINGTON, D.C. 20555